Title

Ubiquitylation and Phosphorylation Regulate Cell Cycle Progression

Author

Ong, Joseph Yeejoo

Publication Date

2022

Peer reviewed|Thesis/dissertation

UNIVERSITY OF CALIFORNIA

Los Angeles

Ubiquitylation and Phosphorylation Regulate Cell Cycle Progression

A dissertation submitted in partial satisfaction of the

requirements for the degree Doctor of Philosophy

in Biochemistry, Molecular and Structural Biology

by

Joseph Yeejoo Ong

2022

ABSTRACT OF THE DISSERTATION

Ubiquitylation and Phosphorylation Regulate Cell Cycle Progression

by

Joseph Yeejoo Ong

Doctor of Philosophy in Biochemistry, Molecular and Structural Biology

University of California, Los Angeles, 2022

Professor Jorge Torres, Chair

Cell division and cell cycle progression are regulated by various proteins. The activity of these proteins are fine-tuned by post-translational modifications such as ubiquitylation and phosphorylation. Identifying what proteins are modified, the enzymes that performed the modification, and the consequence of the modification has been a core component of understanding the regulation of cell cycle progression. Here, I present my thesis on examining various aspects of these post-translational modifications as they apply to cell cycle progression. First, I discuss the Cul3 substrate adaptor SPOP and its role in regulation of Nup153. Next, I discuss KCTD proteins and their ability to bind to Cul3. Finally, I characterize Cdk15, a putative spindle assembly checkpoint kinase. Altogether, these projects further our understanding of how enzymes and their post-translational modifications orchestrate the various processes necessary for cell division and cell cycle progression and how misregulation of these processes may lead to certain disease states like cancer.

The dissertation of Joseph Yeejoo Ong is approved.

James Akira Wohlschlegel

Steven G. Clarke

Margot Elizabeth Quinlan

Jorge Torres, Committee Chair

University of California, Los Angeles

2022

Table of Contents

List of Figures and Tables

Chapter 2:

Chapter 3:

Chapter 5:

Acknowledgements

I am thankful to all the labs and scientists who have mentored and supported me so far on my scientific journey. These include but are not limited to: Holly Goodson (University of Notre Dame), John MacMillan (UT Southwestern Medical Center), Shyh-Chang Ng (Genome Institute, A*STAR), Steve Clarke, Margot Quinlan, Jorge Torres (UCLA), and Julia Wang and Yu Zhou (Analytical Development, Chemistry – Novartis Gene Therapies, San Diego). There are also many others in neighboring and friendly labs whom are too many to enumerate. I am thankful to all the labs and scientists whom I met at conferences, via Twitter, or elsewhere and who shared offered insight, perspective, and/or reagents.

I am thankful to the UCLA Bruin Bus drivers, facilities management, instrumentation staff Anne Hong-Hermesdorf and Martin Phillips, and to the Department (particularly Marla Gonzalez, Penny Jennings, and Janette Kropat), for keeping everything running. Thank you to undergraduates Katherine, Vivian, Hieu, and Emily for your work.

I am thankful to Tracy Johnson and London Williams for allowing me to lead HHMI Pathways workshops during the academic year and to Tama Hasson and Janet Goins for allowing me to serve as a writing tutor with the URC – Sciences and a lab guide to PEERS students. I am thankful to Roni Lavi from the Career Center for inviting me to serve on graduate student panels for undergraduates and to the staff at the *Daily Bruin* for allowing me to write. I am thankful to the members of the MPSC for allowing me to serve in graduate student government.

I am thankful to the Department Chairs Catherine Clarke and Neil Garg and our CAOs Aaron Sanchez, Eileen Sir, and Amy Ragsdale for their support of the graduate Biochemistry Student Association. I am thankful to my gBSA peers, particularly Orlando Martinez, Maeve Nagle, Jennifer Ngo, Natalie Schibrowsky, Kyle Meador, Dylan Valencia, and Hannah Bailey. Thank you for working with me to improve the culture at UCLA and to serve others.

Finally, I say thank you to my friends and family for your continued support.

Curriculum Vitae

Joseph Yeejoo Ong

EDUCATION

2016-present	PhD, Biochemistry, Structural, and Molecular Biology, University of California, Los Angeles
Spring 2015	Exchange student, National University of Singapore
2012-16	BS, Chemistry (with honors), University of Notre Dame

RESEARCH EXPERIENCE

Summer 2021	Intern, Analytical Chemistry	Novartis Gene Therapies (San Diego)	Supervisor: Yu Zhou, PhD
2016-present	Graduate student	UCLA	Mentor: Jorge Torres, PhD
Jan-Aug 2015	SIPGA fellow	A*STAR (Singapore)	Mentor: Shyh-Chang Ng, PhD
Summer 2014	Undergrad. research fellow	UT Southwestern	Mentor: John MacMillan, PhD
2013-16	Undergrad. research assistant	Uni. of Notre Dame	Mentor: Holly Goodson, PhD

HONORS AND AWARDS

2022	(UCLA) Roberts A. Smith Dissertation Award
2021	(Novartis GTx) Selected (out of 15 interns) to give presentation to San Diego GTx site
2020-21	(UCLA) Whitcome Pre-doctoral Fellowship in Molecular Biology
2020	(UCLA) Ralph and Charlene Bauer Award
2019	ASCB Graduate Student Travel Award
2019	Chinese-American Engineers and Scientists Association Scholarship
2019	ASBMB Graduate Student Travel Award
2017-22	NSF Graduate Research Fellowship Program
2017-19	NIH T32 Cellular and Molecular Biology Training Program
2016-19	(UCLA) Edwin W. Pauley Fellowship
2016	(ND) Best Thesis (Science), Glynn Family Honors Program
2015	(ND) Multicultural Students Programs and Services Research Grant
2015	(ND) Career Center Internship Grant
2015	(ND) Glynn Family Honors Program Summer Undergraduate Research Grant
2015	A*STAR Singapore Institute Pre-Graduate Award
2014	UT Southwestern Medical Center Summer Undergraduate Research Fellowship

PUBLICATIONS

1. Rebeccah A. Warmack, Eric Z. Pang, Esther Peluso, Jonathan D. Lowenson, **Joseph Y. Ong**, Jorge Z. Torres, Steven G. Clarke. The human protein-L-isoaspartate O-methyltransferase domain-

containing protein 1 (PCMTD1) associates with Cullin-RING ligase proteins. Biochemistry. 2022 Apr 29. doi: 10.1021/acs.biochem.2c00130. PMID: 35486881

2. **Joseph Y. Ong**, Julia T. Philip, David C. Molik, Holly V. Goodson. Yeast grown in continuous culture systems can detect mutagens with greater sensitivity than the Ames test. PLoS One. 2021 Mar 17;16(3):e0235303. doi: 10.1371/journal.pone.0235303. eCollection 2021.
3. **Joseph Y. Ong**. Synonymous Mutation Generator: a web tool for designing RNAi-resistant sequences. bioRxiv. 2021.01.02.425100. doi: https://doi.org/10.1101/2021.01.02.425100
4. **Joseph Y. Ong**, Michelle C. Bradley, and Jorge Z. Torres. Phospho-regulation of Mitotic Spindle Assembly. Cytoskeleton (Hoboken). 2020 Dec;77(12):558-578. doi: 10.1002/cm.21649. PMID: 33280275
5. **Joseph Y. Ong** and Jorge Z. Torres. Phase separation in cell division. Review. Mol Cell. 2020 Aug 19;S1097-2765(20)30550-5. doi: 10.1016/j.molcel.2020.08.007 PMID: 32860741
6. **Joseph Y. Ong** and Jorge Z. Torres. Dissecting the mechanisms of cell division. Review. J Biol Chem. 2019 Jul 26;294(30):11382-11390. doi: 10.1074/jbc.AW119.008149 PMID: 31175154
7. Xiaoyu Xia, Yu-Chen Lo, Ankur A. Gholkar, Silvia Senese, **Joseph Y. Ong**, Erick F. Velasquez, Robert Damoiseaux, Jorge Z. Torres. Leukemia Cell Cycle Chemical Profiling Identifies the G2-phase Leukemia Specific Inhibitor Leusin-1. ACS Chem Biol. 2019 May 17;14(5):994-1001. doi: 10.1021/acschembio.9b00173 PMID:31046221
8. **Joseph Y. Ong** and Jorge Z. Torres. "E3 Ubiquitin Ligases in Cancer and their Pharmacological Targeting." Book Chapter, *The Ubiquitin/Proteasome System*, ISBN 978-953-51-7766-1. 2019 Feb. Web link

CONFERENCE PRESENTATIONS (ORAL)

1. **Joseph Ong** and Jorge Z. Torres. SPOP regulates the levels of the nuclear pore protein NupJ. Gordon Research Seminar – Cell Growth and Proliferation, Mt. Snow, VT. July 7, 2019.
2. **Joseph Ong** and Holly V. Goodson. Glynn Family Honors Program Final Thesis Colloquium, University of Notre Dame, IN. Using Yeast as a Biosensor for Mutagenicity. April 21, 2016.
3. **Joseph Ong** and Holly V. Goodson. Scientia: Talk Science, University of Notre Dame, IN. Using Yeast as a Biosensor for Mutagenicity. February 4, 2016.
4. **Joseph Ong** and Holly V. Goodson. 8th Annual College of Science Joint Annual Meeting, University of Notre Dame, IN. Using Yeast as a Biosensor for Mutagenicity. May 2, 2014.

Chapter 1: E3 ubiquitin ligases and cancer progression

This chapter is reproduced from:

> Joseph Y. Ong and Jorge Z. Torres. “E3 Ubiquitin Ligases in Cancer and their Pharmacological Targeting.” Book Chapter, The Ubiquitin/Proteasome System, ISBN 978-953-51-7766-1. 2019 Feb.

This chapter introduces ubiquitin and the E3 ubiquitin ligases that are responsible for ubiquitylating proteins and how misregulation of E3 ubiquitin ligases can result in disease states like cancer.

Chapter

E3 Ubiquitin Ligases in Cancer and Their Pharmacological Targeting

Joseph Y. Ong and Jorge Z. Torres

Abstract

Ubiquitination plays many critical roles in protein function and regulation. Consequently, mutation and aberrant expression of E3 ubiquitin ligases can drive cancer progression. Identifying key ligase-substrate relationships is crucial to understanding the molecular basis and pathways behind cancer and toward identifying novel targets for cancer therapeutics. Here, we review the importance of E3 ligases in the regulating the hallmarks of cancer, discuss some of the key and novel E3 ubiquitin ligases that drive tumor formation and angiogenesis, and review the clinical development of inhibitors that antagonize their function. We conclude with perspectives on the field and future directions toward understanding ubiquitination and cancer progression.

Keywords: E3 ubiquitin ligase, cancer, pharmacological targeting

1. Introduction

The regulation and turnover of proteins is an essential aspect of cell homeostasis and one that is commonly disrupted in cancer cells [1]. Regulation of a protein's levels, activity, or localization is affected by ubiquitination, a posttranslational modification that involves the covalent attachment of a 76 amino acid ubiquitin molecule onto a substrate protein [2, 3]. Depending on the cellular context, ubiquitinated proteins can affect a myriad of cellular processes, including signaling [4], epigenetics [5], endosome trafficking [6], DNA repair [7] and protein stability via the 26S-proteasome [8].

The outcome of protein ubiquitination is affected primarily by two properties: what kind of ubiquitin linkage and how many ubiquitin molecules are present [2]. Ubiquitin is usually covalently attached to its substrate via a nucleophilic lysine residue on the substrate and the ubiquitin carboxy terminus. Ubiquitin itself can serve as a nucleophile via one of seven lysine residues (K6, K11, K27, K29, K33, K48, and K63) [9, 10] though K48- and K63-linkages seem to be the most abundant and are the most well-studied. In some cases, the N-terminal amide of the initiator methionine (M1) of the substrate can serve as the nucleophile [11, 12]. If one of the lysine residues or the initiator methionine of ubiquitin serves as the nucleophile for another ubiquitin molecule, a polyubiquitin chain is formed. A K48-linked polyubiquitin chain of four or more ubiquitin molecules is typically enough to target the substrate for 26S-proteasome mediated degradation [13]. Meanwhile, poly-K63 linkages are involved in many processes, including endocytic trafficking, inflammation, and DNA repair [5, 6, 14]. Other ubiquitin linkages [11], combinations of

linkages (mixed or branched chains) [15–17], monoubiquitination [5, 18], and multi-monoubiquitination [19, 20] events have other diverse functions within the cell.

Ubiquitination occurs in three main steps [21, 22]. First, the E1 ubiquitin-activating enzyme (two in the human genome) covalently attaches to a ubiquitin molecule via a thioester bond in an ATP-dependent process. Next, the E1 enzyme transfers ubiquitin onto an E2 ubiquitin-conjugating enzyme (about 40 in the human genome). Finally, the E2 enzyme binds a substrate-bound E3 ligase (about 600 in the human genome) to transfer ubiquitin onto a lysine residue of the substrate. Repeating the cycle creates a polyubiquitin chain.

E3 ligases can function either as single peptides (like Parkin), simple complexes (e.g.: hetero/homodimers, like MDM2/MDMX or XIAP), or as large complexes (like Cullin-RING-ligase complexes or the anaphase promoting complex/cyclosome). There are two main classes of E3 ligases [23]: HECT (about 30 in the human genome) and RING ligases (including RING and RING-like ligases and their accessory proteins, about 600 in the human genome).

HECT ligases contain a C-terminus HECT domain that accepts the ubiquitin molecule from an E2 conjugating enzyme via a thioester bond before transferring the ubiquitin to the substrate [24]. RING ligases contain a zinc finger domain, and these proteins allow the E2 to transfer ubiquitin directly onto the substrate [25]. A subclass of RING ligases known as RING-between-RING (RBR) ligases contain two RING domains that have elements of both HECT and RING ligases: one RING domain binds the charged E2, while the other RING domain accepts the ubiquitin molecule before transferring it onto the substrate [26].

As E3 ligases ultimately determine the target of the ubiquitination machinery, they play a critical role in cell regulation. They regulate key players in processes like apoptosis (caspases), cell senescence and growth (p53, p21, p27; Hippo and

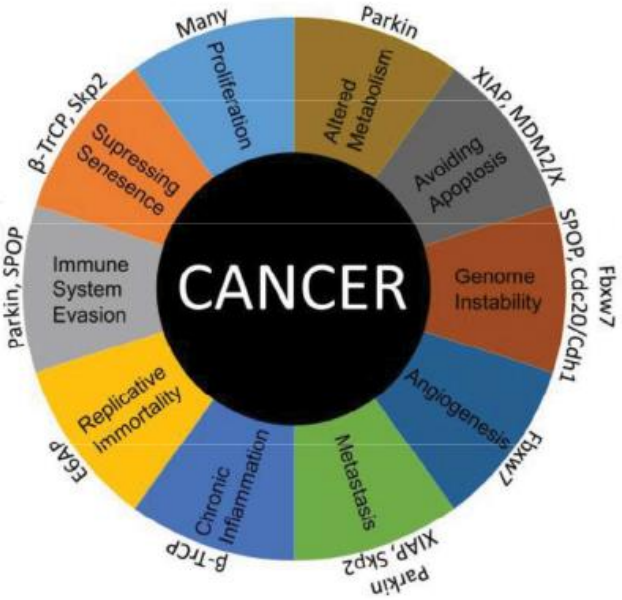

Figure 1.
E3 ubiquitin ligases (outer circle) regulate hallmarks of cancer (inner circle) to drive cancer progression.

Hedgehog signaling), proliferation and genomic stability (c-Myc, cyclins), immune system evasion (PD-L1), inflammation (NFκB), and metastasis and angiogenesis (Wnt signaling) (**Figure 1**). Misregulation or mutation of E3 ligases can lead to overexpression of oncogenes or downregulation of tumor suppressor genes, leading to cancer progression. Consequently, understanding the molecular targets and functions of E3 ligases serves as the basis for designing new cancer therapies.

Here, we describe some central and novel E3 ligases related to cancer development, pharmacological targeting of those ligases, and perspectives on understanding the role of E3 ligases in cancer progression.

2. E3 ligases and cancer progression

2.1 TP53

The tumor protein p53 (TP53) is a transcription factor that serves as one of the principal regulators of cell function and survival (reviewed in [27]), mediating cellular responses to proliferation, cell cycle control, DNA damage response pathways, and apoptosis. Consequently, it is mutated in approximately 50% of all cancer types. Thus, regulators of p53 serve as ideal candidates to understand and address cancer cell progression (**Table 1**).

E6AP (Ube3a) is a 100 kDa HECT domain ligase discovered for mediating the interaction between human papillomavirus protein E6 and p53 [28]. Neither E6AP nor E6 alone have a strong affinity for p53, but together, the E6/E6AP complex binds to p53 and changes the substrate specificity of E6AP [28], allowing E6AP to ubiquitinate p53 at the N-terminal DNA binding domain and target it for

E3 ligase		Notable substrates and binding partners	Expression in cancer	Cancer types
TP53	E6AP	p53	Gain of function via HPV E6	Cervical, breast [38, 166]
	MDM2/X	p53	Overexpressed	Many; liposarcomas [48, 167]
SCF	Skp2	p21, p27	Overexpressed	Many [95, 168]
	Fbxw7	Cyclin E, mTOR	Downregulated or dominant-negative mutant	Many; endometrial, cervical, blood [64, 67, 169]
	β-TrCP	IkB, β-catenin, Wee1, Cdc25a/b	Overexpressed (in some tissues)	Many [60, 168]
APC/C	Cdc20	Cyclin A/B, securin	Overexpressed	Pancreatic, lung, gastric [95, 168, 170]
	Cdh1	Cdc20, Plk1, Aurora kinase A/B	Underexpressed	Many [171]
Other	XIAP	Caspases 3, 7, 9	Overexpressed	Many [98, 99]
	Park2	Cyclin D/E, Cdc20/Cdh1, tubulin	Underexpressed	Breast, pancreatic, colorectal, ovarian [172]
	SPOP	PD-L1, androgen and estrogen receptor	Downregulated or dominant-negative mutant	Prostate, endometrial, kidney [139, 141, 150]

Table 1.
E3 ligases and cancer progression.

degradation [29]. Consequently, E6AP may play a role in HPV-mediated cervical cancers [30], particularly for those mediated by high-risk HPV16 strain, as E6 proteins from lower-risk strains of HPV lack the ability to degrade p53 [31].

The E6/E6AP complex plays other roles in cancer cell progression. Neither E6 nor E6AP alone can activate the hTERT promoter, but together, the E6/E6AP complex can activate the hTERT promoter, perhaps via interactions with c-Myc and NFX-1 to respectively activate and repress promoter activity [32]. The E6/E6AP complex has also been implicated in the ubiquitination of apoptosis-inducing proteins Bak [33], Fas [34], and TNFR1 [35]. Independent of E6 binding, endogenous E6AP targets include the tumor suppressor PML [36]; cell cycle regulators p27 [36], Cdk1, Cdk4; cell proliferation regulator MAPK1 [37];, and guanine nucleotide exchange factor ECT2 [38]. A published list of 130 likely substrates of E6AP includes β-catenin and PRMT5, proteins involved in cancer progression [37].

MDM2 is best known as a regulator of p53. MDM2 is a RING ligase [39] that forms stable heterodimers with a homolog, **MDMX** (MDM4), via their RING domains [40]. MDM2 localizes primarily in the nucleus bound to p300/CBP [41]. When complexed to p53, MDM2 inhibits p53 activity in two ways: first, MDM2 binds the N-terminal transactivation domain [42], inhibiting p53-mediated transcription [43]; secondly, MDM2 modulates p53 protein levels via ubiquitination near the C-terminus [44]. After MDM2 monoubiquitinates p53, p300 and CBP catalyze the polyubiquitination of p53, leading to p53 degradation [8, 41, 45]. Overexpression of MDM2 [46, 47], seen in many cancers where p53 is not mutated [48], leads to a loss of p53 activity.

During p53 activation, p53 is phosphorylated by multiple serine/threonine kinases at residues near the N-terminus, disrupting p53/MDM2 binding and stabilizing p53. For example, ATM kinase phosphorylates p53 at S15 [49] to promote p53-mediated transcription. Additionally, ATM phosphorylation of MDM2 on S395 disrupts the MDM2/p53 complex, allowing p53 to accumulate [50].

2.2 SCF complexes

The SCF complex is a multimeric ubiquitination complex with multiple roles in cell regulation (**Table 1**). The main scaffold of the SCF complex, Cullin 1 (Cul1), recruits the substrate to be ubiquitinated at the N-terminus and the charged ubiquitin at the C-terminus. Rather than bind the substrate directly, Cul1 uses two adaptor proteins: Cul1 binds directly to Skp1, which then binds to one of about 70 F-box proteins [51] that directly bind their substrates. At the C-terminus, Cul1 binds an adaptor protein, either Rbx1 or Rbx2 (also known as Roc1 or Roc2), that will bind a charged E2 ubiquitin conjugating enzyme [52, 53] .

Skp2 (Fbxl1) is a F-box protein that is most active during S-phase [54]. During S phase, Skp2 binds and ubiquitinates phosphorylated p27 [55] by binding the Cdk2-cyclin E complex [56]. Degradation of p27 frees inhibition of Cdk2-cyclinA/E complexes, allowing for progression into S-phase and entry into mitosis [57]. Other targets of Skp2 include p21 [58] and E-cadherin [59]. In some cases, Skp2 requires an accessory protein Cks1 to enhance binding to the substrate [60]. Skp2 both enhances c-Myc transcriptional activity and promotes c-Myc degradation [61]. Interestingly, p300-mediated acetylation of Skp2 changes the localization of Skp2 from nuclear to cytoplasmic, increasing cellular proliferation, motility, and tumorigenesis [59]. Skp2 is commonly overexpressed in a variety of cancers [62], including blood, colorectal, stomach, ovarian, and cervical cancers [60].

Fbxw7 (in yeast, Cdc4) contains a homodimerization domain, an F-box domain that binds Skp1, and eight WD40 repeats that form a beta-propeller structure to bind substrates [63]. Substrate binding is dependent on interaction between the

arginine residues of the Fbxw7 WD40 domains and phosphorylated residues of the substrate in a recognition motif termed the Cdc4 phosphodegron (CPD) [63]. Mutations that disrupt substrate binding, especially point mutations of the arginine residues of the WD40 region, are commonly found in tumor samples [64]. Because Fbxw7 homodimerizes, these mutations may have a dominant-negative effect [65], as wild-type Fbxw7-mutant Fbxw7 dimers are able to effectively bind but not ubiquitinate their substrates [66]. Fbxw7 is deleted [67] or mutated in many cancers, with mutations being especially common in cancers of the bile duct and blood [68].

One well-characterized substrate of Fbxw7 is cyclin E [69]. The ubiquitination and degradation of cyclin E is dependent on phosphorylation of by Cdk2 and glycogen synthase kinase 3 (GSK3) [70]. Dimerization of Fbxw7 can also change its affinity for cyclin E as well as other substrates [71]. Other substrates of Fbxw7 include transcription factors c-Myc [72]; c-JUN, Notch 1; DNA-binding protein DEK [73]; and nutrient sensing protein mTOR [74]. Interestingly, the SV40 large T antigen contains a decoy CPD that can mislocalize Fbxw7 and inhibit Fbxw7-mediated degradation of cyclin E [75].

β-TrCP (BTRC), **Fbxw1a** (β-TrCP1) and **Fbxw11** (β-TrCP2) are protein homologs that appear to have redundant roles [76]. These F-box proteins can form homo- and hetereodimers with each other [76] and use WD40 domains to bind a DSG phosphodegron motif (such as DpSGXXpS) [60]. Overexpression of β-TrCP is seen in various types of cancers, including colorectal, pancreatic, breast, ovarian and melanomas [77].

β-TrCP plays an important role as a regulator of Cdk1. One substrate of β-TrCP is Wee1, a kinase that inhibits Cdk1 activity [78]. Phosphorylation of Wee1 at S53 and S123 by Plk1 and Cdk1 respectively allow β-TrCP to bind to and ubiquitinate Wee1, activating Cdk1 during G2 to promote rapid entry into mitosis. Similarly, in prophase, β-TrCP also ubiquitinates Emi1, an inhibitor of the APC/C [79]. Consequently, β-TrCP accelerates mitotic progression both by increasing Cdk1 activity and activating the APC/C. In the case of DNA damage, checkpoint proteins hyperphosphorylate Cdc25a [80], a phosphatase that activates Cdk1 by removing repressive phosphorylation events. β-TrCP binds to and ubiquitinates hyperphosphorylated Cdc25a, deactivating Cdk1 and delaying the cell cycle. β-TrCP also ubiquitinates Cdc25b [81], a phosphatase that activates Cdk2/cyclin A and Cdk1/cyclin B to progress through the G2/M transition [82]. Other β-TrCP substrates that are linked to cancer progression include the IkB family [83], β-catenin [76] and MDM2 [84].

2.3 APC/C

Proper cell cycling and successful mitotic events rely on the coordinated accumulation and destruction of cyclins [85]. Disruption of this coordination can lead to aberrant mitotic events, aneuploidy, and cancer [86] (**Table 1**). While entry into mitosis is mediated by activation of Cdk1/2, progression through and exit from mitosis is mediated principally by the anaphase promoting complex or cyclosome (**APC/C**).

The APC/C is a 1.2 megadalton complex whose activity is necessary for entry to and exit from mitosis [87]. The structure of the human APC/C was solved via cryoEM to 7.4 angstrom resolution, allowing for the identification of 20 subunits of the APC/C and a mechanistic understanding of its function [88]. APC/C ubiquitin ligase activity depends on two activating subunits, **Cdc20** or **Cdh1** (coded by gene FRZ1; not to be confused with the gene CDH1, which codes for E-cadherin), which are necessary for APC/C binding to substrate and subsequent degradation [89] via

K11 ubiquitin linkages [90]. In early mitosis, APC/C-Cdc20 degrades proteins such as cyclins A and B and Securin, the inhibitor of separase [91]. In later stages of mitosis and early G1, APC/C-Cdh1 degrades Cdc20, mitotic kinases like Plk1 and Aurora kinases A/B, and the contractile ring protein Anillin to ensure exit from mitosis and proper transition into G1 [92]. Binding of the substrate to APC/C is mediated by two main modalities [93]: for some substrates, Cdc20/Cdh1 binds the substrate through a KEN box motif; for others, both the APC/C subunit Apc10 and Cdc20/Cdh1 "sandwich" the substrate at the substrate's D box. Some substrates have both and/or additional motifs to bind the APC/C and Cdc20/Cdh1 [92].

Cdc20 is found overexpressed in many cancers, including lung, oral, liver, and colon cancers [94, 95]. Cdh1 is generally a tumor suppressor, as downregulation of Cdh1 is found in some aggressive cancer cell types [95], and loss of Cdh1 sensitizes cells to DNA damage [96].

2.4 Other

X-linked inhibitor of apoptosis protein (**XIAP**) is a IAP family E3 ligase characterized by three N-terminal baculovirus IAP repeat domains and a C-terminal RING domain [97]. Like other IAPs, XIAP plays a central role in mediating the cell's response to apoptosis. XIAP is overexpressed in many cancer cell lines, particularly in kidney and skin cancers [98, 99].

The linker region of XIAP between BIR1 and BIR2 binds to the active site and inhibits caspase 3 and caspase 7 [100]. The BIR3 domain of XIAP also binds to caspase 9, inhibiting caspase 9 dimerization and activity [101]. Moreover, XIAP ubiquitinates caspase 3 [102], caspase 9 [103], and caspase 7 [104] and targets them for degradation. As a final level of regulation, in addition to its ubiquitin E3 ligase role, XIAP can also function as a neddylation E3 ligase, neddylating and inhibiting the activity of caspases [105].

XIAP also plays important roles in cell motility. On one hand, XIAP degrades COMMD1 [106], a regulator of NFκB [107] and copper homeostasis. XIAP also binds to MAP3K7IP1, an event that activates kinase MAP3K7 to phosphorylate substrates leading to removal of NFκB inhibition [108]. XIAP also binds to survivin [109], activating NFκB signaling and encouraging cell metastasis by activating cell motility kinases Fadk1 and Src [110]. Conversely, XIAP has also been show to inhibit cell migration by binding to and ubiquitinating c-RAF to direct another ubiquitin ligase (CHIP) to degrade c-RAF [111]. Under non-stressed conditions, XIAP ubiquitinates and degrades MDM2, stabilizing p53 and inhibiting autophagy [112]. XIAP also binds to and monoubiquitinates TLE3, allowing β-catenin to activate Wnt-mediated transcription [113]. Finally, in addition to inflammation involving the NFκB pathway, XIAP suppresses TLR-based inflammation [114].

Park2 (PARKIN) is an RBR-E3 ligase with both RING and HECT ligase characteristics [115]. The Park2 locus is commonly deleted in cancers [116]. In mouse models, loss of Park2 causes spontaneous liver cancer [117] and contributes to colorectal cancer in mouse models [118]. Additionally, Park2 plays a central role in mitophagy [119], which may affect cell redox state [120], proliferation, and metastasis [121].

Park2 plays a prominent role in regulating cyclin levels. Park2 degrades cyclins D [122] and E [123] in a Cul1-dependent manner [124]. Park2 mutations found in cancer lead to stabilization of these G1/S-phase cyclins, an increase in the number of cells in S and G2/M phase [123, 124], and increased rates of cellular proliferation [122]. Moreover, Park2 associates with Cdc20 and Cdh1 during mitosis in an APC/C-independent manner and regulates the levels of many APC/C substrates including mitotic kinases and mitotic cyclins [125]. Park2 regulates microtubules

and the mitotic spindle, cytokinetic bridge [126], cell motility [127], and invasion [128]. Park2 ubiquitinates and degrades HIF-1α to contribute to cell migration, and loss of Park2 leads to tumor metastasis in mouse models [129].

In Park2 knock-out mouse models, the resulting oxidative stress and the Warburg effect [130] caused an increase in the mRNA of Aim2, a protein involved in cytokine production [131]. In these mouse models, activation of Aim2 ultimately led to upregulation of PD-L1 in pancreatic tumors and lower rates of survival, an effect seen in human pancreatic tumors and patients [131]. Thus, Park2's roles in metabolism may affect the ability of the immune system to regulate cancer progression.

SPOP is a Cul3 substrate adaptor mutated in about 10% of prostate cancers and some kidney cancers [132]. SPOP has three basic domains: an N-terminal MATH domain for substrate recognition [133], a BTB domain for dimerization and interaction with Cul3 [134], and a BACK domain which assembles SPOP dimers into oligomers [134], a mechanism which increases SPOP binding to and ubiquitination of the substrate [135]. As SPOP regulates many proteins responsible for maintaining cell integrity, mutations in the MATH domain that disrupt binding to substrate encourage cancer progression [136].

SPOP plays a role in immunotherapy by ubiquitinating and degrading PD-L1 [137]. SPOP binding mutants cannot ubiquitinate PD-L1, resulting in larger tumor growth and fewer tumor-infiltrating lymphocytes compared to tumors harboring wild-type SPOP in mouse models [137]. Similarly, pancreatic cancer samples with mutant SPOP had higher levels of PD-L1, demonstrating a role for SPOP in immune system invasion [137].

Other notable SPOP substrates include the apoptotic protein Daxx [138, 139], deSUMOlyase SENP7 [140], c-Myc [141], HDAC6 [142], Cdc20 [143], proto-oncogene DEK [144], phosphatases PTEN and Dusp7 [139], hedgehog pathway proteins Gli2 and Gli3 [145, 146], and BET transcriptional coactivators BRD2–4 [147–149]. SPOP is also closely tied to hormone-activated pathways, as steroid receptor coactivator SRC-3 [150], androgen receptor (AR) [151], enhancer of AR-mediated transcriptional activity TRIM24 [144], and estrogen receptor α (ERα) [136] are all substrates of SPOP. Finally, wild-type, but not mutant SPOP degrades ERG [152]. Interestingly, in some prostate cancer samples, some tumors expressed a fused ERG protein due to genome rearrangements, a phenotype driven by SPOP mutation [153]. Unlike wild-type ERG, these ERG-fusions lack an SPOP binding site, contributing to cancer progression [154].

3. E3 ligases and their inhibitors

One ubiquitin-proteasome inhibitor has already found use in the treatment of cancer: Bortezomib is a 26S-proteasome inhibitor approved for treating certain types of myeloma and lymphoma that binds to and inhibits the proteasome from degrading other proteins [155]. Another compound still in clinical development is MLN4924 (Pevonedistat), an inhibitor of the Nedd8-activating enzyme and thus of Cullin RING ligase complexes [155]. As ubiquitination plays many important roles in cell regulation, these broad inhibitors can affect many cellular pathways, not just those that are therapeutically useful. As E3 ligases are specific for their substrates, E3 ligases serve as precise targets for therapeutic intervention (**Table 2**). Inhibition of E3 ligases will hopefully minimize off-target effects. Moreover, as some E3 ligases have many oncogenes as their substrates, targeting E3 ligases may serve to be more efficient than targeting individual substrates.

While most inhibitors have been identified via high throughput screens, the most clinically relevant inhibitors have been derived from structure–function

analyses of E3 ligases complexed to their substrates. For example, the crystal structure of MDM2 bound to p53 allowed for the identification of the MDM2-p53 binding pocket and the design of small molecules [156] (like Nutlins and their derivatives) and stapled peptides [157] that bind to MDM2 and inhibit p53 binding. Similarly, the structure of the IAP family of E3 ligases and their endogenous inhibitors, the SMAC peptides, allowed for the development of higher affinity peptides [158] and peptidomimetics and the discovery of one small molecule inhibitor, Embelin [159]. Of the inhibitors mentioned here, MDM2 and XIAP inhibitors have advanced the farthest in clinical trials. A crystal structure of the SPOP substrate binding domain was also used to develop an SPOP inhibitor, suggesting that structural studies may greatly enhance development of small molecule inhibitors [160].

Most inhibitors disrupt E3 ligase-substrate binding by blocking the binding pocket of the E3 ligase. However, because HECT domains first transfer the ubiquitin molecule to themselves via a thioester bond [24], HECT ligases have an

E3 ligase		Therapeutic	Mechanism	Model			In clinical trials
				In vitro assay	Cell culture	Mouse model	
TP53	E6AP	CM-11 peptides [161]	Binds HECT domain	X	X		
		Compound 9 [173]	Binds HPV E6	X	X		
	MDM2/X	Nutlins [156], RG7112 [174]	Binds p53 binding site	X	X	X	
		Idasanutlin (RG7388) [175]		X	X	X	X
		MI-888 [176], SAR405838 [151]	Binds p53 binding site	X	X	X	X
		AMG-232 [177]	Binds p53 binding site	X	X	X	X
		NVP-CGM097 [178], HDM201 [179]	Binds p53 binding site	X	X	X	X
		JNJ-26854165 (Serdemetan)	Assumed to bind to RING domain of MDM2 [180]		X	X	X
		ALRN-6924 [157]	Stapled peptide binds MDM2 and MDMX at p53 binding site	X	X	X	X
SCF	Skp2	Compound #25 [181]	Binds Skp1 binding site	X	X	X	
		C1, C2, C16, C20 [163, 182]	Presumed: Binds Skp2, Cks1 at p27 binding site	X	X		
		CpdA [165]	Inhibits Skp2-Skp1 binding	X	X		
		NSC689857, NSC681152 [164]	Inhibits Skp2-Cks1 binding	X			
	Fbxw7	Oridonin [183]	Stabilizes Fbxw7, increases the activity of kinase Gsk-3	X	X		

E3 ligase		Therapeutic	Mechanism	Model			In clinical trials
				In vitro assay	Cell culture	Mouse model	
	β-TrCP	Erioflorin [184]	Inhibits β-TrCP1 binding to substrate	X	X		
		GS143 [185]	Presumed: Inhibits binding of β-TrCP1 and p-IkBa	X	X		
APC/C	Cdc20	Apcin [186]	Binds to D-box binding site of Cdc20	X	X		
	Cdc20/ Cdh1	ProTAME [187]	Inhibits formation of APC/C-Cdc20, -Cdh1	X	X	X	
Other	XIAP	LCL161 [158]	Binds to BIR3 domain of XIAP [188]	X	X	X	X
		AEG 35156 [189]	XIAP antisense oligonucleotide		X		X
	SPOP	Palbociclib [137]	Cdk4 phosphorylates SPOP, destabilizes PD-L1	X	X	X	*
		Compound 6b [160]	Binds to substrate pocket	X	X	X	

**Palbociclib is clinically approved for treatment of breast cancer.*

Table 2.
E3 ligases and their inhibitors.

additional mode of pharmacological inhibition. The CM-11 peptides (E6AP inhibitors) are one such therapy that takes advantage of this step to inhibit or disrupt the HECT-Ubiquitin transthiolation reaction [161]. Future work may focus on designing small molecules that disrupt this function of the HECT domain.

To degrade its most clinically relevant targets p21 and p27, Skp2 functions with an adaptor protein, Cks1 [162]. At least two classes of inhibitors (NSC689857/NSC681152 [163] and the C1/2/16/20 compounds [164]) have been developed that disrupt the Skp2-Cks1 interaction. Similarly, the SCF ligase complex is only active upon the binding of an F-box protein to Skp1. CpdA inhibits Skp2-Skp1 binding [165]. These results suggest that another method of inhibitor design may focus on disrupting crucial activators and binding partners of E3 ligases instead of merely disrupting E3 ligase-substrate binding.

Upon phosphorylation by Cdk4, SPOP protein levels are stabilized, and PD-L1 expression levels decrease [137]. To improve the efficiency of anti-PD-L1 immunotherapies, mice treated with both Cdk4/6 inhibitors (to destabilize SPOP and thus stabilize PD-L1) and anti-PD-L1 immunotherapy showed improved survival when compared to untreated mice or mice with each individual treatment [137]. In this case, stabilization of an oncogenic protein led to improved efficacy of a complimentary therapy. Whether a similar combination of therapies can be used to improve the overall survival rate in other pathways remains to be seen.

4. Conclusions and perspectives

Recent research has highlighted the role of ubiquitination in cell regulation, division, and cancer cell progression. While much work has advanced the identification of E3 ubiquitin ligases and their substrates, untangling how these ligases act upon interconnected pathways remains a challenge in cancer cell biology. For example, understanding in which contexts certain E3 ligases are tumor-supportive or tumor-suppressive (like β-TrCP) is still not clear. Genome-wide analyses and advancements in systems biology have aided in and will continue to contribute to addressing these issues.

The tumor microenvironment has established itself as a central component in understanding and treating cancer progression. The macro-level questions of tumors—how cancers induce angiogenesis, interact with the immune system and cytokines, interact with the microbiome, and metastasize—are some questions that are best addressed with research in animal models, not human cell culture models. For example, the recent discoveries that both SPOP and Park2 play a role in mediating PD-L1 stability demonstrate the need to study the roles of E3 ligases in animal models. Given the recent success of immuno-oncology and CAR-T cell therapy, a further understanding how E3 ligases affect macro-level phenotypes like tumor sensitivity to immunotherapies may influence the design of clinical therapies.

While many E3 ligase inhibitors are being identified via high-throughput small molecule screens that assess inhibition of E3 ligase-substrate binding or ubiquitination activity, the most clinically advanced inhibitors have been refined from structural analysis of the E3 ligase binding pocket. The structures of many E3 ligases have already been determined (for example, all 11 ligases discussed here have at least a partial structure), so further pharmacological development may involve identifying binding pockets and designing inhibitors to perturb ligase function, and optimizing already identified inhibitors. On the other hand, E3 ligases are often redundant, so inhibition of one ligase may not completely stabilize a beneficial substrate. Nonetheless, the early clinical success of some E3 ligase inhibitors suggests that ubiquitin ligase inhibition is a promising venue for therapeutic intervention in cancer patients.

Author details

Joseph Y. Ong and Jorge Z. Torres*
Department of Chemistry and Biochemistry, University of California, Los Angeles, CA, USA

*Address all correspondence to: torres@chem.ucla.edu

References

[1] Hanahan D, Weinberg RA. Hallmarks of cancer: The next generation. Cell. 2011;**144**:646-674

[2] Komander D, Rape M. The ubiquitin code. Annual Review of Biochemistry. 2012;**81**:203-229

[3] Yau R, Rape M. The increasing complexity of the ubiquitin code. Nature Cell Biology. 2016;**18**:579-586

[4] Tao M et al. ITCH K63-ubiquitinates the NOD2 binding protein, RIP2, to influence inflammatory signaling pathways. Current Biology. 2009;**19**: 1255-1263

[5] Sigismund S, Polo S, Di Fiore PP. Signaling through monoubiquitination. Current Topics in Microbiology and Immunology. 2004;**286**:149-185

[6] Williams RL, Urbé S. The emerging shape of the ESCRT machinery. Nature Reviews. Molecular Cell Biology. 2007; **8**:355-368

[7] Hoege C, Pfander B, Moldovan G-L, Pyrowolakis G, Jentsch S. RAD6-dependent DNA repair is linked to modification of PCNA by ubiquitin and SUMO. Nature. 2002;**419**:135-141

[8] Haupt Y, Maya R, Kazaz A, Oren M. Mdm2 promotes the rapid degradation of p 53. Nature. 1997;**387**:296-299

[9] Xu P et al. Quantitative proteomics reveals the function of unconventional ubiquitin chains in proteasomal degradation. Cell. 2009;**137**:133-145

[10] Peng J et al. A proteomics approach to understanding protein ubiquitination. Nature Biotechnology. 2003;**21**:921-926

[11] Emmerich CH et al. Activation of the canonical IKK complex by K63/M1-linked hybrid ubiquitin chains. Proceedings of the National Academy of Sciences of the United States of America. 2013;**110**:15247-15252

[12] Kirisako T et al. A ubiquitin ligase complex assembles linear polyubiquitin chains. The EMBO Journal. 2006;**25**: 4877-4887

[13] Thrower JS, Hoffman L, Rechsteiner M, Pickart CM. Recognition of the polyubiquitin proteolytic signal. The EMBO Journal. 2000;**19**:94-102

[14] Chen ZJ, Sun LJ. Nonproteolytic functions of ubiquitin in cell signaling. Molecular Cell. 2009;**33**:275-286

[15] Ben-Saadon R, Zaaroor D, Ziv T, Ciechanover A. The polycomb protein Ring1B generates self atypical mixed ubiquitin chains required for its In vitro histone H2A ligase activity. Molecular Cell. 2006;**24**:701-711

[16] Liu C, Liu W, Ye Y, Li W. Ufd2p synthesizes branched ubiquitin chains to promote the degradation of substrates modified with atypical chains. Nature Communications. 2017;**8**:14274

[17] Ohtake F, Tsuchiya H, Saeki Y, Tanaka K. K63 ubiquitylation triggers proteasomal degradation by seeding branched ubiquitin chains. Proceedings of the National Academy of Sciences of the United States of America. 2018;**115**: E1401-E1408

[18] Alpi AF, Pace PE, Babu MM, Patel KJ. Mechanistic insight into site-restricted monoubiquitination of FANCD2 by Ube2t, FANCL, and FANCI. Molecular Cell. 2008;**32**:767-777

[19] Braten O et al. Numerous proteins with unique characteristics are degraded by the 26S proteasome following monoubiquitination. Proceedings of the National Academy of Sciences of the

United States of America. 2016;**113**: E4639-E4647

[20] Kravtsova-Ivantsiv Y, Cohen S, Ciechanover A. Modification by single ubiquitin moieties rather than polyubiquitination is sufficient for proteasomal processing of the p105 NF-κB precursor. Molecular Cell. 2009;**33**: 496-504

[21] George AJ, Hoffiz YC, Charles AJ, Zhu Y, Mabb AM. A comprehensive atlas of E3 ubiquitin ligase mutations in neurological disorders. Frontiers in Genetics. 2018;**9**:29

[22] Weissman AM, Shabek N, Ciechanover A. The predator becomes the prey: Regulating the ubiquitin system by ubiquitylation and degradation. Nature Reviews. Molecular Cell Biology. 2011;**12**:605-620

[23] Li W et al. Genome-wide and functional annotation of human E3 ubiquitin ligases identifies MULAN, a mitochondrial E3 that regulates the Organelle's dynamics and signaling. PLoS One. 2008;**3**:e1487

[24] Scheffner M, Kumar S. Mammalian HECT ubiquitin-protein ligases: Biological and pathophysiological aspects. Biochimica et Biophysica Acta (BBA)—Molecular Cell Research. 2014; **1843**:61-74

[25] Lipkowitz S, Weissman AM. RINGs of good and evil: RING finger ubiquitin ligases at the crossroads of tumour suppression and oncogenesis. Nature Reviews. Cancer. 2011;**11**: 629-643

[26] Dove KK, Stieglitz B, Duncan ED, Rittinger K, Klevit RE. Molecular insights into RBR E3 ligase ubiquitin transfer mechanisms. EMBO Reports. 2016;**17**:1221-1235

[27] Kastenhuber ER, Lowe SW. Putting p53 in context. Cell. 2017;**170**:1062-1078

[28] Scheffner M, Werness BA, Huibregtse JM, Levine AJ, Howley PM. The E6 oncoprotein encoded by human papillomavirus types 16 and 18 promotes the degradation of p53. Cell. 1990;**63**:1129-1136

[29] Martinez-Zapien D et al. Structure of the E6/E6AP/p53 complex required for HPV-mediated degradation of p53. Nature. 2016;**529**:541-545

[30] Alejo M et al. Contribution of human papillomavirus in neuroendocrine tumors from a series of 10,575 invasive cervical cancer cases. Papillomavirus Research. 2018;**5**: 134-142

[31] Elbel M, Carl S, Spaderna S, Iftner T. A comparative analysis of the interactions of the E6 proteins from cutaneous and genital papillomaviruses with p53 and E6AP in correlation to their transforming potential. Virology. 1997;**239**:132-149

[32] Liu X et al. HPV E6 protein interacts physically and functionally with the cellular telomerase complex. Proceedings of the National Academy of Sciences. 2009;**106**:18780-18785

[33] Thomas M, Banks L. Inhibition of Bak-induced apoptosis by HPV-18 E6. Oncogene. 1998;**17**:2943-2954

[34] Filippova M, Parkhurst L, Duerksen-Hughes PJ. The human papillomavirus 16 E6 protein binds to Fas-associated death domain and protects cells from Fas-triggered apoptosis. The Journal of Biological Chemistry. 2004;**279**:25729-25744

[35] Filippova M, Song H, Connolly JL, Dermody TS, Duerksen-Hughes PJ. The human papillomavirus 16 E6 protein binds to tumor necrosis factor (TNF) R1 and protects cells from TNF-induced apoptosis. The Journal of Biological Chemistry. 2002;**277**:21730-21739

[36] Raghu D et al. E6AP promotes prostate cancer by reducing p27 expression. Oncotarget. 2017;**8**: 42939-42948

[37] Wang Y et al. Identifying the ubiquitination targets of E6AP by orthogonal ubiquitin transfer. Nature Communications. 2017;**8**:2232

[38] Mansour M et al. The E3-ligase E6AP represses breast cancer metastasis via regulation of ECT2-rho signaling. Cancer Research. 2016;**76**:4236-4248

[39] Fang S, Jensen JP, Ludwig RL, Vousden KH, Weissman AM. Mdm2 is a RING finger-dependent ubiquitin protein ligase for itself and p53. The Journal of Biological Chemistry. 2000; **275**:8945-8951

[40] Wang X, Wang J, Jiang X. MdmX protein is essential for Mdm2 protein-mediated p53 polyubiquitination. The Journal of Biological Chemistry. 2011; **286**:23725-23734

[41] Ferreon JC et al. Cooperative regulation of p53 by modulation of ternary complex formation with CBP/ p300 and HDM2. Proceedings of the National Academy of Sciences. 2009; **106**:6591-6596

[42] Kussie PH et al. Structure of the MDM2 oncoprotein bound to the p53 tumor suppressor transactivation domain. Science. 1996;**274**:948-953

[43] Oliner JD et al. Oncoprotein MDM2 conceals the activation domain of tumour suppressor p53. Nature. 1993; **362**:857-860

[44] Poyurovsky MV et al. The C terminus of p53 binds the N-terminal domain of MDM2. Nature Structural & Molecular Biology. 2010;**17**:982-989

[45] Grossman SR et al. Polyubiquitination of p53 by a ubiquitin ligase activity of p300. Science (80-). 2003;**300**:342-344

[46] Zack TI et al. Pan-cancer patterns of somatic copy number alteration. Nature Genetics. 2013;**45**:1134-1140

[47] Beroukhim R et al. The landscape of somatic copy-number alteration across human cancers. Nature. 2010;**463**: 899-905

[48] Oliner JD, Saiki AY, Caenepeel S. The role of MDM2 amplification and overexpression in tumorigenesis. Cold Spring Harbor Perspectives in Medicine. 2016;**6**:a026336

[49] Canman CE et al. Activation of the ATM kinase by ionizing radiation and phosphorylation of p53. Science. 1998; **281**:1677-1679

[50] Gannon HS, Woda BA, Jones SN. ATM phosphorylation of Mdm2 Ser394 regulates the amplitude and duration of the DNA damage response in mice. Cancer Cell. 2012;**21**:668-679

[51] Lydeard JR, Schulman BA, Harper JW. Building and remodelling Cullin-RING E3 ubiquitin ligases. EMBO Reports. 2013;**14**:1050-1061

[52] Wei D, Sun Y. Small RING finger proteins RBX1 and RBX2 of SCF E3 ubiquitin ligases: The role in cancer and as cancer targets. Genes & Cancer. 2010;**1**:700-707

[53] Lyapina SA, Correll CC, Kipreos ET, Deshaies RJ. Human CUL1 forms an evolutionarily conserved ubiquitin ligase complex (SCF) with SKP1 and an F-box protein. Proceedings of the National Academy of Sciences of the United States of America. 1998;**95**: 7451-7456

[54] Nakayama K et al. Skp2-mediated degradation of p27 regulates progression into mitosis. Developmental Cell. 2004; **6**:661-672

[55] Carrano AC, Eytan E, Hershko A, Pagano M. SKP2 is required for ubiquitin-mediated degradation of the CDK inhibitor p27. Nature Cell Biology. 1999;**1**:193-199

[56] Ungermannova D, Gao Y, Liu X. Ubiquitination of p27Kip1 requires physical interaction with cyclin E and probable phosphate recognition by SKP2. The Journal of Biological Chemistry. 2005;**280**:30301-30309

[57] Zhang H, Kobayashi R, Galaktionov K, Beach D. p19Skp1 and p45Skp2 are essential elements of the cyclin A-CDK2 S phase kinase. Cell. 1995;**82**:915-925

[58] Yu ZK, Gervais JL, Zhang H. Human CUL-1 associates with the SKP1/SKP2 complex and regulates p21(CIP1/WAF1) and cyclin D proteins. Proceedings of the National Academy of Sciences of the United States of America. 1998;**95**:11324-11329

[59] Inuzuka H et al. Acetylation-dependent regulation of Skp2 function. Cell. 2012;**150**:179-193

[60] Frescas D, Pagano M. Deregulated proteolysis by the F-box proteins SKP2 and beta-TrCP: Tipping the scales of cancer. Nature Reviews. Cancer. 2008;**8**: 438-449

[61] von der Lehr N et al. The F-box protein Skp2 participates in c-Myc proteosomal degradation and acts as a cofactor for c-Myc-regulated transcription. Molecular Cell. 2003;**11**: 1189-1200

[62] Wei Z et al. Downregulation of Skp2 inhibits the growth and metastasis of gastric cancer cells in vitro and in vivo. Tumor Biology. 2013;**34**:181-192

[63] Hao B, Oehlmann S, Sowa ME, Harper JW, Pavletich NP. Structure of a Fbw7-Skp1-Cyclin E complex: Multisite-phosphorylated substrate recognition by SCF ubiquitin ligases. Molecular Cell. 2007;**26**:131-143

[64] Davis RJ, Welcker M, Clurman BE. Tumor suppression by the Fbw7 ubiquitin ligase: Mechanisms and opportunities. Cancer Cell. 2014;**26**: 455-464

[65] Tang X et al. Suprafacial orientation of the SCFCdc4 dimer accommodates multiple geometries for substrate ubiquitination. Cell. 2007;**129**:1165-1176

[66] O'Neil J et al. FBW7 mutations in leukemic cells mediate NOTCH pathway activation and resistance to gamma-secretase inhibitors. The Journal of Experimental Medicine. 2007;**204**: 1813-1824

[67] Yeh C-H, Bellon M, Nicot C. FBXW7: A critical tumor suppressor of human cancers. Molecular Cancer. 2018; **17**:115

[68] Akhoondi S et al. *FBXW7/hCDC4* is a general tumor suppressor in human cancer. Cancer Research. 2007;**67**: 9006-9012

[69] Strohmaier H et al. Human F-box protein hCdc4 targets cyclin E for proteolysis and is mutated in a breast cancer cell line. Nature. 2001;**413**: 316-322

[70] Welcker M et al. Multisite phosphorylation by Cdk2 and GSK3 controls cyclin E degradation. Molecular Cell. 2003;**12**:381-392

[71] Welcker M et al. Fbw7 dimerization determines the specificity and robustness of substrate degradation. Genes & Development. 2013;**27**: 2531-2536

[72] Yada M et al. Phosphorylation-dependent degradation of c-Myc is mediated by the F-box protein Fbw7. The EMBO Journal. 2004;**23**:2116-2125

[73] Babaei-Jadidi R et al. FBXW7 influences murine intestinal homeostasis and cancer, targeting Notch, Jun, and DEK for degradation. The Journal of Experimental Medicine. 2011;**208**:295-312

[74] Mao J-H et al. FBXW7 targets mTOR for degradation and cooperates with PTEN in tumor suppression. Science. 2008;**321**:1499-1502

[75] Welcker M, Clurman BE. The SV40 large T antigen contains a decoy phosphodegron that mediates its interactions with Fbw7/hCdc4. The Journal of Biological Chemistry. 2005; **280**:7654-7658

[76] Nakayama K et al. Impaired degradation of inhibitory subunit of NF-kappa B (I kappa B) and beta-catenin as a result of targeted disruption of the beta-TrCP1 gene. Proceedings of the National Academy of Sciences of the United States of America. 2003;**100**: 8752-8757

[77] Zheng N, Zhou Q, Wang Z, Wei W. Recent advances in SCF ubiquitin ligase complex: Clinical implications. Biochimica et Biophysica Acta. 2016; **1866**:12-22

[78] Watanabe N et al. M-phase kinases induce phospho-dependent ubiquitination of somatic Wee1 by SCFbeta-TrCP. Proceedings of the National Academy of Sciences of the United States of America. 2004;**101**: 4419-4424

[79] Guardavaccaro D et al. Control of meiotic and mitotic progression by the F box protein beta-Trcp1 in vivo. Developmental Cell. 2003;**4**:799-812

[80] Busino L et al. Degradation of Cdc25A by β-TrCP during S phase and in response to DNA damage. Nature. 2003;**426**:87-91

[81] Kanemori Y, Uto K, Sagata N. Beta-TrCP recognizes a previously undescribed nonphosphorylated destruction motif in Cdc25A and Cdc25B phosphatases. Proceedings of the National Academy of Sciences of the United States of America. 2005;**102**: 6279-6284

[82] Lammer C et al. The cdc25B phosphatase is essential for the G2/M phase transition in human cells. Journal of Cell Science. 1998;**111**(Pt 16): 2445-2453

[83] Shirane M, Hatakeyama S, Hattori K, Nakayama K, Nakayama K. Common pathway for the ubiquitination of IkappaBalpha, IkappaBbeta, and IkappaBepsilon mediated by the F-box protein FWD1. The Journal of Biological Chemistry. 1999;**274**:28169-28174

[84] Inuzuka H et al. Phosphorylation by casein kinase I promotes the turnover of the Mdm2 oncoprotein via the SCF (beta-TRCP) ubiquitin ligase. Cancer Cell. 2010;**18**:147-159

[85] Satyanarayana A, Kaldis P. Mammalian cell-cycle regulation: Several Cdks, numerous cyclins and diverse compensatory mechanisms. Oncogene. 2009;**28**:2925-2939

[86] Malumbres M, Barbacid M. Cell cycle, CDKs and cancer: A changing paradigm. Nature Reviews. Cancer. 2009;**9**:153-166

[87] Zhang J, Wan L, Dai X, Sun Y, Wei W. Functional characterization of anaphase promoting complex/ cyclosome (APC/C) E3 ubiquitin ligases in tumorigenesis. Biochimica et Biophysica Acta. 2014;**1845**:277-293

[88] Chang L, Zhang Z, Yang J, McLaughlin SH, Barford D. Atomic structure of the APC/C and its mechanism of protein ubiquitination. Nature. 2015;**522**:450-454

[89] Primorac I, Musacchio A. Panta rhei: The APC/C at steady state. The Journal of Cell Biology. 2013;**201**: 177-189

[90] Williamson A et al. Identification of a physiological E2 module for the human anaphase-promoting complex. Proceedings of the National Academy of Sciences of the United States of America. 2009;**106**: 18213-18218

[91] Pines J. Cubism and the cell cycle: The many faces of the APC/C. Nature Reviews. Molecular Cell Biology. 2011; **12**:427-438

[92] Davey NE, Morgan DO. Building a regulatory network with short linear sequence motifs: Lessons from the degrons of the anaphase-promoting complex. Molecular Cell. 2016;**64**:12-23

[93] He J et al. Insights into degron recognition by APC/C coactivators from the structure of an Acm1-Cdh1 complex. Molecular Cell. 2013;**50**:649-660

[94] Wu W et al. CDC20 overexpression predicts a poor prognosis for patients with colorectal cancer. Journal of Translational Medicine. 2013;**11**:142

[95] Lehman NL et al. Oncogenic regulators and substrates of the anaphase promoting complex/ cyclosome are frequently overexpressed in malignant tumors. The American Journal of Pathology. 2007;**170**: 1793-1805

[96] Ishizawa J et al. FZR1 loss increases sensitivity to DNA damage and consequently promotes murine and human B-cell acute leukemia. Blood. 2017;**129**:1958-1968

[97] Gyrd-Hansen M, Meier P. IAPs: From caspase inhibitors to modulators of NF-κB, inflammation and cancer. Nature Reviews. Cancer. 2010;**10**: 561-574

[98] Fong WG et al. Expression and genetic analysis of XIAP-associated factor 1 (XAF1) in cancer cell lines. Genomics. 2000;**70**:113-122

[99] Tamm I et al. Expression and prognostic significance of IAP-family genes in human cancers and myeloid leukemias. Clinical Cancer Research. 2000;**6**:1796-1803

[100] Paulsen M et al. Interaction with XIAP prevents full caspase-3/-7 activation in proliferating human tlymphocytes. European Journal of Immunology. 2008;**38**:1979-1987

[101] Shiozaki EN et al. Mechanism of XIAP-mediated inhibition of caspase-9. Molecular Cell. 2003;**11**:519-527

[102] Suzuki Y, Nakabayashi Y, Takahashi R. Ubiquitin-protein ligase activity of X-linked inhibitor of apoptosis protein promotes proteasomal degradation of caspase-3 and enhances its anti-apoptotic effect in Fas-induced cell death. Proceedings of the National Academy of Sciences. 2001;**98**: 8662-8667

[103] Morizane Y, Honda R, Fukami K, Yasuda H. X-linked inhibitor of apoptosis functions as ubiquitin ligase toward mature caspase-9 and cytosolic Smac/DIABLO. Journal of Biochemistry. 2005;**137**:125-132

[104] Creagh EM, Murphy BM, Duriez PJ, Duckett CS, Martin SJ. Smac/Diablo antagonizes ubiquitin ligase activity of inhibitor of apoptosis proteins. The Journal of Biological Chemistry. 2004; **279**:26906-26914

[105] Broemer M et al. Systematic In vivo RNAi analysis identifies IAPs as NEDD8-E3 ligases. Molecular Cell. 2010;**40**:810-822

[106] Burstein E et al. A novel role for XIAP in copper homeostasis through

regulation of MURR1. The EMBO Journal. 2004;**23**:244-254

[107] Ganesh L et al. The gene product Murr1 restricts HIV-1 replication in resting CD4+ lymphocytes. Nature. 2003;**426**:853-857

[108] Lu M et al. XIAP induces NF-κB activation via the BIR1/TAB1 interaction and BIR1 dimerization. Molecular Cell. 2007;**26**:689-702

[109] Arora V et al. Degradation of survivin by the X-linked inhibitor of apoptosis (XIAP)-XAF1 complex. The Journal of Biological Chemistry. 2007; **282**:26202-26209

[110] Mehrotra S et al. IAP regulation of metastasis. Cancer Cell. 2010;**17**:53-64

[111] Dogan T et al. X-linked and cellular IAPs modulate the stability of C-RAF kinase and cell motility. Nature Cell Biology. 2008;**10**:1447-1455

[112] Huang X, Wu Z, Mei Y, Wu M. XIAP inhibits autophagy via XIAP-Mdm2-p53 signalling. The EMBO Journal. 2013;**32**:2204-2216

[113] Hanson AJ et al. XIAP monoubiquitylates Groucho/TLE to promote canonical Wnt signaling. Molecular Cell. 2012;**45**:619-628

[114] Lawlor KE et al. XIAP loss triggers RIPK3- and caspase-8-driven IL-1β activation and cell death as a consequence of TLR-MyD88-induced cIAP1-TRAF2 degradation. Cell Reports. 2017;**20**:668-682

[115] Riley BE et al. Structure and function of Parkin E3 ubiquitin ligase reveals aspects of RING and HECT ligases. Nature Communications. 2013; **4**:1982

[116] Cesari R et al. Parkin, a gene implicated in autosomal recessive juvenile parkinsonism, is a candidate tumor suppressor gene on chromosome 6q25-q27. Proceedings of the National Academy of Sciences. 2003;**100**: 5956-5961

[117] Fujiwara M et al. Parkin as a tumor suppressor gene for hepatocellular carcinoma. Oncogene. 2008;**27**: 6002-6011

[118] Poulogiannis G et al. PARK2 deletions occur frequently in sporadic colorectal cancer and accelerate adenoma development in Apc mutant mice. Proceedings of the National Academy of Sciences of the United States of America. 2010;**107**:15145-15150

[119] Chourasia AH, Boland ML, Macleod KF. Mitophagy and cancer. Cancer & Metabolism. 2015;**3**:4

[120] Suen D-F, Narendra DP, Tanaka A, Manfredi G, Youle RJ. Parkin overexpression selects against a deleterious mtDNA mutation in heteroplasmic cybrid cells. Proceedings of the National Academy of Sciences. 2010;**107**:11835-11840

[121] Gupta A et al. PARK2 depletion connects energy and oxidative stress to PI3K/Akt activation via PTEN S-nitrosylation. Molecular Cell. 2017;**65**: 999-1013.e7

[122] Yeo CWS et al. Parkin pathway activation mitigates glioma cell proliferation and predicts patient survival. Cancer Research. 2012;**72**: 2543-2553

[123] Staropoli JF et al. Parkin is a component of an SCF-like ubiquitin ligase complex and protects postmitotic neurons from kainate excitotoxicity. Neuron. 2003;**37**:735-749

[124] Gong Y et al. Pan-cancer genetic analysis identifies PARK2 as a master regulator of G1/S cyclins. Nature Genetics. 2014;**46**:588-594

[125] Lee SB et al. Parkin regulates mitosis and genomic stability through Cdc20/Cdh1. Molecular Cell. 2015;**60**: 21-34

[126] Sun X et al. Parkin deficiency contributes to pancreatic tumorigenesis by inducing spindle multipolarity and misorientation. Cell Cycle. 2013;**12**: 1133-1141

[127] Tay S-P et al. Parkin enhances the expression of cyclin-dependent kinase 6 and negatively regulates the proliferation of breast cancer cells. The Journal of Biological Chemistry. 2010; **285**:29231-29238

[128] Wang H et al. PARK2 negatively regulates the metastasis and epithelial-mesenchymal transition of glioblastoma cells via ZEB1. Oncology Letters. 2017; **14**:2933-2939

[129] Liu J et al. Parkin targets HIF-1α for ubiquitination and degradation to inhibit breast tumor progression. Nature Communications. 2017;**8**:1823

[130] Zhang C et al. Parkin, a p53 target gene, mediates the role of p53 in glucose metabolism and the Warburg effect. Proceedings of the National Academy of Sciences of the United States of America. 2011;**108**:16259-16264

[131] Li C et al. PINK1 and PARK2 suppress pancreatic tumorigenesis through control of mitochondrial iron-mediated immunometabolism. Developmental Cell. 2018;**46**:441-455.e8

[132] Frank S, Nelson P, Vasioukhin V. Recent advances in prostate cancer research: Large-scale genomic analyses reveal novel driver mutations and DNA repair defects. F1000 Research. 2018;**7**: 1173

[133] Zhuang M et al. Structures of SPOP-substrate complexes: Insights into molecular architectures of BTB-Cul3 ubiquitin ligases. Molecular Cell. 2009; **36**:39-50

[134] van Geersdaele LK et al. Structural basis of high-order oligomerization of the cullin-3 adaptor SPOP. Acta Crystallographica. Section D, Biological Crystallography. 2013;**69**:1677-1684

[135] Pierce WK et al. Multiple weak linear motifs enhance recruitment and processivity in SPOP-mediated substrate ubiquitination. Journal of Molecular Biology. 2016;**428**:1256-1271

[136] Zhang P et al. Endometrial cancer-associated mutants of SPOP are defective in regulating estrogen receptor-α protein turnover. Cell Death & Disease. 2015;**6**:e1687

[137] Zhang J et al. Cyclin D-CDK4 kinase destabilizes PD-L1 via cullin 3-SPOP to control cancer immune surveillance. Nature. 2017;**553**:91-95

[138] Kwon JE et al. BTB domain-containing speckle-type POZ protein (SPOP) serves as an adaptor of Daxx for ubiquitination by Cul3-based ubiquitin ligase. The Journal of Biological Chemistry. 2006;**281**:12664-12672

[139] Li G et al. SPOP promotes tumorigenesis by acting as a key regulatory hub in kidney cancer. Cancer Cell. 2014;**25**:455-468

[140] Zhu H et al. SPOP E3 ubiquitin ligase adaptor promotes cellular senescence by degrading the SENP7 deSUMOylase. Cell Reports. 2015;**13**: 1183-1193

[141] Geng C et al. SPOP regulates prostate epithelial cell proliferation and promotes ubiquitination and turnover of c-MYC oncoprotein. Oncogene. 2017; **36**:4767-4777

[142] Tan Y et al. Cullin 3 SPOP ubiquitin E3 ligase promotes the poly-ubiquitination and degradation of

HDAC6. Oncotarget. 2017;**8**: 47890-47901

[143] Wu F et al. Prostate cancer-associated mutation in SPOP impairs its ability to target Cdc20 for poly-ubiquitination and degradation. Cancer Letters. 2017;**385**:207-214

[144] Theurillat J-PP et al. Ubiquitylome analysis identifies dysregulation of effector substrates in SPOP-mutant prostate cancer. Science. 2014;**346**(80): 85-89

[145] Chen M-H et al. Cilium-independent regulation of Gli protein function by Sufu in hedgehog signaling is evolutionarily conserved. Genes & Development. 2009;**23**:1910-1928

[146] Cai H, Liu A. Spop promotes skeletal development and homeostasis by positively regulating Ihh signaling. Proceedings of the National Academy of Sciences. 2016;**113**:14751-14756

[147] Dai X et al. Prostate cancer-associated SPOP mutations confer resistance to BET inhibitors through stabilization of BRD4. Nature Medicine. 2017;**23**: 1063-1071

[148] Zhang P et al. Intrinsic BET inhibitor resistance in SPOP-mutated prostate cancer is mediated by BET protein stabilization and AKT–mTORC1 activation. Nature Medicine. 2017;**23**: 1055-1062

[149] Janouskova H et al. Opposing effects of cancer-type-specific SPOP mutants on BET protein degradation and sensitivity to BET inhibitors. Nature Medicine. 2017;**23**:1046-1054

[150] Geng C et al. Prostate cancer-associated mutations in speckle-type POZ protein (SPOP) regulate steroid receptor coactivator 3 protein turnover. Proceedings of the National Academy of Sciences. 2013;**110**:6997-7002

[151] Wang S et al. SAR405838: An optimized inhibitor of MDM2-p53 interaction that induces complete and durable tumor regression. Cancer Research. 2014;**74**:5855-5865

[152] Gan W et al. SPOP promotes ubiquitination and degradation of the ERG oncoprotein to suppress prostate cancer progression. Molecular Cell. 2015;**59**:917-930

[153] Boysen G et al. SPOP mutation leads to genomic instability in prostate cancer. eLife. 2015;**4**:1-18. e09207

[154] An J et al. Truncated ERG oncoproteins from TMPRSS2-ERG fusions are resistant to SPOP-mediated proteasome degradation. Molecular Cell. 2015;**59**:904-916

[155] Zhao Y, Sun Y. Cullin-RING ligases as attractive anti-cancer targets. Current Pharmaceutical Design. 2013;**19**: 3215-3225

[156] Vassilev LT et al. In vivo activation of the p53 pathway by small-molecule antagonists of MDM2. Science (80-). 2004;**303**:844-848

[157] Carvajal LA et al. Dual inhibition of MDMX and MDM2 as a therapeutic strategy in leukemia. Science Translational Medicine. 2018;**10**: eaao3003

[158] Weisberg E et al. Smac mimetics: Implications for enhancement of targeted therapies in leukemia. Leukemia. 2010;**24**:2100-2109

[159] Nikolovska-Coleska Z et al. Discovery of embelin as a cell-permeable, small-molecular weight inhibitor of XIAP through structure-based computational screening of a traditional herbal medicine three-dimensional structure database. Journal of Medicinal Chemistry. 2004;**47**:2430-2440

[160] Guo Z-Q et al. Small-molecule targeting of E3 ligase adaptor SPOP in kidney cancer. Cancer Cell. 2016;**30**: 474-484

[161] Yamagishi Y et al. Natural product-like macrocyclic N-methyl-peptide inhibitors against a ubiquitin ligase uncovered from a ribosome-expressed de novo library. Chemistry & Biology. 2011;**18**:1562-1570

[162] Ganoth D et al. The cell-cycle regulatory protein Cks1 is required for SCFSkp2-mediated ubiquitinylation of p27. Nature Cell Biology. 2001;**3**:321-324

[163] Pavlides SC et al. Inhibitors of SCF-Skp2/Cks1 E3 ligase block estrogen-induced growth stimulation and degradation of nuclear $p27^{kip1}$: Therapeutic potential for endometrial cancer. Endocrinology. 2013;**154**: 4030-4045

[164] Ungermannova D et al. High-throughput screening AlphaScreen assay for identification of small-molecule inhibitors of ubiquitin E3 ligase $SCF^{Skp2-Cks1}$. Journal of Biomolecular Screening. 2013;**18**: 910-920

[165] Chen Q et al. Targeting the p27 E3 ligase SCF(Skp2) results in p27- and Skp2-mediated cell-cycle arrest and activation of autophagy. Blood. 2008; **111**:4690-4699

[166] Beaudenon S, Huibregtse JM. HPV E6, E6AP and cervical cancer. BMC Biochemistry. 2008;**9**:S4

[167] Wade M, Li Y-C, Wahl GM. MDM2, MDMX and p53 in oncogenesis and cancer therapy. Nature Reviews. Cancer. 2013;**13**:83-96

[168] Nakayama KI, Nakayama K. Ubiquitin ligases: Cell-cycle control and cancer. Nature Reviews. Cancer. 2006; **6**:369-381

[169] Lau AW, Fukushima H, Wei W. The Fbw7 and betaTRCP E3 ubiquitin ligases and their roles in tumorigenesis. Frontiers in Bioscience (Landmark Ed.). 2012;**17**:2197-2212

[170] Manchado E et al. Targeting mitotic exit leads to tumor regression In vivo: Modulation by Cdk1, Mastl, and the PP2A/B55α,δ phosphatase. Cancer Cell. 2010;**18**:641-654

[171] Wäsch R, Robbins JA, Cross FR. The emerging role of APC/CCdh1 in controlling differentiation, genomic stability and tumor suppression. Oncogene. 2010;**29**:1-10

[172] Xu L, Lin D, Yin D, Koeffler HP. An emerging role of PARK2 in cancer. Journal of Molecular Medicine. 2014;**92**: 31-42

[173] Baleja JD et al. Identification of inhibitors to papillomavirus typ. 16 E6 protein based on three-dimensional structures of interacting proteins. Antiviral Research. 2006;**72**:49-59

[174] Vu B et al. Discovery of RG7112: A small-molecule MDM2 inhibitor in clinical development. ACS Medicinal Chemistry Letters. 2013;**4**:466-469

[175] Ding Q et al. Discovery of RG7388, a potent and selective p53–MDM2 inhibitor in clinical development. Journal of Medicinal Chemistry. 2013; **56**:5979-5983

[176] Zhao Y et al. A potent small-molecule inhibitor of the MDM2–p53 interaction (MI-888) achieved complete and durable tumor regression in mice. Journal of Medicinal Chemistry. 2013; **56**:5553-5561

[177] Sun D et al. Discovery of AMG 232, a potent, selective, and orally bioavailable MDM2–p53 inhibitor in clinical development. Journal of Medicinal Chemistry. 2014;**57**: 1454-1472

[178] Jeay S et al. A distinct p53 target gene set predicts for response to the selective p53-HDM2 inhibitor NVP-CGM097. eLife. 2015;**4**:1-23. e06498

[179] Furet P et al. Discovery of a novel class of highly potent inhibitors of the p53–MDM2 interaction by structure-based design starting from a conformational argument. Bioorganic & Medicinal Chemistry Letters. 2016;**26**: 4837-4841

[180] Yuan Y, Liao Y-M, Hsueh C-T, Mirshahidi HR. Novel targeted therapeutics: Inhibitors of MDM2, ALK and PARP. Journal of Hematology & Oncology. 2011;**4**:16

[181] Chan C-H et al. Pharmacological inactivation of Skp2 SCF ubiquitin ligase restricts cancer stem cell traits and cancer progression. Cell. 2013;**154**: 556-568

[182] Wu L et al. Specific small molecule inhibitors of Skp2-mediated p27 degradation. Chemistry & Biology. 2012;**19**:1515-1524

[183] Huang H-L et al. Triggering Fbw7-mediated proteasomal degradation of c-Myc by oridonin induces cell growth inhibition and apoptosis. Molecular Cancer Therapeutics. 2012;**11**:1155-1165

[184] Blees JS et al. Erioflorin stabilizes the tumor suppressor Pdcd4 by inhibiting its interaction with the E3-ligase β-TrCP1. PLoS One. 2012;**7**: e46567

[185] Nakajima H, Fujiwara H, Furuichi Y, Tanaka K, Shimbara N. A novel small-molecule inhibitor of NF-κB signaling. Biochemical and Biophysical Research Communications. 2008;**368**: 1007-1013

[186] Sackton KL et al. Synergistic blockade of mitotic exit by two chemical inhibitors of the APC/C. Nature. 2014; **514**:646-649

[187] Zeng X et al. Pharmacologic inhibition of the anaphase-promoting complex induces a spindle checkpoint-dependent mitotic arrest in the absence of spindle damage. Cancer Cell. 2010;**18**: 382-395

[188] Sharma SK, Straub C, Zawel L. Development of peptidomimetics targeting IAPs. International Journal of Peptide Research and Therapeutics. 2006;**12**:21-32

[189] McManus DC et al. Loss of XIAP protein expression by RNAi and antisense approaches sensitizes cancer cells to functionally diverse chemotherapeutics. Oncogene. 2004;**23**: 8105-8117

Chapter 2: Cul3 substrate adaptor SPOP targets Nup153 for degradation

Abstract

SPOP is a Cul3 substrate adaptor responsible for degradation of many proteins related to cell growth and proliferation. Because mutation or misregulation of SPOP drives cancer progression, understanding the suite of SPOP substrates is important to understanding regulation of cell proliferation. Here, we identify Nup153, a component of the nuclear basket of the nuclear pore complex, as a novel substrate of SPOP. SPOP and Nup153 bind to each other and colocalize at the nuclear envelope and some nuclear foci in cells. The binding interaction between SPOP and Nup153 is complex and probably multivalent. Nup153 is ubiquitylated and degraded upon expression of $SPOP^{WT}$ but not its substrate binding-deficient mutant $SPOP^{F102C}$. Loss of SPOP via siRNAs leads to Nup153 stabilization. Upon overexpression of $SPOP^{WT}$, the localization of spindle assembly checkpoint protein Mad1, which is tethered to the nuclear envelope by Nup153, is weaker. Altogether, our results demonstrate SPOP regulates Nup153 and expands our understanding of the role of SPOP in protein homeostasis.

Introduction

The Cullin subset of proteins are E3 ubiquitin ligases responsible for about 20% of ubiquitin-mediated proteasomal degradation within a cell (Soucy et al., 2009). Cul3 assembles an active E3 ubiquitin ligase complex by simultaneously binding an E2 ubiquitin conjugating enzyme charged with the ubiquitin and a BTB-domain containing substrate adaptor which bound to the substrate to be ubiquitylated (Petroski and Deshaies, 2005). Prominent Cul3 substrate adaptors include Keap1, LZTR1, and SPOP. Keap1 binds to and targets the transcription factor Nrf2, a protein responsible for responses to oxidative conditions and cellular stress, for degradation (Cullinan et al., 2004; Furukawa and Xiong, 2005). LZTR1 binds to and targets the

Ras family of GTPases (Steklov et al., 2018; Bigenzahn et al., 2018) and Ras-related GTPase RIT1 (Castel et al., 2019) for degradation.

SPOP is a Cul3 substrate adaptor with three main domains: a MATH domain that binds to substrates, a BTB domain that causes SPOP to dimerize and also mediates interaction with Cul3, and an oligomerization BACK domain through which SPOP dimers can chain to form higher-order structures (Marzahn et al., 2016). Hydrophobic residues within the MATH, such as Y87, F102, Y123, W131, and F133, mediate the interaction between SPOP and its substrates (Zhuang et al., 2009), and mutations of these residues generally disrupt the ability of SPOP to bind to its substrates (Geng et al., 2013a; Janouskova et al., 2017; Ostertag et al., 2019a). Because SPOP plays important roles in cell grow regulation, SPOP is commonly mutated or misregulated in cancers, suggesting an important role for SPOP as a tumor suppressor (Barbieri et al., 2012; Le Gallo et al., 2012; Hu et al., 2016; Wang et al., 2020b).

Whereas the principle substrate of Keap1 is Nrf2 and that of LZTR1 are Ras-related GTPases, SPOP regulates many proteins involved in cell growth and proliferation. For example, androgen receptor (AR)-mediated signaling regulates cell proliferation and differentiation transcriptional programs (Culig and Santer, 2014). SPOP mediates the degradation of AR (An et al., 2014; Geng et al., 2014), its co-activator SRC-3 (Geng et al., 2013b; Zhou et al., 2010), and TRIM24, an enhancer of AR-mediated gene activation (Groner et al., 2016), and SPOP mutations derived from prostate cancers disrupt SPOP's ability to regulate AR-signaling. Similarly, SPOP targets estrogen-receptor for degradation in endometrial cancers (Zhang et al., 2015). In development, SPOP regulates Hedgehog signaling by degrading transcription factors Gli2 and Gli3 (Chen et al., 2009) and consequently influences morphogenesis in both Drosophila and vertebrates (Cai and Liu, 2016, 2017; Schwend et al., 2013; Seong and Ishii, 2013; Kent et al., 2006). Correspondingly, SPOP misregulation is associated with dysfunction of Hedgehog signaling in a variety of cancer types (Li et al., 2014; Zhi et al., 2016; Jin et al., 2019b; Zeng et al., 2014; Li et al., 2019; Burleson et al., 2022). In some cancer types, the

cancer stem cell-associated transcription factors c-Myc (Luo et al., 2018; Geng et al., 2017) and Nanog (Wang et al., 2019; Zhang et al., 2019) are also degradation targets of SPOP.

More broadly, wild-type SPOP promotes genomic stability, and loss of SPOP function can result in defects in DNA replication stress (Hjorth-Jensen et al., 2018), double-stranded break repair (Boysen et al., 2015), and the DNA-damage response (Jin et al., 2021). Altogether, given SPOP's regulatory roles in cell growth, proliferation, and development, understanding the suite of SPOP substrates is crucial to understanding SPOP's role in cell biology and its pathological roles when mutated or misregulated.

The human nuclear pore complex (NPC) is an approximately 120 MDa complex consisting of multiple copies of about 30 proteins termed nuclear pore complex proteins (Nups) (Beck and Hurt, 2016). As the main channel between the nucleoplasm and the cytoplasm, the NPC plays a crucial role in the trafficking of proteins and RNAs in and out of the nucleus (Beck and Hurt, 2016). The NPC also plays other roles in transcription and gene regulation, cytoskeletal regulation, and nuclear membrane architecture (Strambio-De-Castillia et al., 2010). During mammalian cell division, the NPC disassembles during open mitosis/meiosis and reassembles upon completion of chromosome segregation (Otsuka and Ellenberg, 2018). Emerging work demonstrates that the Nups, despite NPC disassembly, are not passive during cell division. Many Nups have roles during cell division including the promotion of microtubule nucleation, regulation of the anaphase promoting complex/cyclosome, and localization of spindle assembly checkpoint proteins Mad1 and Mad2 (Mossaid and Fahrenkrog, 2015; Garcia et al., 2021). For example, during interphase, Nup153 is a nuclear pore complex protein in the nuclear basket that plays roles in nuclear trafficking (Ball and Ullman, 2005) and transcription (Toda et al., 2017), but during mitosis, Nup153 plays roles in nuclear pore complex assembly and nuclear envelope modeling (Duheron et al., 2014; Vollmer et al., 2015) and spindle assembly checkpoint regulation via an interaction with Mad1 (Lussi et al., 2010; Mossaid et al., 2020).

Here, we identify Nup153 as a novel SPOP substrate. We demonstrate that SPOP binds, ubiquitylates, and degrades Nup153. We also demonstrate that SPOP overexpression results in the mislocalization of the spindle assembly checkpoint protein Mad1 from the nuclear envelope, presumably via depletion of Nup153. Altogether, our results demonstrate Nup153 is a substrate of SPOP and suggest that the SPOP-Nup153 axis may be a mechanism by which SPOP regulates aspects of cell cycle progression and cell division.

Methods

Molecular cloning

To generate pDONR221 vectors containing the coding sequence (or truncated coding sequence) of each protein used in this study, primers containing Gateway cloning sites were designed against the coding sequence (or the desired truncation) of each gene and the genes were amplified via PCR. The PCR products were extracted and purified from an agarose gel. The appropriate pDONR221 plasmids and subsequent destination vectors were generated with Gateway cloning as previously described (Torres et al., 2009).

To generate amino acid substitution and deletion mutants, primers were designed with Agilent's QuikChange Primer Design program and the mutagenesis was performed with Agilent QuikChange Lightning using the appropriate pDONR as a template according to manufacturer's instructions.

Cell culture, drug treatments, and transfections

Cells were maintained in DMEM/F12 media supplemented with 10% FBS (v/v) and penicillin/streptomycin at 37°C in 5% CO2. HeLa and HEK293T cells were maintained with standard FBS, and Flp-In T-REx cells were maintained with FBS that contained no detectable tetracycline. The doxycycline-inducible Flp-In T-REx cell lines were generated as previously described (Bradley et al., 2016). The doxycycline-inducible protein was induced in Flp-In T-REx cells by addition of 0.1 µg/mL doxycycline for 16-24 hours. Cells were discarded within 12 weeks of thawing to avoid high passage numbers.

For plasmid DNA and siRNA transfections, for one well of a 12-well plate (surface area 3.5 cm2), about 80,000 cells were plated. The next day, the cells (at about 70% confluence) were transfected. For plasmid DNA transfection, 1 µg of total DNA was transfected with 4 µL of Fugene HD in 100 µL of Opti-MEM, according to manufacturer's instructions. For control

plasmid DNA transfections, non-coding DNA (pCS2-Myc empty plasmid) was used. For siRNA transfection, 0.3 µL of 100 µM siRNA was transfected with 5 µL of Lipofectamine RNAiMax in 100 µL of Opti-MEM, according to manufacturer's instructions (final concentration of siRNA: 30 nM). For control siRNA transfections, siGLO was used. The media was changed about 6-8 hours after plasmid DNA transfection and the next day (about 20 hours) after siRNA transfection. DNA transfected cells were assayed after 48 hours, while siRNA transfected cells were assayed after 72 hours.

For cell cycle arrests, cells were treated with 2 mM thymidine or 232 nM Taxol for 16-20 hours. For protein degradation experiments, cells were transfected with indicated plasmids, then, 48 hours after transfection, treated with 20 µM MG132, 50 mM chloroquine, or both for 5 hours. For in cell ubiquitylation experiments, pgLAP1-Nup153 HeLa cells were treated with 20 µM MG132 for 4-5 hours before lysis.

Mass spectrometry

pgLAP2-SPOP WT HEK293 Flp-In T-Rex cells were generated and tandem affinity purification was performed as previously described (Torres et al., 2009). The eluates were run onto an SDS-PAGE gel and gel slices were subjected for in-gel digestion with trypsin. Mass spectrometry and sequence analysis was performed at the Harvard Microchemistry and Proteomics Analysis Facility by microcapillary reverse-phase HPLC nano-electrospray tandem mass spectrometry (µLC/MS/MS) on a Thermo LTQ-Orbitrap mass spectrometer as previously described (Taniguchi et al., 2002).

Cell lysis, co-immunoprecipitations, SDS-PAGE, and immunoblotting

To produce cell lysates, the media was removed and cells were lifted from the plate using cell dissociation solution (5% (v/v) glycerol, 1 mM EDTA, 1 mM EGTA in PBS) for 5 minutes at 37°C. The cells were pelleted by centrifugation at 500 x g for 5 minutes. Cell lysates,

co-immunoprecipitations, SDS-PAGE, and immunoblotting were performed as previously described with the following modifications (Cheung et al., 2016):

1. The salt and detergent concentration in the lysis buffer was increased to 200 mM KCl and 1% (v/v) NP40. ATP was not added to the lysis buffer.
2. Cells were lysed on ice by vortexing for 3 seconds every 3 minutes, 5 times total, before clearing via centrifugation at 13.1k x g at 4°C for 10 minutes.
3. For co-immunoprecipitations, the lysis buffer was supplemented with 10 μM of MG132, 10 mM of NEM, and phosphatase inhibitor cocktail. Two volumes of lysis buffer without NP40 was added to the cell lysate during the binding so that the final concentration of NP40 during binding was 0.33%. Lysates were incubated with solid phase for 2 hours at 4°C on a rotating platform. The solid phase was washed with the supplemented lysis buffer containing 0.2% NP40.
4. For co-immunoprecipitation experiments using S-Tag agarose, 200 μL S-Tag agarose slurry was used (about 100 μL packed volume). The agarose solid phase was collected by centrifugation at 500 x g for 2 minutes at 4°C.
5. The lysates were run on 4-20% 15-well SDS-PAGE gels.

For immunoblots, molecular weight markers are shown to the right in kDa. Blots were imaged on a LI-COR Odyssey fluorescent scanner. In some cases, for a given experiment, lysates were loaded equivalently onto multiple gels and/or the blot was cut horizontally to allow for probing by multiple antibodies. See Supplementary File 1 for antibodies used and their dilutions.

In vitro transcription/translation and binding experiments

To produce IVT-expressed protein, 200 ng of indicated pCS2 plasmid was added to 8 μL of SP6 TNT-master mix, 0.5 μL of 1 mM methionine, and the volume was brought to 10 μL per

reaction. The tubes were incubated at 30°C for 1.5 hours with shaking at 250 rpm. Upon completion of the incubation, 0.5 µL (approximately 5%) of the protein was saved as for the input portion of a gel and heated at 95°C for 5 minutes with 3 µL of water and 5 µL of 2x Lammeli buffer. The binding reaction, washing, and elution was performed in the same way as detailed for co-immunoprecipitations, except the concentration of NP40 was 0.25% throughout.

Immunofluorescence and microscopy

For fixed cell immunofluorescence microscopy, HeLa cells were plated onto poly-D-lysine coated coverslips in a 24-well plate. The same transfection procedures as a 12-well plate were followed, except everything was halved to adjust for the smaller surface area. Fixation with PFA, staining, and microscopy were performed as previously described (Guo et al., 2021). Methanol fixation was performed via the addition of absolute methanol cooled to -20°C and fixing the cells at -20°C for 20 minutes. See Supplementary File 1 for antibodies used and their dilutions.

Images were acquired as a single plane or as a z-stack of 8 images encompassing a z-volume of 6.23 microns. For z-stack images, the maximum projection of the images is presented. Figures were processed in FIJI and exported as .tif files.

CellProfiler quantification and other code

A Python script used to identify SPOP consensus binding sites is available on Github: https://github.com/jong2ucla/PythonScripts/blob/main/SPOP_ConsensusFinder.

The CellProfiler pipeline used to quantify nuclear Nup153/nuclear DNA fluorescence is available on Github: https://github.com/jong2ucla/CellProfiler/blob/main/rbNup153toDNA.cppipe.

The CellProfiler pipeline used to quantify nuclear nuclear envelope Mad1/nuclear CREST fluorescence is available on Github: https://github.com/jong2ucla/CellProfiler/blob/main/Mad1toCREST.cppipe. Here, we normalized

Mad1 intensity to CREST instead of DNA fluorescence because with the z-stacks used in image acquisition in this experiment, DNA fluorescence produced too much out of focus signal that posed a technical challenge for quantification.

RT-qPCR

For RNA extraction, between 70-72 hours after siRNA transfection, the media was removed from HeLa cells and 200 µL of TriReagent was added directly to the wells of the plate to lyse the cells. RNA extraction and Dnase I digestion, RT-PCR, and qPCR were performed as previously described (Guo et al., 2021). For RT reaction, 750-1500 ng of RNA was used, and for qPCR reaction, 75-150 ng of cDNA with 400 nM each of forward and reverse qPCR primer was used.

Data were processed using the delta delta Ct method as previously described, using Gapdh as a housekeeping gene for normalization (Livak and Schmittgen, 2001). qPCR values were normalized to cells transfected with siGLO.

Statistical analyses

For image quantification, statistical significance was determined via one-way ANOVA and Tukey-HSD. For qPCR quantification, each siRNA transfection, RNA extraction, and RT-PCR were performed three separate times (three biological replicates). For each biological replicate, the cDNA was assayed twice via qPCR (two technical replicates). For reported knockdown efficiencies, the two technical replicates of a biological replicate were averaged, and these averaged values were used to calculate the reported average and standard deviation (avg±SD) of the three biological replicates. Statistical significance was determined via one-way ANOVA and Tukey-HSD.

STAR Protocols

REAGENT or RESOURCE	SOURCE	IDENTIFIER
Recombinant DNA		
See Supplementary File 1 for all plasmids and vectors used in this study.		
Oligonucleotides		
SPOP siRNA #100	Millipore Sigma	siRNA ID: SASI_Hs01_00034100
SPOP siRNA #101	Millipore Sigma	siRNA ID: SASI_Hs01_00034101
SPOP siRNA #102	Millipore Sigma	siRNA ID: SASI_Hs01_00034102
siGLO Red Transfection Indicator	Dharmacon	D-001630-02-05
Oligonucleotide sequences for siRNA, qPCR primers, and primers used for cloning are in Supplementary File 1	Eurofins Genomics	See Supplementary File 1
Experimental Models: Cell Lines		
HeLa Flp-In T-REx	Stephen Taylor (University of Manchester)	PMID: 18541701 (Tighe et al., 2008)
pgLAP1-Nup153 HeLa Flp-In	This paper	

T-REx		
Flp-In™ T-REx™ 293 Cell Line	Invitrogen	R78007
pgLAP2-SPOP WT HEK293 Flp-In T-REx	This paper	
HeLa	ATCC	CCL-2
HEK293T	ATCC	CRL-3216
Antibodies		
See Supplementary File 1 for all primary and secondary antibodies used for immunoblotting and immunofluorescence microscopy in this study.		
Critical Commercial Assays		
QuikChange Lightning Site-Directed Mutagenesis Kit	Agilent	210518
Fetal Bovine Serum – Premium	Atlanta Biologicals	Cat No: S10350, Lot No: F17085
4–20% Mini-PROTEAN® TGX™ Precast Protein Gels, 15-well, 15 µL	BIORAD Life Science Group	#4561096
Precision Plus Protein Dual Color Standards, 500 µL	BIORAD Life Science Group	#1610374

Fetal Bovine Serum - Premium, USDA Origin Tetracycline Free	BIOWEST LLC	Cat No: S162TA, Lot No: 045G19
Gibco™ Opti-MEM™ I Reduced Serum Medium	Fisher Scientific	31-985-070
MilliporeSigma™ Immobilon-FL PVDF Membrane	Fisher Scientific Co.	IPFL00005
qPCRBIO SyGreen Blue Mix Separate-ROX	Genesee Scientific	17-507
UltraScript 2.0 cDNA Synthesis Kit	Genesee Scientific	17-702
DMEM/Ham's F-12, with L-Glutamine	Genesee Scientific	25-503
Trypsin-EDTA, 0.25% 1X, phenol red	Genesee Scientific	25-510
BP Clonase II	Invitrogen	11789020
LR Clonase II	Invitrogen	11791020
Anti-HA-tag mAb-Magnetic Beads (Monoclonal Antibody)	MBL International	M132-11

Phosphatase Inhibitor Cocktail 2	Millipore Sigma	P5726-1ML
TNT® SP6 Quick Coupled Transcription/Translation System	Promega	L2080
FuGENE® HD Transfection Reagent, 1ML	Promega	E2311
QIAquick DNA gel extraction kit	Qiagen	28706
Anti-FLAG® M2 Magnetic Beads	Sigma-Aldrich Corp.	M8823-1ML
Platinum Taq DNA Polymerase	Thermo Fisher Scientific	10966018
Pierce™ Protease Inhibitor Tablets, EDTA-free	Thermo Fisher Scientific	A32965
Tris-Glycine-SDS, 10X Solution (Electrophoresis), Fisher BioReagents	Thermo Fisher Scientific	BP13414
PBS, Phosphate Buffered Saline, 10X Solution, Fisher BioReagents	Thermo Fisher Scientific	BP39920

TAE Buffer, Tris-Acetate-EDTA, 50X Solution, Electrophoresis, Fisher BioReagents	Thermo Fisher Scientific	BP13324
Lipofectamine™ RNAiMAX Transfection Reagent	Thermo Fisher Scientific	13778150
Invitrogen™ Molecular Probes™ ProLong™ Gold Antifade Mountant	Thermo Fisher Scientific	P36934
EMD Millipore™ Novagen™ S-protein Agarose	Thermo Fisher Scientific	Novagen 69704-4
Hardware and Software		
S1000 Thermal Cycler with Dual 48/48 Fast Reaction Module	BIORAD Life Science Group	1852148
CFX Connect Real-Time PCR Detection System; software: CFX Manager, Version 3.0	BIORAD Life Science Group	1855201
CellProfiler v4.2.1	https://cellprofiler.org/	PMID: 34507520 (Stirling et al., 2021)

ImageJ2/FIJI	https://imagej.net/software/fiji/	PMID: 22743772 (Schindelin et al., 2012)
Leica DMI6000 microscope (Leica DFC360 FX Camera, 63x/1.40–0.60 NA oil objective); software: Leica AF6000	Leica	
LI-COR Odyssey Imager; software: Odyssey v3.0	LI-COR	Model 9120
NanoDrop 2000c; software: NanoDrop 2000/2000c version 1.6.198	Thermo Fisher Scientific	ND-2000C
SuperPlots of Data	https://huygens.science.uva.nl/SuperPlotsOfData/	PMID: 33476183 (Goedhart, 2021)
Inkscape 0.92.4	https://inkscape.org/	

Results

SPOP binds Nup153

To identify novel substrates of SPOP, we overexpressed tagged SPOP in HEK293 cells and analyzed affinity-purified complexes via mass spectrometry (Supplementary Figure 1A). Our results showed a number of known SPOP substrates and interactors, such as Caprin1 (Shi et al., 2019) and G3BP1 (Mukhopadhyay et al., 2021). The most abundant protein identified was Nup153, a nuclear pore complex protein, and its binding partners Nup50 and some importin subunits like KPNA6. A direct interaction between these proteins is involved in nuclear trafficking through the nuclear pore complex (Makise et al., 2012). Given that Nup153 (Lan et al., 2019), Nup50 (Hjorth-Jensen et al., 2018), KPNA6 (Ewing et al., 2007; Yuan et al., 2020), and other importin subunits (Huttlin et al., 2021; Yuan et al., 2020) have all been identified as possible interactors of SPOP by mass spectrometry, and given their high abundance in our mass spectrometry results, we pursued these proteins as possible substrates of SPOP.

To determine whether SPOP binds these substrates, we expressed HA-tagged $SPOP^{WT}$, its binding mutant $SPOP^{F102C}$, and FLAG-tagged Nup153, Nup50, and KPNA6 in a cell-free, in vitro transcription and translation rabbit reticulolysate system (hereafter, IVT-expressed protein). We also expressed FLAG-tagged Cdc20, a known SPOP substrate (Wu et al., 2017), as a positive control, and Plk1, which lacks SPOP binding consensus motifs (Zhuang et al., 2009), as a negative control. Binding reactions between these SPOP constructs and potential substrates demonstrated that $SPOP^{WT}$ could readily immunoprecipitate the positive control Cdc20, Nup153, Nup50, and KPNA6, and the binding mutant $SPOP^{F102C}$ could only weakly immunoprecipitate KPNA6 (Figure 1A).

Having established that SPOP and these potential substrates can associate as proteins expressed in a cell-free system, we sought next to establish if these proteins associate in human cell lysates via co-immunoprecipitation experiments. We first observed that Nup153 and

known SPOP substrates Caprin1 and Myd88 was able to co-immunoprecipitate with exogenous HA-SPOP^{WT} but not binding mutant HA-SPOP^{F102C} (Supplementary Figure 1B). We also observed that Nup153 levels, but Nup50 levels, increased in cells arrested in mitosis via Taxol treatment relative to cells arrested in G1/S phase via thymidine treatment (Figure 1B). Such a result is consistent with previous reports that some nucleoporins, including Nup153, generally increase from G1 to G2/M (Chakraborty et al., 2008), coinciding with nuclear pore complex synthesis and assembly during S phase. Another SPOP substrate, like DAXX, also increased in Taxol-arrested cells relative to asynchronous cells (Kwon et al., 2006); in contrast, the levels of another SPOP substrate, DEK, did not have a cell cycle phase dependence (Theurillat et al., 2014), suggesting that cell cycle-dependent protein levels are not shared among all SPOP substrates.

We wondered then if SPOP regulation of the substrates we identified could be differentially regulated in mitosis. This question was supported by two opposing reasons: first, SPOP-substrate interactions have been known to be enhanced by or dependent on substrate phosphorylation (Wang et al., 2020a, 2021; Gan et al., 2015; Li et al., 2011; Jiang et al., 2021) (although phosphorylation of some substrates weaken SPOP-substrate binding (Ostertag et al., 2019b; Zhuang et al., 2009; Zhang et al., 2009; Wang et al., 2019)). Nuclear pore complex proteins are phosphorylated by mitotic kinases as the cell enters into mitosis, an event that precedes nuclear envelope breakdown and the dissociation of the nuclear pore complex (Linder et al., 2017; Martino et al., 2017). Indeed, we observed a significant decrease in the mobility of Nup98 in the mitotic population, suggestive of post-translational modifications such as phosphorylation (Figure 1B). While not as dramatic, we also observed a slight decrease in mobility for Nup153 and Nup50 in the mitotic population as well, suggestive of post-translational modifications such phosphorylation, a modification which has been previously documented (Ball and Ullman, 2005). Whether or not these mitotic phosphorylation events would promote or decrease SPOP binding to our substrates was an open question.

On the other hand, during mitosis, the nuclear envelope is disassembled and SPOP can no longer associate with the nuclear pore complex proteins. Dilution of SPOP into the cytoplasm could weaken the SPOP-nuclear pore complex protein interaction. In a similar vein, SPOP was previously reported to be active in interphase and deactivated during late mitosis due to degradation by the APC/C substrate adaptor Cdh1/Fzr1 (Zhang et al., 2017a). We note that whereas Zhang et al. observe a decrease of SPOP protein levels in mitosis and an increase of SPOP protein levels in interphase via immunoblotting, we observe no difference in SPOP levels between the two phases (Figure 1B). Whether or not inactivation of SPOP during mitosis, either due to degradation or dilution (or some other mechanism), was also an open question.

To assess whether mitotic events could mediate the effect of SPOP binding to our identified substrates, we performed co-immunoprecipitation experiments with asynchronous, cycling cells (about 80% in G1/S) and Taxol-arrested mitotic cells (about 80% in M phase) (Figure 1C,D). We observed that, similar to before, Nup153 co-immunoprecipitates with SPOP in the asynchronous cell population. However, the amount of immunoprecipitated Nup153 was less in the mitotic cell population than the asynchronous population, suggesting that the SPOP-Nup153 interaction is weaker in mitotic cells (when Nup153 is hyperphosphorylated and the nuclear envelope has broken down) than in interphase cells (which contain an intact nuclear envelope).

Despite observing a binding interaction between SPOP and Nup50 with IVT-expressed proteins, we did not observe co-immunoprecipitation of Nup50 with SPOP in either an asynchronous or mitotic cell lysates (Figure 1C). This result may suggest that the SPOP-Nup50 interaction may be weak or transient within cells. Such an idea is supported by the highly mobile nature of Nup50 and its transient association with the nuclear pore complex (and thus perhaps SPOP) (Buchwalter et al., 2014). We also observed that KPNA6 co-immunoprecipitated with both SPOPWT and its binding mutant $SPOP^{F102C}$ in both the asynchronous and mitotic cell lysates (Figure 1D). Why the mutant construct of SPOP can bind KPNA6 in cell lysates but not

with IVT-expressed protein is unclear. One possibility is that in cell lysates, endogenous SPOP can oligomerize with the mutant SPOP such that the interaction between exogenous SPOPF102C and endogenous KPNA6 is mediated through endogenous, wild-type SPOP (Pierce et al., 2016) (also note the stronger co-immunoprecipitation of endogenous SPOP with exogenous HA-SPOP^{F102C} than HA-SPOP^{WT} in Figure 1C). Consistent with this idea, we also observe that, in HEK293 cells, expression of SPOP^{F102C} also results in weaker (relative to SPOP^{WT}) but detectable co-immunoprecipitation of Nup153 and KPNA6 (Supplementary Figure 1C).

Because Nup153 presented the clearest case of SPOP binding (that is, we observe the SPOP-Nup153 interaction in both IVT-expressed proteins and in HeLa cell lysates, and the interaction is disrupted by the canonical SPOP binding mutant F102C), we proceeded to examine the possibility of Nup153 as an SPOP substrate. We first sought to determine if the two proteins colocalize in the nucleus by transiently DNA coding for both proteins into HeLa cells. We observed that SPOP^{WT} and Nup153 colocalize along the nuclear envelope and in some nuclear speckles, similar to the localization observed with SPOP and other SPOP substrates (Bunce et al., 2008; Marzahn et al., 2016). In contrast, the binding mutant SPOP^{F102C} has a different localization, and these nuclear speckles exclude Nup153. In particular, Nup153 lacks nuclear speckle localization when co-expressed with SPOPF102C, suggesting that Nup153 associates with SPOP^{WT} but not SPOP^{F102C} compartments, similar to what has been observed previously for other SPOP-substrates coacervates (Bouchard et al., 2018).

Altogether, these results demonstrate SPOP binds to and colocalizes with Nup153, suggesting that Nup153 is a substrate of SPOP.

SPOP binds to Nup153 at least within the N-terminal Nuclear Pore Complex domain

The SPOP MATH domain binds to an SPOP binding consensus site on its substrates, a canonical five amino acid motif of nonpolar–polar–S–S/T–S/T, though some motifs with

mismatches (underlined in this sentence) are known, such as with GL9 (Zhang et al., 2021) (GL9 SPOP site #1: AD<u>T</u>TS; GL9 SPOP site #2: AD<u>T</u>TT) and Myd88 (Guillamot et al., 2019; Jin et al., 2019a) (VDSS<u>V</u>). One SPOP substrate, Pdx1, has SPOP binding consensus sites that are significantly different from the canonical SPOP binding consensus site (Pdx1 SPOP site #1 (Ostertag et al., 2019b): VTS<u>GE</u>; Pdx1 SPOP site #2 (Usher et al., 2021): PQ<u>P</u>SS) but nonetheless use the same binding modality in the MATH domain. We sought to determine the SPOP binding consensus sites on Nup153.

Unfortunately, unlike other SPOP substrates which tend to have only a few SPOP binding consensus sites, Nup153 contains 15 SPOP canonical binding consensus motifs (and many more “near-miss” binding sites where a mismatch is allowed). Individually mutating these sites was deemed impractical. Instead, we opted to first truncate Nup153 to determine which domains could bind to SPOP, and then mutate the SPOP binding consensus motifs of the Nup153 domains that did bind to SPOP. Accordingly, Nup153 was truncated according to its three domains: the N-terminal nuclear pore complex domain (NPC), the central zinc finger domain (ZnF), and the C-terminal phenylalanine and glycine repeat domains (FG). We also generated the NPCZnF and ZnFFG domains (Figure 2A). Immunoprecipitation experiments using IVT-expressed protein demonstrated that SPOP binds to the Nup153 NPC, NPCZnF, ZnFFG, and FG truncations (Figure 2B). Altogether, these results suggest that SPOP binds to the Nup153 NPC and the FG domains and not the ZnF domain.

To further verify that SPOP can bind to the NPC and FG domains of Nup153, we co-expressed each Nup153 truncation with $SPOP^{WT}$ in HeLa cells. We observed co-localization of SPOP and Nup153 NPC and NPCZnF, but not any of the other truncations (Figure 2E and E’). We note that the truncations of Nup153 that lack the N-terminal NPC domain did not localize within the nucleus and thus would not bind to the nuclear protein SPOP (Ball and Ullman, 2005). The mislocalization of these Nup153 truncations that do not contain the N-terminal NPC domain may bias the interpretation of this experiment, at least for these truncations. In particular, the

observation that SPOP does not co-localize with the Nup153 FG domain does not rule out the possibility that SPOP may bind to the FG domain of Nup153. Nonetheless, these microscopy results suggest that the Nup153 NPC domain co-localized with SPOP, further suggesting that SPOP binds to Nup153 at least within the N-terminal NPC domain. Given the easy read-out that we could obtain via microscopy, we opted to continue characterization of the Nup153 NPC domain instead of the FG domain.

The Nup153 NPC domain contains three SPOP binding consensus sites at amino acids ^{303}VTSST^{308}, ^{479}ITSSS^{484}, and ^{561}GSSST^{566}. To determine which binding site(s) were sites of SPOP-Nup153 NPC binding, we mutated the middle three amino acids (underlined in the previous sentence) to three alanine residues, generating Nup153 NPC 304AAA, 480AAA, and 562AAA, an approach adopted from studies of other SPOP substrates like Geminin (Ma et al., 2021) and GLP (Zhang et al., 2021). We also generated a construct of the Nup153 NPC whereby all three aforementioned sites were mutated to AAA (3xAAA). LCMT1, a protein that contains no SPOP consensus binding sites, was used as a negative control (Xia et al., 2015).

Surprisingly, all four alanine constructs of the Nup153 NPC, including the 3xAAA where all three SPOP binding consensus sites were mutated, still bound to SPOP (Figure 2C). Intrigued, we again truncated the Nup153 NPC into two truncations, chosen to avoid disrupting secondary structures within the NPC: NPC amino acids 1-330 and NPC amino acids 331-619. Binding experiments with IVT-expressed proteins demonstrated that the Nup153 NPC 1-330 but not 331-619 binds to SPOP (Figure 2D). Via microscopy, the Nup153 NPC 1-330 domain localized within the nucleus but Nup153 NPC 331-619 did not. Similar to how the Nup153 FG domain does not localize within the nucleus, we were also unable to use the localization of the Nup153 NPC 331-619 to support an SPOP binding site. Nonetheless, given the binding of Nup153 NPC 1-330 to and colocalization with SPOP, we pursued the SPOP binding site within the first 330 amino acids of Nup153.

SPOP binding to the Nup153 NPC is not dependent on traditional SPOP binding consensus motifs

To determine where the SPOP-Nup153 1-330 binding site is located, we again mutated Nup153 1-330 by introducing premature stop codons about every 30 amino acids (with some consideration to not disrupt predicted secondary structure) to generate C-terminally truncated constructs of Nup153 that spanned from the full 1-330 amino acids to the smallest segment generated, 1-167 amino acids. Binding reactions with these IVT-expressed proteins demonstrated that SPOP binds only to the full 1-330 amino acids, as Nup153 1-300 and smaller constructs exhibited weaker binding to SPOP (Supplementary Figure 2A). We thus further examined these final 30 amino acids in detail. In these 30 amino acids (^{301}SYGVTSSTARRILQSLEKMSSPLADAKRIPS^{330}), we identified three polar amino acid stretches (underlined in this sentence) that could serve as potential SPOP-Nup153 1-330 binding sites: amino acids 303-307 (the exact match to SPOP binding consensus motifs previously mutated to AAA), amino acids 312-316 (which resembles the first Pdx1 SPOP consensus binding site VTSGE as both sites contain a mismatch in the fourth position and a glutamate residue in the fifth position), and amino acids 319-214 (which we selected for its serine residues). We deleted these amino acids to generate Nup153 NPC 1-330 Δ303-307, Nup153 NPC 1-330 Δ312-316, and Nup153 NPC 1-330 Δ319-324.

Surprisingly, mutation of any one of these sites did not disrupt the Nup153 NPC 1-330 construct from binding to SPOP (Supplementary Figure 2B). We confirmed that binding of Nup153 NPC 1-330 was dependent on the substrate-binding MATH domain of SPOP by performing the same experiment but with the SPOP mutant F102C (Supplementary Figure 2C). Combining two these deletions in the Nup153 1-330 also did not disrupt Nup153 1-330 binding to SPOP, as the double deletion constructs (denoted as Δ1+Δ2, Δ1+Δ3, and Δ2+Δ3 for which deletions were generated) also bound to SPOP with the same affinity as the intact Nup153 1-330 construct (Supplementary Figure 2D). These results suggested that unlike other SPOP

substrate binding interfaces, which can be easily disrupted by deleting or mutating approximately 5 amino acids, the SPOP-Nup153 binding interface within the Nup153 1-330 may span over a larger stretch of amino acids and/or may involve structural motifs in three-dimensional space that are not disrupted by deletions of small portions of the substrate. Consistent with this idea, deleting the same three regions either individually or simultaneously within the entire Nup153 NPC (amino acids 1-619) did not disrupt SPOP-Nup153 binding (Supplementary Figure 2E). This result suggests that other amino acids within Nup153 residues 331-619 can compensate for the lack of the potential SPOP binding site within Nup153 residues 300-330. One hypothesis is that SPOP forms oligomers that can bind to multiple binding motifs on its substrate (Pierce et al., 2016). Consequently, an oligomeric chain of SPOP may bind to the Nup153 NPC (or full length Nup153) at multiple locations, granting an interaction with higher avidity. An additional SPOP binding site(s) – particularly a non-canonical binding site that does not match the usual consensus motif – within the Nup153 NPC may explain why deletion of residues 300-330 within the Nup153 NPC does not abrogate binding to SPOP. Altogether, these results suggest that the SPOP-Nup153 NPC binding interface is not dependent on canonical SPOP consensus binding sites and is complex.

SPOP targets Nup153 for ubiquitin-mediated degradation

Having established that SPOP binds Nup153, we sought to establish the consequence of this interaction: namely, does SPOP target Nup153 for ubiquitin-mediated degradation? Most SPOP substrates are degraded (Wang et al., 2020b; Cuneo and Mittag, 2019), but some, such as MacroH2A (Hernández-Muñoz et al., 2005), HIPK2 (Jin et al., 2021), and G3PB1 (Mukhopadhyay et al., 2021), are not. We began by overexpressing SPOP WT or its binding mutant F102C and probing the substrates of SPOP by immunoblotting. We saw a decrease in Nup153 and KPNA6, but not Nup50, upon expression of $SPOP^{WT}$ but not $SPOP^{F102C}$ (Figure 3A). We saw a corresponding decrease in known SPOP substrates Caprin1 and Myd88. These

results suggest that SPOP targets Nup153 and KPNA6, but not Nup50, for degradation. We note that the observed pattern for protein degradation is the same as our co-immunoprecipitation results (Figure 1B,C): that is, we neither detected co-immunoprecipitation of Nup50 by SPOP nor a change in Nup50 levels upon SPOP overexpression.

To determine the mechanism of Nup153 degradation, we again overexpressed SPOP WT or its binding mutant F102C and treated the cells with proteasomal inhibitor MG132, lysosomal inhibitor chloroquine (an inhibitor of autophagy (Mauthe et al., 2018)), both MG132 and chloroquine, or left the cells untreated. Both MG132 and chloroquine prevented $SPOP^{WT}$-mediated degradation of Nup153, suggesting that Nup153 degradation may be both via proteasomal and lysosomal degradation.

Having determined that SPOP overexpression degrades Nup153, we sought to determine whether SPOP ubiquitylates Nup153. We generated a HeLa cell line that expressed GFP-S Tag-Nup153 in a doxycycline-inducible manner (Torres et al., 2009), overexpressed either SPOP WT or its binding mutant F102C, induced exogenous Nup153 overexpression via doxycycline addition to cell culture media, and precipitated the exogenously expressed Nup153. We probed immunoblots from these lysates with an antibody that detects polyubiquitin chains. These blots showed that polyubiquitylation of Nup153 is increased when $SPOP^{WT}$, but not $SPOP^{F102C}$, is overexpressed (Figure 3C), suggesting that the degradation of Nup153 by SPOP is mediated through ubiquitylation. However, whether this degradation is proteasomal or lysosomal (or both) is not clear.

We then determined the effect of SPOP knockdown on Nup153 levels. We tested three siRNAs against SPOP, siSPOP #100, #101, and #102. While we had difficulty detecting endogenous SPOP via western blotting, we were able to readily detect knockdown of SPOP mRNA levels via RT-qPCR (normalized to Gapdh mRNA levels and relative to control, non-targeting siRNA siGLO; Figure 3D) with siSPOP #101 (24±9% SPOP mRNA remaining) and #102 (27±10% SPOP mRNA remaining) but not siSPOP #100 (128±13% SPOP mRNA

remaining). In HeLa cells, use of these siRNAs demonstrated that siSPOP #101 and #102, but not the SPOP siRNA #100 (that did not knockdown SPOP) nor the control siGLO, resulted in an increase in Nup153 and Caprin1 protein levels and a modest increase in Myd88 levels (Figure 3E). No change in protein levels was detected for KPNA6 or Nup50. We note that protein levels of KPNA6, which co-immunoprecipitates with SPOP and is degraded upon SPOP overexpression, do not change upon SPOP knockdown. We are unsure as to whether the moderate change in Myd88 levels, a known SPOP substrate of degradation, and the apparent no change in protein levels for KPNA6 are due to an incomplete loss of SPOP. Similarly, the protein levels of Nup50, which only binds to SPOP from IVT-expressed proteins but neither co-immunoprecipitates with SPOP from HeLa cell lysates nor is degraded upon SPOP overexpression, also do not change upon SPOP knockdown.

Finally, we used immunofluorescence microscopy to confirm that SPOP overexpression depletes Nup153 levels. We saw a moderate decrease of endogenous Nup153 fluorescence upon overexpression of $SPOP^{WT}$ (an average of 82% of Nup153 levels in untransfected cells) but not $SPOP^{F102C}$ (an average of 105% of Nup153 levels in untransfected cells) (Figure 3F, G) upon normalization to DNA fluorescence. We normalized to DNA fluorescence here because the number of nuclear pore complex proteins (and thus Nup153 fluorescence) should roughly scale with DNA synthesis (and thus the amount of DNA fluorescence) in S phase (Maul et al., 1972). Altogether, these results suggest SPOP targets Nup153 for ubiquitin-mediated degradation, similar to many other SPOP substrates already identified.

SPOP overexpression results in Mad1 mislocalization

The nucleoporin Nup153 plays many roles in cell biology. One such role involves regulating the localization and thus function of Mad1, a spindle assembly checkpoint protein (Lussi et al., 2010). Lussi et al. showed that loss of Nup153 via siRNAs resulted in a weakened localization of Mad1 at the nuclear envelope, a stronger Mad1 association with the mitotic

spindle, and cytokinetic defects (Lussi et al., 2010). We sought to determine whether loss of Nup153 via SPOP overexpression could also recapitulate the Mad1 phenotypes observed due to loss of Nup153 via siRNA knockdown.

We sought to determine whether Mad1 was mis-localized in cells overexpressing $SPOP^{WT}$. To this aim, we quantified the amount of Mad1 localized to the nuclear envelope in cells expressing $SPOP^{WT}$ or $SPOP^{F102C}$. We again observed a moderate decrease in Mad1 at the nuclear envelope in cells expressing $SPOP^{WT}$ (average of 71% relative to untransfected cells) but not $SPOP^{F102C}$ (average of 91% relative to untransfected cells) when Mad1 intensity was normalized to CREST fluorescence.

However, our results must be interpreted with caution. Without a construct of Nup153 that does not bind to SPOP, overexpression of SPOP, in addition to decreasing Nup153 levels, may also decrease other proteins that can result in the observed phenotype.

Discussion

The nuclear pore complex is a crucial structure to scaffold other proteins and regulate nuclear trafficking. Here, we demonstrate that the Cul3 substrate adaptor SPOP binds to Nup153 and targets Nup153 for degradation. We also show that overexpression of SPOP leads to loss of Mad1 at the nuclear envelope, presumably via lower levels of Nup153 available to scaffold Mad1 to the nuclear envelope.

Most SPOP substrates are degraded through the ubiquitin proteasome system, but recent reports have demonstrated that, at least in *Saccharomyces cerevisiae*, the nuclear pore complex is degraded through the autophagy via recognition of Nup159 on the cytoplasmic side of the NPC (Lee et al., 2020; Tomioka et al., 2020). It is unclear how the protein stability of the nuclear pore complex is regulated in vertebrates. Here, we show that SPOP can degrade Nup153 but does not rule out autophagy as a means of degradation of the nuclear pore complex. Understanding the relationship between nutrient flux (for example, low nutrient

conditions to stimulate autophagy) and SPOP-mediated degradation of Nup153 remains to be determined, as SPOP regulation can change under autophagy-inducing conditions. Indeed, SPOP mutants that no longer degrade BRD4 result in AKT and mTORC1 activation in prostate cancer cells and cell proliferation (Zhang et al., 2017b); perhaps the nuclear pore complex is degraded “in bulk” via autophagy during nutrient-poor conditions but Nup153 levels are “fine-tuned” via SPOP during nutrient-rich, proliferative conditions.

One possible piece of evidence to support this idea comes from the half-life of the NPC components: whereas NPC proteins in the central channel generally have a long half-life (approximately 200-700 hours in some cell types), Nup153 has a shorter half-life on the scale of about 50 hours (Mathieson et al., 2018). The observation that some NPC components are long-lived and obdurate whereas Nup153 is a more dynamic and readily-turned over NPC component is also generally true in C. elegans models of aging (D’Angelo et al., 2009). Of the NPC protein components, Nup153 and Nup50 are the most dynamic, only transiently interacting with the NPC (Rabut et al., 2004) and perhaps are accessible to be regulated by SPOP. Thus, SPOP-specific mediated regulation of one component of the NPC, Nup153, may be one component of Nup153’s relatively rapid protein turnover. We note that while proteasomes have been shown to localize at the nuclear basket (where Nup153 resides) in yeasts and C. reinhardtii (Albert et al., 2017) and some mammalian NPC components are ubiquitylated (Chakraborty et al., 2008), we believe the SPOP-Nup153 interaction is the first identification of an E3 ubiquitin ligase for the nuclear pore complex in mammals. Generally, few E3 ubiquitin ligases have been recognized that target the nuclear pore complex: one example would be a Cdc53-Skp1-Grr1 complex (homologous to mammalian Cul1-Skp1-F box complex) that monoubiquitylates Nup159 in S. cerevisiae to control nuclear migration during mitosis (Hayakawa et al., 2012).

Indeed, how SPOP expression and activity can change in different cellular conditions, such as nutrient flux, is an important question for SPOP regulation. For example, in kidney

cancers, SPOP increases during hypoxia and relocalizes into the cytoplasm where it gains a new suite of non-nuclear substrates (Li et al., 2014). During DNA damage, ATM kinase phosphorylates SPOP in the MATH domain and increases the affinity of SPOP for the substrates 53BP1 (Wang et al., 2021) and HIPK2 (Jin et al., 2021) (of note, these two SPOP substrates are ubiquitylated but not degraded). In proliferative, cycling cells, Aurora A kinase also phosphorylates SPOP in the MATH domain (Nikhil et al., 2020). While this phosphorylation was suggested to promote SPOP degradation (Nikhil et al., 2020), whether or not phosphorylation of SPOP in the MATH domain also allows SPOP to interact with a new suite of substrates is unclear. At least for one cell cycle-related kinase, Cdk4-mediated phosphorylation of SPOP resulted in association of SPOP with 14-3-3γ, an event that protected SPOP from Cdh1/Fzr1 binding and resulting degradation (Zhang et al., 2017a). Phenotypes related to SPOP-mediated degradation of Caprin1 were only evident when cells underwent stress and form stress granules (Shi et al., 2019). Finally, SPOP-mediated degradation of Cyclin E1 was only observed in some prostate and bladder cancer cells and not in the other tested cell types (Ju et al., 2018). Given the changing roles of SPOP under varied cellular conditions and cell type, there is a possibility that the effect of SPOP on Nup153 degradation may be stronger than the modest effect we see here or previously reported under other cellular conditions (Lan et al., 2019).

Acknowledgements

We thank the labs of Prasad Jallepalli (MSKCC), Sabrina Spencer (CU Boulder), Tom Misteli (NCI, NIH), Wenjian Gan (Medical University of South Carolina), Gerd Blobel (Upenn), and Cai-Guang Yang (Shanghai Institute of Materia Medica, CAS) for materials and reagents which were ultimately not used in this publication.

Funding

This work was supported by a NIH-NIGMS Ruth L. Kirschstein National Research Service Award GM007185, a National Science Foundation Graduate Research Fellowship DGE-1650604, and a Whitcome Pre-doctoral Fellowship in Molecular Biology from the UCLA MBI to J.Y.O.

References

Albert, S., M. Schaffer, F. Beck, S. Mosalaganti, S. Asano, H.F. Thomas, J.M. Plitzko, M. Beck, W. Baumeister, and B.D. Engel. 2017. Proteasomes tether to two distinct sites at the nuclear pore complex. Proc. Natl. Acad. Sci. U. S. A. 114:13726–13731. doi:10.1073/PNAS.1716305114/SUPPL_FILE/PNAS.1716305114.SM02.MOV.

An, J., C. Wang, Y. Deng, L. Yu, and H. Huang. 2014. Destruction of Full-Length Androgen Receptor by Wild-Type SPOP, but Not Prostate-Cancer-Associated Mutants. Cell Rep. 6:657–669. doi:10.1016/j.celrep.2014.01.013.

Ball, J.R., and K.S. Ullman. 2005. Versatility at the nuclear pore complex: Lessons learned from the nucleoporin Nup153. Chromosoma. 114:319–330. doi:10.1007/S00412-005-0019-3/FIGURES/3.

Barbieri, C.E., S.C. Baca, M.S. Lawrence, F. Demichelis, M. Blattner, J.P. Theurillat, T.A. White, P. Stojanov, E. Van Allen, N. Stransky, E. Nickerson, S.S. Chae, G. Boysen, D. Auclair, R.C. Onofrio, K. Park, N. Kitabayashi, T.Y. MacDonald, K. Sheikh, T. Vuong, C. Guiducci, K. Cibulskis, A. Sivachenko, S.L. Carter, G. Saksena, D. Voet, W.M. Hussain, A.H. Ramos, W. Winckler, M.C. Redman, K. Ardlie, A.K. Tewari, J.M. Mosquera, N. Rupp, P.J. Wild, H. Moch, C. Morrissey, P.S. Nelson, P.W. Kantoff, S.B. Gabriel, T.R. Golub, M. Meyerson, E.S. Lander, G. Getz, M.A. Rubin, and L.A. Garraway. 2012. Exome sequencing identifies recurrent SPOP, FOXA1 and MED12 mutations in prostate cancer. Nat. Genet. 44:685–689. doi:10.1038/NG.2279.

Beck, M., and E. Hurt. 2016. The nuclear pore complex: understanding its function through structural insight. Nat. Rev. Mol. Cell Biol. 2016 182. 18:73–89. doi:10.1038/nrm.2016.147.

Bigenzahn, J.W., G.M. Collu, F. Kartnig, M. Pieraks, G.I. Vladimer, L.X. Heinz, V. Sedlyarov, F. Schischlik, A. Fauster, M. Rebsamen, K. Parapatics, V.A. Blomen, A.C. Müller, G.E. Winter, R.

Kralovics, T.R. Brummelkamp, M. Mlodzik, and G. Superti-Furga. 2018. LZTR1 is a regulator of RAS ubiquitination and signaling. Science. 362:1171. doi:10.1126/SCIENCE.AAP8210.

Bouchard, J.J., J.H. Otero, D.C. Scott, E. Szulc, E.W. Martin, N. Sabri, D. Granata, M.R. Marzahn, K. Lindorff-Larsen, X. Salvatella, B.A. Schulman, and T. Mittag. 2018. Cancer Mutations of the Tumor Suppressor SPOP Disrupt the Formation of Active, Phase-Separated Compartments. Mol. Cell. 72:19-36.e8.

Boysen, G., C.E. Barbieri, D. Prandi, M. Blattner, S.-S. Chae, A. Dahija, S. Nataraj, D. Huang, C. Marotz, L. Xu, J. Huang, P. Lecca, S. Chhangawala, D. Liu, P. Zhou, A. Sboner, J.S. de Bono, F. Demichelis, Y. Houvras, and M.A. Rubin. 2015. SPOP mutation leads to genomic instability in prostate cancer. Elife. 4. doi:10.7554/eLife.09207.

Bradley, M., I. Ramirez, K. Cheung, A.A. Gholkar, and J.Z. Torres. 2016. Inducible LAP-tagged Stable Cell Lines for Investigating Protein Function, Spatiotemporal Localization and Protein Interaction Networks. J. Vis. Exp. doi:10.3791/54870.

Buchwalter, A.L., Y. Liang, and M.W. Hetzer. 2014. Nup50 is required for cell differentiation and exhibits transcription-dependent dynamics. Mol. Biol. Cell. 25:2472–2484. doi:10.1091/MBC.E14-04-0865/ASSET/IMAGES/LARGE/2472FIG9.JPEG.

Bunce, M.W., I. V. Boronenkov, and R.A. Anderson. 2008. Coordinated Activation of the Nuclear Ubiquitin Ligase Cul3-SPOP by the Generation of Phosphatidylinositol 5-Phosphate *. J. Biol. Chem. 283:8678–8686. doi:10.1074/JBC.M710222200.

Burleson, M., J.J. Deng, T. Qin, T.M. Duong, Y. Yan, X. Gu, D. Das, A. Easley, M.A. Liss, P. Renee Yew, R. Bedolla, A.P. Kumar, T. Hui-Ming Huang, Y. Zou, Y. Chen, C.L. Chen, H. Huang, L.Z. Sun, and T.G. Boyer. 2022. GLI3 Is Stabilized by SPOP Mutations and Promotes Castration Resistance via Functional Cooperation with Androgen Receptor in Prostate Cancer. Mol. Cancer Res. 20:62–76. doi:10.1158/1541-7786.MCR-21-0108.

Cai, H., and A. Liu. 2016. Spop promotes skeletal development and homeostasis by positively regulating Ihh signaling. 113:14751–14756.

Cai, H., and A. Liu. 2017. Spop regulates Gli3 activity and Shh signaling in dorsoventral patterning of the mouse spinal cord. Dev. Biol. 432:72–85. doi:10.1016/J.YDBIO.2017.04.002.

Castel, P., A. Cheng, A. Cuevas-Navarro, D.B. Everman, A.G. Papageorge, D.K. Simanshu, A. Tankka, J. Galeas, A. Urisman, and F. McCormick. 2019. RIT1 oncoproteins escape LZTR1-mediated proteolysis. Science. 363:1226. doi:10.1126/SCIENCE.AAV1444.

Chakraborty, P., Y. Wang, J.H. Wei, J. van Deursen, H. Yu, L. Malureanu, M. Dasso, D.J. Forbes, D.E. Levy, J. Seemann, and B.M.A. Fontoura. 2008. Nucleoporin Levels Regulate Cell Cycle Progression and Phase-Specific Gene Expression. Dev. Cell. 15:657. doi:10.1016/J.DEVCEL.2008.08.020.

Chen, M.-H., C.W. Wilson, Y.-J. Li, K.K. Lo Law, C.-S. Lu, R. Gacayan, X. Zhang, C. Hui, and P.-T. Chuang. 2009. Cilium-independent regulation of Gli protein function by Sufu in Hedgehog signaling is evolutionarily conserved. Genes Dev. 23:1910–1928. doi:10.1101/gad.1794109.

Cheung, K., S. Senese, J. Kuang, N. Bui, C. Ongpipattanakul, A. Gholkar, W. Cohn, J. Capri, J.P. Whitelegge, and J.Z. Torres. 2016. Proteomic Analysis of the Mammalian Katanin Family of Microtubule-severing Enzymes Defines Katanin p80 subunit B-like 1 (KATNBL1) as a Regulator of Mammalian Katanin Microtubule-severing. Mol. Cell. Proteomics. 15:1658–69. doi:10.1074/mcp.M115.056465.

Culig, Z., and F.R. Santer. 2014. Androgen receptor signaling in prostate cancer. Cancer Metastasis Rev. 33:413–427. doi:10.1007/S10555-013-9474-0.

Cullinan, S.B., J.D. Gordan, J. Jin, J.W. Harper, and J.A. Diehl. 2004. The Keap1-BTB Protein Is an Adaptor That Bridges Nrf2 to a Cul3-Based E3 Ligase: Oxidative Stress Sensing by a

Cul3-Keap1 Ligase. Mol. Cell. Biol. 24:8477–8486. doi:10.1128/MCB.24.19.8477-8486.2004/ASSET/CD1AEB31-DD00-4CD7-9D3E-19688F6DB403/ASSETS/GRAPHIC/ZMB0190444350007.JPEG.

Cuneo, M.J., and T. Mittag. 2019. The ubiquitin ligase adaptor SPOP in cancer. FEBS J. 286:3946–3958. doi:10.1111/FEBS.15056.

D'Angelo, M.A., M. Raices, S.H. Panowski, and M.W. Hetzer. 2009. Age-Dependent Deterioration of Nuclear Pore Complexes Causes a Loss of Nuclear Integrity in Postmitotic Cells. Cell. 136:284–295. doi:10.1016/J.CELL.2008.11.037.

Daigle, N., J. Beaudouin, L. Hartnell, G. Imreh, E. Hallberg, J. Lippincott-Schwartz, and J. Ellenberg. 2001. Nuclear pore complexes form immobile networks and have a very low turnover in live mammalian cells. J. Cell Biol. 154:71–84. doi:10.1083/JCB.200101089.

Duheron, V., G. Chatel, U. Sauder, V. Oliveri, and B. Fahrenkrog. 2014. Structural characterization of altered nucleoporin Nup153 expression in human cells by Thin-Section electron microscopy. Nucleus. 5:601–612. doi:10.4161/19491034.2014.990853/SUPPL_FILE/KNCL_A_990853_SM3357.PDF.

Elia, A.E.H., L.C. Cantley, and M.B. Yaffe. 2003. Proteomic Screen Finds pSer/pThr-Binding Domain Localizing Plk1 to Mitotic Substrates. Science (80-.). 299:1228–1231. doi:10.1126/science.1079079.

Ewing, R.M., P. Chu, F. Elisma, H. Li, P. Taylor, S. Climie, L. McBroom-Cerajewski, M.D. Robinson, L. O'Connor, M. Li, R. Taylor, M. Dharsee, Y. Ho, A. Heilbut, L. Moore, S. Zhang, O. Ornatsky, Y. V. Bukhman, M. Ethier, Y. Sheng, J. Vasilescu, M. Abu-Farha, J.P. Lambert, H.S. Duewel, I.I. Stewart, B. Kuehl, K. Hogue, K. Colwill, K. Gladwish, B. Muskat, R. Kinach, S.L. Adams, M.F. Moran, G.B. Morin, T. Topaloglou, and D. Figeys. 2007. Large-scale mapping of

human protein-protein interactions by mass spectrometry. Mol. Syst. Biol. 3. doi:10.1038/MSB4100134.

Furukawa, M., and Y. Xiong. 2005. BTB protein Keap1 targets antioxidant transcription factor Nrf2 for ubiquitination by the Cullin 3-Roc1 ligase. Mol. Cell. Biol. 25:162–171. doi:10.1128/MCB.25.1.162-171.2005.

Le Gallo, M., A.J. O'Hara, M.L. Rudd, M.E. Urick, N.F. Hansen, N.J. O'Neil, J.C. Price, S. Zhang, B.M. England, A.K. Godwin, D.C. Sgroi, P. Hieter, J.C. Mullikin, M.J. Merino, and D.W. Bell. 2012. Exome sequencing of serous endometrial tumors identifies recurrent somatic mutations in chromatin-remodeling and ubiquitin ligase complex genes. Nat. Genet. 44:1310–1315. doi:10.1038/NG.2455.

Gan, W., X. Dai, A. Lunardi, Z. Li, H. Inuzuka, P. Liu, S. Varmeh, J. Zhang, L. Cheng, Y. Sun, J.M.M. Asara, A.H.H. Beck, J. Huang, P.P.P. Pandolfi, and W. Wei. 2015. SPOP Promotes Ubiquitination and Degradation of the ERG Oncoprotein to Suppress Prostate Cancer Progression. 59:917–930.

Garcia, Y.A., E.F. Velasquez, L.W. Gao, A.A. Gholkar, K.M. Clutario, K. Cheung, T. Williams-Hamilton, J.P. Whitelegge, and J.Z. Torres. 2021. Mapping Proximity Associations of Core Spindle Assembly Checkpoint Proteins. J. Proteome Res. 20:3414–3427. doi:10.1021/ACS.JPROTEOME.0C00941.

Geng, C., B. He, L. Xu, C.E. Barbieri, V.K. Eedunuri, S.A. Chew, M. Zimmermann, R. Bond, J. Shou, C. Li, M. Blattner, D.M. Lonard, F. Demichelis, C. Coarfa, M.A. Rubin, P. Zhou, B.W. O'Malley, and N. Mitsiades. 2013a. Prostate cancer-associated mutations in speckle-type POZ protein (SPOP) regulate steroid receptor coactivator 3 protein turnover. Proc. Natl. Acad. Sci. 110:6997–7002. doi:10.1073/pnas.1304502110.

Geng, C., B. He, L. Xu, C.E. Barbieri, V.K. Eedunuri, S.A. Chew, M. Zimmermann, R. Bond, J. Shou, C. Li, M. Blattner, D.M. Lonard, F. Demichelis, C. Coarfa, M.A. Rubin, P. Zhou, B.W. O'Malley, and N. Mitsiades. 2013b. Prostate cancer-associated mutations in speckle-type POZ protein (SPOP) regulate steroid receptor coactivator 3 protein turnover. 110:6997–7002.

Geng, C., S. Kaochar, M. Li, K. Rajapakshe, W. Fiskus, J. Dong, C. Foley, B. Dong, L. Zhang, O.-J.J. Kwon, S.S. Shah, M. Bolaki, L. Xin, M. Ittmann, B.W. O'Malley, C. Coarfa, and N. Mitsiades. 2017. SPOP regulates prostate epithelial cell proliferation and promotes ubiquitination and turnover of c-MYC oncoprotein. Oncogene. 36:4767–4777.

Geng, C., K. Rajapakshe, S.S. Shah, J. Shou, V.K. Eedunuri, C. Foley, W. Fiskus, M. Rajendran, S.A. Chew, M. Zimmermann, R. Bond, B. He, C. Coarfa, and N. Mitsiades. 2014. Androgen Receptor Is the Key Transcriptional Mediator of the Tumor Suppressor SPOP in Prostate Cancer. Cancer Res. 74:5631–5643. doi:10.1158/0008-5472.CAN-14-0476.

Goedhart, J. 2021. SuperPlotsOfData - A web app for the transparent display and quantitative comparison of continuous data from different conditions. Mol. Biol. Cell. 32:470–474. doi:10.1091/MBC.E20-09-0583/ASSET/IMAGES/LARGE/MBC-32-470-G003.JPEG.

Groner, A.C., L. Cato, J. de Tribolet-Hardy, T. Bernasocchi, H. Janouskova, D. Melchers, R. Houtman, A.C.B. Cato, P. Tschopp, L. Gu, A. Corsinotti, Q. Zhong, C. Fankhauser, C. Fritz, C. Poyet, U. Wagner, T. Guo, R. Aebersold, L.A. Garraway, P.J. Wild, J.P. Theurillat, and M. Brown. 2016. TRIM24 Is an Oncogenic Transcriptional Activator in Prostate Cancer. Cancer Cell. 29:846–858. doi:10.1016/J.CCELL.2016.04.012.

Guillamot, M., D. Ouazia, I. Dolgalev, S.T. Yeung, N. Kourtis, Y. Dai, K. Corrigan, L. Zea-Redondo, A. Saraf, L. Florens, M.P. Washburn, A.N. Tikhonova, M. Malumbres, Y. Gong, A. Tsirigos, C. Park, C. Barbieri, K.M. Khanna, L. Busino, and I. Aifantis. 2019. The E3 ubiquitin

ligase SPOP controls resolution of systemic inflammation by triggering MYD88 degradation. Nat. Immunol. 2019 209. 20:1196–1207. doi:10.1038/s41590-019-0454-6.

Guo, X., I. Ramirez, Y.A. Garcia, E.F. Velasquez, A.A. Gholkar, W. Cohn, J.P. Whitelegge, B. Tofig, R. Damoiseaux, and J.Z. Torres. 2021. DUSP7 regulates the activity of ERK2 to promote proper chromosome alignment during cell division. J. Biol. Chem. 296. doi:10.1016/J.JBC.2021.100676.

Hansen, D. V., A. V. Loktev, K.H. Ban, and P.K. Jackson. 2004. Plk1 regulates activation of the anaphase promoting complex by phosphorylating and triggering SCFbetaTrCP-dependent destruction of the APC Inhibitor Emi1. Mol. Biol. Cell. 15:5623–5634. doi:10.1091/MBC.E04-07-0598.

Hayakawa, A., A. Babour, L. Sengmanivong, and C. Dargemont. 2012. Ubiquitylation of the nuclear pore complex controls nuclear migration during mitosis in S. cerevisiae. J. Cell Biol. 196:19–27. doi:10.1083/JCB.201108124.

Hernández-Muñoz, I., A.H. Lund, P. Van Der Stoop, E. Boutsma, I. Muijrers, E. Verhoeven, D.A. Nusinow, B. Panning, Y. Marahrens, and M. Van Lohuizen. 2005. Stable X chromosome inactivation involves the PRC1 Polycomb complex and requires histone MACROH2A1 and the CULLIN3/SPOP ubiquitin E3 ligase. Proc. Natl. Acad. Sci. U. S. A. 102:7635–7640. doi:10.1073/PNAS.0408918102.

Hjorth-Jensen, K., A. Maya-Mendoza, N. Dalgaard, J.O. Sigurðsson, J. Bartek, D. Iglesias-Gato, J. V. Olsen, and A. Flores-Morales. 2018. SPOP promotes transcriptional expression of DNA repair and replication factors to prevent replication stress and genomic instability. Nucleic Acids Res. 46:9484–9495. doi:10.1093/NAR/GKY719.

Hu, X., Z. Yang, M. Zeng, Y. Liu, X. Yang, Y. Li, X. Li, and Q. Yu. 2016. Speckle-type POZ (pox virus and zinc finger protein) protein gene deletion in ovarian cancer: Fluorescence in situ

hybridization analysis of a tissue microarray. Oncol. Lett. 12:658–662. doi:10.3892/OL.2016.4643.

Huttlin, E.L., R.J. Bruckner, J. Navarrete-Perea, J.R. Cannon, K. Baltier, F. Gebreab, M.P. Gygi, A. Thornock, G. Zarraga, S. Tam, J. Szpyt, B.M. Gassaway, A. Panov, H. Parzen, S. Fu, A. Golbazi, E. Maenpaa, K. Stricker, S. Guha Thakurta, T. Zhang, R. Rad, J. Pan, D.P. Nusinow, J.A. Paulo, D.K. Schweppe, L.P. Vaites, J.W. Harper, and S.P. Gygi. 2021. Dual proteome-scale networks reveal cell-specific remodeling of the human interactome. Cell. 184:3022-3040.e28. doi:10.1016/J.CELL.2021.04.011.

Janouskova, H., G. El Tekle, E. Bellini, N.D. Udeshi, A. Rinaldi, A. Ulbricht, T. Bernasocchi, G. Civenni, M. Losa, T. Svinkina, C.M. Bielski, G. V Kryukov, L. Cascione, S. Napoli, R.I. Enchev, D.G. Mutch, M.E. Carney, A. Berchuck, B.J.N. Winterhoff, R.R. Broaddus, P. Schraml, H. Moch, F. Bertoni, C. V Catapano, M. Peter, S.A. Carr, L.A. Garraway, P.J. Wild, and J.-P.P. Theurillat. 2017. Opposing effects of cancer-type-specific SPOP mutants on BET protein degradation and sensitivity to BET inhibitors. Nat. Med. 23:1046–1054. doi:10.1038/nm.4372.

Jiang, Q., N. Zheng, L. Bu, X. Zhang, X. Zhang, Y. Wu, Y. Su, L. Wang, X. Zhang, S. Ren, X. Dai, D. Wu, W. Xie, W. Wei, Y. Zhu, and J. Guo. 2021. SPOP-mediated ubiquitination and degradation of PDK1 suppresses AKT kinase activity and oncogenic functions. Mol. Cancer. 20:1–18. doi:10.1186/S12943-021-01397-5/FIGURES/7.

Jin, X., S. Qing, Q. Li, H. Zhuang, L. Shen, J. Li, H. Qi, T. Lin, Z. Lin, J. Wang, X. Cao, J. Yang, Q. Ma, L. Cong, Y. Xi, S. Fang, X. Meng, Z. Gong, M. Ye, S. Wang, C. Wang, and K. Gao. 2021. Prostate cancer-associated SPOP mutations lead to genomic instability through disruption of the SPOP-HIPK2 axis. Nucleic Acids Res. 49:6788–6803. doi:10.1093/NAR/GKAB489.

Jin, X., Q. Shi, Q. Li, L. Zhou, J. Wang, L. Jiang, X. Zhao, K. Feng, T. Lin, Z. Lin, H. Zhuang, J. Yang, C. Hu, L. Zhang, L. Shen, Y. Lu, J. Zhu, H. Wang, H. Qi, X. Meng, Y. Xi, J. Pan, S. Fang, H. Tian, C. Zhou, P. Zhang, K. Gao, S. min Zhao, Y. Li, Z. Gong, and C. Wang. 2019a. CRL3–SPOP ubiquitin ligase complex suppresses the growth of diffuse large B-cell lymphoma by negatively regulating the MyD88/NF-κB signaling. Leuk. 2019 345. 34:1305–1314. doi:10.1038/s41375-019-0661-z.

Jin, X., J. Wang, Q. Li, H. Zhuang, J. Yang, Z. Lin, T. Lin, Z. Lv, L. Shen, C. Yan, J. Zheng, J. Zhu, Z. Gong, C. Wang, and K. Gao. 2019b. SPOP targets oncogenic protein ZBTB3 for destruction to suppress endometrial cancer. Am. J. Cancer Res. 9:2797.

Ju, L.G., Y. Zhu, Q.Y. Long, X.J. Li, X. Lin, S.B. Tang, L. Yin, Y. Xiao, X.H. Wang, L. Li, L. Zhang, and M. Wu. 2018. SPOP suppresses prostate cancer through regulation of CYCLIN E1 stability. Cell Death Differ. 2018 266. 26:1156–1168. doi:10.1038/s41418-018-0198-0.

Kent, D., E.W. Bush, and J.E. Hooper. 2006. Roadkill attenuates Hedgehog responses through degradation of Cubitus interruptus. Development. 133:2001–2010. doi:10.1242/DEV.02370.

Kwon, J.E., M. La, K.H. Oh, Y.M. Oh, G.R. Kim, J.H. Seol, S.H. Baek, T. Chiba, K. Tanaka, O.S. Bang, C.O. Joe, and C.H. Chung. 2006. BTB Domain-containing Speckle-type POZ Protein (SPOP) Serves as an Adaptor of Daxx for Ubiquitination by Cul3-based Ubiquitin Ligase. J. Biol. Chem. 281:12664–12672. doi:10.1074/jbc.M600204200.

Lan, X., E. Khandros, P. Huang, S.A. Peslak, S.K. Bhardwaj, J.D. Grevet, O. Abdulmalik, H. Wang, C.A. Keller, B. Giardine, J. Baeza, E.R. Duffner, O. El Demerdash, X.S. Wu, C.R. Vakoc, B.A. Garcia, R.C. Hardison, J. Shi, and G.A. Blobel. 2019. The E3 ligase adaptor molecule SPOP regulates fetal hemoglobin levels in adult erythroid cells. Blood Adv. 3:1586–1597. doi:10.1182/BLOODADVANCES.2019032318.

Lee, C.W., F. Wilfling, P. Ronchi, M. Allegretti, S. Mosalaganti, S. Jentsch, M. Beck, and B. Pfander. 2020. Selective autophagy degrades nuclear pore complexes. Nat. Cell Biol. 22:159–166. doi:10.1038/S41556-019-0459-2.

Li, C., J. Ao, J. Fu, D.F. Lee, J. Xu, D. Lonard, and B.W. O'Malley. 2011. Tumor-suppressor role for the SPOP ubiquitin ligase in signal-dependent proteolysis of the oncogenic co-activator SRC-3/AIB1. Oncogene. 30:4350–4364. doi:10.1038/ONC.2011.151.

Li, G., W. Ci, S. Karmakar, K. Chen, R. Dhar, Z. Fan, Z. Guo, J. Zhang, Y. Ke, L. Wang, M. Zhuang, S. Hu, X. Li, L. Zhou, X. Li, M.F. Calabrese, E.R. Watson, S.M. Prasad, C. Rinker-Schaeffer, S.E. Eggener, T. Stricker, Y. Tian, B.A. Schulman, J. Liu, and K.P. White. 2014. SPOP promotes tumorigenesis by acting as a key regulatory hub in kidney cancer. Cancer Cell. 25:455–468. doi:10.1016/J.CCR.2014.02.007.

Li, Y., Q. Yu, R. Li, J. Luo, D. Yuan, J. Song, Y. Sun, T. Long, and Z. Yang. 2019. SPOP Regulates The Biological Mechanism Of Ovarian Cancer Cells Through The Hh Signaling Pathway. Onco. Targets. Ther. 12:9239–9248. doi:10.2147/OTT.S215940.

Linder, M.I., M. Köhler, P. Boersema, M. Weberruss, C. Wandke, J. Marino, C. Ashiono, P. Picotti, W. Antonin, and U. Kutay. 2017. Mitotic Disassembly of Nuclear Pore Complexes Involves CDK1- and PLK1-Mediated Phosphorylation of Key Interconnecting Nucleoporins. Dev. Cell. 43:141-156.e7. doi:10.1016/J.DEVCEL.2017.08.020.

Liu, X., T. Zhou, R. Kuriyama, and R.L. Erikson. 2004. Molecular interactions of Polo-like-kinase 1 with the mitotic kinesin-like protein CHO1/MKLP-1. J. Cell Sci. 117:3233–3246. doi:10.1242/jcs.01173.

Livak, K.J., and T.D. Schmittgen. 2001. Analysis of Relative Gene Expression Data Using Real-Time Quantitative PCR and the 2−ΔΔCT Method. Methods. 25:402–408. doi:10.1006/METH.2001.1262.

Luo, L., H. Tang, L. Ling, N. Li, X. Jia, Z. Zhang, X. Wang, L. Shi, J. Yin, N. Qiu, H. Liu, Y. Song, K. Luo, H. Li, Z. He, G. Zheng, and X. Xie. 2018. LINC01638 lncRNA activates MTDH-Twist1 signaling by preventing SPOP-mediated c-Myc degradation in triple-negative breast cancer. Oncogene. 37:6166–6179. doi:10.1038/S41388-018-0396-8.

Lussi, Y.C., D.K. Shumaker, T. Shimi, and B. Fahrenkrog. 2010. The nucleoporin Nup153 affects spindle checkpoint activity due to an association with Mad1. Nucleus. 1:71–84. doi:10.4161/NUCL.1.1.10244.

Ma, J., Q. Shi, G. Cui, H. Sheng, M.V. Botuyan, Y. Zhou, Y. Yan, Y. He, L. Wang, Y. Wang, G. Mer, D. Ye, C. Wang, and H. Huang. 2021. SPOP mutation induces replication over-firing by impairing Geminin ubiquitination and triggers replication catastrophe upon ATR inhibition. Nat. Commun. 2021 121. 12:1–14. doi:10.1038/s41467-021-26049-6.

Makise, M., D.R. Mackay, S. Elgort, S.S. Shankaran, S.A. Adam, and K.S. Ullman. 2012. The Nup153-Nup50 protein interface and its role in nuclear import. J. Biol. Chem. 287:38515–38522. doi:10.1074/JBC.M112.378893.

Martino, L., S. Morchoisne-Bolhy, D.K. Cheerambathur, L. Van Hove, J. Dumont, N. Joly, A. Desai, V. Doye, and L. Pintard. 2017. Channel Nucleoporins Recruit PLK-1 to Nuclear Pore Complexes to Direct Nuclear Envelope Breakdown in C. elegans. Dev. Cell. 43:157-171.e7. doi:10.1016/J.DEVCEL.2017.09.019.

Marzahn, M.R., S. Marada, J. Lee, A. Nourse, S. Kenrick, H. Zhao, G. Ben-Nissan, R. Kolaitis, J.L. Peters, S. Pounds, W.J. Errington, G.G. Privé, J.P. Taylor, M. Sharon, P. Schuck, S.K. Ogden, and T. Mittag. 2016. Higher-order oligomerization promotes localization of SPOP to liquid nuclear speckles. EMBO J. 35:1254–1275. doi:10.15252/embj.201593169.

Mathieson, T., H. Franken, J. Kosinski, N. Kurzawa, N. Zinn, G. Sweetman, D. Poeckel, V.S. Ratnu, M. Schramm, I. Becher, M. Steidel, K.M. Noh, G. Bergamini, M. Beck, M. Bantscheff, and M.M. Savitski. 2018. Systematic analysis of protein turnover in primary cells. Nat. Commun. 2018 91. 9:1–10. doi:10.1038/s41467-018-03106-1.

Maul, G.G., H.M. Maul, J.E. Scogna, M.W. Lieberman, G.S. Stein, B.Y.L. Hsu, and T.W. Borun. 1972. TIME SEQUENCE OF NUCLEAR PORE FORMATION IN PHYTOHEMAGGLUTININ-STIMULATED LYMPHOCYTES AND IN HELA CELLS DURING THE CELL CYCLE. J. Cell Biol. 55:433. doi:10.1083/JCB.55.2.433.

Mauthe, M., I. Orhon, C. Rocchi, X. Zhou, M. Luhr, K.J. Hijlkema, R.P. Coppes, N. Engedal, M. Mari, and F. Reggiori. 2018. Chloroquine inhibits autophagic flux by decreasing autophagosome-lysosome fusion. Autophagy. 14:1435. doi:10.1080/15548627.2018.1474314.

Mossaid, I., G. Chatel, V. Martinelli, M. Vaz, and B. Fahrenkrog. 2020. Mitotic checkpoint protein Mad1 is required for early Nup153 recruitment to chromatin and nuclear envelope integrity. J. Cell Sci. 133. doi:10.1242/JCS.249243.

Mossaid, I., and B. Fahrenkrog. 2015. Complex Commingling: Nucleoporins and the Spindle Assembly Checkpoint. Cells. 4:706. doi:10.3390/CELLS4040706.

Mukhopadhyay, C., C. Yang, L. Xu, D. Liu, Y. Wang, D. Huang, L.D. Deonarine, J. Cyrta, E. Davicioni, A. Sboner, B.D. Robinson, A.M. Chinnaiyan, M.A. Rubin, C.E. Barbieri, and P. Zhou. 2021. G3BP1 inhibits Cul3 SPOP to amplify AR signaling and promote prostate cancer. Nat. Commun. 12. doi:10.1038/S41467-021-27024-X.

Nikhil, K., M. Kamra, A. Raza, H.S. Haymour, and K. Shah. 2020. Molecular Interplay between AURKA and SPOP Dictates CRPC Pathogenesis via Androgen Receptor. Cancers 2020, Vol. 12, Page 3247. 12:3247. doi:10.3390/CANCERS12113247.

Ostertag, M.S., W. Hutwelker, O. Plettenburg, M. Sattler, and G.M. Popowicz. 2019a. Structural Insights into BET Client Recognition of Endometrial and Prostate Cancer-Associated SPOP Mutants. J. Mol. Biol. 431:2213–2221. doi:10.1016/J.JMB.2019.04.017.

Ostertag, M.S., A.C. Messias, M. Sattler, and G.M. Popowicz. 2019b. The Structure of the SPOP-Pdx1 Interface Reveals Insights into the Phosphorylation-Dependent Binding Regulation. Structure. 27:327-334.e3. doi:10.1016/J.STR.2018.10.005.

Otsuka, S., and J. Ellenberg. 2018. Mechanisms of nuclear pore complex assembly – two different ways of building one molecular machine. Febs Lett. 592:475. doi:10.1002/1873-3468.12905.

Petroski, M.D., and R.J. Deshaies. 2005. Function and regulation of cullin–RING ubiquitin ligases. Nat. Rev. Mol. Cell Biol. 2005 61. 6:9–20. doi:10.1038/nrm1547.

Pierce, W.K., C.R. Grace, J. Lee, A. Nourse, M.R. Marzahn, E.R. Watson, A.A. High, J. Peng, B.A. Schulman, and T. Mittag. 2016. Multiple Weak Linear Motifs Enhance Recruitment and Processivity in SPOP-Mediated Substrate Ubiquitination. J. Mol. Biol. 428:1256–1271. doi:10.1016/j.jmb.2015.10.002.

Rabut, G., V. Doye, and J. Ellenberg. 2004. Mapping the dynamic organization of the nuclear pore complex inside single living cells. Nat. Cell Biol. 2004 611. 6:1114–1121. doi:10.1038/ncb1184.

Schindelin, J., I. Arganda-Carreras, E. Frise, V. Kaynig, M. Longair, T. Pietzsch, S. Preibisch, C. Rueden, S. Saalfeld, B. Schmid, J.Y. Tinevez, D.J. White, V. Hartenstein, K. Eliceiri, P. Tomancak, and A. Cardona. 2012. Fiji: an open-source platform for biological-image analysis. Nat. Methods. 9:676–682. doi:10.1038/NMETH.2019.

Schwend, T., Z. Jin, K. Jiang, B.J. Mitchell, J. Jia, and J. Yang. 2013. Stabilization of speckle-type POZ protein (Spop) by Daz interacting protein 1 (Dzip1) is essential for Gli turnover and the proper output of Hedgehog signaling. J. Biol. Chem. 288:32809–32820. doi:10.1074/JBC.M113.512962.

Seong, K.H., and S. Ishii. 2013. Su(fu) switches Rdx functions to fine-tune hedgehog signaling in the Drosophila wing disk. Genes to Cells. 18:66–78. doi:10.1111/GTC.12018.

Shi, Q., Y. Zhu, J. Ma, K. Chang, D. Ding, Y. Bai, K. Gao, P. Zhang, R. Mo, K. Feng, X. Zhao, L. Zhang, H. Sun, D. Jiao, Y. Chen, Y. Sun, S.M. Zhao, H. Huang, Y. Li, S. Ren, and C. Wang. 2019. Prostate Cancer-associated SPOP mutations enhance cancer cell survival and docetaxel resistance by upregulating Caprin1-dependent stress granule assembly. Mol. Cancer. 18. doi:10.1186/S12943-019-1096-X.

Soucy, T.A., P.G. Smith, M.A. Milhollen, A.J. Berger, J.M. Gavin, S. Adhikari, J.E. Brownell, K.E. Burke, D.P. Cardin, S. Critchley, C.A. Cullis, A. Doucette, J.J. Garnsey, J.L. Gaulin, R.E. Gershman, A.R. Lublinsky, A. McDonald, H. Mizutani, U. Narayanan, E.J. Olhava, S. Peluso, M. Rezaei, M.D. Sintchak, T. Talreja, M.P. Thomas, T. Traore, S. Vyskocil, G.S. Weatherhead, J. Yu, J. Zhang, L.R. Dick, C.F. Claiborne, M. Rolfe, J.B. Bolen, and S.P. Langston. 2009. An inhibitor of NEDD8-activating enzyme as a new approach to treat cancer. Nature. 458:732. doi:10.1038/nature07884.

Steklov, M., S. Pandolfi, M.F. Baietti, A. Batiuk, P. Carai, P. Najm, M. Zhang, H. Jang, F. Renzi, Y. Cai, L. Abbasi Asbagh, T. Pastor, M. De Troyer, M. Simicek, E. Radaelli, H. Brems, E. Legius, J. Tavernier, K. Gevaert, F. Impens, L. Messiaen, R. Nussinov, S. Heymans, S. Eyckerman, and A.A. Sablina. 2018. Mutations in LZTR1 drive human disease by dysregulating RAS ubiquitination. Science. 362:1177–1182. doi:10.1126/SCIENCE.AAP7607.

Stirling, D.R., M.J. Swain-Bowden, A.M. Lucas, A.E. Carpenter, B.A. Cimini, and A. Goodman. 2021. CellProfiler 4: improvements in speed, utility and usability. BMC Bioinformatics. 22. doi:10.1186/S12859-021-04344-9.

Strambio-De-Castillia, C., M. Niepel, and M.P. Rout. 2010. The nuclear pore complex: bridging nuclear transport and gene regulation. Nat. Rev. Mol. Cell Biol. 2010 117. 11:490–501. doi:10.1038/nrm2928.

Taniguchi, T., I. Garcia-Higuera, B. Xu, P.R. Andreassen, R.C. Gregory, S.T. Kim, W.S. Lane, M.B. Kastan, and A.D. D'Andrea. 2002. Convergence of the Fanconi Anemia and Ataxia Telangiectasia Signaling Pathways. Cell. 109:459–472. doi:10.1016/S0092-8674(02)00747-X.

Theurillat, J.P.P.J.-P.P., N.D. Udeshi, W.J. Errington, T. Svinkina, S.C. Baca, M. Pop, P.J. Wild, M. Blattner, A.C. Groner, M.A. Rubin, H. Moch, G.G. Prive, S.A. Carr, L.A. Garraway, G.G. Privé, S.A. Carr, and L.A. Garraway. 2014. Ubiquitylome analysis identifies dysregulation of effector substrates in SPOP-mutant prostate cancer. Science (80-.). 346:85–89.

Tighe, A., O. Staples, and S. Taylor. 2008. Mps1 kinase activity restrains anaphase during an unperturbed mitosis and targets Mad2 to kinetochores. J. Cell Biol. 181:893–901. doi:10.1083/JCB.200712028.

Toda, T., J.Y. Hsu, S.B. Linker, L. Hu, S.T. Schafer, J. Mertens, F. V. Jacinto, M.W. Hetzer, and F.H. Gage. 2017. Nup153 Interacts with Sox2 to Enable Bimodal Gene Regulation and Maintenance of Neural Progenitor Cells. Cell Stem Cell. 21:618-634.e7. doi:10.1016/J.STEM.2017.08.012.

Tomioka, Y., T. Kotani, H. Kirisako, Y. Oikawa, Y. Kimura, H. Hirano, Y. Ohsumi, and H. Nakatogawa. 2020. TORC1 inactivation stimulates autophagy of nucleoporin and nuclear pore complexes. J. Cell Biol. 219. doi:10.1083/JCB.201910063/151819.

Torres, J.Z., J.J. Miller, and P.K. Jackson. 2009. High-throughput generation of tagged stable cell lines for proteomic analysis. Proteomics. 9:2888–2891. doi:10.1002/pmic.200800873.

Tsvetkov, L.M., R.T. Tsekova, X. Xu, and D.F. Stern. 2005. The Plk1 Polo Box Domain Mediates a Cell Cycle and DNA Damage Regulated Interaction with Chk2. Cell Cycle. 4:602–610. doi:10.4161/cc.4.4.1599.

Usher, E.T., N. Sabri, R. Rohac, A.K. Boal, T. Mittag, and S.A. Showalter. 2021. Intrinsically disordered substrates dictate SPOP subnuclear localization and ubiquitination activity. J. Biol. Chem. 296:100693. doi:10.1016/J.JBC.2021.100693.

Vollmer, B., M. Lorenz, D. Moreno-Andrés, M. Bodenhöfer, P. De Magistris, S.A. Astrinidis, A. Schooley, M. Flötenmeyer, S. Leptihn, and W. Antonin. 2015. Nup153 Recruits the Nup107-160 Complex to the Inner Nuclear Membrane for Interphasic Nuclear Pore Complex Assembly. Dev. Cell. 33:717–728. doi:10.1016/J.DEVCEL.2015.04.027.

Wang, D., J. Ma, M.V. Botuyan, G. Cui, Y. Yan, D. Ding, Y. Zhou, E.W. Krueger, J. Pei, X. Wu, L. Wang, H. Pei, M.A. McNiven, D. Ye, G. Mer, and H. Huang. 2021. ATM-phosphorylated SPOP contributes to 53BP1 exclusion from chromatin during DNA replication. Sci. Adv. 7:9208–9226. doi:10.1126/SCIADV.ABD9208/SUPPL_FILE/SCIADV.ABD9208_SM.PDF.

Wang, L., M. Lin, M. Chu, Y. Liu, J. Ma, Y. He, and Z. wei Wang. 2020a. SPOP promotes ubiquitination and degradation of LATS1 to enhance kidney cancer progression. EBioMedicine. 56:102795. doi:10.1016/J.EBIOM.2020.102795/ATTACHMENT/18FAB33E-E985-4038-9A1C-61654CAB391F/MMC1.PDF.

Wang, X., J. Jin, F. Wan, L. Zhao, H. Chu, C. Chen, G. Liao, J. Liu, Y. Yu, H. Teng, L. Fang, C. Jiang, W. Pan, X. Xie, J. Li, X. Lu, X. Jiang, X. Ge, D. Ye, and P. Wang. 2019. AMPK Promotes SPOP-Mediated NANOG Degradation to Regulate Prostate Cancer Cell Stemness. Dev. Cell. 48:345-360.e7. doi:10.1016/J.DEVCEL.2018.11.033.

Wang, Z., Y. Song, M. Ye, X. Dai, X. Zhu, and W. Wei. 2020b. The diverse roles of SPOP in prostate cancer and kidney cancer. Nat. Rev. Urol. 17:339–350. doi:10.1038/S41585-020-0314-Z.

Wu, F., X. Dai, W. Gan, L. Wan, M. Li, N. Mitsiades, W. Wei, Q. Ding, and J. Zhang. 2017. Prostate cancer-associated mutation in SPOP impairs its ability to target Cdc20 for poly-ubiquitination and degradation. Cancer Lett. 385:207–214. doi:10.1016/j.canlet.2016.10.021.

Xia, X., A. Gholkar, S. Senese, and J.Z. Torres. 2015. A LCMT1-PME-1 methylation equilibrium controls mitotic spindle size. Cell Cycle. 14:1938–47. doi:10.1080/15384101.2015.1026487.

Yuan, D., Y. Chen, Z. Yang, G. Li, M. Wu, J. Jiang, D. Li, and Q. Yu. 2020. SPOP attenuates migration and invasion of choriocarcinoma cells by promoting DHX9 degradation. Am. J. Cancer Res. 10:2428.

Zeng, C., Y. Wang, Q. Lu, J. Chen, J. Zhang, T. Liu, N. Lv, and S. Luo. 2014. SPOP suppresses tumorigenesis by regulating Hedgehog/Gli2 signaling pathway in gastric cancer. J. Exp. Clin. Cancer Res. 33. doi:10.1186/S13046-014-0075-8.

Zhang, J., X. Bu, H. Wang, Y. Zhu, Y. Geng, N.T. Nihira, Y. Tan, Y. Ci, F. Wu, X. Dai, J. Guo, Y.-H. Huang, C. Fan, S. Ren, Y. Sun, G.J. Freeman, P. Sicinski, and W. Wei. 2017a. Cyclin D–CDK4 kinase destabilizes PD-L1 via cullin 3–SPOP to control cancer immune surveillance. Nature. 553:91–95. doi:10.1038/nature25015.

Zhang, J., M. Chen, Y. Zhu, X. Dai, F. Dang, J. Ren, S. Ren, Y. V. Shulga, F. Beca, W. Gan, F. Wu, Y.M. Lin, X. Zhou, J.A. DeCaprio, A.H. Beck, K.P. Lu, J. Huang, C. Zhao, Y. Sun, X. Gao, P.P. Pandolfi, and W. Wei. 2019. SPOP Promotes Nanog Destruction to Suppress Stem Cell Traits and Prostate Cancer Progression. Dev. Cell. 48:329-344.e5. doi:10.1016/J.DEVCEL.2018.11.035.

Zhang, J.J., K. Gao, H. Xie, D. Wang, P. Zhang, T. Wei, Y. Yan, Y. Pan, W. Ye, H. Chen, Q. Shi, Y. Li, S. min Zhao, X. Hou, S.J. Weroha, Y. Wang, J.J. Zhang, R.J. Karnes, H.H. He, L. Wang, C. Wang, and H. Huang. 2021. SPOP mutation induces DNA methylation via stabilizing GLP/G9a. Nat. Commun. 12. doi:10.1038/S41467-021-25951-3.

Zhang, P., K. Gao, X. Jin, J. Ma, J. Peng, R. Wumaier, Y. Tang, Y. Zhang, J. An, Q. Yan, Y. Dong, H. Huang, L. Yu, and C. Wang. 2015. Endometrial cancer-associated mutants of SPOP are defective in regulating estrogen receptor-α protein turnover. Cell Death Dis. 6:e1687. doi:10.1038/cddis.2015.47.

Zhang, P., D. Wang, Y. Zhao, S. Ren, K. Gao, Z. Ye, S. Wang, C.-W. Pan, Y. Zhu, Y. Yan, Y. Yang, D. Wu, Y. He, J. Zhang, D. Lu, X. Liu, L. Yu, S. Zhao, Y. Li, D. Lin, Y. Wang, L. Wang, Y. Chen, Y. Sun, C. Wang, and H. Huang. 2017b. Intrinsic BET inhibitor resistance in SPOP-mutated prostate cancer is mediated by BET protein stabilization and AKT–mTORC1 activation. Nat. Med. 23:1055–1062. doi:10.1038/nm.4379.

Zhang, Q., Q. Shi, Y. Chen, T. Yue, S. Li, B. Wang, and J. Jiang. 2009. Multiple Ser/Thr-rich degrons mediate the degradation of Ci/Gli by the Cul3-HIB/SPOP E3 ubiquitin ligase. Proc. Natl. Acad. Sci. U. S. A. 106:21191–21196. doi:10.1073/PNAS.0912008106/SUPPL_FILE/APPENDIX_PDF.PDF.

Zhi, X., J. Tao, L. Zhang, R. Tao, L. Ma, and J. Qin. 2016. Silencing speckle-type POZ protein by promoter hypermethylation decreases cell apoptosis through upregulating Hedgehog signaling pathway in colorectal cancer. Cell Death Dis. 7. doi:10.1038/CDDIS.2016.435.

Zhou, X.E., K.M. Suino-Powell, J. Li, Y. He, J.P. MacKeigan, K. Melcher, E.L. Yong, and H.E. Xu. 2010. Identification of SRC3/AIB1 as a Preferred Coactivator for Hormone-activated Androgen Receptor. J. Biol. Chem. 285:9161. doi:10.1074/JBC.M109.085779.

Zhuang, M., M.F. Calabrese, J. Liu, M.B. Waddell, A. Nourse, M. Hammel, D.J. Miller, H. Walden, D.M. Duda, S.N. Seyedin, T. Hoggard, J.W. Harper, K.P. White, and B.A. Schulman. 2009. Structures of SPOP-Substrate Complexes: Insights into Molecular Architectures of BTB-Cul3 Ubiquitin Ligases. Mol. Cell. 36:39–50. doi:10.1016/j.molcel.2009.09.022.

References in Supplementary Files

Other plasmids were obtained from PMID: 26929214 (Cheung et al., 2016), PMID: 11448991 (Daigle et al., 2001), PMID: 15469984 (Hansen et al., 2004), and PMID: 25839665 (Xia et al., 2015).

Figures and figure legends

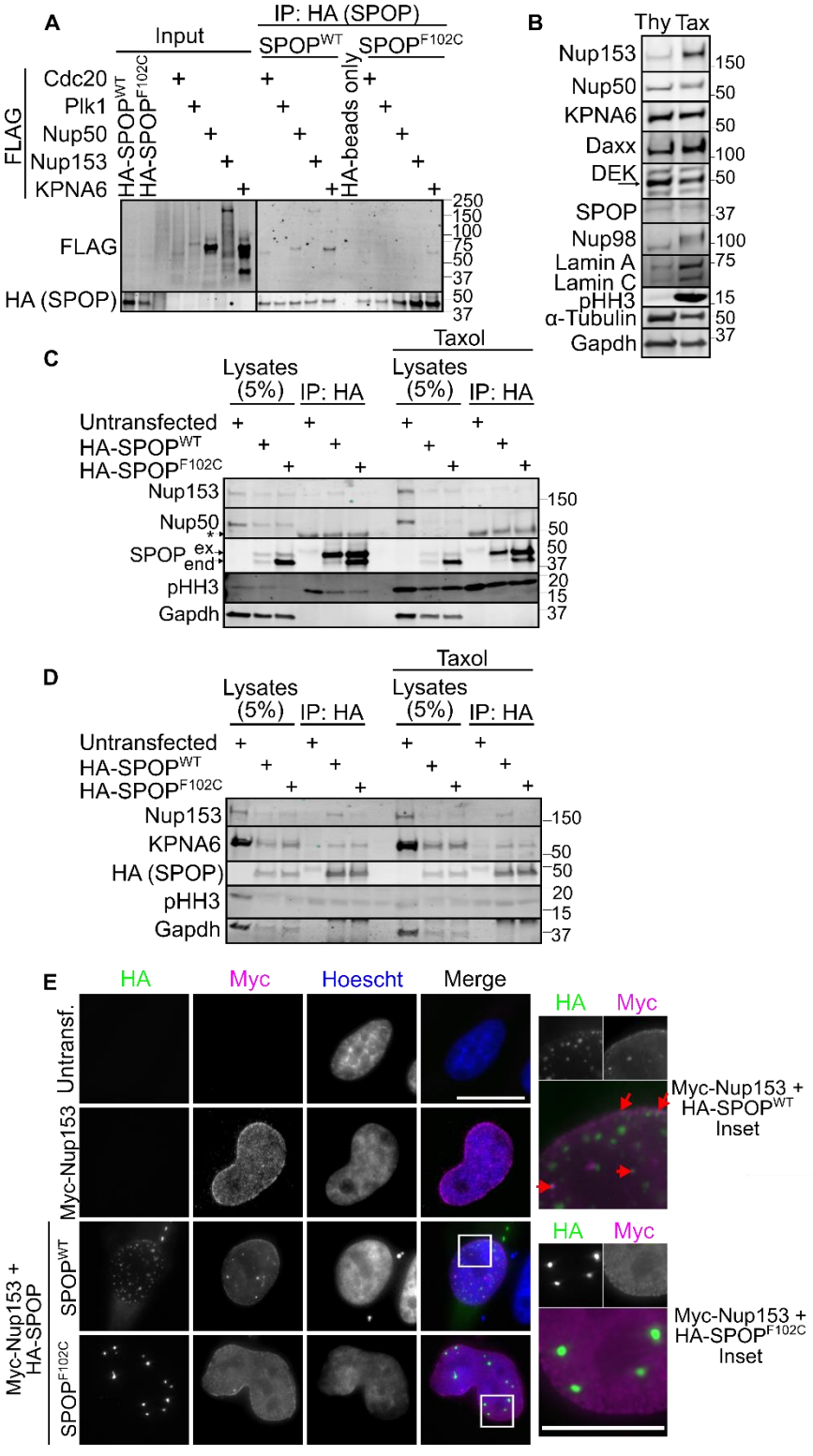

Figure 1. SPOP binds to and colocalizes with Nup153. (A) IVT-expressed HA-SPOP and FLAG-substrates underwent HA-immunoprecipitation to determine which substrates can bind to

SPOP. Cdc20 is used as a known SPOP substrate (positive control) and Plk1 is a negative control. (B) HeLa cells were arrested with 2 mM thymidine (Thy) or 232 nM Taxol (Tax) 17 hours and the lysates were probed for the indicated proteins. pHH3 serves as a mitotic marker. (C, D) HeLa cells were transfected with HA-SPOP and either left asynchronous or treated with 232 nM Taxol. The lysates were subjected to HA-immunoprecipitation and the resulting blots were probed with the indicated antibodies. In (C), *ex* refers to exogenous (HA-tagged) and *end* refers to endogenous SPOP. (E) HeLa cells transfected with Myc-Nup153 and HA-SPOP were imaged (z-stack) after staining with the indicated antibodies. The scale bars in both the full images and the insets are 10 μm.

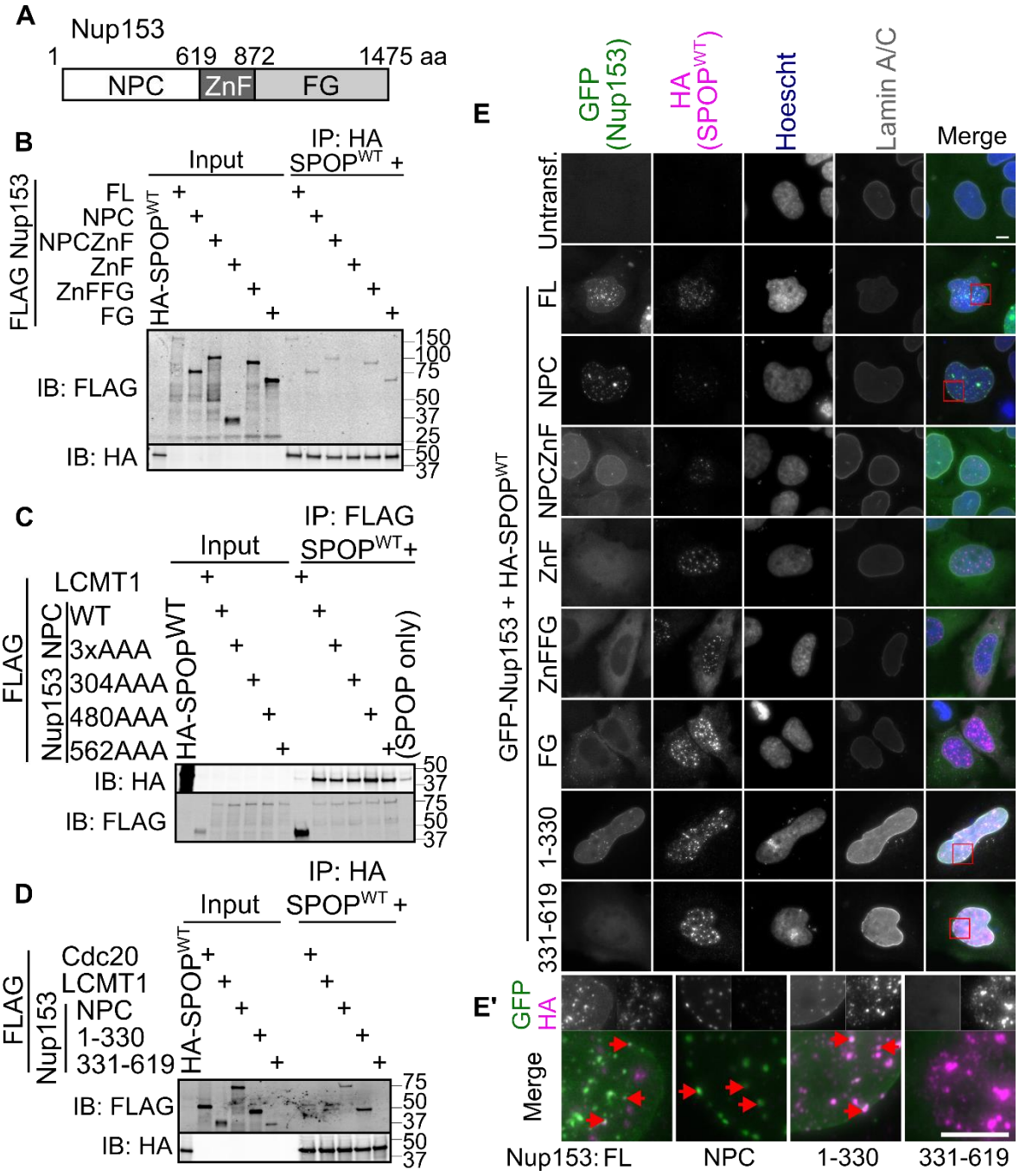

Figure 2. SPOP binds at least to the N-terminal NPC domain of Nup153. (A) Nup153 was truncated according to its domains. (B) IVT-expressed HA-SPOP and FLAG-Nup153 truncations were subjected to HA-immunoprecipitation and the resulting blots probed with HA and FLAG antibodies. (C) IVT-expressed HA-SPOP and FLAG-Nup153 NPC with indicated alanine substitutions were subjected to FLAG-immunoprecipitation and the resulting blots probed with

HA and FLAG antibodies. FLAG-LCMT1 serves as a negative control. SPOP only refers to a condition with HA-SPOP and the FLAG beads (no FLAG tagged protein). (D) Same as (C), except with FLAG-Nup153 NPC, 1-330, or 331-619. FLAG-Cdc20 is used as a known SPOP substrate (positive control). (E) HeLa cells transfected with (GFP) pgLAP1-Nup153 truncations and HA-SPOP were imaged (z-stack) after staining with the indicated antibodies. (E') Insets showing colocalization of HA-SPOP and GFP-Nup153. The scale bars in both the full images and the insets are 10 μm.

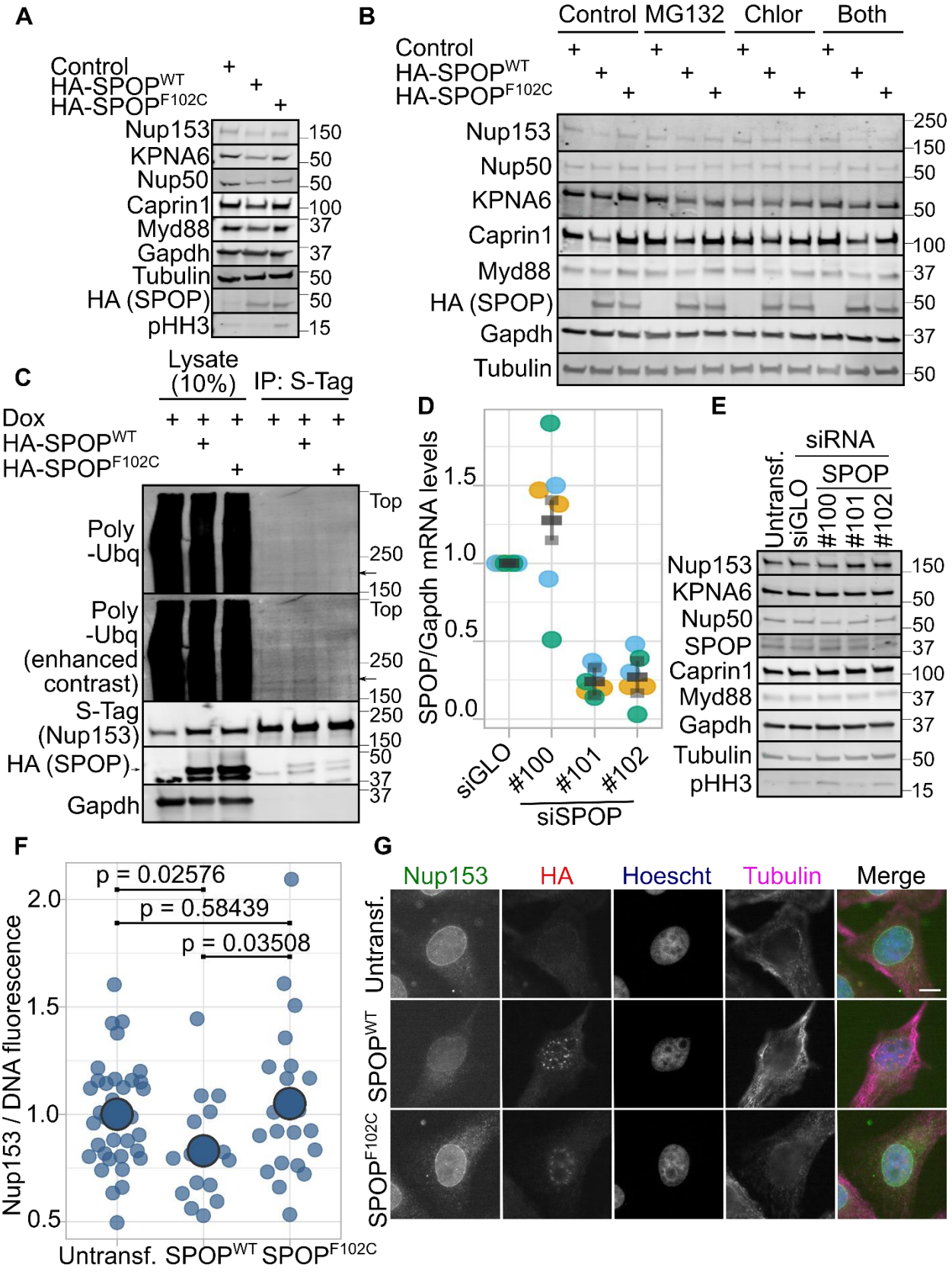
A
Control
HA-SPOP^WT
HA-SPOP^F102C
Nup153
KPNA6
Nup50
Caprin1
Myd88
Gapdh
Tubulin
HA (SPOP)
pHH3
150
50
50
100
37
37
50
50
15
B
Control
MG132
Chlor
Both
Control
HA-SPOP^WT
HA-SPOP^F102C
Nup153
Nup50
KPNA6
Caprin1
Myd88
HA (SPOP)
Gapdh
Tubulin
250
150
50
50
100
37
50
37
50
C
Lysate (10%)
IP: S-Tag
Dox
HA-SPOP^WT
HA-SPOP^F102C
Poly -Ubq
Poly -Ubq (enhanced contrast)
S-Tag (Nup153)
HA (SPOP)
Gapdh
Top
250
150
Top
250
150
250
150
50
37
37
D
SPOP/Gapdh mRNA levels
1.5
1.0
0.5
0.0
siGLO
#100
#101
#102
siSPOP
E
siRNA
Untransf.
siGLO
SPOP
#100
#101
#102
Nup153
KPNA6
Nup50
SPOP
Caprin1
Myd88
Gapdh
Tubulin
pHH3
150
50
50
37
100
37
37
50
15
F
p = 0.02576
p = 0.58439
p = 0.03508
Nup153 / DNA fluorescence
2.0
1.5
1.0
0.5
Untransf.
SPOP^WT
SPOP^F102C
G
Nup153
HA
Hoescht
Tubulin
Merge
Untransf.
SPOP^WT
SPOP^F102C

Figure 3. SPOP degrades Nup153. (A) Immunoblots from lysates from HeLa cells overexpressing HA-SPOP WT or F102C were probed with the indicated antibodies. (B) HeLa cells transfected with HA-SPOP WT or F102C were left untreated, treated with 20 μM of MG132, 50 μM of chloroquine, or both for 5 hours. (C) pgLAP1-Nup153 HeLa cells were transfected HA-SPOP WT or F102C and pgLAP1-Nup153 expression was induced with doxycycline (dox). The lysates were subjected to S-Tag immunoprecipitation and probed with the indicated antibodies. The arrow indicates the location of pgLAP1-Nup153, and *Top* indicates the top of the gel. (D) mRNA levels of SPOP relative to Gapdh, normalized to siGLO, were determined by qPCR in HeLa cells transfected with the indicated siRNAs. Each color corresponds to a different biological replicate, and cDNA from each biological replicate was analyzed twice. Error bars represent the mean and standard deviation. p-values compared to siGLO: siSPOP #100: $p=0.030$; siSPOP #101: $p<0.00001$; siSPOP #102: $p<0.00001$. (E) Immunoblots from lysates from HeLa cells overexpressing HA-SPOP WT or F102C were probed with the indicated antibodies. (F) HeLa cells overexpressing HA-SPOP were imaged (single plane) and the (G) ratio of nuclear Nup153 / nuclear DNA fluorescence was determined using CellProfiler. Untransf., untransfected. Number of cells quantified: untransfected, 36; HA-SPOP^{WT}: 16; HA-SPOP^{F102C}: 21. The scale bar is 10 μm. All p-values in this figure were determined by one-way ANOVA and Tukey-HSD.

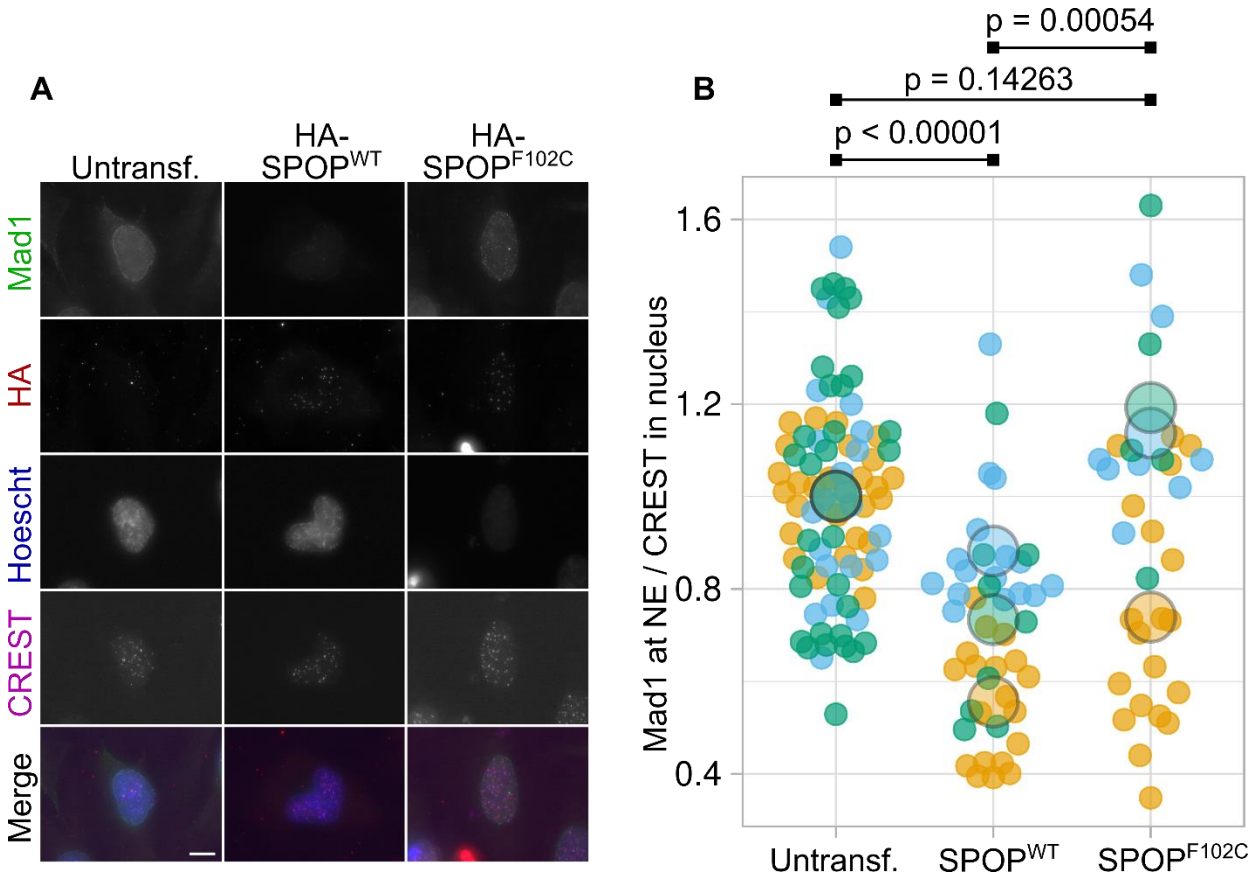

Figure 4. SPOP overexpression reduces Mad1 levels at the nuclear envelope. (A) HeLa cells transfected with HA-SPOP were imaged (z-stack) after staining with the indicated antibodies and the (B) ratio of Mad1 at the nuclear envelope / nuclear CREST fluorescence was determined using CellProfiler. Untransf., untransfected; NE, nuclear envelope. The different colors represent different biological replicates. The large circles are the median of each biological replicate. Total number of cells analyzed: untransfected, 79; $SPOP^{WT}$, 44; $SPOP^{F102C}$, 33. All p-values in this figure were determined by one-way ANOVA and Tukey-HSD. The scale bar is 10 μm.

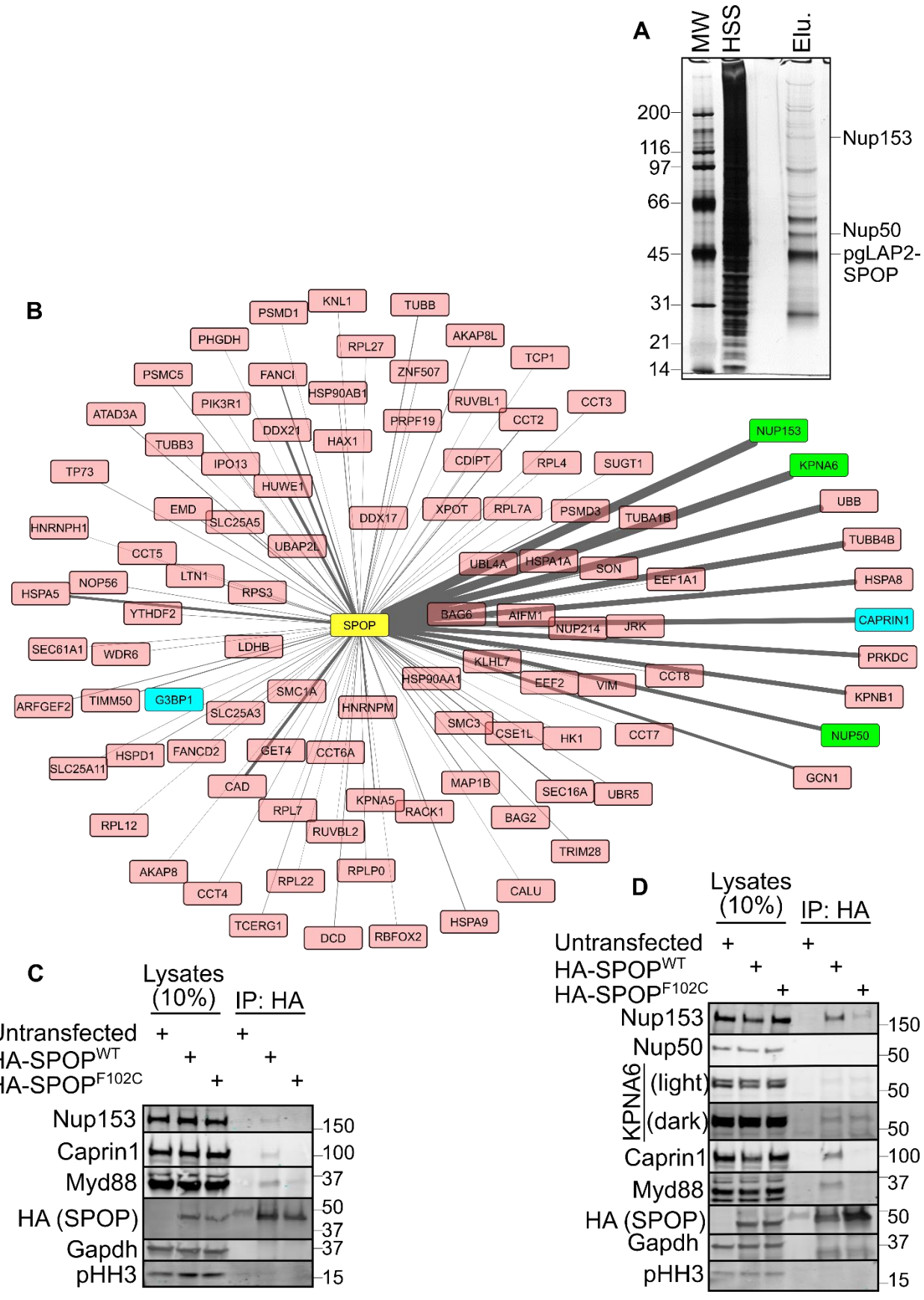
A
MW
HSS
Elu.
200
116
97
66
45
31
21
14
Nup153
Nup50
pgLAP2-SPOP
B
SPOP
NUP153
KPNA6
UBB
TUBB4B
HSPA8
CAPRIN1
PRKDC
KPNB1
NUP50
GCN1
KNL1
TUBB
PSMD1
PHGDH
AKAP8L
RPL27
TCP1
PSMC5
FANCI
ZNF507
HSP90AB1
PIK3R1
RUVBL1
CCT3
ATAD3A
PRPF19
CCT2
DDX21
HAX1
TUBB3
IPO13
CDIPT
RPL4
SUGT1
TP73
HUWE1
EMD
SLC25A5
DDX17
XPOT
RPL7A
PSMD3
TUBA1B
HNRNPH1
CCT5
UBAP2L
UBL4A
HSPA1A
SON
EEF1A1
LTN1
NOP56
RPS3
HSPA5
YTHDF2
BAG6
AIFM1
NUP214
JRK
SEC61A1
WDR6
LDHB
KLHL7
HSP90AA1
EEF2
VIM
CCT8
ARFGEF2
TIMM50
G3BP1
SMC1A
SLC25A3
HNRNPM
SMC3
CSE1L
HK1
CCT7
HSPD1
FANCD2
GET4
CCT6A
SLC25A11
CAD
MAP1B
SEC16A
UBR5
KPNA5
RACK1
RPL7
BAG2
RPL12
RUVBL2
TRIM28
AKAP8
RPL22
RPLP0
CCT4
CALU
TCERG1
DCD
RBFOX2
HSPA9
C
Lysates (10%)
IP: HA
Untransfected + +
HA-SPOP^WT + +
HA-SPOP^F102C + +
Nup153
Caprin1
Myd88
HA (SPOP)
Gapdh
pHH3
150
100
37
50
37
37
15
D
Lysates (10%)
IP: HA
Untransfected + +
HA-SPOP^WT + +
HA-SPOP^F102C + +
Nup153
Nup50
KPNA6 (light)
KPNA6 (dark)
Caprin1
Myd88
HA (SPOP)
Gapdh
pHH3
150
50
50
50
100
37
50
37
15

Supplementary Figure 1. Identification and validation of SPOP-Nup153 binding interaction. (A) Coomassie-stained gel from tandem affinity purification of pgLAP2-SPOP from HEK293 cells. MW, molecular weight marker, given to left in kDa. HSS, high spin supernatant. Elu., elution. Proteins of interest are noted on the right. (B) Cytoscape analysis of proteins detected by mass spectrometry. The thickness of the line is proportional to the peptide count. Known SPOP interactors are in blue, and SPOP interactors focused on in this study are in green. The ten most abundant hits are on the right. (C) Lysates from HeLa cells or (D) from HEK293T cells transfected with the indicated HA-SPOP plasmids were subjected to HA-immunoprecipitation and the resulting blots were probed with the indicated proteins. In (D), light and dark refer to low and high intensity scans. For (C) and (D), molecular weight markers are shown to the right in kDa.

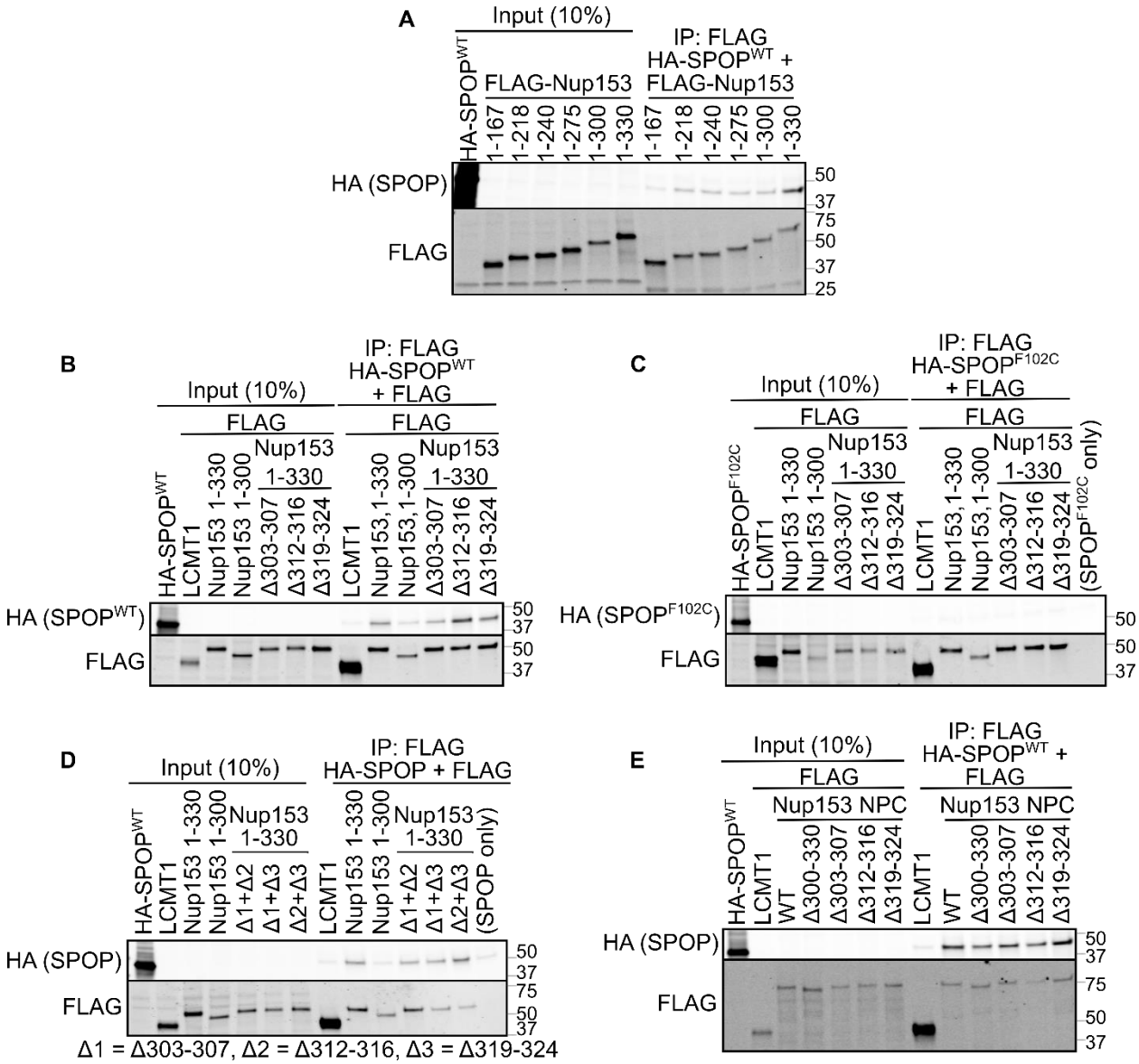

Supplementary Figure 2. SPOP binds to Nup153 1-330 but not Nup153 1-300. (A) IVT-expressed HA-SPOP^{WT} and increasing N-terminal segments of FLAG-Nup153 were subjected to FLAG-immunoprecipitation. (B) IVT-expressed HA-SPOP^{WT} and (C) binding mutant HA-SPOP^{F102C} and FLAG-Nup153 1-330 with single deletions in the 300-330 region were subjected to FLAG-immunoprecipitation. (D) IVT-expressed HA-SPOP^{WT} and FLAG-Nup153 1-330 with double deletions in the 300-330 region were subjected to FLAG-immunoprecipitation. The double deletions in Nup153 are noted below the blot. (E) IVT-expressed HA-SPOP^{WT} and FLAG-Nup153 NPC with single deletions in or the complete deletion of the 300-330 region were

subjected to FLAG-immunoprecipitation. For all blots, FLAG-LCMT1 is used as a negative control, SPOP only refers to HA-SPOP and the FLAG beads (no FLAG-tagged protein), and molecular weight markers are shown to the right in kDa.

Chapter 3: Determination of which KCTD proteins can bind to Cul3

Abstract

Cul3 binds to substrates via a BTB domain-containing substrate adaptor, but which BTB domain-containing proteins can bind to Cul3 and which cannot is unclear. Using the KCTD family of BTB proteins as a model set, we investigated which KCTD proteins can bind to Cul3. Via *in vitro* binding reactions using *in vitro* translated/transcribed proteins and co-immunoprecipitation experiments from HeLa cells, we show that KCTD3, KCTD18 (previously only shown to associate with Cul3 via mass spectrometry), KCTD4 and KCTD19 (unknown as to whether these can associate with Cul3) can bind to Cul3, but KCTD14 cannot. Interpretation of whether KCTD8 can bind to Cul3 was more complicated and requires further validation. We also characterize the localization of these proteins via immunofluorescence microscopy. Overall, our work expands on the knowledge of what BTB proteins can function as Cul3 substrate adaptors.

Materials and Methods

The reagents and experimental procedures are the same as Chapter 2 (SPOP) with the following modifications:

1. For co-transfections of HA-Cul3 and a KCTD protein, twice the amount of DNA for KCTD protein was added relative to HA-Cul3 (for example, 333 ng of KCTD and 167 ng of Cul3)

The primers and plasmids used in this study are found in Supplementary File 1. The FLAG-EGFP construct (pCS2 FLAG S-Tag EGFP) was a gift from PMID: 33865857 (Guo et al., 2021).

Introduction

Cul3 regulates many proteins via a BTB domain-containing substrate adaptor (Cheng et al., 2018). There are about 400 BTB domain-containing proteins in the human genome, and which one of these can function as Cul3 substrate adaptors is not known (Liu et al., 2013). To identify new substrate adaptors of Cul3, we performed mass spectrometry. Tandem-affinity purification of HEK293 cells expressing pgLAP2 Cul3 revealed a number of BTB proteins that may be potential Cul3 substrate adaptors (Figure 1A). For these BTB proteins, the sequences for the BTB domains were aligned in Clustal Omega and a phylogenetic tree was generated (using EMBL-EBI Simple Phylogeny tool) (Sievers and Higgins, 2018) (Figure 1B). From the phylogenetic analysis, we identified three main classes of BTB proteins that co-purified with Cul3. We generated amino acid conservation images (Crooks et al., 2004) for these three different clades and superimposed secondary structural elements predicted from PsiPred (McGuffin et al., 2000) (Figure 1C). Class 2, which primarily composes the KCTD family of proteins, has a unique protein sequence within the BTB domain.

The KCTD family of proteins are generally poorly characterized at a molecular level, but mutations of these proteins are nonetheless implicated in a number of neurodevelopmental and neurological disorders (Teng et al., 2019). Broadly, the KCTD proteins are predominantly expressed in neurons and regulate different signaling pathways including Wnt, Sonic hedgehog, and GABA signaling (Liu et al., 2013), and misregulation of KCTD proteins has been implicated in cancer progression (Angrisani et al., 2021). KCTD proteins tend to form oligomers (usually, but not necessarily, tetramers or pentamers), and those that can bind Cul3 bind an equivalent molar amount of Cul3 (for example, a pentamer of KCTD proteins will bind five Cul3 proteins) (Ji et al., 2016; Smaldone et al., 2015; Pinkas et al., 2017).

Most, but not all, KCTD proteins can bind to Cul3. For example, KCTD1, KCTD16, KCTD12, and KCTD15 have been shown not to bind to Cul3 via biophysical experiments such as isothermal calorimetry or analytical size exclusion chromatography (Ji et al., 2016; Smaldone et al., 2015; Pinkas et al., 2017). Interestingly, KCTD12 was shown to associate with Cul3 in

one mass spectrometry experiment (Bennett et al., 2010), creating an inconsistency within our knowledge of Cul3-binding KCTD proteins. KCTD5, KCTD9, KCTD10, the long isoform of KCTD11, KCTD13, KCTD17, and SHKBP1 have all been shown to bind to Cul3 via a biophysical experiment (Ji et al., 2016; Smaldone et al., 2015; Pinkas et al., 2017). BACD2, KCTD2, KCTD3, KCTD6, KCTD7, KCTD18, and KCTD21 have all been shown to associate with Cul3, but only via mass spectrometry (that is, these results are not supported by a biophysical experiment). Finally, KCTD4, KCTD8, KCTD14, and KCTD19 have neither been identified as potential Cul3-interacting proteins via mass spectrometry, nor have they been ruled out as potential Cul3-interacting proteins via a biophysical experiment.

Given that the KCTD family of proteins is generally poorly molecularly characterized, is relatively small (about 25 protein members) and thus would serve as a good set to examine in its entirety, and has both some preliminary information and some controversy as to which KCTD proteins can bind to Cul3, we set out to determine which KCTD proteins can bind to Cul3. We chose the following KCTD proteins to test Cul3 binding: KCTD9 (positive control); KCTD1 (negative control); KCTD12 (controversial); KCTD4, KCTD8, KCTD14, and KCTD19 (all poorly characterized); KCTD3 and KCTD18 (only validated as Cul3-binding via mass spectrometry via other groups and our results here but not validated via biophysical studies). Our results expand the suite of Cul3 substrate adaptors and may assist in the identification of novel substrates of these new Cul3 substrate adaptors.

Results

To identify which KCTD proteins can bind to Cul3, we expressed each KCTD protein as an IVT protein and subjected them to HA-immunoprecipitations with HA-Cul3. We opted for this approach first because there is the possibility that KCTD proteins can oligomerize with each other; using the IVT-expression system to avoid a situation where KCTD proteins could form

“mix and match” oligomers simplified our analysis. In this way, we observed KCTD4, KCTD18, KCTD3, KCTD8, and KCTD19 all bound to Cul3 (Figure 2A and 2B).

To further validate our results, we performed the same co-immunoprecipitation reactions but from lysates prepared from HeLa cells co-transfected with HA¬-Cul3 and a FLAG-tagged KCTD protein. Again, we observed that KCTD9, KCTD4, KCTD18, KCTD3, and KCTD19 were able to co-immunoprecipitate HA-Cul3 (Figure 3A and 3B). Interestingly, in contrast with the results obtained via IVT-expressed protein, KCTD8 was not able to co-immunoprecipitate HA-Cul3 (Figure 3B). We repeated the experiment but with HA-Cul3 and a C-terminally GFP-tagged KCTD protein (KCTD-GFP) (Figure 4A and 4B). In this case, KCTD8 was able to co-immunoprecipitate HA-Cul3 (Figure 4B). Whether KCTD8 can actually bind Cul3 thus remains an open question. While artifacts due to protein tags are well established, it is unclear as to why the smaller FLAG-tag would disfavor Cul3-KCTD8 binding while the larger GFP-tag would promote it. Perhaps the N-terminal FLAG tag, despite being relatively small, prohibits BTB-mediated oligomerization in KCTD8 (which is also at the N-terminus in KCTD8) necessary for Cul3-binding.

To clarify whether KCTD8 can actually bind to Cul3, we examined the localization of Cul3 and the KCTD proteins in HeLa cells (Figure 5). Transfection of Cul3 only showed that Cul3 has a moderate nuclear localization and weaker cytoplasmic localization. KCTD1, KCTD3, KCTD4, KCTD9, KCTD12, and KCTD14 all have a prominent cytoplasmic localization. The cytoplasmic localization does not seem to correlate with the KCTD’s ability to bind to Cul3; for example, KCTD1, which does not bind to Cul3, and KCTD9, which does bind to Cul3, both are cytoplasmic whereas Cul3 is nuclear. Interestingly, KCTD18 and KCTD19, which both do bind Cul3, are nuclear proteins. Sequence analysis of KCTD18 and KCTD19 did not show any obvious nuclear localization signals (Nguyen Ba et al., 2009), although some basic regions were identified (for KCTD18, ^{311}RKRR^{314} and ^{377}RRKAAQR^{383}; for KCTD19, ^{779}PPKRAG^{784}) that may

serve as nuclear localization signals. Finally, KCTD8 was observed to form filaments within the cytoplasm. Tubulin filaments formed similar structures as these KCTD8 filaments.

Discussion

There are roughly 600 E3 ubiquitin ligases and their associated proteins. Most of these ubiquitin ligases are “orphan” ligases in that they have no known substrates. Here, we have identified a number of putative Cul3 KCTD proteins that may serve as substrate adaptors for Cul3. This work helps complete our understanding of Cul3-KCTD ubiquitin-mediated regulation in cell biology.

The work presented here takes a molecular biology approach. Structural and computational approaches would both strengthen the results presented here: namely, instead of asking which KCTD proteins can bind to Cul3, these approaches would allow us to ask why can some KCTD proteins bind to Cul3 and some cannot? Information contained within the three-dimensional structure and information that can be gleamed from the primary amino acid sequence may be of use to make rules as to what determines whether a KCTD protein is a Cul3-binding substrate adaptor or not. For example, previous work has identified that Cul3 interacts with its substrate adaptors via a negatively charged patch on Cul3, so BTB domain-containing proteins tend to have a corresponding positive patch. Preliminary work that examines the charge of each predicted Cul3-binding interface suggests that charge is one element that can be used to form rules as to which KCTD protein can bind to Cul3. Given that KCTD proteins bind to Cul3 using two interfaces – Cul3 is “sandwiched” between two KCTD molecules in the oligomer such that the back of Cul3 touches both the front of one KCTD protein and the front of Cul3 touches the back of another KCTD protein (Ji et al., 2016) – structural information would allow for better identification of where the positive charges would accumulate and how they would present a proper binding patch in the KCTD surface. Computational approaches that can identify what other elements, besides charges, may contribute to this binding interaction.

Given that it is unclear whether these KCTD proteins can “mix and match” in their oligomers (for example, a KCTD9-KCTD5 pentamer), Cul3-binding experiments should be performed with caution, as a non-binding KCTD protein may appear to be a binding protein if it can associate with a Cul3-binding KCTD oligomer (say, a KCTD1-KCTD9 pentamer). Whether or not these “mix and match” oligomers can form is an interesting question; thus far, structural and biophysical studies that have examined the composition of KCTD oligomers have only expressed and purified one species of KCTD protein at a time.

KCTD8 was observed to form curvy filaments that resemble intermediate filaments, like vimentin (Duarte et al., 2019). Whether or not KCTD8 associates with intermediate filaments is an interesting question, particularly given the role of intermediate filaments in neuronal development, maintenance, and disease progression (Bott and Winckler, 2020) and the known roles of these KCTD proteins in neurological diseases.

References

Angrisani, A., A. Di Fiore, E. De Smaele, and M. Moretti. 2021. The emerging role of the KCTD proteins in cancer. Cell Commun. Signal. 19. doi:10.1186/S12964-021-00737-8.

Bennett, E.J., J. Rush, S.P. Gygi, and J.W. Harper. 2010. Dynamics of cullin-RING ubiquitin ligase network revealed by systematic quantitative proteomics. Cell. 143:951–65. doi:10.1016/j.cell.2010.11.017.

Bott, C.J., and B. Winckler. 2020. Intermediate filaments in developing neurons: Beyond structure. Cytoskeleton. 77:110–128. doi:10.1002/cm.21597.

Cheng, J., J. Guo, Z. Wang, B.J. North, K. Tao, X. Dai, and W. Wei. 2018. Functional analysis of Cullin 3 E3 ligases in tumorigenesis. Biochim. Biophys. Acta - Rev. Cancer. 1869:11–28. doi:10.1016/J.BBCAN.2017.11.001.

Crooks, G.E., G. Hon, J.-M. Chandonia, and S.E. Brenner. 2004. WebLogo: a sequence logo generator. Genome Res. 14:1188–90. doi:10.1101/gr.849004.

Duarte, S., Á. Viedma-Poyatos, E. Navarro-Carrasco, A.E. Martínez, M.A. Pajares, and D. Pérez-Sala. 2019. Vimentin filaments interact with the actin cortex in mitosis allowing normal cell division. Nat. Commun. 10:4200. doi:10.1038/s41467-019-12029-4.

Guo, X., I. Ramirez, Y.A. Garcia, E.F. Velasquez, A.A. Gholkar, W. Cohn, J.P. Whitelegge, B. Tofig, R. Damoiseaux, and J.Z. Torres. 2021. DUSP7 regulates the activity of ERK2 to promote proper chromosome alignment during cell division. J. Biol. Chem. 296. doi:10.1016/J.JBC.2021.100676.

Ji, A.X., A. Chu, T.K. Nielsen, S. Benlekbir, J.L. Rubinstein, and G.G. Privé. 2016. Structural Insights into KCTD Protein Assembly and Cullin3 Recognition. J. Mol. Biol. 428:92–107. doi:10.1016/J.JMB.2015.08.019.

Liu, Z., Y. Xiang, and G. Sun. 2013. The KCTD family of proteins: structure, function, disease relevance. Cell Biosci. 3. doi:10.1186/2045-3701-3-45.

McGuffin, L.J., K. Bryson, and D.T. Jones. 2000. The PSIPRED protein structure prediction server. Bioinformatics. 16:404–5. doi:10.1093/bioinformatics/16.4.404.

Nguyen Ba, A.N., A. Pogoutse, N. Provart, and A.M. Moses. 2009. NLStradamus: a simple Hidden Markov Model for nuclear localization signal prediction. BMC Bioinformatics. 10:202. doi:10.1186/1471-2105-10-202.

Pinkas, D.M., C.E. Sanvitale, J.C. Bufton, F.J. Sorrell, N. Solcan, R. Chalk, J. Doutch, and A.N. Bullock. 2017. Structural complexity in the KCTD family of Cullin3-dependent E3 ubiquitin ligases. Biochem. J. 474:3747–3761. doi:10.1042/BCJ20170527.

Sievers, F., and D.G. Higgins. 2018. Clustal Omega for making accurate alignments of many protein sequences. Protein Sci. 27:135–145. doi:10.1002/pro.3290.

Smaldone, G., L. Pirone, N. Balasco, S. Di Gaetano, E.M. Pedone, and L. Vitagliano. 2015. Cullin 3 Recognition Is Not a Universal Property among KCTD Proteins. PLoS One. 10. doi:10.1371/JOURNAL.PONE.0126808.

Teng, X., A. Aouacheria, L. Lionnard, K.A. Metz, L. Soane, A. Kamiya, and J.M. Hardwick. 2019. KCTD: A new gene family involved in neurodevelopmental and neuropsychiatric disorders. CNS Neurosci. Ther. 25:887–902. doi:10.1111/CNS.13156.

Figures and figure legends

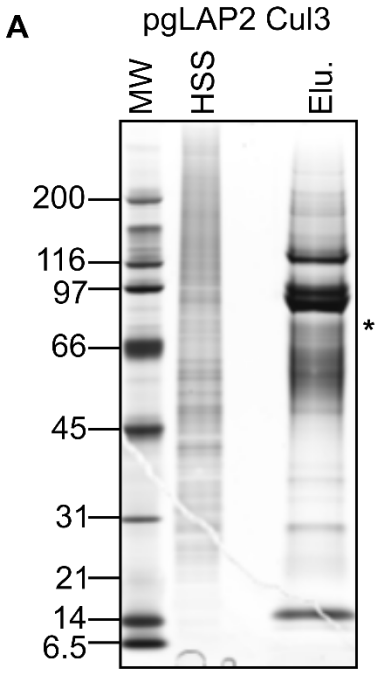

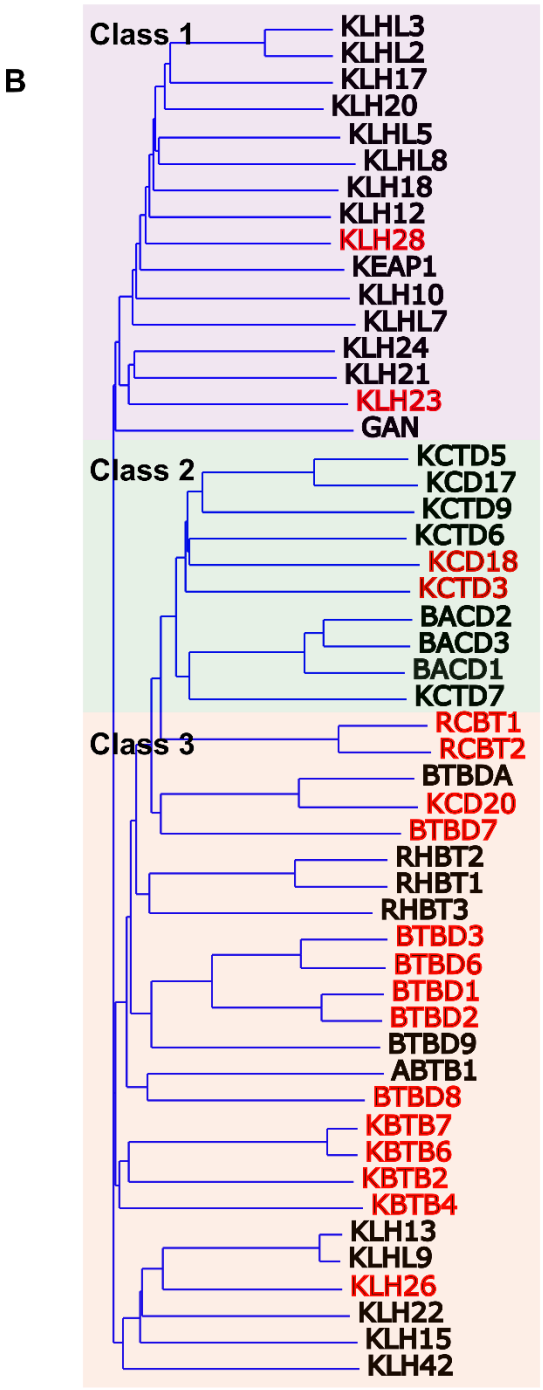

C

sheet helix coil Cul3 binding loop

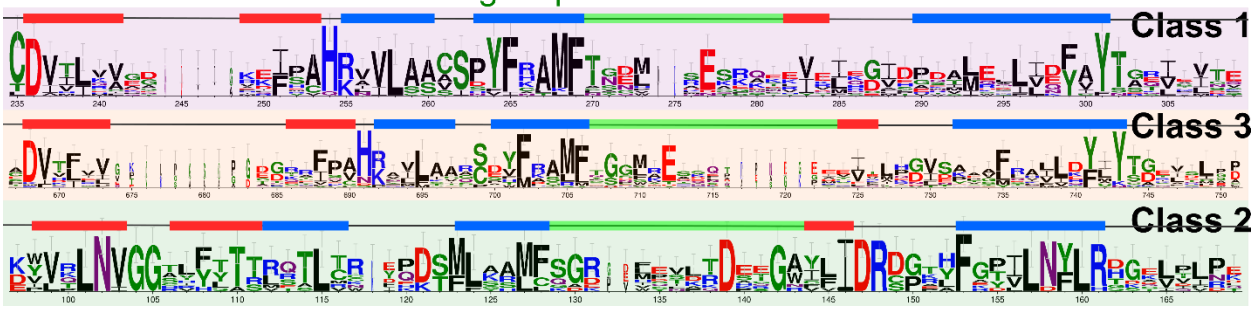

Figure 1. Mass spectrometry of Cul3 identifies novel potential BTB substrate adaptors. (A) Coomassie-stained gel of tandem-affinity purification of pgLAP2-Cul3 from HEK293 cells. MW, molecular weight marker, given to left in kDa. HSS, high spin supernatant. Elu., elution. pgLAP2 Cul3 is marked with an asterisk. (B) Phylogenetic tree of BTB domain-containing proteins identified via mass spectrometry. KCTD proteins in red are KCTD proteins which have not been validated as Cul3 binding partners. (C) Sequence alignment of BTB domains from proteins identified via mass spectrometry. Above the sequence alignment is the secondary structure predicted by PsiPred.

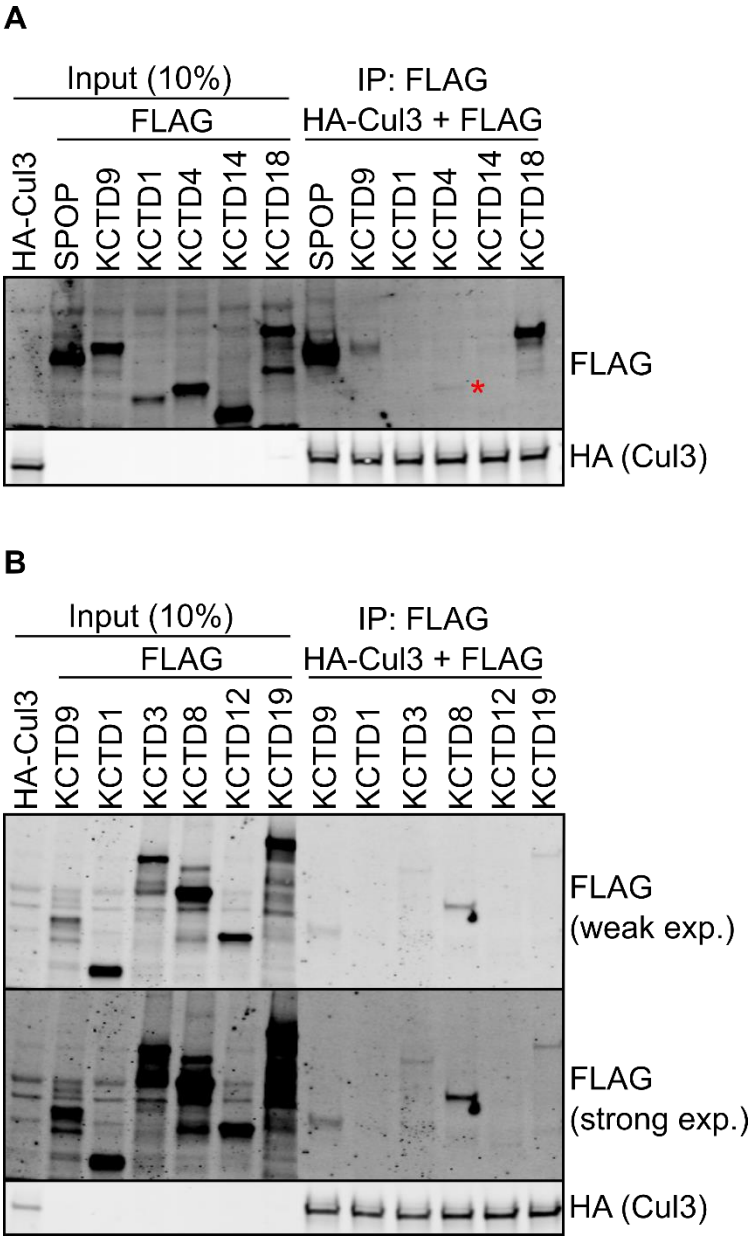

Figure 2. IVT-expressed Cul3 binds to FLAG-KCTD4, KCTD18, KCTD3, KCTD8, and KCTD19. In both (A) and (B), the indicated IVT-expressed proteins were subjected to FLAG-immunoprecipitation and the resulting blots probed with the indicated proteins. In (A), SPOP is used as a positive control (binds to Cul3) and the red asterisk denotes the KCTD4 band. In both, KCTD9 is used as a positive control (binds to Cul3) and KCTD1 is used as a negative control (does not bind to Cul3). In (B), weak or strong exp. (exposure) refers to the low or high intensity scans.

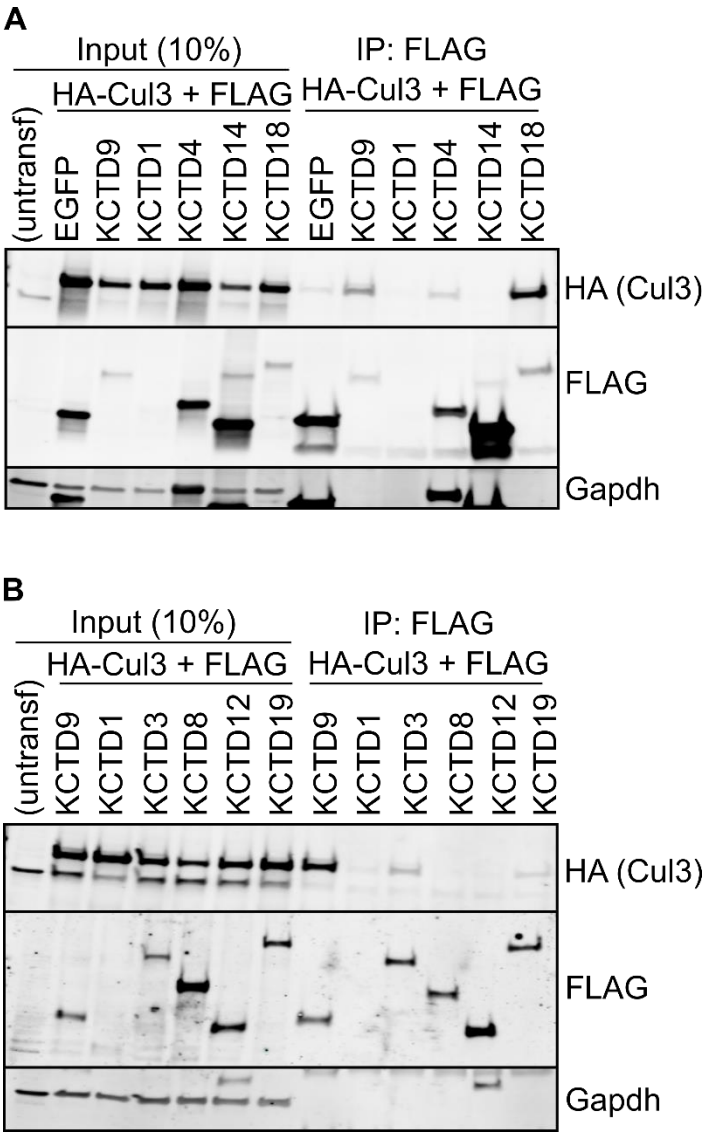

Figure 3. Cul3 co-immunoprecipitates with FLAG-KCTD4, KCTD18, KCTD3, and KCTD19, but not FLAG KCTD8. In both (A) and (B), cell lysates from HeLa cells co-transfected with HA-Cul3 and the indicated FLAG-KCTD proteins were subjected to FLAG-immunoprecipitation and the resulting blots were probed with the indicated proteins. In (A), EGFP serves as a negative control. Because the blots were not stripped between probing with different antibodies, the FLAG bands are still present in the Gapdh images. In both, KCTD9 is used as a positive control (binds to Cul3) and KCTD1 is used as a negative control (does not bind to Cul3).

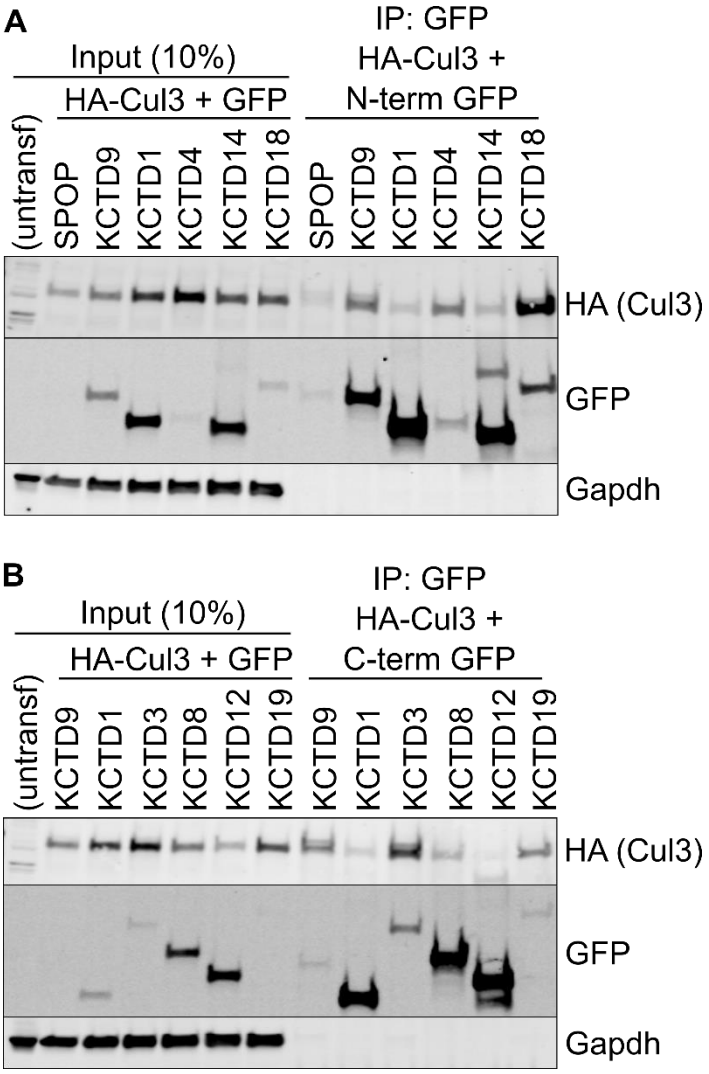

Figure 4. Cul3 co-immunoprecipitates with GFP-KCTD4, KCTD18, KCTD3, KCTD8, and KCTD19. In both (A) and (B), cell lysates from HeLa cells co-transfected with HA-Cul3 and the indicated GFP-KCTD proteins were subjected to GFP-immunoprecipitation and the resulting blots were probed with the indicated proteins. In (A), SPOP serves as a positive control. In both, untransf. refers to an untransfected cell lysate, KCTD9 is used as a positive control (binds to Cul3), and KCTD1 is used as a negative control (does not bind to Cul3).

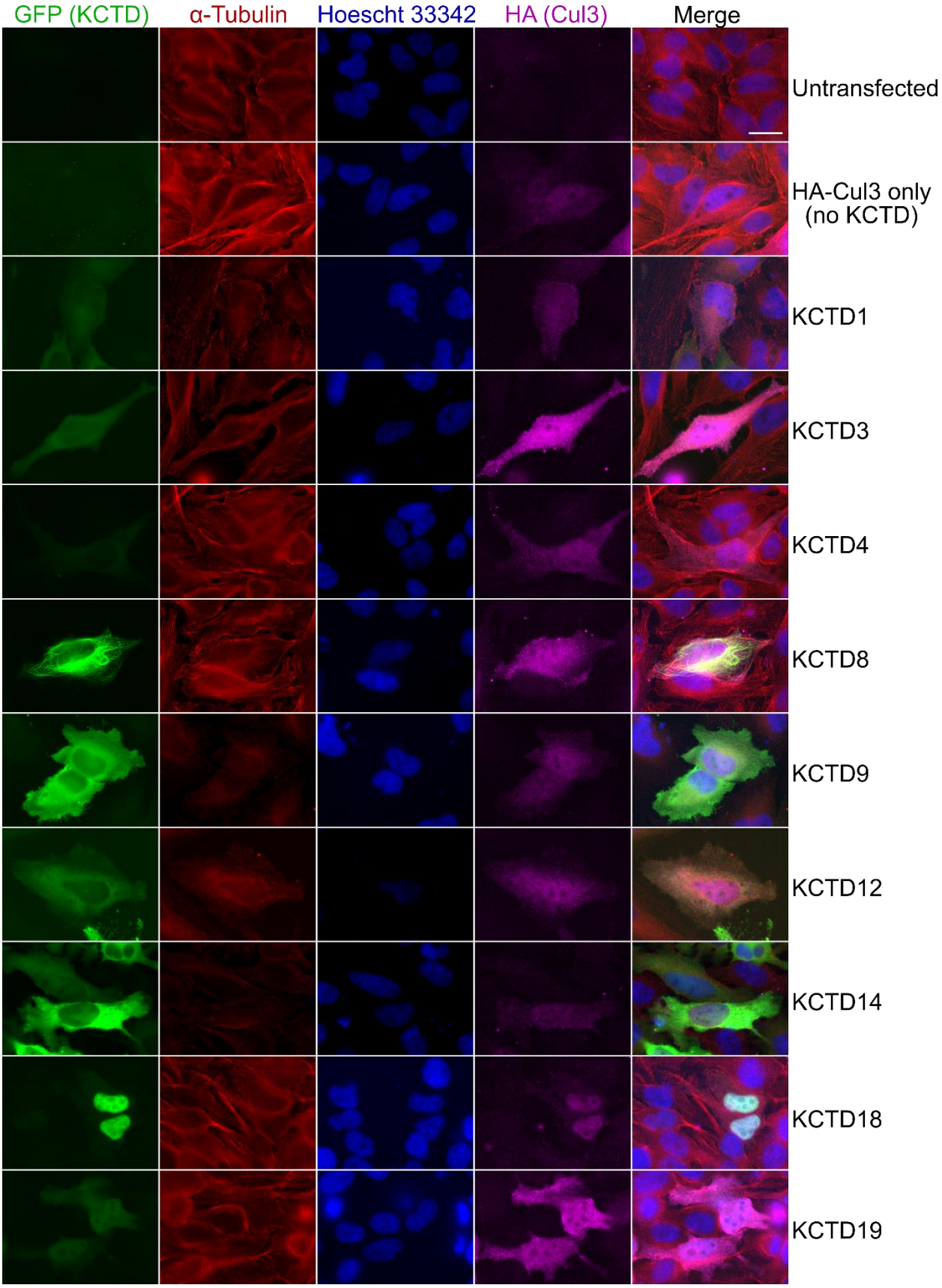
GFP (KCTD)
α-Tubulin
Hoescht 33342
HA (Cul3)
Merge
Untransfected
HA-Cul3 only (no KCTD)
KCTD1
KCTD3
KCTD4
KCTD8
KCTD9
KCTD12
KCTD14
KCTD18
KCTD19

Figure 5. Cul3 shares the same localization as some KCTD proteins. HeLa cells were transfected with plasmids encoding for HA-Cul3 and pgLAP1-KCTD and stained with the indicated antibodies. The scale bar is 20 μm.

Chapter 4: Phosphorylation regulates mitotic spindle assembly

This chapter is reproduced from

> Joseph Y. Ong, Michelle C. Bradley, and Jorge Z. Torres. Phospho-regulation of Mitotic Spindle Assembly. Cytoskeleton (Hoboken). 2020 Dec;77(12):558-578. doi: 10.1002/cm.21649. PMID: 33280275

This chapter introduces phosphorylation and the protein kinases that regulate many aspects of mitotic spindle assembly and cell cycle progression.

Received: 6 August 2020 | Revised: 8 October 2020 | Accepted: 2 December 2020
DOI: 10.1002/cm.21649

REVIEW ARTICLE

WILEY

Phospho-regulation of mitotic spindle assembly

Joseph Y. Ong[1] | Michelle C. Bradley[1] | Jorge Z. Torres[1,2,3]

[1]Department of Chemistry and Biochemistry, University of California, Los Angeles, California
[2]Molecular Biology Institute, University of California, Los Angeles, California
[3]Jonsson Comprehensive Cancer Center, University of California, Los Angeles, California

Correspondence
Jorge Z. Torres, Department of Chemistry and Biochemistry, University of California, 607 Charles E. Young Drive East, Los Angeles, CA 90095.
Email: torres@chem.ucla.edu

Funding information
Division of Graduate Education, Grant/Award Number: DGE-1650604; Division of Molecular and Cellular Biosciences, Grant/Award Number: MCB1912837; National Institute of General Medical Sciences, Grant/Award Numbers: GM007185, R01GM117475

Abstract

The assembly of the bipolar mitotic spindle requires the careful orchestration of a myriad of enzyme activities like protein posttranslational modifications. Among these, phosphorylation has arisen as the principle mode for spatially and temporally activating the proteins involved in early mitotic spindle assembly processes. Here, we review key kinases, phosphatases, and phosphorylation events that regulate critical aspects of these processes. We highlight key phosphorylation substrates that are important for ensuring the fidelity of centriole duplication, centrosome maturation, and the establishment of the bipolar spindle. We also highlight techniques used to understand kinase–substrate relationships and to study phosphorylation events. We conclude with perspectives on the field of posttranslational modifications in early mitotic spindle assembly.

KEYWORDS
centriole, centromere, centrosome, kinase, kinetochore, microtubules, mitotic spindle

1 | INTRODUCTION

The faithful congression and segregation of chromosomes during mitosis requires the assembly and regulation of a large and complex microtubule-based structure called the mitotic spindle. Numerous proteins with structural and signaling roles coordinate to assemble and regulate the mitotic spindle (Prosser & Pelletier, 2017). Importantly, these spindle components are often regulated by posttranslational modifications such as phosphorylation and ubiquitylation that allow for precise spatial and temporal control over their activity (Ong & Torres, 2019). The preparations for mitotic spindle assembly initiate during S phase where centrioles must duplicate and recruit and assemble the appropriate factors to mature into centrosomes (Nigg & Holland, 2018). The centrosomes then disjoin and move to opposite ends of the cell where they will serve as the spindle poles for the bipolar spindle. Subsequently, in early mitosis, the spindle poles nucleate and form the microtubule spindle, which promotes kinetochore-microtubule attachments and the alignment of the chromosomes at the cell mid-plane for cell division (Prosser & Pelletier, 2017). The synchronization and execution of these processes is highly regulated and necessary for faithful cell division, and their dysregulation can lead to chromosomal instability (Maniswami et al., 2018), apoptosis (Steegmaier et al., 2007; Torres et al., 2011), and aneuploidy (Kang et al., 2006; Tan, Caro, Potnis, Lanza, & Slawson, 2013; Yasui et al., 2004). Understanding how centrosomes, microtubule-associated proteins, and the mitotic spindle are regulated are important avenues toward understanding diseases like aging (Fu et al., 2008; Macedo et al., 2018) and cancer (Gordon, Resio, & Pellman, 2012).

Kinases are critical for regulating proteins that have essential roles in early spindle assembly through their ability to transfer phosphate groups onto their substrates to modulate protein activity (Arquint & Nigg, 2016; Johnson & Hunter, 2005; Joukov & De Nicolo, 2018). In particular, phosphorylation regulates centriole duplication and procentriole elongation in S phase, centrosome maturation, disjunction, and separation in G2 phase, and microtubule nucleation and spindle assembly in late G2 and early M phase (Figure 1) (Arquint & Nigg, 2016; Carmena, Wheelock, Funabiki, & Earnshaw, 2012; Johmura et al., 2011; Mardin et al., 2010; Prosser & Pelletier, 2017). Here, we review the activation and roles of the key kinases Plk4, Plk1, Aurora A, Aurora B, and Cdk1, the key

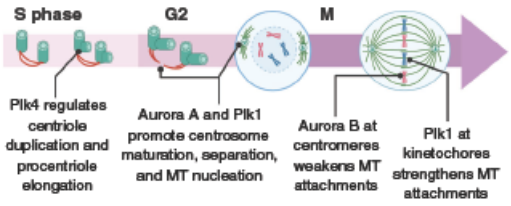

FIGURE 1 Kinases regulate early mitotic spindle assembly. Key kinases, including Plk4, Aurora A, Plk1, and Aurora B regulate aspects of centriole duplication, centrosome maturation, and spindle assembly throughout the cell cycle [Color figure can be viewed at wileyonlinelibrary.com]

phosphatases PP1 and PP2A, and substrates of these enzymes as they function to promote mitotic spindle assembly from S phase to early M phase (Table 1). We discuss useful techniques for understanding the kinase–substrate relationship and identifying and characterizing phosphorylation sites and conclude with perspectives on future avenues into understanding the roles of phosphorylation and other posttranslational modifications on spindle assembly.

2 | CENTRIOLE DUPLICATION AND PROCENTRIOLE ELONGATION

The centrioles are rod-shaped microtubule-based structures that form the core of the future centrosome (Nigg & Holland, 2018). Before S phase, a cell has two centrioles connected by a protein linker (Bahe et al., 2005). During S phase, an emerging procentriole will form at the base of each centriole, eventually forming two centriole pairs (Ohta et al., 2014). Each centriole pair will subsequently serve as one of the two poles of the bipolar spindle (Mardin et al., 2011). Plk4 is a key regulator of centriole biogenesis (Nigg & Holland, 2018) and is recruited to nascent centrioles through its binding to the centriolar proteins Cep152 and Cep192 (Kim et al., 2013; Sonnen, Gabryjonczyk, Anselm, Nigg, & Stierhof, 2013) (Figure 2). Although Plk4 phosphorylates Cep152, which residue(s) it phosphorylates and the importance of this modification is unknown (Hatch et al., 2010). At the centrioles, Plk4 binds STIL, a protein marker for the site of procentriole elongation, activating Plk4 kinase activity via autophosphorylation of its T-loop on Thr170 (Moyer et al., 2015). Once activated, Plk4 phosphorylates STIL at Ser1108 and Ser1116 (Moyer et al., 2015; Moyer & Holland, 2019). These modifications are required for maintaining STIL localization at the centriole (Moyer et al., 2015) and for downstream recruitment of Sas6 (Ohta et al., 2014), which forms the symmetric core of the centriole. Plk4 also phosphorylates STIL at Ser428 (Dzhindzhev et al., 2017; Moyer & Holland, 2019), which promotes the binding of STIL with CPAP, a protein involved in procentriole elongation, and connects the growing microtubule cartwheel to the centriole wall (Moyer & Holland, 2019). While Plk4 is necessary upstream of Sas6, it remains unknown whether Plk4 modifies Sas6 in mammals. In *Caenorhabditis elegans*, Zyg-1 (the ortholog of Plk4) phosphorylates Sas6 at Ser123, to promote centriole formation (Kitagawa et al., 2009). However, this residue is not conserved in the human sequence of Sas6. Beyond its roles in centriole biogenesis, Plk4 also has roles in recruiting the γ-tubulin ring complex (γ-TuRC), a key protein involved in microtubule nucleation, to the centrosome. GCP6 is a member of the γ-TuRC complex and a substrate of Plk4 (Bahtz et al., 2012). Plk4 phosphorylates GCP6 on at least 10 residues throughout the sequence, and these modifications may be required for centriole duplication (Bahtz et al., 2012).

Plk4 protein levels are precisely regulated by posttranslational modifications (Rogers et al., 2009) and misregulation of Plk4 is associated with tumorigenesis (Maniswami et al., 2018). Overexpression of Plk4 leads to centriole over-duplication, whereas loss of Plk4 leads to a reduction in centriole number (Arquint & Nigg, 2016; Habedanck, Stierhof, Wilkinson, & Nigg, 2005; Kleylein-Sohn et al., 2007). Both overexpression and underexpression of Plk4 are characteristic of numerous types of cancers. Plk4 autophosphorylates itself at Ser698, Ser700, Thr704, and Thr707 to promote the formation of phase separated condensates (Park et al., 2019). These condensates localize and concentrate Plk4 and exclude its ubiquitin ligase, β-TrCP, promoting Plk4's stability (Gouveia et al., 2019; Park et al., 2019). Moreover, Plk4 autophosphorylates itself in *trans* at Ser285 and Thr289 (Cunha-Ferreira et al., 2013; Guderian, Westendorf, Uldschmid, & Nigg, 2010). Phosphorylation of these residues generates a phosphodegron recognized by β-TrCP and promotes Plk4 degradation in S and G2 phases (Cunha-Ferreira et al., 2013; Guderian et al., 2010). In *Drosophila melanogaster*, Slimb (β-TrCP ortholog) binding to Plk4 at the centrosome is antagonized by the phosphatase PP2A-Twins, as PP2A-Twins dephosphorylates Plk4, presumably removing the phosphodegron and promoting Plk4 stability (Brownlee et al., 2011). There is no obvious mammalian ortholog of the *Drosophila* PP2A regulatory B subunit Twins in mammalian systems. However, Cdc14B is a likely candidate as a regulator of Plk4 activity, as it localizes to the centrosomes and loss of Cdc14B activity leads to centriole amplification (Wu et al., 2008). As Plk4 localization and concentration both drive Plk4 kinase activity and degradation (autophosphorylation in *trans* both increases kinase activity and recognition by β-TrCP), Plk4 levels and activity are tightly regulated. For example, lysine acetylation on Plk4 at Lys45 and Lys46 by acetyltransferases KAT2A and KAT2B are thought to induce structural changes that inactivate Plk4's kinase activity (Fournier et al., 2016).

3 | CENTROSOME MATURATION AND EARLY SPINDLE POLE ASSEMBLY

To become competent for nucleating mitotic spindle microtubules, centrosomes must undergo a maturation process where they accumulate pericentriolar material (PCM) and recruit the γ-TuRC. These two factors nucleate new microtubules and recruit microtubule-associated proteins for microtubule organization, growth, and stability. The Aurora A kinase regulates many proteins with roles in centrosome maturation, spindle pole assembly, and mitotic spindle integrity

TABLE 1 Summary of kinases, substrates, and phosphatases in mitotic spindle assembly

Kinase	Key substrates	Substrate function	Consequence of phosphorylation	Relevant phosphatases
Centriole duplication and procentriole elongation				
Plk4	Plk4 (*in trans*)	Master kinase involved in centriole duplication and elongation in G1/S	Promotes localization, phase separation, degradation by β-TrCP (Park et al., 2019; Rogers, Rusan, Roberts, Peifer, & Rogers, 2009)	PP2A-Twins (*Drosophila*) (Brownlee, Klebba, Buster, & Rogers, 2011), Cdc14B (mammalian) (Wu et al., 2008)
	STIL	Marks site of procentriole	Promotes STIL localization to centriole and binding of CPAP and Sas6 to STIL to promote centriole elongation (Moyer, Ciutario, Lambrus, Daggubati, & Holland, 2015; Moyer & Holland, 2019; Ohta et al., 2014)	
	Sas6	Forms nine-spoked cartwheel at core of centriole	Promotes centriole formation (in *Caenorhabditis elegans*) (Kitagawa, Busso, Flückiger, & Gönczy, 2009)	
	GCP6	Component of γ-TuRC	Promotes centriole duplication (Bahtz et al., 2012)	
	Cep152	Centrosome-associated protein	Unknown (Hatch, Kulukian, Holland, Cleveland, & Stearns, 2010)	
Centrosome maturation and early spindle pole assembly				
Aurora A	Aurora A	Master G2/M kinase	Autophosphorylation promotes Aurora A kinase activity (Zorba et al., 2014)	PP6 (Zeng, Bastos, Barr, & Gruneberg, 2010)
	TPX2	Nucleator for branched microtubules	Promotes TPX2-CLASP1 interaction and proper spindle length (Fu et al., 2015)	
	TACC3	Microtubule-associated protein; forms TACC3/XMAP215/clathrin complex in mitosis	Promotes TACC3-clathrin binding, TACC3 binding to microtubules, and TACC3/XMAP215/clathrin complex localization to mitotic spindle (Barros, Kinoshita, Hyman, & Raff, 2005; Burgess et al., 2018; Hood et al., 2013; Lin, Hu, & Shih, 2010)	
	NDEL1	Microtubule-associated protein	Promotes NDEL1 localization to centrosomes (Mori et al., 2007)	
	Hice1	Component of Augmin complex, microtubule nucleator	Weakens interaction between Hice1 and microtubules (Tsai et al., 2011)	
Plk1	Cep192	Centrosome-associated protein	Promotes γ-TuRC recruitment to centrosome and centrosome maturation (in *Xenopus laevis*) (Joukov, de Nicolo, Rodriguez, Walter, & Livingston, 2010)	
	PCNT	Principle component of centrosomal matrix	Promotes subsequent microtubule nucleation activity via recruitment of PCM proteins (Lee & Rhee, 2011)	
	Nedd1	Localizes γ-TuRC to centrosome	Phosphorylation and binding by Plk1 requires priming phosphorylation by Cdk1 (Johmura et al., 2011; Zhang et al., 2009); promotes γ-TuRC recruitment to centrosome and phosphorylation of Hice1 (Johmura et al., 2011; Zhang et al., 2009)	
	Hice1	Component of Augmin complex, microtubule nucleator	Promotes Augmin localization to microtubule spindle and microtubule nucleation activity (Johmura et al., 2011)	

TABLE 1 (Continued)

Kinase	Key substrates	Substrate function	Consequence of phosphorylation	Relevant phosphatases
	Kizuna	Centrosomal protein involved in centrosome cohesion	Promotes spindle bistability, centrosome cohesion (Oshimori, Ohsugi, & Yamamoto, 2006)	Cdc25B (Thomas et al., 2014)
	LRRK1	Kinase with various functions	Phosphorylation first by Plk1, then by Cdk1, activates LRRK1 kinase activity; LRRK1 phosphorylates CDK5RAP2, activating its microtubule-nucleating capacity (Hanafusa et al., 2015)	
	NEK9	Kinase with mitotic roles	Phosphorylation by Cdk1 and Plk1 promote NEK9 kinase activity; NEK9 phosphorylates Nedd1 to promote recruitment of Nedd1 to centrosomes (Bertran et al., 2011; Sdelci et al., 2012)	
Centrosome disjunction and separation				
Plk1	Cep85	Centrosome-associated protein; suppresses NEK2A activity	Disrupts Cep85-NEK2A complex and promotes NEK2A kinase activity (Chen et al., 2019)	
	Mst2 (STK3)	Hippo pathway kinase	Phosphorylation of Mst2 causes dissociation of PP1γ from Mst2-NEK2A-PP1γ complex and promotes NEK2A activity and localization to centrosome (Mardin, Agircan, Lange, & Schiebel, 2011; Mardin et al., 2010)	PP1γ (Mardin et al., 2010, 2011)
	NEK9	Kinase with mitotic roles	Phosphorylation by Cdk1 and Plk1 promote NEK9 kinase activity; activated NEK9 phosphorylates NEK6/7 (Belham et al., 2003)	
NEK2A	NEK2A	Kinase with mitotic roles	Autophosphorylation activates NEK2A kinase activity (Rellos et al., 2007)	PP1γ (Meraldi & Nigg, 2001)
	C-Nap1, Rootletin, LRRC45, β-catenin	Form a protein network that connects the duplicated centrosomes	Dissociates protein network and promotes centrosome disjunction (Bahe, Stierhof, Wilkinson, Leiss, & Nigg, 2005; Bahmanyar et al., 2008; Hardy et al., 2014; He et al., 2013)	
NEK9	NEK9	Kinase with mitotic roles	Autophosphorylation activates NEK9 kinase activity (Roig, Groen, Caldwell, & Avruch, 2005)	
	NEK6/7	Kinases with mitotic roles	Activates NEK6/7 kinase activity (Belham et al., 2003)	
NEK6/7	Eg5	Major kinesin involved in centrosome separation and spindle bipolarity	Promotes Eg5-TPX2 binding (Eibes et al., 2018) and consequently Eg5 localization to centrosome (Bertran et al., 2011; Rapley et al., 2008)	
Cdk1			Promotes Eg5-MT binding (Cahu et al., 2008; Slangy et al., 1995)	
SRC kinases			Phosphorylation by c-Src decreases Eg5 motor activity (Bickel et al., 2017)	
Aurora A (in *X. laevis*)			Unknown (Giet, Uzbekov, Cubizolles, Le Guellec, & Prigent, 1999)	
Spindle positioning				

(Continues)

TABLE 1 (Continued)

Kinase	Key substrates	Substrate function	Consequence of phosphorylation	Relevant phosphatases
Cdk1	NuMA	Links mitotic spindle poles to cell membrane	NuMA not phosphorylated at Thr2055 localizes to cell cortex (Kotak, Busso, & Gönczy, 2013)	PP1-Repo-Man (B. H. Lee, Schwager, Meraldi, & Gotta, 2018), PP2A-B55γ (Keshri, Rajeevan, & Kotak, 2020)
	APC/C	Promotes mitotic progression	Regulates APC/C activity in early mitosis by anchoring it to spindle poles via END network (Ban et al., 2007)	PP2A-B55α (Torres, Ban, & Jackson, 2010)
Early spindle assembly—centromere				
Aurora B kinase	Aurora B	Master mitotic kinase	Autophosphorylation in *trans* activates Aurora B kinase activity (Yasui et al., 2004)	PP2A, PP1
	INCENP	Core component of CPC	Phosphorylation of and binding to INCENP activates Aurora B kinase activity (Honda, Körner, & Nigg, 2003)	
	KMN network • Knl1 • Mis12 complex (Mis12, Dsn1, Nnf1, Nsl1) • Ndc80 complex (Ndc80/Hec1, Nuf2, Spc24, Spc25)	Bind kinetochore proteins and microtubules to form kinetochore-MT attachments	Phosphorylation of Knl1, Dsn1, and Hec1 reduces the binding affinity of the KMN network with microtubules (Cheeseman, Chappie, Wilson-Kubalek, & Desai, 2006; DeLuca et al., 2006; Welburn et al., 2010)	
	Ska complex (Ska1-3)	Stabilizes kinetochore-MT attachments	Phosphorylation of Ska1 and Ska3 decreases Ska-KMN network affinity (Chan, Jeyaprakash, Nigg, & Santamaria, 2012)	
	Cdt1	Origin licensing in DNA replication; in mitosis, stabilizes kinetochore-MT attachments	Phosphorylation decreases Cdt1-MT affinity (Agarwal et al., 2018)	
Early mitotic spindle assembly—kinetochore				
Aurora A	Plk1	Master G2/M kinase involved in centrosome maturation	Phosphorylation activates Plk1 kinase activity (Macůrek et al., 2008)	
Cdk1	Mypt1	Regulatory unit of PP1	Phosphorylation promotes Mypt1 localization to kinetochores and binding to Plk1 to antagonize Plk1 activity (Dumitru, Rusin, Clark, Kettenbach, & Compton, 2017; Yamashiro et al., 2008)	
Plk1	PBIP1 (CENP-U)	Centrosome-associated protein	Phosphorylation promotes PBIP1-Plk1 binding and localization to kinetochores (Dumitru et al., 2017; Yamashiro et al., 2008)	PP2A, PP1, Mypt1-PP1 (Dumitru et al., 2017; Yamashiro et al., 2008)
	NudC	Dynein-associated protein	Phosphorylation promotes NudC-Plk1 binding and localization to kinetochores (Nishino et al., 2006)	
	Bub1	Kinetochore protein with roles in promoting spindle assembly checkpoint	Phosphorylation and binding by Plk1 requires priming phosphorylation by Cdk1; phosphorylation promotes Plk1 localization to kinetochores and possibly to enhance Plk1 phosphorylation of other substrates	
	CLASP2	MT plus-end tracking protein	Phosphorylation and binding by Plk1 requires priming phosphorylation by Cdk1; phosphorylation promotes	

TABLE 1 (Continued)

Kinase	Key substrates	Substrate function	Consequence of phosphorylation	Relevant phosphatases
			Plk1 localization to kinetochores and formation of kinetochore-MT attachments	
	CENP-F	In mitosis, recruits other proteins to kinetochores	Phosphorylation possibly promotes CENP-F localization to kinetochores	
	Sgt1	Cochaperone for heat-shock proteins	Phosphorylation promotes KMN complex localization at kinetochores	
	CLIP-170	MT plus-end tracking protein	Phosphorylation promotes CLIP-170 localization at kinetochores and kinetochore-MT attachments	
	BubR1	Component of mitotic checkpoint complex; promotes spindle assembly checkpoint	Phosphorylation and binding by Plk1 requires priming phosphorylation by Cdk1; recruits phosphatase PP2A-B56α to kinetochores to antagonize Aurora B (Wang et al., 2016)	

Abbreviations: APC/C, anaphase promoting complex/cyclosome; CPC, chromosomal passenger complex; MT, microtubules; PP2A, protein phosphatase 2A; γ-TuRC, γ-tubulin ring complex.

(Brittle & Ohkura, 2005) (Figure 3). However, prior to doing so, Aurora A must be activated, a process dependent on phosphorylation and protein–protein interactions. First, Aurora A kinase activity is activated by phosphorylation of Thr288 on its T-loop (Littlepage et al., 2002), a modification that may be carried out by another kinase, such as PAK1 (Zhao, Lim, Ng, Lim, & Manser, 2005), or via autophosphorylation (Zorba et al., 2014). Phosphorylation at Thr288 is opposed by phosphatases, such as PP6 (Zeng et al., 2010). Second, Aurora A activity is further promoted by binding to branched microtubule nucleator TPX2 (Bayliss, Sardon, Vernos, & Conti, 2003; Zorba et al., 2014), a regulatory event that causes a conformational shift in Aurora A toward an open conformation. Moreover, the binding of TPX2 to Aurora A may protect Aurora A from dephosphorylation at Thr288 (Bayliss et al., 2003) and ubiquitin-mediated degradation (Giubettini et al., 2011). Similarly, Aurora A binding to TACC3, a microtubule-associated protein that generally stabilizes microtubules (Peset & Vernos, 2008), promotes activation of Aurora A kinase activity (Burgess et al., 2015). Additionally, Aurora A activity may also be enhanced by incorporation into phase separated condensates via binding to microtubule-associated protein BuGZ at the centromeres (Huang et al., 2018) and by binding to Cep192 (Joukov et al., 2010).

Once activated, Aurora A phosphorylates TPX2 at Ser121 and Ser125, promoting an interaction between TPX2 and CLASP1, a microtubule stabilizing protein (Lawrence, Zanic, & Rice, 2020), and consequently normal spindle length (Fu et al., 2015). Similarly, Aurora A phosphorylates NDEL1, a microtubule-associated protein, on Ser251 (Mori et al., 2007). This modification promotes NDEL1 localization to the centrosomes and may be required for ubiquitin-mediated degradation of NDEL1 (Mori et al., 2007). Moreover, this modification was not required for the binding of NDEL1 to TACC3 but nonetheless may promote the localization of TACC3 and γ-tubulin to the centrosome, suggesting that phosphorylation on Ser251 of NDEL1 serves to recruit other proteins to the centrosome (Mori et al., 2007). Aurora A phosphorylates Ser34, Ser552, and Ser558 on TACC3, a regulator of microtubules and a component of the TACC3/XMAP215/clathrin complex (Kinoshita et al., 2005). Phosphorylation of TACC3 on Ser558 is not necessary for localization to the centrosomes or recruitment of XMAP215 (also known as ch-TOG), a key microtubule nucleator and polymerase (Thawani, Kadzik, & Petry, 2018), to the centrosomes (Barros et al., 2005). Rather, this phosphorylation event promotes TACC3 binding to the minus ends of microtubules, stabilizes astral microtubules (Barros et al., 2005) and promotes the binding of TACC3 to dathrin (Burgess et al., 2018; Hood et al., 2013; Lin et al., 2010). Phosphorylation at Ser552 and Ser558 of TACC3 by Aurora A also promotes TACC3 localization to the centrosome, mitotic spindle, and mitotic spindle assembly (Fu et al., 2010). Similarly, TACC3 binding with Aurora A is necessary for TACC3 targeting to the mitotic spindle (Burgess et al., 2015). Although TACC3 can bind XMAP215 without Aurora A kinase activity (Thakur et al., 2014), TACC3 binding to XMAP215 stimulates XMAP215 microtubule nucleation activity (Kinoshita et al., 2005). Together, the TACC3/XMAP215/clathrin complex localizes to the mitotic spindle and promotes spindle stability (Hood et al., 2013; Lin et al., 2010).

Cep192 binds Aurora A and promotes Aurora A phosphorylation at Thr288 (Joukov, Walter, & De Nicolo, 2014). Once activated, Aurora A phosphorylates Plk1 at Thr210 (Joukov et al., 2014; Macůrek et al., 2008; Seki, Coppinger, Jang, Yates, & Fang, 2008). Plk1 binds to Cep192 via recognition of a phosphorylated Thr46 on Cep192 in *Xenopus laevis* (Thr44 in humans), though whether this modification comes from Plk1 or from another kinase is uncertain (Joukov et al., 2014). Nevertheless, in *Xenopus* egg extracts, once bound to Cep192, Plk1 phosphorylates Ser481, Ser507, Ser509, Ser919, and Ser923 (amino acid numbering refers to *X. laevis* Cep192 sequence), promoting γ-TuRC recruitment and centrosome maturation (Joukov et al., 2014). In human cells, Plk1 also binds Cep192 through the conserved phospho-Thr44 (Meng et al., 2015). However, whether Plk1 also modifies Cep192 for the purpose of γ-TuRC recruitment in humans is unclear, as the phosphorylated serine residues in *X. laevis* are not conserved in humans.

Besides Cep192, Plk1 phosphorylates the long isoform of PCNT, a protein necessary for PCM expansion and centrosome maturation, at Thr1209, Thr1221, Ser1235, and Ser1241 (Lee & Rhee, 2011). While these modifications are not necessary for PCNT targeting to the centrosome, they are required for subsequent microtubule nucleation activity (Lee & Rhee, 2011). In particular, phosphorylation of Ser1235 and Ser1241 promotes bipolar spindle formation and recruitment of PCM proteins including Cep192, Aurora A, Nedd1, Plk1, and γ-tubulin, proteins which are all involved in γ-TuRC recruitment and microtubule nucleation (Lee & Rhee, 2011). Nedd1, the anchor for the γ-TuRC complex in the centrosome, is first phosphorylated on Thr550 by Cdk1, allowing for the binding of Plk1 and subsequent phosphorylation by Plk1 on Thr382, Ser397, Ser426, and Ser637 (Zhang et al., 2009). These modifications promote γ-TuRC recruitment to the centrosome (Zhang et al., 2009). Moreover, Cdk1 also phosphorylates Nedd1 on Ser460, which again promotes Plk1 binding to Nedd1 (Johmura et al., 2011). The Plk1-Nedd1 complex phosphorylates the Hice1 subunit of Augmin, a noncentrosomal microtubule nucleator, at 17 unique sites (Johmura et al., 2011). These modifications drive Augmin binding to the microtubule spindle, microtubule nucleation, and spindle stability (Johmura et al., 2011). Interestingly, Aurora A also phosphorylates Hice1 at a number of residues in its N-terminal microtubule binding region, including Thr17, Ser19, Ser20, and Ser20 (Tsai et al., 2011). In contrast to Plk1 phosphorylation, which promotes Hice1-microtubule binding, Aurora A phosphorylation of Hice1 weakened the affinity of Hice1 for microtubules (Tsai et al., 2011). Plk1 phosphorylation of Kizuna, a centrosomal protein involved in centrosome cohesion, on Thr379 does not affect localization to the centrosomes, but does promote spindle bistability and centrosome cohesion (Oshimori et al., 2006). This modification is antagonized by the phosphatase Cdc25B (Thomas et al., 2014).

Plk1 also activates a number of kinases that regulate processes in centrosome maturation (Figure 4). Plk1 phosphorylates LRRK1, a kinase involved in cytoskeletal regulation and endosome trafficking (Hanafusa et al., 2019; Kedashiro et al., 2015), at Ser1790, then Cdk1

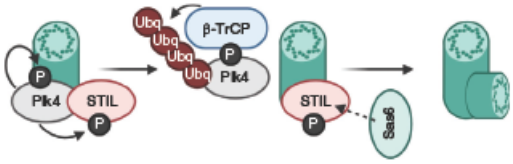

FIGURE 2 Plk4 kinase activity regulates centriole duplication and procentriole elongation. Plk4 binds to STIL, a marker of the site of procentriole formation, and auto-phosphorylates itself in *trans* to activate its kinase activity. Once activated, Plk4 phosphorylates STIL. Sas6 binds to STIL and promotes procentriole elongation. Once autophosphorylated, Plk4 binds to β-TrCP (substrate adaptor for SCF ubiquitin ligase complex), promoting Plk4 degradation [Color figure can be viewed at wileyonlinelibrary.com]

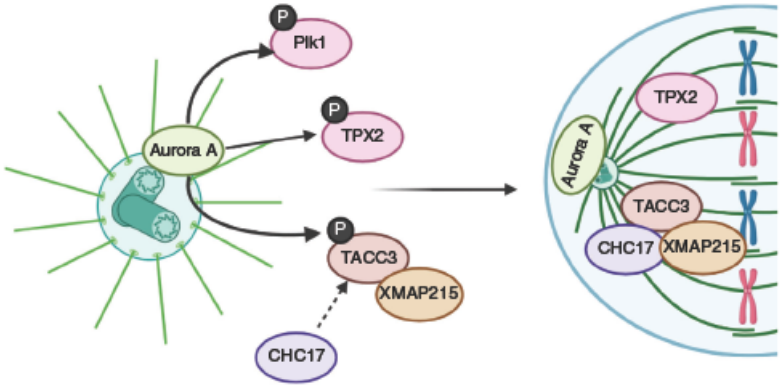

FIGURE 3 Aurora A regulates centrosome maturation and early spindle assembly. Aurora A activates Plk1 at the centrosome and phosphorylates microtubule-associated proteins like TPX2 and TACC3. These microtubule-associated proteins promote centrosome maturation and microtubule organizing center activity, and consequently serve to assemble and stabilize the microtubule spindle [Color figure can be viewed at wileyonlinelibrary.com]

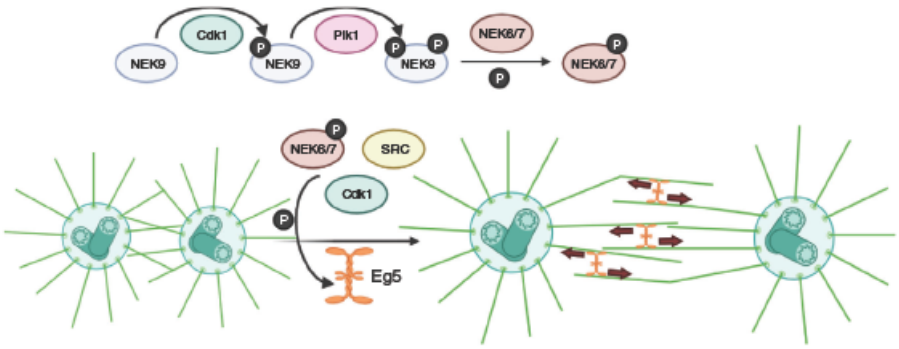

FIGURE 6 Kinases regulate Eg5 in centrosome separation and bipolar spindle formation. Once the centrosomes have disjoined, they need to separate to opposite ends of the cell to form a bipolar spindle. NEK9 activates NEK6 and NEK7, which in turn phosphorylate Eg5, localizing it to the centrosome and promoting centrosome separation and bipolar spindle formation. Other kinases also regulate Eg5 activity [Color figure can be viewed at wileyonlinelibrary.com]

activity (Rellos et al., 2007). Plk1 also phosphorylates an upstream regulator of NEK2A, Mst2 (also known as STK3) (Mardin et al., 2011). NEK2A activity is antagonized by phosphatases (Meraldi & Nigg, 2001), including PP1γ. Conversely, NEK2A binds to and phosphorylates PP1γ at Thr307 and Thr318 to reduce its phosphatase activity (Helps, Luo, Barker, & Cohen, 2000). NEK2A forms a complex with PP1γ and Hippo-pathway kinase Mst2 (Mardin et al., 2010, 2011). Mst2 phosphorylates NEK2A at Ser356, Ser365, Thr406, and Ser438 (Mardin et al., 2010). These modifications do not affect NEK2A kinase activity but are necessary for NEK2A localization to the centrosome (Mardin et al., 2010). To regulate NEK2A activity, Plk1 phosphorylates Mst2 at Ser15, Ser18, and Ser316, disrupting the binding of PP1γ to the NEK2A-PP1γ-Mst2 complex and promoting NEK2A activity (Mardin et al., 2011).

During G2 phase, the two pairs of centrioles are linked by a network of filaments that must be removed for centrosome disjunction and separation (Paintrand, Moudjou, Delacroix, & Bornens, 1992). While the composition of these filaments is not entirely known, a number of candidate proteins have been identified, including C-Nap1 and Rootletin (Hinchcliffe & Sluder, 2001; Wang et al., 2014). When activated, NEK2A phosphorylates 27 residues in the C-terminus of C-Nap1, a protein that resides at the proximal end of centrioles and may serve as the point of attachment for the protein linker network (Hardy et al., 2014). These modifications weaken the affinity of C-Nap1 for Cep135, presumably via electrostatic interactions, and promote the release of C-Nap1 from the centrosome, freeing the pairs of centrioles from each other and promoting centrosome disjunction (Hardy et al., 2014) (Figure 5). Rootletin is a protein that forms fibers that bridge the proximal ends of centrioles and binds to C-Nap1 and is similarly phosphorylated by NEK2A at many sites to promote centrosome disjunction (Bahe et al., 2005). A similar mechanism may apply for NEK2A phosphorylation of protein fiber LRRC45 at Ser661 (He et al., 2013). β-catenin also forms a complex with Rootletin at the centrosomes, is phosphorylated by NEK2A, and plays a role in centrosome separation (Bahmanyar et al., 2008). Whereas C-Nap1 and Rootletin do not localize at the centrosomes during mitosis, β-catenin is found at mitotic centrosomes, suggesting additional roles for β-catenin in centrosome function (Bahmanyar et al., 2008).

Once centrosomes have been disjoined, they must separate to opposite ends of the cell to form a bipolar spindle. Eg5 is a tetrameric bipolar kinesin that acts on antiparallel microtubules to generate forces that separate centrosomes and promote spindle bistability (Kapitein et al., 2005; Shimamoto, Forth, & Kapoor, 2015) (Figure 6). NEK9 is a downstream kinase of Plk1 that phosphorylates NEK6 at Ser206 and NEK7 at Ser195 at the T-loop to activate NEK6/7 (Belham et al., 2003). NEK6/7 phosphorylate Eg5 at Ser1033, promoting Eg5 binding to TPX2 (Eibes et al., 2018), inducing Eg5 localization to the centrosome, and ultimately promoting centrosome separation (Bertran et al., 2011; Rapley et al., 2008). Cdk1 also phosphorylates Eg5 on Thr926 (Slangy et al., 1995), increasing the affinity of Eg5 for microtubules (Cahu et al., 2008).The PP2A-B55α complex dephosphorylates this residue to regulate Eg5 activity (Liu et al., 2017). SRC kinases phosphorylate Eg5 on Tyr125, Tyr211, and Tyr231 (Bickel et al., 2017). These modifications decrease Eg5 motor activity (Bickel et al., 2017). Of interest, Aurora A has been shown to phosphorylate Eg5 in *X. laevis*, but the site of phosphorylation and the consequence of this modification is unknown, and there are no reports of Aurora A phosphorylating Eg5 in human cells (Giet et al., 1999).

5 | EARLY MITOTIC SPINDLE ASSEMBLY—CENTROMERE

Critical to chromosome congression are kinetochore-microtubule attachments. Centromeres are regions of DNA that recruit centromeric proteins (CENPs, such as CENP-A) and function to physically link the chromosomes to the microtubule spindle via the kinetochore (Fukagawa & Earnshaw, 2014). At the centromere, the chromosomal

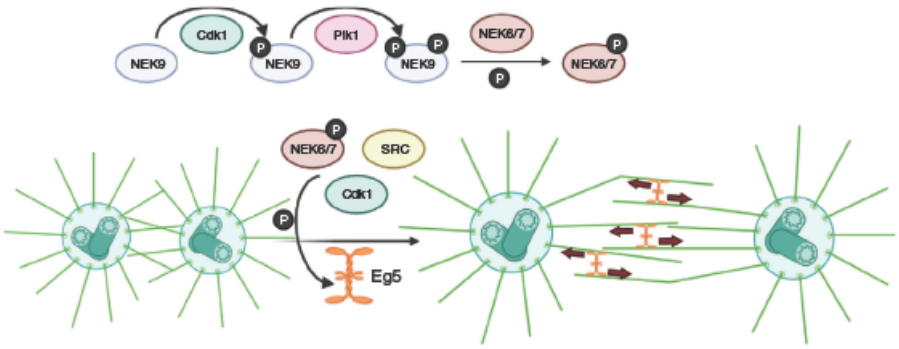

FIGURE 6 Kinases regulate Eg5 in centrosome separation and bipolar spindle formation. Once the centrosomes have disjoined, they need to separate to opposite ends of the cell to form a bipolar spindle. NEK9 activates NEK6 and NEK7, which in turn phosphorylate Eg5, localizing it to the centrosome and promoting centrosome separation and bipolar spindle formation. Other kinases also regulate Eg5 activity [Color figure can be viewed at wileyonlinelibrary.com]

activity (Rellos et al., 2007). Plk1 also phosphorylates an upstream regulator of NEK2A, Mst2 (also known as STK3) (Mardin et al., 2011). NEK2A activity is antagonized by phosphatases (Meraldi & Nigg, 2001), including PP1γ. Conversely, NEK2A binds to and phosphorylates PP1γ at Thr307 and Thr318 to reduce its phosphatase activity (Helps, Luo, Barker, & Cohen, 2000). NEK2A forms a complex with PP1γ and Hippo-pathway kinase Mst2 (Mardin et al., 2010, 2011). Mst2 phosphorylates NEK2A at Ser356, Ser365, Thr406, and Ser438 (Mardin et al., 2010). These modifications do not affect NEK2A kinase activity but are necessary for NEK2A localization to the centrosome (Mardin et al., 2010). To regulate NEK2A activity, Plk1 phosphorylates Mst2 at Ser15, Ser18, and Ser316, disrupting the binding of PP1γ to the NEK2A-PP1γ-Mst2 complex and promoting NEK2A activity (Mardin et al., 2011).

During G2 phase, the two pairs of centrioles are linked by a network of filaments that must be removed for centrosome disjunction and separation (Paintrand, Moudjou, Delacroix, & Bornens, 1992). While the composition of these filaments is not entirely known, a number of candidate proteins have been identified, including C-Nap1 and Rootletin (Hinchcliffe & Sluder, 2001; Wang et al., 2014). When activated, NEK2A phosphorylates 27 residues in the C-terminus of C-Nap1, a protein that resides at the proximal end of centrioles and may serve as the point of attachment for the protein linker network (Hardy et al., 2014). These modifications weaken the affinity of C-Nap1 for Cep135, presumably via electrostatic interactions, and promote the release of C-Nap1 from the centrosome, freeing the pairs of centrioles from each other and promoting centrosome disjunction (Hardy et al., 2014) (Figure 5). Rootletin is a protein that forms fibers that bridge the proximal ends of centrioles and binds to C-Nap1 and is similarly phosphorylated by NEK2A at many sites to promote centrosome disjunction (Bahe et al., 2005). A similar mechanism may apply for NEK2A phosphorylation of protein fiber LRRC45 at Ser661 (He et al., 2013). β-catenin also forms a complex with Rootletin at the centrosomes, is phosphorylated by NEK2A, and plays a role in centrosome separation (Bahmanyar et al., 2008). Whereas C-Nap1 and Rootletin do not localize at the centrosomes during mitosis, β-catenin is found at mitotic centrosomes, suggesting additional roles for β-catenin in centrosome function (Bahmanyar et al., 2008).

Once centrosomes have been disjoined, they must separate to opposite ends of the cell to form a bipolar spindle. Eg5 is a tetrameric bipolar kinesin that acts on antiparallel microtubules to generate forces that separate centrosomes and promote spindle bistability (Kapitein et al., 2005; Shimamoto, Forth, & Kapoor, 2015) (Figure 6). NEK9 is a downstream kinase of Plk1 that phosphorylates NEK6 at Ser206 and NEK7 at Ser195 at the T-loop to activate NEK6/7 (Belham et al., 2003). NEK6/7 phosphorylate Eg5 at Ser1033, promoting Eg5 binding to TPX2 (Eibes et al., 2018), inducing Eg5 localization to the centrosome, and ultimately promoting centrosome separation (Bertran et al., 2011; Rapley et al., 2008). Cdk1 also phosphorylates Eg5 on Thr926 (Slangy et al., 1995), increasing the affinity of Eg5 for microtubules (Cahu et al., 2008).The PP2A-B55α complex dephosphorylates this residue to regulate Eg5 activity (Liu et al., 2017). SRC kinases phosphorylate Eg5 on Tyr125, Tyr211, and Tyr231 (Bickel et al., 2017). These modifications decrease Eg5 motor activity (Bickel et al., 2017). Of interest, Aurora A has been shown to phosphorylate Eg5 in *X. laevis*, but the site of phosphorylation and the consequence of this modification is unknown, and there are no reports of Aurora A phosphorylating Eg5 in human cells (Giet et al., 1999).

5 | EARLY MITOTIC SPINDLE ASSEMBLY—CENTROMERE

Critical to chromosome congression are kinetochore-microtubule attachments. Centromeres are regions of DNA that recruit centromeric proteins (CENPs, such as CENP-A) and function to physically link the chromosomes to the microtubule spindle via the kinetochore (Fukagawa & Earnshaw, 2014). At the centromere, the chromosomal

6 | EARLY SPINDLE ASSEMBLY—KINETOCHORE

Key to ensuring the timing and fidelity of chromosome movements are kinetochore-microtubule attachments. Plk1 kinase activity is necessary for mitotic spindle formation and kinetochore-microtubule attachments (Lera et al., 2016; Liu, Davydenko, & Lampson, 2012) and is tightly regulated by modifications (Figure 7, top). Plk1 kinase activity is activated via phosphorylation of its T-loop on Thr210 by Aurora A kinase (Macůrek et al., 2008; Seki et al., 2008) and possibly by other kinases (Paschal, Maciejowski, & Jallepalli, 2012). Methylation on Lys191 of Plk1 by methyltransferases SET7/9 inhibits Plk1 kinase activity (Yu et al., 2020). This modification presumably allows for fine-tuning of Plk1 activity at the kinetochores, though a demethylase has not yet been identified. Moreover, phosphorylation of Plk1 Thr210 is also regulated by phosphatases. Cdk1/Cyclin A phosphorylates Mypt1, a binding partner and localization subunit for phosphatase PP1 at Ser473 (Dumitru et al., 2017). Phosphorylation at Ser473 promotes Mypt1 localization to the kinetochores (Dumitru et al., 2017) and subsequent binding to Plk1 (Dumitru et al., 2017; Yamashiro et al., 2008). Once bound to Plk1, the Mypt-PP1 complex antagonizes Plk1 function by dephosphorylating Thr210 (Dumitru et al., 2017).

Plk1 localization to the kinetochores is mediated by several protein interactions. Plk1 phosphorylates kinetochore protein PBIP1 at a number of residues, and phosphorylation at Thr78 generates a consensus polo-box domain-binding motif that is necessary for Plk1-PBIP1 binding (Kang et al., 2006). This interaction is required for Plk1 targeting to the kinetochores (Kang et al., 2006). Similarly, NudC, a dynein-associated protein, is phosphorylated by Plk1 at Ser274 and Ser326, and, in the absence of NudC, Plk1 localization at the kinetochores is weakened (Nishino et al., 2006). Cdk1 phosphorylation of kinetochore protein Bub1 at Thr609 also promotes Plk1 binding to Bub1 and localization of Plk1 to the kinetochores (Qi, Tang, & Yu, 2006). Plk1 phosphorylates Bub1, but which residues are phosphorylated and the consequence of the modification are not fully understood (Qi et al., 2006). One possible downstream application of Plk1-Bub1 binding may be to enhance Plk1 phosphorylation of Cdc20 at Ser92, a modification that inhibits the E3 ubiquitin ligase anaphase promoting complex/cyclosome (APC/C) and regulates mitotic progression (Jia, Li, & Yu, 2016). Another consequence of Plk1-Bub1 binding may be that Bub1 serves as a scaffold for Plk1 to phosphorylate other substrates, such as the Mps1 kinase (Ikeda & Tanaka, 2017).

At the kinetochores, Plk1 phosphorylation activates a number of microtubule-associated proteins with the purpose of promoting stable kinetochore-microtubule attachments (Lera et al., 2016; Liu, Davydenko, & Lampson, 2012). Cdk1 phosphorylates CLASP2 at Ser1233, Ser1234, and Ser1250, with Ser1234 being the main modification priming CLASP2 for recognition and subsequent phosphorylation by Plk1 at Ser12348, Ser1255, Ser1274, and Ser1313 (Maia et al., 2012). These modifications are necessary for maintenance of spindle bipolarity and proper kinetochore-microtubule attachments (Maia et al., 2012). CENP-F is a large microtubule-associated protein with roles in stabilizing kinetochore-microtubule attachments (Auckland, Roscioli, Coker, & McAinsh, 2020). Plk1 phosphorylates CENP-F on at least eight residues, and these phosphorylation marks may be important for CENP-F localization at the kinetochores (Santamaria et al., 2011).

Similarly, Plk1 phosphorylates Sgt1, a co-chaperone for heat-shock proteins, at Ser331, and this phosphorylation is necessary for Sgt1 localization at kinetochores and enhances subsequent localization of the KMN microtubule-kinetochore complex (Liu, Song, et al., 2012). In a similar manner, CLIP-170, a major component of the microtubule plus end-binding proteins (Bieling et al., 2008), was phosphorylated by Plk1 at Ser195 and kinase CK2 at Ser1318 (Li et al., 2010). Phosphorylation at Ser195 does not affect CLIP-170 binding to microtubules but enhances the association of kinase CK2 with CLIP-170, CLIP-170 localization to the kinetochores, and the formation of microtubule-kinetochore attachments (Li et al., 2010). After Cdk1 primes kinetochore protein BubR1 by phosphorylating Thr620, Plk1 phosphorylates BubR1 at Ser676 (Elowe, Hümmer, Uldschmid, Li, & Nigg, 2007) and at Thr680 (Suijkerbuijk, Vleugel, Teixeira, & Kops, 2012). Together with other phosphorylation marks by kinases like Mps1 (Huang et al., 2008), these modifications recruit PP2A-B56α which may balance Aurora B activity at the kinetochore (Suijkerbuijk et al., 2012; Xu, Raetz, Kitagawa, Virshup, & Lee, 2013).

7 | PHOSPHATASES IN MITOTIC SPINDLE ASSEMBLY

Phosphatases antagonize the activity of protein kinases. While they play a role in suppressing kinase activity, the timely activation of protein phosphatases is also necessary to promote timely cell cycle progression and spindle assembly. Here, we focus on the two main classes of phosphatases in mitotic spindle assembly: PP1 and PP2A. The PP1 holoenzyme generally consists of the catalytic PP1 subunit and one or more substrate-recognition and/or localization co-factors (Bertolotti, 2018), whereas the PP2A holoenzyme generally consists of a scaffolding A subunit, a catalytic C subunit, and a regulatory, substrate-recognition B subunit (Sents, Ivanova, Lambrecht, Haesen, & Janssens, 2013).

In mitosis, PP2A functions to promote proper kinetochore-microtubule attachments at the kinetochores and centromeres. At the kinetochores, PP2A-B56γ binds to Cdk1- and Plk1-phosphorylated BubR1 (Kruse et al., 2013; Wang et al., 2016). Binding of PP2A to BubR1 may be promoted by the presence of centromeric protein Sgo1 (Vallardi, Allan, Crozier, & Saurin, 2019). At the centromere, PP2A-B56α localization is dependent on Sgo2, not on Sgo1 (Vallardi et al., 2019). Interestingly, however, Sgo1 also binds the CPC via Borealin, and a Borealin-Sgo1-PP2AC complex was reconstituted in vitro from recombinant proteins (Bonner et al., 2020). Together, these data suggest that Sgo1 may coordinate to allow PP2A-B56 to antagonize CPC-based Aurora B activity at the centromere (Meppelink, Kabeche, Vromans, Compton, & Lens, 2015; Vallardi et al., 2019) and inner kinetochore (Suijkerbuijk et al., 2012; Xu et al., 2013). Altogether, PP2A regulates kinetochore-microtubule attachments, as loss of PP2A leads to a

loss of stable k-fibers and chromosome attachment, regulating both Aurora B and Plk1 activity (Foley, Maldonado, & Kapoor, 2011).

In contrast to PP2A, which has roles at both the centromere and kinetochores, PP1 functions mainly at the kinetochores. PP1 binds competitively to kinetochore protein KNL1 at the same location as KNL1's microtubule-binding site, suggesting that KNL1 could either bind microtubules or PP1 (Bajaj, Bollen, Peti, & Page, 2018). Once bound to KNL1, PP1 dephosphorylates KNL1, causing dissociation of spindle assembly checkpoint kinetochore proteins from KNL1, thus silencing spindle assembly checkpoint signaling (Bajaj et al., 2018). PP1 is also recruited to the kinetochores via binding to Ska1 (Sivakumar et al., 2016). At the kinetochores, both PP1 and PP2A dephosphorylate and inactivate Msp1, a master kinase of spindle assembly checkpoint signaling, shutting down the spindle assembly checkpoint (Hayward et al., 2019; Moura et al., 2017). Thus, the proper localization and accumulation of PP1 and PP2A at the kinetochores serve to antagonize Aurora B activity and quench spindle assembly checkpoint signaling.

Besides regulating kinetochore-microtubule attachments, PP1 and PP2A also function to regulate spindle orientation and stability during mitosis. NuMA is a microtubule-binding protein that anchors the mitotic spindle to the cortex via the plasma membrane (Kotak, Busso, Gonczy, & Gönczy, 2014). Cdk1 phosphorylates Thr2055 of NuMA; this phosphorylation event inhibits NuMa localization at the cortex, such that only NuMA not phosphorylated at this residue localizes to the cortex (Kotak et al., 2013). The proper extent of NuMA localization at the cortex is regulated by PP2A-B55γ (Keshri et al., 2020) and by PP1-Repo-Man (Lee et al., 2018). Expression of a construct of NuMA that could not be phosphorylated on Thr2055 resulted in spindle oscillations (i.e., the mitotic spindle wobbled unsteadily) (Kotak et al., 2013), and inhibition of either phosphatase complex resulted in improper metaphase spindle positioning (Keshri et al., 2020; Kotak et al., 2013). During anaphase, when Cdk1 activity is low, these phosphatases promote increased NuMA localization to the cortex, generating dynein-dependent forces that result in spindle elongation and progression through anaphase (Keshri et al., 2020; Kotak et al., 2013). At the spindle poles, NuMA also forms the END (Emi1, NuMA, dynein-dynactin) network, a complex that localizes the APC/C at the spindle poles and inhibits its activity, allowing for proper Cdk1-mediated spindle assembly in early mitosis (Ban et al., 2007). Loss of PP2A-B55α led to the mislocalization of the APC/C from the spindle poles during mitotic spindle assembly, the formation of multipolar spindles, and failures in chromosome congression, suggesting that PP2A antagonizes Cdk1-regulation of APC/C localization at the spindle poles in early mitosis (Torres et al., 2010).

8 | TECHNIQUES IN IDENTIFYING AND STUDYING PHOSPHORYLATION

Numerous methods of identifying and studying phosphorylation and the relationship between kinase and substrate have been developed (Johnson & Hunter, 2005; Xue & Tao, 2013). A traditional method for characterizing a kinase–substrate pair has been an in vitro kinase assay, where the isolated kinase and putative substrate are incubated with radioactive γ-^{32}P ATP and the transfer of the radioactive phosphoryl group onto the substrate is monitored by western blotting and radiometry. If the substrate is phosphorylated, then the reaction is repeated using nonradioactive ATP and the sites of phosphorylation on the substrate are identified via mass spectrometry, as the addition of a phosphate group leads to a detectable mass increase of ~80 Da. These types of approaches have been used to identify numerous Plk1 substrates including the StarD9 protein that is important for PCM cohesion at the centrosome (Senese et al., 2015). Similar experiments can be performed in cells either in the presence or absence of kinase inhibitors or by overexpressing or knocking down/knocking out the kinase of interest and assessing for differential phosphorylation on potential substrates using immunoblotting (with a phospho-specific antibody) or mass spectrometry-based approaches, which have also been used to identify Plk1 substrates (Santamaria et al., 2011).

Other popular approaches include classical yeast two-hybrid approaches or affinity proteomics approaches, which can also identify potential kinase–substrate relationships (Johnson & Hunter, 2005; Xue & Tao, 2013). Once a phosphorylation site has been mapped, a common approach to study the effect of the modification is to mutate the site(s) of phosphorylation to a nonphosphorylatable residue (usually Ser/Thr to Ala and Tyr to Phe) or a phosphomimetic residue (usually to Asp or Glu, though sometimes these phosphomimetic residues do not recapitulate the phosphorylated state of the protein) (Johnson & Hunter, 2005; Xue & Tao, 2013) and analyze the cellular consequences of the modification.

In some cases, understanding what motif the kinase will phosphorylate is useful for identifying additional substrates of that kinase. Computational approaches, such as ScanSite (Obenauer, Cantley, & Yaffe, 2003) or PhosphoPredict (Song et al., 2017) have been developed that analyze phosphosites and their motifs and predict potential substrates, such as the prediction and validation of SPICE1 as an Aurora A and Aurora B substrate (Deretic, Kerr, & Welburn, 2019). Phage display approaches or peptide-library based approaches have also been used to define kinase phosphorylation motifs. In the case of peptide-library based approaches, a microchip with a peptide library is allowed to react with the kinase of interest, such as with the NEK family of kinases (van de Kooij et al., 2019). Phosphorylated peptides are identified and computationally analyzed to identify a consensus phosphorylation motif. In the case of phage-based approaches, phages are modified to display a library of peptides on their surface. The kinase is allowed to react with the peptides, and phages that are phosphorylated are enriched, usually via binding to a phospho-antibody. After sequential rounds of enrichment, the selected phages have their DNA sequenced, and again the selected peptides are computationally analyzed to identify a consensus phosphorylation motif. Such a technique was used to expand the phosphorylation motif for Plk1 (Santamaria et al., 2011).

While these classic approaches have been useful in understanding kinase–substrate relationships, these techniques have difficulty addressing important biological questions. First, in vitro kinase assays

are low-throughput and biased, requiring a guess as to what a kinase's substrate may be. Moreover, while numerous techniques have been used to assay kinase activity in vitro, assessing kinase activity in cells has been a challenge. Finally, chemical inhibitors are useful agents in understanding a kinase's role, but chemical inhibitors lack spatial specificity that make it difficult to study a kinase with more than one localization. Here, we highlight some innovative techniques used for understanding kinase–substrate relationships and kinase activity in cells. We focus on "bump-hole" technology for orthogonal identification of kinase substrates, FRET sensors for in situ readouts of kinase activity in cells, and strategies for localized inhibition of kinases for targeted kinase inhibition. Strategies for studying phosphatases are similar, including techniques in mass spectrometry and the use of FRET- or fluorescence-based assays, and are reviewed elsewhere (Fahs, Lujan, & Köhn, 2016).

8.1 | Bump-hole

While mass spectrometry can identify phosphorylation sites that increase or decrease in abundance upon expression or inhibition of a kinase, these modifications may come about from the activation or inactivation of downstream kinases. For example, many Cdk1 phosphorylation events serve as priming modifications for later binding and phosphorylation by Plk1 (Elowe et al., 2007; Maia et al., 2012; Qi et al., 2006; Zhang et al., 2009). Thus, if mass spectrometry is performed on cell lysates where Cdk1 is overexpressed, the identified phosphorylation sites may not simply be Cdk1 sites but also Plk1 sites. While in vitro kinase assays can confirm whether or not those sites are due to Cdk1, such assays are time-consuming and/or expensive. A high-throughput, unbiased, and more direct method of identifying kinase substrates employs "bump-hole" technology (Figure 8a′). First, an analogue of ATP is synthesized that is sterically larger than unmodified ATP. This increased steric size creates a "bump" in ATP that renders it unable to bind to unmodified kinases or ATPases (Figure 8a′, Circle 1) (Liu, Shah, Yang, Witucki, & Shokat, 1998; Shah, Liu, Deirmengian, & Shokat, 1997). The gamma phosphate of the modified ATP analogue (i.e., the phosphate group that is transferred to the substrate) is also modified to contain a thiophosphate group for later detection (Blethrow, Glavy, Morgan, & Shokat, 2008; Hengeveld et al., 2012). Mutation of a bulky "gatekeeper" residue in the ATP binding pocket to an amino acid with a smaller side chain, such as glycine or alanine, introduces a "hole" into the kinase of interest. This "hole" allows the mutated kinase of interest, but not other kinases or ATPases, to bind to the "bumpy" substrate (Figure 8a′, Circle 2) (Liu et al., 1998; Shah et al., 1997). Since the mutated kinase can bind the analogue of ATP, these kinases are often referred to as "analog sensitive" enzymes. Importantly, the "hole" also decreases the affinity of the mutated enzyme for unmodified ATP, allowing the mutated enzyme to bind to and use "bumpy" ATP with reasonable selectivity for its enzymatic reactions (Figure 8a′, Circle 3). Proteins modified by the "bumpy" substrate can subsequently be isolated via enrichment for the thiophosphate tag and analyzed via mass spectrometry, allowing for high-throughput and unbiased identification of substrates of a particular kinase (Figure 8a") (Blethrow et al., 2008; Hengeveld et al., 2012). Such an approach has been used to identify substrates of Aurora B (Hengeveld et al., 2012) and Cdk1 (Blethrow et al., 2008) via mass spectrometry. One limitation of this approach is that due to poor cell permeability of the ATP analogue, these experiments are usually performed in cell extracts, not in whole cells. However, some cell-permeable inhibitors have been identified, allowing for more physiological labeling conditions (Bishop et al., 1998, 1999, 2000). Additionally, further developments have allowed the generation of otherwise cell-impermeable ATP analogues within cells (Hertz et al., 2013) and for the use of ATP analogues in animal models (Cibrián Uhalte et al., 2012; Soskis et al., 2012).

8.2 | FRET sensors

In vitro kinase assays are useful for assessing kinase activity. These assays typically employ a means of measuring ATP hydrolysis over time (e.g., with colorimetric assays) or of measuring phosphorylation of the substrate over time (e.g., via intensity of the phosphoprotein band by western blotting or via radiolabeled phosphate incorporation on the substrate) (Johnson & Hunter, 2005; Xue & Tao, 2013). However, a read-out of kinase activity within living cells had been largely intractable until the recent development of fluorescence resonance energy transfer (FRET)-based sensors. From N-terminus to C-terminus, an FRET construct for kinase activity consists of an FRET donor (CFP), a phospho-amino acid binding domain, a linker peptide with a phosphorylation motif for the kinase of interest, and an FRET acceptor (YFP) (Zhang, Ma, Taylor, & Tsien, 2001). When the kinase is inactive, excitation of the FRET donor results in a low or no FRET signal, as the FRET donor is usually not within the vicinity of the FRET acceptor for an FRET signal to occur (Figure 8b, left). When the kinase is active, however, it phosphorylates the phosphorylation motif within the linker peptide. The phosphorylated residue binds to the phospho-amino acid binding domain, bringing the FRET acceptor closer to the FRET donor and increasing the FRET signal (Figure 8b, right). Assessing the FRET signal over time and distance allows for an understanding of when and where a kinase is active in situ. Such a reporter was used to determine the spatial and temporal activity of Aurora B (Fuller et al., 2008).

8.3 | Localized inhibition

While small molecule inhibitors have been useful tools to elucidate kinase function, they lack precise temporal or spatial precision. For example, Plk1 is an enzyme with prominent roles at both the centrosome and the kinetochores. If one has an interest in the role of Plk1 at the centrosome, adding a Plk1 inhibitor will disturb Plk1 signaling at both the centrosome and the kinetochores, causing unwanted artifacts and complicating subsequent analysis (Figure 8c, left). Conversely, if one has an interest in the role of Plk1 at the kinetochore, a

Plk1 inhibitor will disturb the function of Plk1 at the centrosome, inhibiting downstream mitotic spindle assembly and potentially introducing artifacts into the analysis of the kinetochore. One recent technological advancement that provides for localized inhibition of kinases employs the use of localized kinase inhibition (LoKI) (Bucko et al., 2019). An LoKI construct consists of two self-labeling protein SNAP-tags followed by a localization domain, such as the PACT domain for centrosome localization (Bucko et al., 2019) (Figure 8c, right; only one SNAP-tag is shown in Figure 8c for clarity). The inhibitor of interest is chemically modified such that it is compatible with the self-labeling protein tag (i.e., it will form a covalent bond with the protein tag) while still retaining its abilities to inhibit the kinase of interest. Adding the modified inhibitor to a cell expressing the LoKI construct will localize the inhibitor to the region of interest, allowing for acute and region-specific inhibition of a kinase (Figure 8c, right). The original LoKI construct could be targeted to centrosomes, kinetochores, mitochondria, and the plasma membrane. In theory, LoKI can be targeted to any cellular location, as long as an appropriate localization signal is used. Similarly, while Plk1 and Aurora A inhibitors have been used for this purpose, any kinase inhibitor can be used with the LoKI system as long as the inhibitor can be chemically adapted to be compatible with the self-labeling protein tag without the loss of function.

While the original LoKI construct used two SNAP-tags, in theory, other self-labeling protein tags, such as the HaloTag or CLIP-tag, could be used as well (Gautier et al., 2008; Stagge, Mitronova, Belov, Wurm, & Jakobs, 2013). These tags could be used in the same LoKI construct to fine-tune control of enzyme activity for downstream analyses. For example, a construct may consist of an LoKI construct with an SNAP-tag and a HaloTag, used in conjunction with an SNAP-modified Plk1 inhibitor and a Halo-modified APC/C inhibitor. In this way, one LoKI construct will contain two (or more, if multiple self-labeling protein domains are used) inhibitors, allowing for localized and specific inhibition of two (or more) biological processes within one region.

Other localization-based kinase inhibition strategies have also been developed. In one example, Lera et al. generated two alleles of Plk1 within one cell (Lera et al., 2016). The first allele coded for an analogue sensitive construct of Plk1 with mutations that rendered it sensitive to the "bumpy" inhibitor 3-MB-PP1 but insensitive to the Plk1 ATP-competitive inhibitor BI-2536. This allele retained the wild-type localization of Plk1. The other allele coded for a construct of

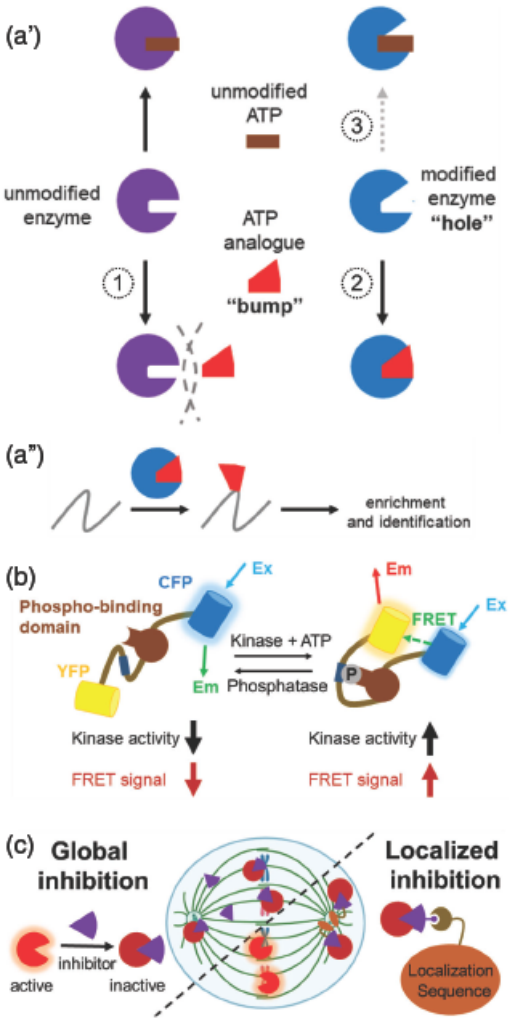

FIGURE 8 Selected techniques in determining kinase function. (a) Bump-hole technology. (a') A "bump" is chemically added to ATP (brown) to make it sterically bulky (red) and unable to bind to a wild-type kinase (left, purple) (Circle 1). A corresponding "hole" is made in a modified kinase (right, blue) that allows it to bind to and use the modified ATP analogue (Cirde 2). The catalytic efficiency of the modified kinase for unmodified ATP is usually weakened (Circle 3). (a") The modified kinase selectively incorporates the ATP analogue onto its substrates. These substrates are then enriched and identified via mass spectrometry-based approaches. (b) Fluorescence resonance energy transfer (FRET) sensors. When the kinase is inactive (left), the FRET donor and acceptor are not within FRET distance and the FRET signal is low. When the kinase is active (right), the kinase phosphorylates a phosphosite (dark blue) in the linker sequence, causing the linker sequence to bind to the phospho-binding domain (dark brown),which brings the FRET donor and acceptor close to each other, producing an FRET signal. (c) Localized kinase inhibition (LoKI). A kinase inhibitor (purple triangle) has poor location specificity, inhibiting its target kinase (red circular sector) at all locations and prohibiting the study of the kinase at a specific location (left, centrosome and kinetochores used as examples). In an LoKI construct (right), the inhibitor is covalently bound via an SNAP-tag (brown) to a protein targeting domain (orange; centrosome-targeting sequence used as example). The LoKI construct promotes inhibition of the kinase only at that domain (here, only at the centrosome and not at the kinetochores) [Color figure can be viewed at wileyonlinelibrary.com]

Plk1 that was wild-type in the ATP binding pocket but with varying C-terminal localization domains that localized it to chromatin, the inner centromere and outer kinetochore, or the inner kinetochore. The localization-specific construct of Plk1 was sensitive to the inhibitor BI-2536 but insensitive to the inhibitor 3-MB-PP1. Thus, by using different combinations of inhibitors and localization constructs, the authors were able to selectively inhibit Plk1 at different cellular structures to understand the different functions of Plk1 at each structure. For example, the authors found that Plk1 localized to the inner centromere and outer kinetochore, but not Plk1 localized to chromatin or the inner kinetochore, was responsible for chromosome alignment in metaphase. These experiments were performed under 3-MB-PP1 inhibition (suppressing the activity of the analog sensitive Plk1 with wild-type localization) to allow for precise control of Plk1 localization. Furthermore, the authors showed that the ability of Plk1 to localize to the inner centromere and outer kinetochore to promote chromosome alignment was due to Plk1 activity, as the phenotype was sensitive to BI-2536 treatment.

9 | CONCLUSIONS AND PERSPECTIVES

Although this review has focused on the phosphoregulation of mitotic spindle assembly, many other posttranslational modifications have key roles in regulating various aspects of early mitotic spindle assembly. The APC/C, for example, promotes mitotic progression by ubiquitylating and degrading substrates throughout mitosis (Pines, 2011; Primorac & Musacchio, 2013). Misregulation of the APC/C can lead to defects in spindle assembly and in cyclin B distribution on the mitotic spindle (Torres et al., 2010). Moreover, tubulin itself is heavily modified in mitosis. Besides phosphorylation, tubulin is also modified via detyrosination, acetylation, and polyglutamylation (Barisic & Maiato, 2016; Ferreira, Figueiredo, Orr, Lopes, & Maiato, 2018; Janke & Magiera, 2020). In some cases, these modifications promote or direct motor localization or activity, but understanding how these modifications "cross-talk" and how the ensemble of these modifications gives rise to the complex dynamics of mitosis remains an open question (Barisic & Maiato, 2016; Ferreira et al., 2018; Janke & Magiera, 2020). Other modifications, such as the addition and removal of *O*-linked *N*-acetylglucosamine (*O*-GlcNAc) to serine or threonine residues of nuclear or cytoplasmic proteins is essential for cell cycle progression. Misregulation of *O*-GlcNAc cycling leads to defects in spindle size and shape (Slawson et al., 2005), in part due to misregulation of Cdk1 and Aurora B (Tan et al., 2013). Most of the identified *O*-GlcNAc sites in mitosis are in close proximity or lie within known phosphorylation sites, causing altered phosphorylation of proteins associated with the mitotic spindle (Wang et al., 2010). Other modifications, including farnesylation (Moudgil et al., 2015) and myristoylation (Timm, Titus, Bernd, & Barroso, 1999), promote the localization of microtubule-associated proteins to the mitotic spindle.

Thus, while phosphorylation and ubiquitylation have been heavily studied as regulators of the events leading to mitotic spindle assembly (Ong & Torres, 2019), other posttranslational modifications have received less attention, perhaps because of the difficulty of studying these modifications in a high-throughput manner with mass spectrometry (An, Froehlich, & Lebrilla, 2009; Tate, Kalesh, Lanyon-Hogg, Storck, & Thinon, 2015). Nonetheless, improvements in computation and analytical techniques have emerged to aid our understanding of the role of these modifications in spindle assembly (Klamer, Hsueh, Ayala-Talavera, & Haab, 2019). Altogether, understanding how the myriad of modifications coordinate as a signaling network to give rise to the dynamic process of mitotic spindle assembly will be a prime future goal for the field of cell division.

ACKNOWLEDGMENTS

The authors apologize to colleagues whose work could not be cited due to space constraints. This material is based upon work supported by the National Institutes of Health NIGMS grant number R01GM117475 and National Science Foundation grant number MCB1912837 to J. Z. T. Any opinions, findings, and conclusions or recommendations expressed in this material are those of the authors and do not necessarily reflect the views of the National Institutes of Health or the National Science Foundation. This work was also supported by an NIH-NIGMS Ruth L. Kirschstein National Research Service Award GM007185 and a Whitcome Pre-doctoral Fellowship in Molecular Biology from the UCLA MBI to J. Y. O and M. C. B; and a National Science Foundation Graduate Research Fellowship DGE-1650604 to J. Y. O. Figures 1–7 and parts of Figure 8c were created with BioRender.com.

CONFLICT OF INTEREST

The authors declare no conflict of interest.

AUTHOR CONTRIBUTIONS

Michelle C. Bradley, Jorge Z. Torres: Conceptualization. **Joseph Y. Ong, Michelle C. Bradley**: Writing – original draft. **Joseph Y. Ong, Michelle C. Bradley**, and **Jorge Z. Torres**: Writing – review and editing. **Jorge Z. Torres**: Supervision.

DATA AVAILABILITY STATEMENT

Data sharing is not applicable to this article as no new data were created or analyzed in this study.

ORCID

Jorge Z. Torres https://orcid.org/0000-0002-2158-889X

REFERENCES

Agarwal, S., Smith, K. P., Zhou, Y., Suzuki, A., McKenney, R. J., & Varma, D. (2018). Cdt1 stabilizes kinetochore-microtubule attachments via an Aurora B kinase-dependent mechanism. *Journal of Cell Biology*, *217* (10), 3446–3463. https://doi.org/10.1083/JCB.201705127

An, H. J., Froehlich, J. W., & Lebrilla, C. B. (2009). Determination of glycosylation sites and site-specific heterogeneity in glycoproteins. *Current Opinion in Chemical Biology*, *13*(4), 421–426. https://doi.org/10.1016/j.cbpa.2009.07.022

Andrews, P. D., Ovechkina, Y., Morrice, N., Wagenbach, M., Duncan, K., Wordeman, L., & Swedlow, J. R. (2004). Aurora B regulates MCAK at the mitotic centromere. *Developmental Cell*, *6*(2), 253–268. https://doi.org/10.1016/S1534-5807(04)00025-5

Plk1 that was wild-type in the ATP binding pocket but with varying C-terminal localization domains that localized it to chromatin, the inner centromere and outer kinetochore, or the inner kinetochore. The localization-specific construct of Plk1 was sensitive to the inhibitor BI-2536 but insensitive to the inhibitor 3-MB-PP1. Thus, by using different combinations of inhibitors and localization constructs, the authors were able to selectively inhibit Plk1 at different cellular structures to understand the different functions of Plk1 at each structure. For example, the authors found that Plk1 localized to the inner centromere and outer kinetochore, but not Plk1 localized to chromatin or the inner kinetochore, was responsible for chromosome alignment in metaphase. These experiments were performed under 3-MB-PP1 inhibition (suppressing the activity of the analog sensitive Plk1 with wild-type localization) to allow for precise control of Plk1 localization. Furthermore, the authors showed that the ability of Plk1 to localize to the inner centromere and outer kinetochore to promote chromosome alignment was due to Plk1 activity, as the phenotype was sensitive to BI-2536 treatment.

9 | CONCLUSIONS AND PERSPECTIVES

Although this review has focused on the phosphoregulation of mitotic spindle assembly, many other posttranslational modifications have key roles in regulating various aspects of early mitotic spindle assembly. The APC/C, for example, promotes mitotic progression by ubiquitylating and degrading substrates throughout mitosis (Pines, 2011; Primorac & Musacchio, 2013). Misregulation of the APC/C can lead to defects in spindle assembly and in cyclin B distribution on the mitotic spindle (Torres et al., 2010). Moreover, tubulin itself is heavily modified in mitosis. Besides phosphorylation, tubulin is also modified via detyrosination, acetylation, and polyglutamylation (Barisic & Maiato, 2016; Ferreira, Figueiredo, Orr, Lopes, & Maiato, 2018; Janke & Magiera, 2020). In some cases, these modifications promote or direct motor localization or activity, but understanding how these modifications "cross-talk" and how the ensemble of these modifications gives rise to the complex dynamics of mitosis remains an open question (Barisic & Maiato, 2016; Ferreira et al., 2018; Janke & Magiera, 2020). Other modifications, such as the addition and removal of *O*-linked *N*-acetylglucosamine (*O*-GlcNAc) to serine or threonine residues of nuclear or cytoplasmic proteins is essential for cell cycle progression. Misregulation of *O*-GlcNAc cycling leads to defects in spindle size and shape (Slawson et al., 2005), in part due to misregulation of Cdk1 and Aurora B (Tan et al., 2013). Most of the identified *O*-GlcNAc sites in mitosis are in close proximity or lie within known phosphorylation sites, causing altered phosphorylation of proteins associated with the mitotic spindle (Wang et al., 2010). Other modifications, including farnesylation (Moudgil et al., 2015) and myristoylation (Timm, Titus, Bernd, & Barroso, 1999), promote the localization of microtubule-associated proteins to the mitotic spindle.

Thus, while phosphorylation and ubiquitylation have been heavily studied as regulators of the events leading to mitotic spindle assembly (Ong & Torres, 2019), other posttranslational modifications have received less attention, perhaps because of the difficulty of studying these modifications in a high-throughput manner with mass spectrometry (An, Froehlich, & Lebrilla, 2009; Tate, Kalesh, Lanyon-Hogg, Storck, & Thinon, 2015). Nonetheless, improvements in computation and analytical techniques have emerged to aid our understanding of the role of these modifications in spindle assembly (Klamer, Hsueh, Ayala-Talavera, & Haab, 2019). Altogether, understanding how the myriad of modifications coordinate as a signaling network to give rise to the dynamic process of mitotic spindle assembly will be a prime future goal for the field of cell division.

ACKNOWLEDGMENTS

The authors apologize to colleagues whose work could not be cited due to space constraints. This material is based upon work supported by the National Institutes of Health NIGMS grant number R01GM117475 and National Science Foundation grant number MCB1912837 to J. Z. T. Any opinions, findings, and conclusions or recommendations expressed in this material are those of the authors and do not necessarily reflect the views of the National Institutes of Health or the National Science Foundation. This work was also supported by an NIH-NIGMS Ruth L. Kirschstein National Research Service Award GM007185 and a Whitcome Pre-doctoral Fellowship in Molecular Biology from the UCLA MBI to J. Y. O and M. C. B; and a National Science Foundation Graduate Research Fellowship DGE-1650604 to J. Y. O. Figures 1–7 and parts of Figure 8c were created with BioRender.com.

CONFLICT OF INTEREST

The authors declare no conflict of interest.

AUTHOR CONTRIBUTIONS

Michelle C. Bradley, Jorge Z. Torres: Conceptualization. **Joseph Y. Ong, Michelle C. Bradley**: Writing – original draft. **Joseph Y. Ong, Michelle C. Bradley**, and **Jorge Z. Torres**: Writing – review and editing. **Jorge Z. Torres**: Supervision.

DATA AVAILABILITY STATEMENT

Data sharing is not applicable to this article as no new data were created or analyzed in this study.

ORCID

Jorge Z. Torres https://orcid.org/0000-0002-2158-889X

REFERENCES

Agarwal, S., Smith, K. P., Zhou, Y., Suzuki, A., McKenney, R. J., & Varma, D. (2018). Cdt1 stabilizes kinetochore-microtubule attachments via an Aurora B kinase-dependent mechanism. *Journal of Cell Biology*, *217* (10), 3446–3463. https://doi.org/10.1083/JCB.201705127

An, H. J., Froehlich, J. W., & Lebrilla, C. B. (2009). Determination of glycosylation sites and site-specific heterogeneity in glycoproteins. *Current Opinion in Chemical Biology*, *13*(4), 421–426. https://doi.org/10.1016/j.cbpa.2009.07.022

Andrews, P. D., Ovechkina, Y., Morrice, N., Wagenbach, M., Duncan, K., Wordeman, L., & Swedlow, J. R. (2004). Aurora B regulates MCAK at the mitotic centromere. *Developmental Cell*, *6*(2), 253–268. https://doi.org/10.1016/S1534-5807(04)00025-5

DeLuca, J. G., Gall, W. E., Ciferri, C., Cimini, D., Musacchio, A., & Salmon, E. D. (2006). Kinetochore microtubule dynamics and attachment stability are regulated by Hec1. *Cell*, *127*(5), 969–982. https://doi.org/10.1016/j.cell.2006.09.047

Deretic, J., Kerr, A., & Welburn, J. P. I. (2019). A rapid computational approach identifies SPICE1 as an Aurora kinase substrate. *Molecular Biology of the Cell*, *30*(3), 312–323. https://doi.org/10.1091/mbc.E18-08-0495

Dumitru, A. M. G., Rusin, S. F., Clark, A. E. M., Kettenbach, A. N., & Compton, D. A. (2017). Cyclin a/Cdk1 modulates Plk1 activity in prometaphase to regulate kinetochore-microtubule attachment stability. *eLife*, *6*. https://doi.org/10.7554/eLife.29303

Dzhindzhev, N. S., Tzolovsky, G., Lipinszki, Z., Abdelaziz, M., Debski, J., Dadlez, M., & Glover, D. M. (2017). Two-step phosphorylation of Ana2 by Plk4 is required for the sequential loading of Ana2 and Sas6 to initiate procentriole formation. *Open Biology*, *7*(12), 170247. https://doi.org/10.1098/rsob.170247

Eibes, S., Gallisà-Suñé, N., Rosas-Salvans, M., Martínez-Delgado, P., Vernos, I., & Roig, J. (2018). Nek9 phosphorylation defines a new role for TPX2 in Eg5-dependent centrosome separation before nuclear envelope breakdown. *Current Biology*, *28*(1), 121–129.e4. https://doi.org/10.1016/j.cub.2017.11.046

Elowe, S., Hümmer, S., Uldschmid, A., Li, X., & Nigg, E. A. (2007). Tension-sensitive Plk1 phosphorylation on BubR1 regulates the stability of kinetochore-microtubule interactions. *Genes and Development*, *21*(17), 2205–2219. https://doi.org/10.1101/gad.436007

Fahs, S., Lujan, P., & Köhn, M. (2016). Approaches to study phosphatases. *ACS Chemical Biology*, *11*(11), 2944–2961. https://doi.org/10.1021/acschembio.6b00570

Ferreira, L. T., Figueiredo, A. C., Orr, B., Lopes, D., & Maiato, H. (2018). Dissecting the role of the tubulin code in mitosis. *Methods in Cell Biology*, *144*, 33–74. https://doi.org/10.1016/bs.mcb.2018.03.040

Foley, E. A., Maldonado, M., & Kapoor, T. M. (2011). Formation of stable attachments between kinetochores and microtubules depends on the B56-PP2A phosphatase. *Nature Cell Biology*, *13*(10), 1265–1271. https://doi.org/10.1038/ncb2327

Fournier, M., Orpinell, M., Grauffel, C., Scheer, E., Garnier, J. M., Ye, T., … Tora, L. (2016). KAT2A/KAT2B-targeted acetylome reveals a role for PLK4 acetylation in preventing centrosome amplification. *Nature Communications*, *7*(1), 1–16. https://doi.org/10.1038/ncomms13227

Fu, J., Bian, M., Xin, G., Deng, Z., Luo, J., Guo, X., … Zhang, C. (2015). TPX2 phosphorylation maintains metaphase spindle length by regulating microtubule flux. *Journal of Cell Biology*, *210*(3), 373–383. https://doi.org/10.1083/jcb.201412109

Fu, W., Tao, W., Zheng, P., Fu, J., Bian, M., Jiang, Q., … Zhang, C. (2010). Clathrin recruits phosphorylated TACC3 to spindle poles for bipolar spindle assembly and chromosome alignment. *Journal of Cell Science*, *123*(21), 3645–3651. https://doi.org/10.1242/jcs.075911

Fu, Z., Malureanu, L., Huang, J., Wang, W., Li, H., van Deursen, J. M., … Chen, J. (2008). Plk1-dependent phosphorylation of FoxM1 regulates a transcriptional programme required for mitotic progression. *Nature Cell Biology*, *10*(9), 1076–1082. https://doi.org/10.1038/ncb1767

Fukagawa, T., & Earnshaw, W. C. (2014). The centromere: Chromatin foundation for the kinetochore machinery. *Developmental Cell*, *30*(5), 496–508. https://doi.org/10.1016/j.devcel.2014.08.016

Fuller, B. G., Lampson, M. A., Foley, E. A., Rosasco-Nitcher, S., Le, K. V., Tobelmann, P., … Kapoor, T. M. (2008). Midzone activation of aurora B in anaphase produces an intracellular phosphorylation gradient. *Nature*, *453*(7198), 1132–1136. https://doi.org/10.1038/nature06923

Gautier, A., Juillerat, A., Heinis, C., Corrêa, I. R., Kindermann, M., Beaufils, F., & Johnsson, K. (2008). An engineered protein tag for multiprotein labeling in living cells. *Chemistry and Biology*, *15*(2), 128–136. https://doi.org/10.1016/j.chembiol.2008.01.007

Giet, R., Uzbekov, R., Cubizolles, F., Le Guellec, K., & Prigent, C. (1999). The *Xenopus laevis* aurora-related protein kinase pEg2 associates with and phosphorylates the kinesin-related protein XlEg5. *Journal of Biological Chemistry*, *274*(21), 15005–15013. https://doi.org/10.1074/jbc.274.21.15005

Giubettini, M., Asteriti, I. A., Scrofani, J., De Luca, M., Lindon, C., Lavia, P., & Guarguaglini, G. (2011). Control of Aurora-A stability through interaction with TPX2. *Journal of Cell Science*, *124*(1), 113–122. https://doi.org/10.1242/jcs.075457

Gordon, D. J., Resio, B., & Pellman, D. (2012). Causes and consequences of aneuploidy in cancer. *Nature Reviews Genetics*, *13*(3), 189–203. https://doi.org/10.1038/nrg3123

Gouveia, S. M., Zitouni, S., Kong, D., Duarte, P., Gomes, B. F., Sousa, A. L., … Bettencourt-Dias, M. (2019). PLK4 is a microtubule-associated protein that self-assembles promoting de novo MTOC formation. *Journal of Cell Science*, *132*(4), jcs219501. https://doi.org/10.1242/jcs.219501

Guderian, G., Westendorf, J., Uldschmid, A., & Nigg, E. A. (2010). Plk4 trans-autophosphorylation regulates centriole number by controlling βTrCP-mediated degradation. *Journal of Cell Science*, *123*(13), 2163–2169. https://doi.org/10.1242/jcs.068502

Habedanck, R., Stierhof, Y. D., Wilkinson, C. J., & Nigg, E. A. (2005). The polo kinase Plk4 functions in centriole duplication. *Nature Cell Biology*, *7*(11), 1140–1146. https://doi.org/10.1038/ncb1320

Hames, R. S., & Fry, A. M. (2002). Alternative splice variants of the human centrosome kinase Nek2 exhibit distinct patterns of expression in mitosis. *Biochemical Journal*, *361*(1), 77–85. https://doi.org/10.1042/0264-6021:3610077

Hanafusa, H., Kedashiro, S., Tezuka, M., Funatsu, M., Usami, S., Toyoshima, F., & Matsumoto, K. (2015). PLK1-dependent activation of LRRK1 regulates spindle orientation by phosphorylating CDK5RAP2. *Nature Cell Biology*, *17*(8), 1024–1035. https://doi.org/10.1038/ncb3204

Hanafusa, H., Yagi, T., Ikeda, H., Hisamoto, N., Nishioka, T., Kaibuchi, K., … Matsumoto, K. (2019). LRRK1 phosphorylation of Rab7 at S72 links trafficking of EGFR-containing endosomes to its effector RILP. *Journal of Cell Science*, *132*(11), jcs228809. https://doi.org/10.1242/jcs.228809

Hardy, T., Lee, M., Hames, R. S., Prosser, S. L., Cheary, D. M., Samant, M. D., … Fry, A. M. (2014). Multisite phosphorylation of C-Nap1 releases it from Cep135 to trigger centrosome disjunction. *Journal of Cell Science*, *127*(11), 2493–2506. https://doi.org/10.1242/jcs.142331

Hatch, E. M., Kulukian, A., Holland, A. J., Cleveland, D. W., & Stearns, T. (2010). Cep152 interacts with Plk4 and is required for centriole duplication. *Journal of Cell Biology*, *191*(4), 721–729. https://doi.org/10.1083/jcb.201006049

Hayward, D., Bancroft, J., Mangat, D., Alfonso-Pérez, T., Dugdale, S., McCarthy, J., … Gruneberg, U. (2019). Checkpoint signaling and error correction require regulation of the MPS1 T-loop by PP2A-B56. *Journal of Cell Biology*, *218*(10), 3188–3199. https://doi.org/10.1083/JCB.201905026

He, R., Huang, N., Bao, Y., Zhou, H., Teng, J., & Chen, J. (2013). LRRC45 is a centrosome linker component required for centrosome cohesion. *Cell Reports*, *4*(6), 1100–1107. https://doi.org/10.1016/j.celrep.2013.08.005

Helps, N. R., Luo, X., Barker, H. M., & Cohen, P. T. W. (2000). NIMA-related kinase 2 (Nek2), a cell-cycle-regulated protein kinase localized to centrosomes, is complexed to protein phosphatase 1. *Biochemical Journal*, *349*(2), 509–518. https://doi.org/10.1042/0264-6021:3490509

Hengeveld, R. C. C., Hertz, N. T., Vromans, M. J. M., Zhang, C., Burlingame, A. L., Shokat, K. M., & Lens, S. M. A. (2012). Development of a chemical genetic approach for human Aurora B kinase identifies novel substrates of the chromosomal passenger complex. *Molecular & Cellular Proteomics*, *11*(5), 47–59. https://doi.org/10.1074/mcp.M111.013912

Hertz, N. T., Berthet, A., Sos, M. L., Thorn, K. S., Burlingame, A. L., Nakamura, K., & Shokat, K. M. (2013). A neo-substrate that amplifies catalytic activity of Parkinson's-disease-related kinase PINK1. *Cell*, *154*(4), 737–747. https://doi.org/10.1016/j.cell.2013.07.030

Hinchcliffe, E. H., & Sluder, G. (2001). "It takes two to tango": Understanding how centrosome duplication is regulated throughout the cell cycle. *Genes and Development*, *15*(10), 1167–1181. https://doi.org/10.1101/gad.894001

Honda, R., Körner, R., & Nigg, E. A. (2003). Exploring the functional interactions between Aurora B, INCENP, and survivin in mitosis. *Molecular Biology of the Cell*, *14*(8), 3325–3341. https://doi.org/10.1091/mbc.E02-11-0769

Hood, F. E., Williams, S. J., Burgess, S. G., Richards, M. W., Roth, D., Straube, A., … Royle, S. J. (2013). Coordination of adjacent domains mediates TACC3-ch-TOG-clathrin assembly and mitotic spindle binding. *Journal of Cell Biology*, *202*(3), 463–478. https://doi.org/10.1083/jcb.201211127

Huang, H., Hittle, J., Zappacosta, F., Annan, R. S., Hershko, A., & Yen, T. J. (2008). Phosphorylation sites in BubR1 that regulate kinetochore attachment, tension, and mitotic exit. *Journal of Cell Biology*, *183*(4), 667–680. https://doi.org/10.1083/jcb.200805163

Huang, Y., Li, T., Ems-McClung, S. C., Walczak, C. E., Prigent, C., Zhu, X., … Zheng, Y. (2018). Aurora A activation in mitosis promoted by BuGZ. *Journal of Cell Biology*, *217*(1), 107–116. https://doi.org/10.1083/jcb.201706103

Ikeda, M., & Tanaka, K. (2017). Plk1 bound to Bub1 contributes to spindle assembly checkpoint activity during mitosis. *Scientific Reports*, *7*(1), 1–15. https://doi.org/10.1038/s41598-017-09114-3

Janke, C., & Magiera, M. M. (2020). The tubulin code and its role in controlling microtubule properties and functions. *in Nature Reviews Molecular Cell Biology*. *Nature Research.*, *21*, 307–326. https://doi.org/10.1038/s41580-020-0214-3

Jia, L., Li, B., & Yu, H. (2016). The Bub1–Plk1 kinase complex promotes spindle checkpoint signalling through Cdc20 phosphorylation. *Nature Communications*, *7*, 10818. https://doi.org/10.1038/NCOMMS10818

Johmura, Y., Soung, N. K., Park, J. E., Yu, L. R., Zhou, M., Bang, J. K., … Lee, K. S. (2011). Regulation of microtubule-based microtubule nucleation by mammalian polo-like kinase 1. *Proceedings of the National Academy of Sciences of the United States of America*, *108*(28), 11446–11451. https://doi.org/10.1073/pnas.1106223108

Johnson, S. A., & Hunter, T. (2005). Kinomics: Methods for deciphering the kinome. *Nature Methods*, *2*(1), 17–25. https://doi.org/10.1038/nmeth731

Joukov, V., & de Nicolo, A. (2018). Aurora-PLK1 cascades as key signaling modules in the regulation of mitosis. *Science Signaling*, *11*(543), eaar4195. https://doi.org/10.1126/scisignal.aar4195

Joukov, V., de Nicolo, A., Rodriguez, A., Walter, J. C., & Livingston, D. M. (2010). Centrosomal protein of 192 kDa (Cep192) promotes centrosome-driven spindle assembly by engaging in organelle-specific Aurora A activation. *Proceedings of the National Academy of Sciences of the United States of America*, *107*(49), 21022–21027. https://doi.org/10.1073/pnas.1014664107

Joukov, V., Walter, J. C., & De Nicolo, A. (2014). The Cep192-organized Aurora A-Plk1 Cascade is essential for centrosome cycle and bipolar spindle assembly. *Molecular Cell*, *55*(4), 578–591. https://doi.org/10.1016/j.molcel.2014.06.016

Kang, Y. H., Park, J. E., Yu, L. R., Soung, N. K., Yun, S. M., Bang, J. K., … Lee, K. S. (2006). Self-regulated Plk1 recruitment to kinetochores by the Plk1-PBIP1 interaction is critical for proper chromosome segregation. *Molecular Cell*, *24*(3), 409–422. https://doi.org/10.1016/j.molcel.2006.10.016

Kapitein, L. C., Peterman, E. J. G., Kwok, B. H., Kim, J. H., Kapoor, T. M., & Schmidt, C. F. (2005). The bipolar mitotic kinesin Eg5 moves on both microtubules that it crosslinks. *Nature*, *435*(7038), 114–118. https://doi.org/10.1038/nature03503

Kedashiro, S., Pastuhov, S. I., Nishioka, T., Watanabe, T., Kaibuchi, K., Matsumoto, K., & Hanafusa, H. (2015). LRRK1-phosphorylated CLIP-170 regulates EGFR trafficking by recruiting p150Glued to microtubule plus ends. *Journal of Cell Science*, *128*(2), 385–396. https://doi.org/10.1242/jcs.161547

Kelly, A. E., Ghenoiu, C., Xue, J. Z., Zierhut, C., Kimura, H., & Funabiki, H. (2010). Survivin reads phosphorylated histone H3 threonine 3 to activate the mitotic kinase Aurora B. *Science*, *330*(6001), 235–239. https://doi.org/10.1126/science.1189505

Keshri, R., Rajeevan, A., & Kotak, S. (2020). PP2A–B55γ counteracts Cdk1 and regulates proper spindle orientation through the cortical dynein adaptor NuMA. *Journal of Cell Science*, *133*(14), jcs243857. https://doi.org/10.1242/jcs.243857

Kim, T. S., Park, J. E., Shukla, A., Choi, S., Murugan, R. N., Lee, J. H., … Lee, K. S. (2013). Hierarchical recruitment of Plk4 and regulation of centriole biogenesis by two centrosomal scaffolds, Cep192 and Cep152. *Proceedings of the National Academy of Sciences of the United States of America*, *110*(50), E4849–E4857. https://doi.org/10.1073/pnas.1319656110

Kinoshita, K., Noetzel, T. L., Pelletier, L., Mechtler, K., Drechsel, D. N., Schwager, A., … Hyman, A. A. (2005). Aurora A phosphorylation of TACC3/maskin is required for centrosome-dependent microtubule assembly in mitosis. *Journal of Cell Biology*, *170*(7), 1047–1055. https://doi.org/10.1083/jcb.200503023

Kitagawa, D., Busso, C., Flückiger, I., & Gönczy, P. (2009). Phosphorylation of SAS-6 by ZYG-1 is critical for centriole formation in *C. elegans* embryos. *Developmental Cell*, *17*(6), 900–907. https://doi.org/10.1016/j.devcel.2009.11.002

Klamer, Z., Hsueh, P., Ayala-Talavera, D., & Haab, B. (2019). Deciphering protein glycosylation by computational integration of on-chip profiling, glycan-array data, and mass spectrometry. *Molecular and Cellular Proteomics*, *18*(1), 28–40. https://doi.org/10.1074/mcp.RA118.000906

Kleylein-Sohn, J., Westendorf, J., Le Clech, M., Habedanck, R., Stierhof, Y. D., & Nigg, E. A. (2007). Plk4-induced centriole biogenesis in human cells. *Developmental Cell*, *13*(2), 190–202. https://doi.org/10.1016/j.devcel.2007.07.002

Kotak, S., Busso, C., & Gönczy, P. (2013). NuMA phosphorylation by CDK1 couples mitotic progression with cortical dynein function. *The EMBO Journal*, *32*(18), 2517–2529. https://doi.org/10.1038/emboj.2013.172

Kotak, S., Busso, C., Gonczy, P., & Gönczy, P. (2014). NuMA interacts with phosphoinositides and links the mitotic spindle with the plasma membrane. *The EMBO Journal*, *33*(16), 1815–1830. https://doi.org/10.15252/embj.201488147

Kruse, T., Zhang, G., Larsen, M. S. Y., Lischetti, T., Streicher, W., Nielsen, T. K., … Nilsson, J. (2013). Direct binding between BubR1 and B56-PP2A phosphatase complexes regulate mitotic progression. *Journal of Cell Science*, *126*(5), 1086–1092. https://doi.org/10.1242/jcs.122481

Lan, W., Zhang, X., Kline-Smith, S. L., Rosasco, S. E., Barrett-Wilt, G. A., Shabanowitz, J., … Stukenberg, P. T. (2004). Aurora B phosphorylates Centromeric MCAK and regulates its localization and microtubule Depolymerization activity. *Current Biology*, *14*(4), 273–286. https://doi.org/10.1016/j.cub.2004.01.055

Lawrence, E. J., Zanic, M., & Rice, L. M. (2020). CLASPs at a glance. *Journal of Cell Science*, *133*(8), jcs243097. https://doi.org/10.1242/jcs.243097

Lee, B. H., Schwager, F., Meraldi, P., & Gotta, M. (2018). p37/UBXN2B regulates spindle orientation by limiting cortical NuMA recruitment via PP1/repo-man. *Journal of Cell Biology*, *217*(2), 483–593. https://doi.org/10.1083/jcb.201707050

Lee, K., & Rhee, K. (2011). PLK1 phosphorylation of pericentrin initiates centrosome maturation at the onset of mitosis. *Journal of Cell Biology*, *195*(7), 1093–1101. https://doi.org/10.1083/jcb.201106093

Lera, R. F., Potts, G. K., Suzuki, A., Johnson, J. M., Salmon, E. D., Coon, J. J., & Burkard, M. E. (2016). Decoding polo-like kinase

1 signaling along the kinetochore-centromere axis. *Nature Chemical Biology*, *12*(6), 411–418. https://doi.org/10.1038/nchembio.2060

Li, H., Liu, X. S., Yang, X., Wang, Y., Wang, Y., Turner, J. R., & Liu, X. (2010). Phosphorylation of CLIP-170 by Plk1 and CK2 promotes timely formation of kinetochore-microtubule attachments. *EMBO Journal*, *29*(17), 2953–2965. https://doi.org/10.1038/emboj.2010.174

Lin, C. H., Hu, C. K., & Shih, H. M. (2010). Clathrin heavy chain mediates TACC3 targeting to mitotic spindles to ensure spindle stability. *Journal of Cell Biology*, *189*(7), 1097–1105. https://doi.org/10.1083/jcb.200911120

Littlepage, L. E., Wu, H., Andresson, T., Deanehan, J. K., Amundadottir, L. T., & Ruderman, J. V. (2002). Identification of phosphorylated residues that affect the activity of the mitotic kinase Aurora-A. *Proceedings of the National Academy of Sciences of the United States of America*, *99*(24), 15440–15445. https://doi.org/10.1073/pnas.202606599

Liu, D., Davydenko, O., & Lampson, M. A. (2012). Polo-like kinase-1 regulates kinetochore-microtubule dynamics and spindle checkpoint silencing. *Journal of Cell Biology*, *198*(4), 491–499. https://doi.org/10.1083/jcb.201205090

Liu, X. S., Song, B., Tang, J., Liu, W., Kuang, S., & Liu, X. (2012). Plk1 phosphorylates Sgt1 at the kinetochores to promote timely kinetochore-microtubule attachment. *Molecular and Cellular Biology*, *32*(19), 4053–4067. https://doi.org/10.1128/mcb.00516-12

Liu, Y., Zhang, Z., Liang, H., Zhao, X., Liang, L., Wang, G., … Yin, Y. (2017). Protein phosphatase 2A (PP2A) regulates EG5 to control mitotic progression. *Scientific Reports*, *7*(1), 1–13. https://doi.org/10.1038/s41598-017-01915-w

Liu, Y., Shah, K., Yang, F., Witucki, L., & Shokat, K. M. (1998). Engineering Src family protein kinases with unnatural nucleotide specificity. *Chemistry and Biology*, *5*(2), 91–101. https://doi.org/10.1016/S1074-5521(98)90143-0

Macedo, J. C., Vaz, S., Bakker, B., Ribeiro, R., Bakker, P. L., Escandell, J. M., … Logarinho, E. (2018). FoxM1 repression during human aging leads to mitotic decline and aneuploidy-driven full senescence. *Nature Communications*, *9*(1), 2834. https://doi.org/10.1038/s41467-018-05258-6

Macûrek, L., Lindqvist, A., Lim, D., Lampson, M. A., Klompmaker, R., Freire, R., … Medema, R. H. (2008). Polo-like kinase-1 is activated by Aurora A to promote checkpoint recovery. *Nature*, *455*(7209), 119–123. https://doi.org/10.1038/nature07185

Maia, A. R. R., Garcia, Z., Kabeche, L., Barisic, M., Maffini, S., Macedo-Ribeiro, S., … Maiato, H. (2012). Cdk1 and Plk1 mediate a CLASP2 phospho-switch that stabilizes kinetochore-microtubule attachments. *Journal of Cell Biology*, *199*(2), 285–301. https://doi.org/10.1083/jcb.201203091

Maney, T., Hunter, A. W., Wagenbach, M., & Wordeman, L. (1998). Mitotic centromere-associated kinesin is important for anaphase chromosome segregation. *Journal of Cell Biology*, *142*(3), 787–801. https://doi.org/10.1083/jcb.142.3.787

Maniswami, R. R., Prashanth, S., Karanth, A. V., Koushik, S., Govindaraj, H., Mullangi, R., … Jegatheesan, S. K. (2018). PLK4: A link between centriole biogenesis and cancer. *Expert Opinion on Therapeutic Targets*, *22*(1), 59–73. https://doi.org/10.1080/14728222.2018.1410140

Mardin, B. R., Agircan, F. G., Lange, C., & Schiebel, E. (2011). Plk1 controls the Nek2A-PP1γ antagonism in centrosome disjunction. *Current Biology*, *21*(13), 1145–1151. https://doi.org/10.1016/j.cub.2011.05.047

Mardin, B. R., Lange, C., Baxter, J. E., Hardy, T., Scholz, S. R., Fry, A. M., & Schiebel, E. (2010). Components of the hippo pathway cooperate with Nek2 kinase to regulate centrosome disjunction. *Nature Cell Biology*, *12*(12), 1166–1176. https://doi.org/10.1038/ncb2120

Meng, L., Park, J.-E., Kim, T.-S., Lee, E. H., Park, S.-Y., Zhou, M., … Lee, K. S. (2015). Bimodal interaction of mammalian polo-like kinase 1 and a Centrosomal scaffold, Cep192, in the regulation of bipolar spindle formation. *Molecular and Cellular Biology*, *35*(15), 2626–2640. https://doi.org/10.1128/mcb.00068-15

Meppelink, A., Kabeche, L., Vromans, M. J. M., Compton, D. A., & Lens, S. M. A. (2015). Shugoshin-1 balances Aurora B kinase activity via PP2A to promote chromosome bi-orientation. *Cell Reports*, *11*(4), 508–515. https://doi.org/10.1016/j.celrep.2015.03.052

Meraldi, P., & Nigg, E. A. (2001). Centrosome cohesion is regulated by a balance of kinase and phosphatase activities. *Journal of Cell Science*, *114*(Pt 20), 3749–3757.

Moniz, L., Dutt, P., Haider, N., & Stambolic, V. (2011). Nek family of kinases in cell cycle, checkpoint control and cancer. *Cell Division*, *6*, 18. https://doi.org/10.1186/1747-1028-6-18

Mori, D., Yano, Y., Toyo-oka, K., Yoshida, N., Yamada, M., Muramatsu, M., … Hirotsune, S. (2007). NDEL1 phosphorylation by Aurora-A kinase is essential for Centrosomal maturation, separation, and TACC3 recruitment. *Molecular and Cellular Biology*, *27*(1), 352–367. https://doi.org/10.1128/mcb.00878-06

Moudgil, D. K., Westcott, N., Famulski, J. K., Patel, K., Macdonald, D., Hang, H., & Chan, G. K. T. (2015). A novel role of farnesylation in targeting a mitotic checkpoint protein, human spindly, to kinetochores. *Journal of Cell Biology*, *208*(7), 881–896. https://doi.org/10.1083/jcb.201412085

Moura, M., Osswald, M., Leça, N., Barbosa, J., Pereira, A. J., Maiato, H., … Conde, C. (2017). Protein phosphatase 1 inactivates Mps1 to ensure efficient spindle assembly checkpoint silencing. *eLife*, *6*. https://doi.org/10.7554/eLife.25366

Moyer, T. C., Clutario, K. M., Lambrus, B. G., Daggubati, V., & Holland, A. J. (2015). Binding of STIL to Plk4 activates kinase activity to promote centriole assembly. *Journal of Cell Biology*, *209*(6), 863–878. https://doi.org/10.1083/jcb.201502088

Moyer, T. C., & Holland, A. J. (2019). Plk4 promotes centriole duplication by phosphorylating stil to link the procentriole cartwheel to the microtubule wall. *eLife*, *8*. https://doi.org/10.7554/eLife.46054

Nigg, E. A., & Holland, A. J. (2018). Once and only once: Mechanisms of centriole duplication and their deregulation in diseases. *Nature Reviews Molecular Cell Biology*, *19*(5), 297–312. https://doi.org/10.1038/nrm.2017.127

Nishino, M., Kurasawa, Y., Evans, R., Lin, S. H., Brinkley, B. R., & Yu-Lee, L. y. (2006). NudC is required for Plk1 targeting to the kinetochore and chromosome Congression. *Current Biology*, *16*(14), 1414–1421. https://doi.org/10.1016/j.cub.2006.05.052

Obenauer, J. C., Cantley, L. C., & Yaffe, M. B. (2003). Scansite 2.0: Proteome-wide prediction of cell signaling interactions using short sequence motifs. *Nucleic Acids Research*, *31*(13), 3635–3641. https://doi.org/10.1093/nar/gkg584

Ohta, M., Ashikawa, T., Nozaki, Y., Kozuka-Hata, H., Goto, H., Inagaki, M., … Kitagawa, D. (2014). Direct interaction of Plk4 with STIL ensures formation of a single procentriole per parental centriole. *Nature Communications*, *5*, 5267. https://doi.org/10.1038/ncomms6267

Ong, J. Y., & Torres, J. Z. (2019). Dissecting the mechanisms of cell division. *Journal of Biological Chemistry*, *294*(30), 11382–11390. https://doi.org/10.1074/jbc.AW119.008149

Oshimori, N., Ohsugi, M., & Yamamoto, T. (2006). The Plk1 target Kizuna stabilizes mitotic centrosomes to ensure spindle bipolarity. *Nature Cell Biology*, *8*(10), 1095–1101. https://doi.org/10.1038/ncb1474

Paintrand, M., Moudjou, M., Delacroix, H., & Bornens, M. (1992). Centrosome organization and centriole architecture: Their sensitivity to divalent cations. *Journal of Structural Biology*, *108*(2), 107–128. https://doi.org/10.1016/1047-8477(92)90011-X

Park, J.-E., Zhang, L., Bang, J. K., Andresson, T., DiMaio, F., & Lee, K. S. (2019). Phase separation of polo-like kinase 4 by autoactivation and clustering drives centriole biogenesis. *Nature Communications*, *10*(1), 4959. https://doi.org/10.1038/s41467-019-12619-2

Paschal, C. R., Maciejowski, J., & Jallepalli, P. V. (2012). A stringent requirement for PIK1 T210 phosphorylation during K-fiber assembly and chromosome congression. *Chromosoma*, *121*(6), 565–572. https://doi.org/10.1007/s00412-012-0375-8

Peset, I., & Vernos, I. (2008). The TACC proteins: TACC-ling microtubule dynamics and centrosome function. *Trends in Cell Biology*, *18*(8), 379–388. https://doi.org/10.1016/j.tcb.2008.06.005

Pines, J. (2011). Cubism and the cell cycle: The many faces of the APC/C. *Nature Reviews Molecular Cell Biology*, *12*(7), 427–438. https://doi.org/10.1038/nrm3132

Primorac, I., & Musacchio, A. (2013). Panta rhei: The APC/C at steady state. *The Journal of Cell Biology*, *201*(2), 177–189. https://doi.org/10.1083/jcb.201301130

Prosser, S. L., & Pelletier, L. (2017). Mitotic spindle assembly in animal cells: A fine balancing act. *Nature Reviews Molecular Cell Biology*, *18*(3), 187–201. https://doi.org/10.1038/nrm.2016.162

Qi, W., Tang, Z., & Yu, H. (2006). Phosphorylation- and polo-box-dependent binding of Plk1 to Bub1 is required for the kinetochore localization of Plk1. *Molecular Biology of the Cell*, *17*(8), 3705–3716. https://doi.org/10.1091/mbc.E06-03-0240

Rapley, J., Nicolàs, M., Groen, A., Regué, L., Bertran, M. T., Caelles, C., … Roig, J. (2008). The NIMA-family kinase Nek6 phosphorylates the kinesin Eg5 at a novel site necessary for mitotic spindle formation. *Journal of Cell Science*, *121*(23), 3912–3921. https://doi.org/10.1242/jcs.035360

Redli, P. M., Gasic, I., Meraldi, P., Nigg, E. A., & Santamaria, A. (2016). The Ska complex promotes Aurora B activity to ensure chromosome biorientation. *Journal of Cell Biology*, *215*(1), 77–93. https://doi.org/10.1083/jcb.201603019

Rellos, P., Ivins, F. J., Baxter, J. E., Pike, A., Nott, T. J., Parkinson, D. M., … Smerdon, S. J. (2007). Structure and regulation of the human Nek2 centrosomal kinase. *Journal of Biological Chemistry*, *282*(9), 6833–6842. https://doi.org/10.1074/jbc.M609721200

Rogers, G. C., Rusan, N. M., Roberts, D. M., Peifer, M., & Rogers, S. L. (2009). The SCFSlimb ubiquitin ligase regulates Plk4/Sak levels to block centriole reduplication. *Journal of Cell Biology*, *184*(2), 225–239. https://doi.org/10.1083/jcb.200808049

Roig, J., Groen, A., Caldwell, J., & Avruch, J. (2005). Active Nercc1 protein kinase concentrates at centrosomes early in mitosis and is necessary for proper spindle assembly. *Molecular Biology of the Cell*, *16*(10), 4827–4840. https://doi.org/10.1091/mbc.E05-04-0315

Santamaria, A., Wang, B., Elowe, S., Malik, R., Zhang, F., Bauer, M., … Nigg, E. A. (2011). The Plk1-dependent Phosphoproteome of the early mitotic spindle. *Molecular & Cellular Proteomics*, *10*(1), M110.004457. https://doi.org/10.1074/mcp.M110.004457

Sdelci, S., Schütz, M., Pinyol, R., Bertran, M. T., Regué, L., Caelles, C., … Roig, J. (2012). Nek9 phosphorylation of NEDD1/GCP-WD contributes to Plk1 control of γ-tubulin recruitment to the mitotic centrosome. *Current Biology*, *22*(16), 1516–1523. https://doi.org/10.1016/j.cub.2012.06.027

Seki, A., Coppinger, J. A., Jang, C.-Y., Yates, J. R., & Fang, G. (2008). Bora and the kinase Aurora A cooperatively activate the kinase Plk1 and control mitotic entry. *Science*, *320*(5883), 1655–1658. https://doi.org/10.1126/science.1157425

Senese, S., Cheung, K., Lo, Y.-C., Gholkar, A. A., Xia, X., Wohlschlegel, J. A., & Torres, J. Z. (2015). A unique insertion in STARD9's motor domain regulates its stability. *Molecular Biology of the Cell*, *26*(3), 440–452. https://doi.org/10.1091/mbc.E14-03-0829

Sents, W., Ivanova, E., Lambrecht, C., Haesen, D., & Janssens, V. (2013). The biogenesis of active protein phosphatase 2A holoenzymes: A tightly regulated process creating phosphatase specificity. *FEBS Journal*, *280*(2), 644–661. https://doi.org/10.1111/j.1742-4658.2012.08579.x

Sessa, F., Mapelli, M., Ciferri, C., Tarricone, C., Areces, L. B., Schneider, T. R., … Musacchio, A. (2005). Mechanism of Aurora B activation by INCENP and inhibition by hesperadin. *Molecular Cell*, *18*(3), 379–391. https://doi.org/10.1016/j.molcel.2005.03.031

Shah, K., Liu, Y., Deirmengian, C., & Shokat, K. M. (1997). Engineering unnatural nucleotide specificity for Rous sarcoma virus tyrosine kinase to uniquely label its direct substrates. *Proceedings of the National Academy of Sciences of the United States of America*, *94*(8), 3565–3570. https://doi.org/10.1073/pnas.94.8.3565

Shimamoto, Y., Forth, S., & Kapoor, T. M. (2015). Measuring pushing and braking forces generated by ensembles of kinesin-5 crosslinking two microtubules. *Developmental Cell*, *34*(6), 669–681. https://doi.org/10.1016/j.devcel.2015.08.017

Sivakumar, S., Janczyk, P., Qu, Q., Brautigam, C. A., Stukenberg, P. T., Yu, H., & Gorbsky, G. J. (2016). The human SKA complex drives the metaphase-anaphase cell cycle transition by recruiting protein phosphatase 1 to kinetochores. *eLife*, *5*. https://doi.org/10.7554/eLife.12902

Slangy, A., Lane, H. A., d'Hérin, P., Harper, M., Kress, M., & Niggt, E. A. (1995). Phosphorylation by p34cdc2 regulates spindle association of human Eg5, a kinesin-related motor essential for bipolar spindle formation in vivo. *Cell*, *83*(7), 1159–1169. https://doi.org/10.1016/0092-8674(95)90142-6

Slawson, C., Zachara, N. E., Vosseller, K., Cheung, W. D., Lane, M. D., & Hart, G. W. (2005). Perturbations in O-linked β-N-acetylglucosamine protein modification cause severe defects in mitotic progression and cytokinesis. *Journal of Biological Chemistry*, *280*(38), 32944–32956. https://doi.org/10.1074/jbc.M503396200

Song, J., Wang, H., Wang, J., Leier, A., Marquez-Lago, T., Yang, B., … Daly, R. J. (2017). PhosphoPredict: A bioinformatics tool for prediction of human kinase-specific phosphorylation substrates and sites by integrating heterogeneous feature selection. *Scientific Reports*, *7*(1), 6862. https://doi.org/10.1038/s41598-017-07199-4

Sonnen, K. F., Gabryjonczyk, A. M., Anselm, E., Nigg, E. A., & Stierhof, Y. D. (2013). Human cep192 and cep152 cooperate in plk4 recruitment and centriole duplication. *Journal of Cell Science*, *126*(14), 3223–3233. https://doi.org/10.1242/jcs.129502

Soskis, M. J., Ho, H. Y. H., Bloodgood, B. L., Robichaux, M. A., Malik, A. N., Ataman, B., … Greenberg, M. E. (2012). A chemical genetic approach reveals distinct EphB signaling mechanisms during brain development. *Nature Neuroscience*, *15*(12), 1645–1654. https://doi.org/10.1038/nn.3249

Stagge, F., Mitronova, G. Y., Belov, V. N., Wurm, C. A., & Jakobs, S. (2013). Snap-, CLIP- and halo-tag labelling of budding yeast cells. *PLoS One*, *8*(10), e78745. https://doi.org/10.1371/journal.pone.0078745

Steegmaier, M., Hoffmann, M., Baum, A., Lénárt, P., Petronczki, M., Krssák, M., … Rettig, W. J. (2007). BI 2536, a potent and selective inhibitor of polo-like kinase 1, inhibits tumor growth in vivo. *Current Biology*, *17*(4), 316–322. https://doi.org/10.1016/j.cub.2006.12.037

Suijkerbuijk, S. J. E., Vleugel, M., Teixeira, A., & Kops, G. J. P. L. (2012). Integration of kinase and phosphatase activities by BUBR1 ensures formation of stable kinetochore-microtubule attachments. *Developmental Cell*, *23*(4), 745–755. https://doi.org/10.1016/j.devcel.2012.09.005

Tan, E. P., Caro, S., Potnis, A., Lanza, C., & Slawson, C. (2013). O-linked N-acetylglucosamine cycling regulates mitotic spindle organization. *Journal of Biological Chemistry*, *288*(38), 27085–27099. https://doi.org/10.1074/jbc.M113.470187

Tate, E. W., Kalesh, K. A., Lanyon-Hogg, T., Storck, E. M., & Thinon, E. (2015). Global profiling of protein lipidation using chemical proteomic technologies. *Current Opinion in Chemical Biology*, *24*, 48–57. https://doi.org/10.1016/j.cbpa.2014.10.016

Thakur, H. C., Singh, M., Nagel-Steger, L., Kremer, J., Prumbaum, D., Fansa, E. K., … Piekorz, R. P. (2014). The centrosomal adaptor TACC3 and the microtubule polymerase chTOG interact via defined C-terminal subdomains in an Aurora-A kinase-independent manner. *Journal of Biological Chemistry*, *289*(1), 74–88. https://doi.org/10.1074/jbc.M113.532333

Thawani, A., Kadzik, R. S., & Petry, S. (2018). XMAP215 is a microtubule nucleation factor that functions synergistically with the γ-tubulin ring complex. *Nature Cell Biology*, *20*(5), 575–585. https://doi.org/10.1038/s41556-018-0091-6

Thomas, Y., Peter, M., Mechali, F., Blanchard, J. M., Coux, O., & Baldin, V. (2014). Kizuna is a novel mitotic substrate for CDC25B phosphatase. *Cell Cycle*, *13*(24), 3867–3877. https://doi.org/10.4161/15384101.2014.972882

Timm, S., Titus, B., Bernd, K., & Barroso, M. (1999). The EF-hand Ca2+-binding protein p22 associates with microtubules in an N-myristoylation-dependent manner. *Molecular Biology of the Cell*, *10*(10), 3473–3488. https://doi.org/10.1091/mbc.10.10.3473

Torres, J. Z., Ban, K. H., & Jackson, P. K. (2010). A specific form of phospho protein phosphatase 2 regulates anaphase-promoting complex/cyclosome association with spindle poles. *Molecular Biology of the Cell*, *21*(6), 897–904. https://doi.org/10.1091/mbc.e09-07-0598

Torres, J. Z., Summers, M. K., Peterson, D., Brauer, M. J., Lee, J., Senese, S., … Jackson, P. K. (2011). The STARD9/Kif16a kinesin associates with mitotic microtubules and regulates spindle pole assembly. *Cell*, *147*(6), 1309–1323. https://doi.org/10.1016/J.CELL.2011.11.020

Tsai, C. Y., Ngo, B., Tapadia, A., Hsu, P. H., Wu, G., & Lee, W. H. (2011). Aurora-A phosphorylates augmin complex component hice1 protein at an N-terminal serine/threonine cluster to modulate its microtubule binding activity during spindle assembly. *Journal of Biological Chemistry*, *286*(34), 30097–30106. https://doi.org/10.1074/jbc.M111.266767

Vallardi, G., Allan, L. A., Crozier, L., & Saurin, A. T. (2019). Division of labour between pp2a-b56 isoforms at the centromere and kinetochore. *eLife*, *8*. https://doi.org/10.7554/eLife.42619

van de Kooij, B., Creixell, P., van Vlimmeren, A., Joughin, B. A., Miller, C. J., Haider, N., … Yaffe, M. B. (2019). Comprehensive substrate specificity profiling of the human nek kinome reveals unexpected signaling outputs. *eLife*, *8*, 8. https://doi.org/10.7554/eLife.44635

Varma, D., Chandrasekaran, S., Sundin, L. J. R., Reidy, K. T., Wan, X., Chasse, D. A. D., … Cook, J. G. (2012). Recruitment of the human Cdt1 replication licensing protein by the loop domain of Hec1 is required for stable kinetochore-microtubule attachment. *Nature Cell Biology*, *14*(6), 593–603. https://doi.org/10.1038/ncb2489

Wang, G., Jiang, Q., & Zhang, C. (2014). The role of mitotic kinases in coupling the centrosome cycle with the assembly of the mitotic spindle. *Journal of Cell Science*, *127*(19), 4111–4122. https://doi.org/10.1242/jcs.151753

Wang, J., Wang, Z., Yu, T., Yang, H., Virshup, D. M., Kops, G. J. P. L., … Rao, Z. (2016). Crystal structure of a PP2A B56-BubR1 complex and its implications for PP2A substrate recruitment and localization. *Protein & Cell*, *7*(7), 516–526. https://doi.org/10.1007/s13238-016-0283-4

Wang, Z., Udeshi, N. D., Slawson, C., Compton, P. D., Sakabe, K., Cheung, W. D., … Hart, G. W. (2010). Extensive crosstalk between O-GlcNAcylation and phosphorylation regulates cytokinesis. *Science Signaling*, *3*(104), ra2. https://doi.org/10.1126/scisignal.2000526

Welburn, J. P. I., Grishchuk, E. L., Backer, C. B., Wilson-Kubalek, E. M., Yates, J. R., & Cheeseman, I. M. (2009). The human kinetochore Ska1 complex facilitates microtubule depolymerization-coupled motility. *Developmental Cell*, *16*(3), 374–385. https://doi.org/10.1016/j.devcel.2009.01.011

Welburn, J. P. I., Vleugel, M., Liu, D., Yates, J. R., Lampson, M. A., Fukagawa, T., & Cheeseman, I. M. (2010). Aurora B phosphorylates spatially distinct targets to differentially regulate the kinetochore-microtubule interface. *Molecular Cell*, *38*(3), 383–392. https://doi.org/10.1016/j.molcel.2010.02.034

Wu, J., Cho, H. P., Rhee, D. B., Johnson, D. K., Dunlap, J., Liu, Y., & Wang, Y. (2008). Cdc14B depletion leads to centriole amplification, and its overexpression prevents unscheduled centriole duplication. *Journal of Cell Biology*, *181*(3), 475–483. https://doi.org/10.1083/jcb.200710127

Xu, P., Raetz, E. A., Kitagawa, M., Virshup, D. M., & Lee, S. H. (2013). BUBR1 recruits PP2A via the B56 family of targeting subunits to promote chromosome congression. *Biology Open*, *2*(5), 479–486. https://doi.org/10.1242/bio.20134051

Xue, L., & Tao, W. A. (2013). Current technologies to identify protein kinase substrates in high throughput. *Frontiers in Biology*, *8*(2), 216–227. https://doi.org/10.1007/s11515-013-1257-z

Yamashiro, S., Yamakita, Y., Totsukawa, G., Goto, H., Kaibuchi, K., Ito, M., … Matsumura, F. (2008). Myosin phosphatase-targeting subunit 1 regulates mitosis by antagonizing polo-like kinase 1. *Developmental Cell*, *14*(5), 787–797. https://doi.org/10.1016/j.devcel.2008.02.013

Yasui, Y., Urano, T., Kawajiri, A., Nagata, K. I., Tatsuka, M., Saya, H., … Inagaki, M. (2004). Autophosphorylation of a newly identified site of Aurora-B is indispensable for cytokinesis. *Journal of Biological Chemistry*, *279*(13), 12997–13003. https://doi.org/10.1074/jbc.M311128200

Yu, R., Wu, H., Ismail, H., Du, S., Cao, J., Wang, J., … Yao, X. (2020). Methylation of PLK1 by SET7/9 ensures accurate kinetochore–microtubule dynamics. *Journal of Molecular Cell Biology*, *12*(6), 462–476. https://doi.org/10.1093/jmcb/mjz107

Zeng, K., Bastos, R. N., Barr, F. A., & Gruneberg, U. (2010). Protein phosphatase 6 regulates mitotic spindle formation by controlling the T-loop phosphorylation state of Aurora A bound to its activator TPX2. *Journal of Cell Biology*, *191*(7), 1315–1332. https://doi.org/10.1083/jcb.201008106

Zhang, J., Ma, Y., Taylor, S. S., & Tsien, R. Y. (2001). Genetically encoded reporters of protein kinase a activity reveal impact of substrate tethering. *Proceedings of the National Academy of Sciences of the United States of America*, *98*(26), 14997–15002. https://doi.org/10.1073/pnas.211566798

Zhang, Q., Sivakumar, S., Chen, Y., Gao, H., Yang, L., Yuan, Z., … Liu, H. (2017). Ska3 phosphorylated by Cdk1 binds Ndc80 and recruits Ska to kinetochores to promote mitotic progression. *Current Biology*, *27*(10), 1477–1484.e4. https://doi.org/10.1016/j.cub.2017.03.060

Zhang, X., Chen, Q., Feng, J., Hou, J., Yang, F., Liu, J., … Zhang, C. (2009). Sequential phosphorylation of Nedd1 by Cdk1 and Plk1 is required for targeting of the γTuRC to the centrosome. *Journal of Cell Science*, *122*(13), 2240–2251. https://doi.org/10.1242/jcs.042747

Zhang, X., Lan, W., Ems-McClung, S. C., Stukenberg, P. T., & Walczak, C. E. (2007). Aurora B phosphorylates multiple sites on mitotic centromere-associated kinesin to spatially and temporally regulate its function. *Molecular Biology of the Cell*, *18*(9), 3264–3276. https://doi.org/10.1091/mbc.E07-01-0086

Zhao, Z. S., Lim, J. P., Ng, Y. W., Lim, L., & Manser, E. (2005). The GIT-associated kinase PAK targets to the centrosome and regulates Aurora-A. *Molecular Cell*, *20*(2), 237–249. https://doi.org/10.1016/j.molcel.2005.08.035

Zorba, A., Buosi, V., Kutter, S., Kern, N., Pontiggia, F., Cho, Y. J., & Kern, D. (2014). Molecular mechanism of Aurora A kinase autophosphorylation and its allosteric activation by TPX2. *eLife*, *2014*(3). https://doi.org/10.7554/eLife.02667.001

How to cite this article: Ong JY, Bradley MC, Torres JZ. Phospho-regulation of mitotic spindle assembly. *Cytoskeleton*. 2020;77:558–578. https://doi.org/10.1002/cm.21649

Chapter 5: Molecular characterization of Cdk15, a putative spindle assembly checkpoint regulator

Abstract

The spindle assembly checkpoint (SAC) regulates the metaphase to anaphase transition in cell division. While many aspects of SAC signaling and regulation have been identified, much about SAC signaling is still being discovered. We identified a novel kinase Cdk15 as a potential regulator of the SAC. Here, we demonstrate that Cdk15 can bind to important mitotic regulators Mad2, Plk1, Aurora Kinase B, and Survivin both from in vitro transcribed and translated proteins and from HeLa cell lysates. For Plk1, we suggest that Plk1 is a substrate of Cdk15 and that Cdk15 is not a substrate of Plk1. We also show that the localization of Cdk15 to the nucleus during interphase is dependent on a canonical nuclear localization sequence. Altogether, we present some elements of the molecular characterization of this putative SAC kinase.

Introduction

The faithful segregation of chromosomes during mitosis is regulated by the spindle assembly checkpoint (SAC), which delays the metaphase to anaphase transition and is composed of two main modules (Musacchio and Salmon, 2007). The first module involves the anaphase promoting complex/cyclosome (APC/C). The APC/C is a mitotic E3 ubiquitin ligase responsible for two major events in mitosis: (1) the ubiquitylation and subsequent degradation of securin, the inhibitor of the protease separase; once uninhibited, separase degrades the cohesion proteins that binds sister chromosomes together during metaphase; and (2) the degradation of cyclin B1, which inactivates Cdk1 and promotes mitotic exit (Pines, 2011; Primorac and Musacchio, 2013). In the first module of the SAC, a mitotic checkpoint complex (MCC) comprised of Mad2, Cdc20, BubR1, and Bub3 is generated at unattached kinetochores and inhibits the APC/C, thus preventing sister chromosome separation until all the kinetochores are attached to microtubules.

In the second module of SAC regulation, the chromosomal passenger complex (CPC) comprised of Aurora Kinase B, Survivin, INCENP, and Borealin phosphorylates microtubule-associated proteins like the Ndc80 complex, phosphorylation events that broadly serve to weaken microtubule-kinetochore attachments (Ong et al., 2020). In this way, incorrect microtubule-kinetochore attachments are disrupted and the kinetochore gets another “chance” at capturing a microtubule. Only when an amphitelic (bipolar) microtubule attachment has been generated at each kinetochore, and tension is generated across the sister chromosomes such that the microtubule-kinetochore sites are now pulled away from the centrosomes and the CPC, are the microtubule-associated proteins free from Aurora Kinase B-mediated regulation of kinetochore attachment. Thus, in this parallel module of SAC regulation, cell division is prohibited until proper (bipolar and with tension) spindle-chromosome attachments are generated.

The SAC is a highly controlled process. In order to further understand SAC regulation, we performed an siRNA screen against the “druggable” human genome using the HeLa FUCCI cell line (Sakaue-Sawano et al., 2008). Briefly, HeLa FUCCI cells were treated with a library of siRNAs and treated with 6 nM Taxol. Cells whose SAC was not perturbed will arrest in mitosis and fluoresce green; cells whose SAC function was compromised will continue through with cell division and fluoresce red. By quantifying the ratio of red:green cells, siRNAs may modulate SAC function can be determined. Through this method, we identified Cdk15, a cyclin dependent kinase whose knockdown via siRNA resulted in SAC bypass. Cdk15 is a poorly studied protein implicated in some cancer types via broad genetic analyses; generally, higher Cdk15 expression corresponds to a worse prognosis (Shiraishi et al., 2014; Zhang et al., 2021). Few studies have examined Cdk15 at a molecular basis: one study identifies Survivin as a substrate of Cdk15 (Park et al., 2014) and suggests a role in protecting some cell types from apoptosis, and another identifies Pak4 as a substrate and suggests that Cdk15 phosphorylation of Pak4 leads to subsequent amplified ERK signaling, cell proliferation, and tumor growth of colorectal cancer cells

(Huang et al., 2022). Given that Cdk15 is an emerging factor in cell proliferation, we sought to characterize Cdk15 and its effects on mitosis and the SAC.

Materials and Methods

The reagents and experimental procedures are the same as Chapter 2 (SPOP) with the following modifications:

1. The solid phase for Myc-immunoprecipitations is Anti-Myc-tag mAb-Magnetic Beads (MBL, M047-11).
2. The Survivin antibody (Abcam, ab76424) used for immunoblotting was used at 1:1000.
3. pDONR221 Mad2, Aurora B Kinase, and Survivin were already generated in the Torres lab.
4. The purchased Cdk15 ORF (GenScript) codes for the 429 amino acid isoform given by Uniprot ID Q96Q40-5.

Primers used for Gateway cloning are as follows and are all from Eurofins:

Primer name	Sequence (5'-3')
Cdk15 Fwd	GGGGACAAGTTTGTACAAAAAAGCAGGCTTCGAAGG AGATAGAACCATGGGTCAAGAGCTGTGTGCAAAGAC
Cdk15 NT_RevS	GGGGACCACTTTGTACAAGAAAGCTGGGTCCTATGA GGCTGCCCCAAAAGGGAGG
Cdk15 KD_Fwd	GGGGACAAGTTTGTACAAAAAAGCAGGCTTCGAAGG AGATAGAACCATGGGGTCTTACTTGAACTTGGAGAAGC
Cdk15 KD_RevS	GGGGACCACTTTGTACAAGAAAGCTGGGTCCTAGAA ATAATCATGAACAAGTGC

Cdk15 CT_Fwd	GGGGACAAGTTTGTACAAAAAAGCAGGCTTCGAAGG AGATAGAACCATGGGGAGCGCCCTGCCATCTCAGC
Cdk15 RevS	GGGGACCACTTTGTACAAGAAAGCTGGGTCCTACCA GCATTTGCTAAACTGGGC
Plk1 Fwd	GGGGACAAGTTTGTACAAAAAAGCAGGCTTCGAAGG AGATAGAACCATGGGGAGTGCTGCAGTGACTGC
Plk1 KD_RevS	GGGGACCACTTTGTACAAGAAAGCTGGGTCCTAAAA GAACTCGTCATTAAGCAGC
Plk1 LinkPDB_Fwd	GGGGACAAGTTTGTACAAAAAAGCAGGCTTCGAAGG AGATAGAACCATGGGGACTTCTGGCTATATCCCTGCC
Plk1 PDB_Fwd	GGGGACAAGTTTGTACAAAAAAGCAGGCTTCGAAGG AGATAGAACCATGGGGATGCTGCAGCAGCTGCACAGTG
Plk1 RevS	GGGGACCACTTTGTACAAGAAAGCTGGGTCCTAGGA GGCCTTGAGACGGTTGCTGG

Results

Cdk15 binds to mitotic proteins Mad2, Plk1, Aurora Kinase B, and Survivin

We began by analyzing the domains of Cdk15. By homology to other Cdks, we identified the only domain in Cdk15 as the kinase domain. We thus truncated Cdk15 according to its domains using PCR: full length (FL, amino acids 1-429); N-terminus (NT, 1-101); kinase domain (KD, 102-387); C-terminus (CT, 388-429); NTKD (1-387); and KDCT (102-429).

We next sought to determine the binding partners of Cdk15. We chose a subset of mitotic proteins of interest determined via mass spectrometry of overexpressed Cdk15: Mad2, Plk1, Aurora Kinase B (AurK B), and Survivin. First, we expressed these proteins via IVT and

subjected them to binding experiments with Cdk15 FL, NT, KD, or CT (Figure 1A-D). In all cases, the Cdk15 FL and KD, but not the NT or CT, co-immunoprecipitated with the mitotic protein. Broadly, this is not altogether unsurprising, considering neither the NT nor the CT of Cdk15 have any structural elements that would support binding. We sought to validate whether these binding interactions could be recapitulated in HeLa cell lysates. HeLa cells were transfected with Myc-Cdk15 and the four mitotic proteins, treated with Taxol to arrest the cells in mitosis, and subjected to Myc-immunoprecipitation. Again, Cdk15 was able to co-immunoprecipitate HA-Plk1 and Mad2 (Figure 2A) and FLAG-AurK B and Survivin (Figure 2B). Altogether, these results suggest that Cdk15 can interact with these four proteins with key roles in the spindle assembly checkpoint, albeit while both proteins are overexpressed.

Cdk15 binds to the kinase domain of Plk1

We were interested in examining the interaction between Cdk15 and Plk1, as both are kinases. In particular, we sought to determine the kinase relationship between the two: does Cdk15 phosphorylate Plk1; does Plk1 phosphorylate Cdk15; or do they phosphorylate each other? Preliminary kinase assays using 32P-labeled ATP were technically challenging, so we opted for another approach. Plk1 binds to its substrates using its polo box domains (PBD). Broadly, the PBD recognizes phosphorylated peptides (for example, a residue phosphorylated by a priming kinase like Cdk1) and allows for subsequent Plk1 phosphorylation on a different residue (Tsvetkov et al., 2005; Liu et al., 2004; Elia et al., 2003). Thus, if Cdk15 is a substrate of Plk1, it should bind to the PBD of Plk1.

We truncated Plk1 into its different domains (Lee et al., 2014; Schmucker and Sumara, 2014): full length (FL, amino acids 1-603); kinase domain (KD, 1-305); polo box domains (PDB, 377-603); and Linker + PBD (306-603). Given that the PDB of Plk1 often requires phosphorylated substrates and we did not know the kinase that would phosphorylate Cdk15, we opted to perform this binding reaction in asynchronous HeLa cells instead of with IVT protein, as

this approach would give us the highest likelihood that the necessary phosphorylation to mediate Cdk15-Plk1 binding would be present. A co-immunoprecipitation demonstrated that both Plk1 FL and KD, but not the domains containing the PBD, bound to Cdk15 (Figure 3). Thus, at least using the basis that substrates of Plk1 bind to its PBD, it seems that Cdk15 is not a substrate of Plk1. Rather, it seems that Cdk15 binds to (and possibly phosphorylates) Plk1 at the kinase domain of Plk1.

Cdk15 nuclear localization is dependent on a classical nuclear localization sequence

Having established that Cdk15 can bind to mitotic proteins, we next sought to determine the localization of Cdk15 in cells. We could not determine a clear mitotic localization for Cdk15. However, we did observe that Cdk15 FL localized slightly within the nucleus. Using a computational tool (Nguyen Ba et al., 2009) to identify canonical nuclear localization signals (NLS; we used a cut off value of 0.4 instead of the default 0.5), we identified a putative monopartite NLS within the N-terminus of Cdk15: 67KFKSKRP73. As NLS tend to involve basic residues, we disrupted the NLS via mutation of amino acids KR (underlined in previous sentence) to AA, giving Cdk15 KR71AA. We transfected pgLAP1-tagged Cdk15 WT or KR71AA into HeLa cells and assessed the localization of each protein (Figure 4). For Cdk15 FL and NTKD, mutation of these residues to alanine significantly weakened the nuclear localization of Cdk15. For the Cdk15 NT, mutation of these residues did not have as significant an effect on the nuclear localization of the Cdk15 NT. Given that pgLAP1 Cdk15 NT is about 30 kDa (28 kDa EGFP-S Tag + 1.3 kDa Cdk15 N-terminus), the Cdk15 NT is small enough to avoid exclusion by the nuclear pore complex, which generally excludes molecules larger than approximately 60 kDa (Wang and Brattain, 2007).

Discussion

The full ensemble of proteins that regulate the spindle assembly checkpoint are unknown. Here, we describe Cdk15 as a potential regulator of the spindle assembly checkpoint and document its ability to bind the key mitotic proteins Mad2, Plk1, Aurora Kinase B, and Survivin and its nuclear localization, dependent on a nuclear localization sequence.

We initially identified Cdk15 as a novel mitotic regulator via a high-throughput siRNA screen. Subsequent experimentation has suggested that the original siRNAs used in the screen to identify Cdk15 as a novel mitotic regulator may have also had off-target effects on Mad2, a common off-target effect of siRNAs (Hübner et al., 2010). In particular, loss of Cdk15 via some siRNAs also led to loss of Mad2 via immunoblotting. Thus, Cdk15 may be a false positive as a regulator of the spindle assembly checkpoint. Why the key mitotic proteins Mad2, Plk1, Aurora Kinase B, and Survivin thus seem to bind to Cdk15 is unclear. Perhaps, if the loss of Mad2 via Cdk15 siRNAs is due to off-target effects, Cdk15 may nonetheless be an important mitotic regulator like Cdk1. On the other hand, the consistent loss of Mad2 by various Cdk15 siRNAs may suggest that Cdk15 may serve a role in stabilizing Mad2, either transcriptionally (discussed below) or directly through protein-protein interactions.

The observation of Cdk15 in the nucleus is reminiscent of transcriptional Cdks, like Cdk5 or Cdk9. These transcriptional kinases bind to cyclins that are not cell-cycle regulated and thus the regulation of these kinases is not cell cycle-dependent (Malumbres, 2014). However, Cdks cannot be simply divided into “transcriptional” or “cell cycle” Cdks. Indeed, in S. cerevisiae, Cdk1, a canonical “cell cycle” Cdk, has strong roles in transcriptional activation of RNA polymerase and promoting the transcription of S-phase genes (Kõivomägi et al., 2021). Perhaps Cdk15 is also similarly responsible for the transcription of other genes necessary for cell cycle progression.

Key questions in understanding the role of Cdk15 remain. What is the cyclin that binds to and regulates Cdk15? We were unable to pursue any viable in vitro kinase assays with Cdk15 because Cdks are not active in the absence of their cyclin. Consequently, we were unable to

determine the substrates of Cdk15. These experiments were done with exogenous Cdk15 because no commercial antibody against Cdk15 could be validated. The localization and role of endogenous Cdk15, which would be possible via good antibodies against Cdk15 and/or CRISPR-based tagging or disruption of the genetic locus of Cdk15, would greatly aid our understanding of Cdk15. Similarly, the reagents available to disrupt Cdk15 (while leaving Mad1 intact) to study its function are necessary for understanding the role of Cdk15 within the cell.

Acknowledgements

We thank Katherine Morillo (summer student in 2017), Vivian Yang (2017-2019), and Hieu Nguyen (2018-2021) for their work on the project.

References

Elia, A.E.H., L.C. Cantley, and M.B. Yaffe. 2003. Proteomic Screen Finds pSer/pThr-Binding Domain Localizing Plk1 to Mitotic Substrates. Science (80-.). 299:1228–1231. doi:10.1126/science.1079079.

Huang, C., R. Du, X. Jia, K. Liu, Y. Qiao, Q. Wu, N. Yao, L. Yang, L. Zhou, X. Liu, P. Xiang, M. Xin, Y. Wang, X. Chen, D.J. Kim, Z. Dong, and X. Li. 2022. CDK15 promotes colorectal cancer progression via phosphorylating PAK4 and regulating β-catenin/ MEK-ERK signaling pathway. Cell Death Differ. 29:14–27. doi:10.1038/s41418-021-00828-6.

Hübner, N.C., L.H.C. Wang, M. Kaulich, P. Descombes, I. Poser, and E.A. Nigg. 2010. Re-examination of siRNA specificity questions role of PICH and Tao1 in the spindle checkpoint and identifies Mad2 as a sensitive target for small RNAs. Chromosoma. 119:149. doi:10.1007/S00412-009-0244-2.

Kõivomägi, M., M.P. Swaffer, J.J. Turner, G. Marinov, and J.M. Skotheim. 2021. G1 cyclin-Cdk promotes cell cycle entry through localized phosphorylation of RNA polymerase II. Science. 374:347–351. doi:10.1126/science.aba5186.

Lee, K.S., J.-E. Park, Y.H. Kang, T.-S. Kim, and J.K. Bang. 2014. Mechanisms Underlying Plk1 Polo-Box Domain-Mediated Biological Processes and Their Physiological Significance. Mol. Cells. 37:286–294. doi:10.14348/molcells.2014.0002.

Liu, X., T. Zhou, R. Kuriyama, and R.L. Erikson. 2004. Molecular interactions of Polo-like-kinase 1 with the mitotic kinesin-like protein CHO1/MKLP-1. J. Cell Sci. 117:3233–3246. doi:10.1242/jcs.01173.

Malumbres, M. 2014. Cyclin-dependent kinases. Genome Biol. 15:122. doi:10.1186/gb4184.

Musacchio, A., and E.D. Salmon. 2007. The spindle-assembly checkpoint in space and time. Nat. Rev. Mol. Cell Biol. 8:379–393. doi:10.1038/nrm2163.

Nguyen Ba, A.N., A. Pogoutse, N. Provart, and A.M. Moses. 2009. NLStradamus: a simple Hidden Markov Model for nuclear localization signal prediction. BMC Bioinformatics. 10:202. doi:10.1186/1471-2105-10-202.

Ong, J.Y., M.C. Bradley, and J.Z. Torres. 2020. Phospho‐regulation of mitotic spindle assembly. Cytoskeleton. 77:558–578. doi:10.1002/cm.21649.

Park, M.H., S.Y. Kim, Y.J. Kim, and Y.-H. Chung. 2014. ALS2CR7 (CDK15) attenuates TRAIL induced apoptosis by inducing phosphorylation of survivin Thr34. Biochem. Biophys. Res. Commun. 450:129–134. doi:10.1016/j.bbrc.2014.05.070.

Pines, J. 2011. Cubism and the cell cycle: the many faces of the APC/C. Nat. Rev. Mol. Cell Biol. 12:427–438. doi:10.1038/nrm3132.

Primorac, I., and A. Musacchio. 2013. Panta rhei: the APC/C at steady state. J. Cell Biol. 201:177–89. doi:10.1083/jcb.201301130.

Sakaue-Sawano, A., H. Kurokawa, T. Morimura, A. Hanyu, H. Hama, H. Osawa, S. Kashiwagi, K. Fukami, T. Miyata, H. Miyoshi, T. Imamura, M. Ogawa, H. Masai, and A. Miyawaki. 2008. Visualizing Spatiotemporal Dynamics of Multicellular Cell-Cycle Progression. Cell. 132:487–498. doi:10.1016/J.CELL.2007.12.033.

Schmucker, S., and I. Sumara. 2014. Molecular dynamics of PLK1 during mitosis. Mol. Cell. Oncol. 1:e954507. doi:10.1080/23723548.2014.954507.

Shiraishi, Y., A. Fujimoto, M. Furuta, H. Tanaka, K. Chiba, K.A. Boroevich, T. Abe, Y. Kawakami, M. Ueno, K. Gotoh, S. Ariizumi, T. Shibuya, K. Nakano, A. Sasaki, K. Maejima, R. Kitada, S. Hayami, Y. Shigekawa, S. Marubashi, T. Yamada, M. Kubo, O. Ishikawa, H. Aikata,

K. Arihiro, H. Ohdan, M. Yamamoto, H. Yamaue, K. Chayama, T. Tsunoda, S. Miyano, and H. Nakagawa. 2014. Integrated Analysis of Whole Genome and Transcriptome Sequencing Reveals Diverse Transcriptomic Aberrations Driven by Somatic Genomic Changes in Liver Cancers. PLoS One. 9:e114263. doi:10.1371/journal.pone.0114263.

Tsvetkov, L.M., R.T. Tsekova, X. Xu, and D.F. Stern. 2005. The Plk1 Polo Box Domain Mediates a Cell Cycle and DNA Damage Regulated Interaction with Chk2. Cell Cycle. 4:602–610. doi:10.4161/cc.4.4.1599.

Wang, R., and M.G. Brattain. 2007. The maximal size of protein to diffuse through the nuclear pore is larger than 60kDa. FEBS Lett. 581:3164–70. doi:10.1016/j.febslet.2007.05.082.

Zhang, X., Q. Wang, Y. Luo, M. Song, Z. Zhou, L. Zeng, M. Hu, and C. Yang. 2021. Cyclin-dependent kinase 15 upregulation is correlated with poor prognosis for patients with breast cancer. J. Int. Med. Res. 49:300060521999552. doi:10.1177/0300060521999552.

Figures and figure legends

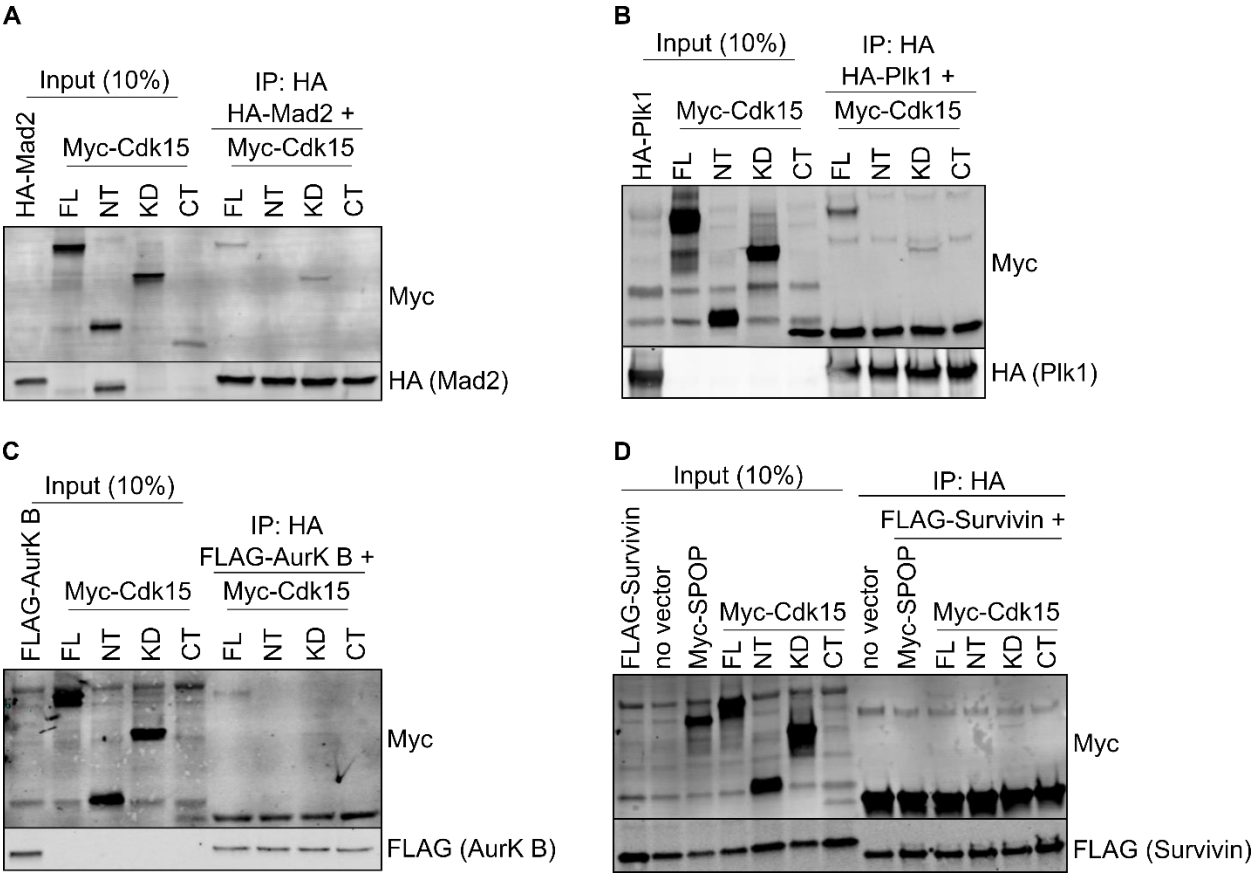

Figure 1. The Cdk15 kinase domain binds to Plk1, Mad2, Aurora Kinase B, and Survivin. IVT-expressed Myc-Cdk15 full length (FL, amino acids 1-429), N-terminus (NT, 1-101), kinase domain (KD, 102-387), or C-terminus (CT, 388-429) and (A) HA-Mad2, (B) HA-Plk1, (C) FLAG-Aurora Kinase B (AurK B), and (D) FLAG-Survivin were subjected to Myc-immunoprecipitation and the resulting blots probed with the indicated antibodies. In (D), no vector refers to no Myc-tagged protein (just the IVT master mix and water), and Myc-SPOP is used as a negative control.

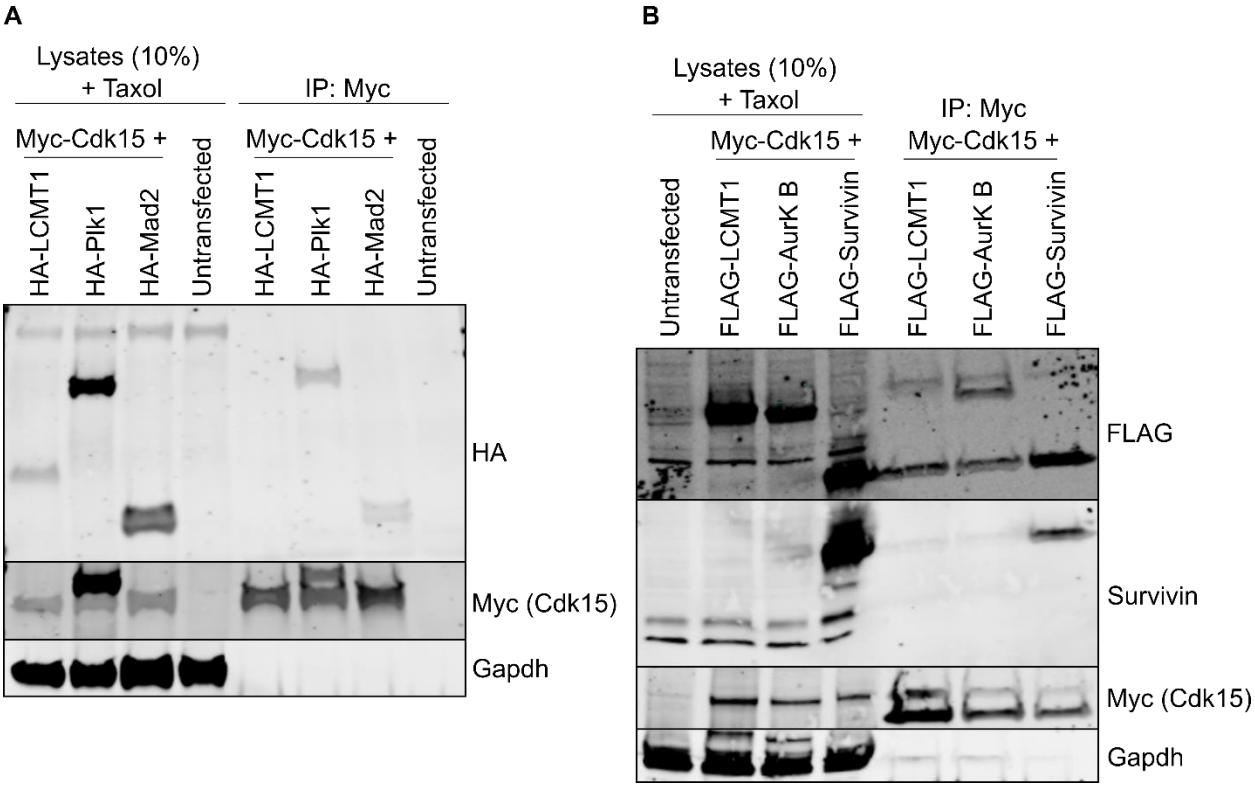

Figure 2. Plk1, Mad2, Aurora Kinase B, and Survivin co-immunoprecipitate with Cdk15 from HeLa lysates. (A) Lysates from HeLa cells co-transfected with Myc-Cdk15 and HA-Plk1 or HA-Mad2 were subjected to Myc-immunoprecipitaiton and the resulting blot probed with the indicated antibodies. (B) Same as (A), except with FLAG-AurK B and FLAG-Survivin and subjected to Myc-immunoprecipitation. Because FLAG-Survivin migrates at the same weight as the IgG light chain, the blot was also probed with a Survivin antibody. LCMT1 was used as a negative control.

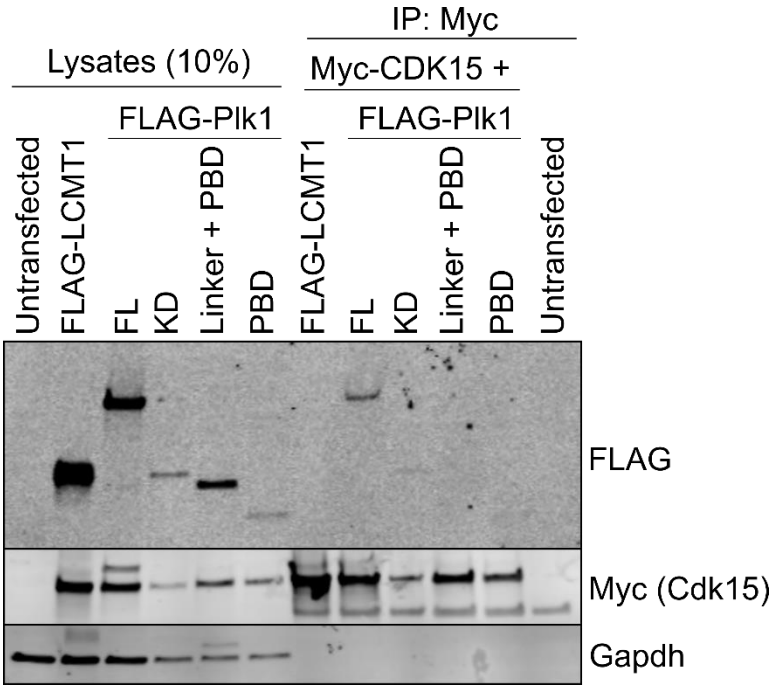

Figure 3. Cdk15 binds to the kinase domain of Plk1. Lysates from HeLa cells co-transfected with Myc-Cdk15 and FLAG-LCMT1 or FLAG-Plk1 truncations (FL, full length: amino acids 1-603; KD, kinase domain: 1-305; Linker + PBD: 306-603; PBD, polo box domains: 377-603) were subjected to Myc-immunoprecipitaiton and the resulting blot probed with the indicated antibodies. LCMT1 was used as a negative control.

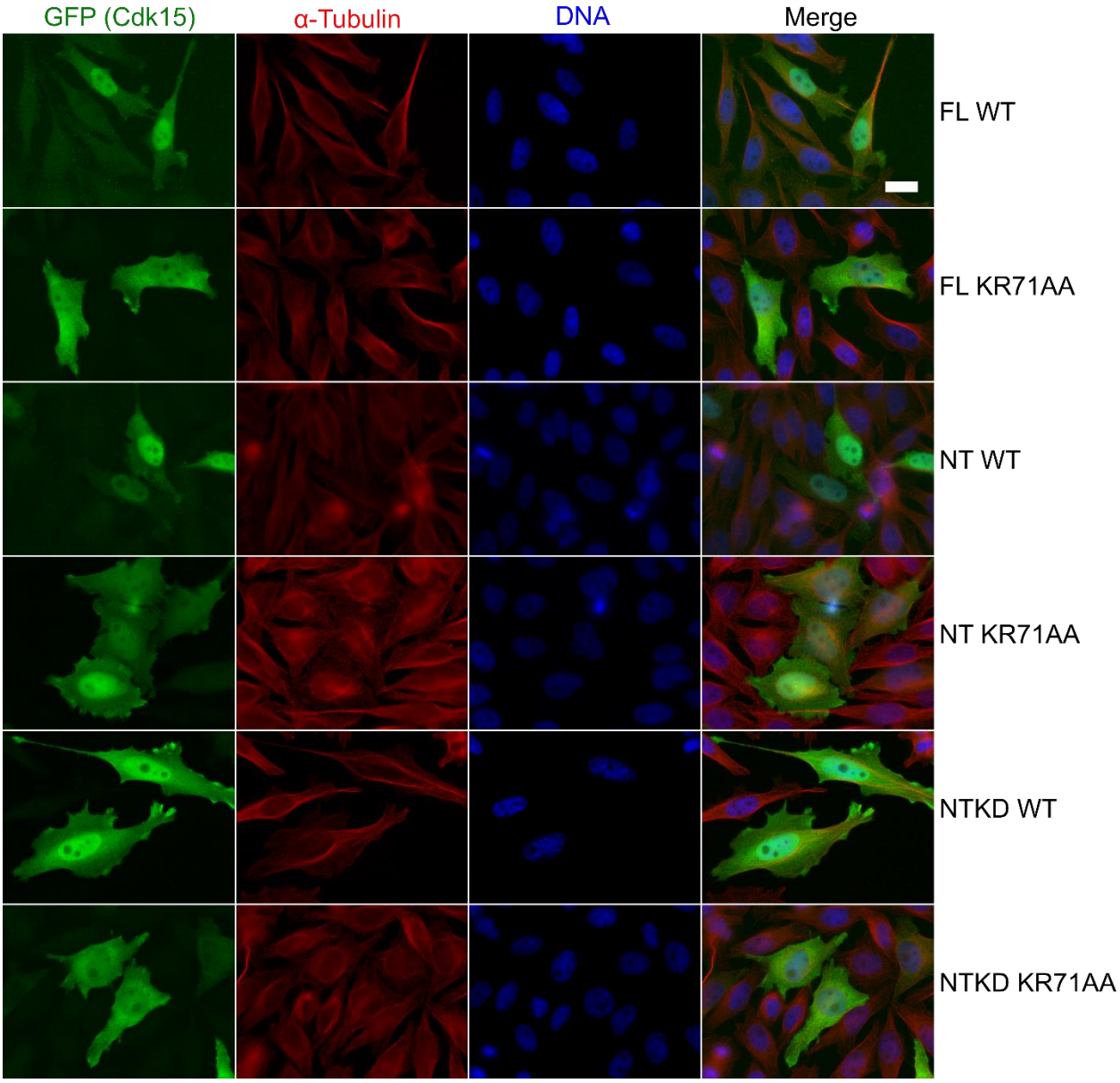

Figure 4. The nuclear localization of Cdk15 is dependent on an N-terminal NLS. HeLa cells were transfected with pgLAP1 Cdk15 FL, NT, NTKD, either WT or with the putative N-terminal NLS mutated (KR71AA) and stained with the indicated antibodies. The scale bar is 20 μm.

Appendix Chapter 1: Dissecting the mechanisms of cell division

This chapter is reproduced from

Joseph Y. Ong and Jorge Z. Torres. Dissecting the mechanisms of cell division. Review. J Biol Chem. 2019 Jul 26;294(30):11382-11390. doi: 10.1074/jbc.AW119.008149 PMID: 31175154

JBC ASBMB AWARD ARTICLE

Dissecting the mechanisms of cell division

Published, Papers in Press, June 7, 2019, DOI 10.1074/jbc.AW119.008149

Joseph Y. Ong[‡] and Jorge Z. Torres[‡§¶1]

From the [‡]Department of Chemistry and Biochemistry, [§]The Jonsson Comprehensive Cancer Center, and the [¶]Molecular Biology Institute, UCLA, Los Angeles, California 90095

Edited by Enrique M. De La Cruz

Cell division is a highly regulated and carefully orchestrated process. Understanding the mechanisms that promote proper cell division is an important step toward unraveling important questions in cell biology and human health. Early studies seeking to dissect the mechanisms of cell division used classical genetics approaches to identify genes involved in mitosis and deployed biochemical approaches to isolate and identify proteins critical for cell division. These studies underscored that post-translational modifications and cyclin–kinase complexes play roles at the heart of the cell division program. Modern approaches for examining the mechanisms of cell division, including the use of high-throughput methods to study the effects of RNAi, cDNA, and chemical libraries, have evolved to encompass a larger biological and chemical space. Here, we outline some of the classical studies that established a foundation for the field and provide an overview of recent approaches that have advanced the study of cell division.

Introduction to cell division

Cell division, or mitosis, is the process by which a mother cell divides its nuclear and cytoplasmic components into two daughter cells. Mitosis is divided into four major phases: prophase, metaphase, anaphase, and telophase. Careful regulation of the cell division program is crucial for proper cell growth, development, and gametogenesis. Dysfunction or misregulation of cell division can lead to growth defects (1, 2) and proliferative diseases like cancer (3) and aging-related diseases (4), including Alzheimer's disease (5). Therefore, analyses of the pathways and mechanisms that promote proper cell division are important avenues through which we can understand cell regulation and its misregulation in human disease.

Cell division is driven by two main modes of post-translational modifications. First, protein kinases like cyclin-dependent kinases (CDKs)[2] (6, 7) and Polo-like kinases (8) phosphorylate their substrates to modify their activity or stability; this modification is opposed by protein phosphatase–mediated dephosphorylation (for example, Cdc25 (9) and various PP2A (10) complexes). Second, E3 ubiquitin ligases like the anaphase-promoting complex/cyclosome (APC/C) (11) and Cullin 1-based SCF (Skp-Cullin-F box) (12) complexes ubiquitylate their substrates and target them for proteasomal degradation; this modification is opposed by deubiquitylases such as USP37 (13) and Cezanne (14). Spatiotemporal control of when these post-translational modifications occur gives rise to the ordered events of cell division. Our current understanding of key regulators of cell division is founded upon many classical genetic and biochemical studies aimed at understanding the cell cycle. We begin by highlighting some of these seminal studies, transition to discussing modern techniques and approaches used to dissect the mechanisms of cell division, and conclude with future directions and perspectives on the cell division field.

Classical studies of cell division: post-translational regulation

Early cell cycle studies established that phosphorylation was important for cell division. These studies assessed the DNA content, size, and doubling time of mutant strains of the yeast *Schizosaccharomyces pombe* to identify genes, termed cell division cycle (*cdc*) genes (15). One of the first *cdc* genes to be characterized was *cdc9-50*, later renamed *WEE1* (16). *WEE1*-mutant yeast divided at a smaller size than their WT counterparts, suggesting that loss of Wee1p activity accelerated mitotic entry and that Wee1p was an inhibitor of mitosis. Later, it was discovered that overexpression of the *S. pombe* gene *cdc25*, determined to encode a protein phosphatase (17), led to increased rates of mitotic entry (18). Moreover, Wee1p and Cdc25p worked in opposition to each other, suggesting a balancing act between these two proteins to regulate the initiation of mitosis (19). The cloning of *WEE1* indicated that it resembled a protein kinase (20), suggesting that phosphorylation could regulate cell division. This analysis also suggested that a common substrate of Cdc25p and Wee1p was Cdc2p, a protein kinase (21) known to be involved in the initiation of DNA replication (Cdc2p in *S. pombe* and Cdc28p in *Saccharomyces cerevisiae*, now known as CDK1 in humans) (22). The possibility that Wee1p and Cdc25p worked in opposition to each other at the biochemical level was later confirmed when it was shown that Wee1p phosphorylated and inactivated Cdc2p (23) and that Cdc25p dephosphorylated and activated Cdc2p (17). Thus, the ability of Cdc2p to regulate mitotic entry depended on its

This work was supported by National Institutes of Health NIGMS Grant R01GM117475 (to J. Z. T.), Ruth L. Kirschstein National Institutes of Health NRSA Award GM007185 (UCLA Cellular and Molecular Biology Training Program), and National Science Foundation Graduate Research Fellowship DGE-1650604 (to J. Y. O.). The authors declare that they have no conflicts of interest with the contents of this article. The content is solely the responsibility of the authors and does not necessarily represent the official views of the National Institutes of Health.

[1] To whom correspondence should be addressed. Tel.: 310-206-2092; Fax: 310-206-5213; E-mail: torres@chem.ucla.edu.

[2] The abbreviations used are: CDK, cyclin-dependent kinase; APC/C, anaphase-promoting complex/cyclosome; MPF, maturation-promoting factor; ROS, reactive oxygen species.

phosphorylation state (24), a theme that has now extended to other mitotic kinases.

Meanwhile, parallel studies in frog oocytes demonstrated that a cytoplasmic substance, termed maturation-promoting factor (MPF), regulated the initiation of meiosis (25, 26). Curiously, the levels of MPF seemed to go up and down during the different phases of meiosis (27). Purification of MPF (28) suggested that this protein complex contained two proteins: a protein kinase of ~32 kDa, later identified to be a homologue of *S. pombe* Cdc2p (29), and a protein of ~45 kDa, later identified to be cyclin B (30). The interaction between the kinase Cdc2p and cyclins, a class of proteins named because their protein levels cycled with each mitotic division in sea urchins and clams (31), became a key resource for understanding the mechanisms of cell division. The discovery of CDK2 and CDK2–cyclin A complexes (32, 33) and Cdc2–cyclin A and Cdc2–cyclin B complexes (30, 34) suggested that different cyclin-kinase pairs could regulate different aspects of mitotic entry and progression (32). Subsequent studies in model organisms demonstrated that, among its many substrates, Cdc2 phosphorylated nuclear lamins for nuclear envelope breakdown (35, 36) and cytoskeletal elements for important morphological changes during mitosis (37, 38). The ability of cyclins and their kinases to mediate mitotic entry and progression has become the engine that drives cell division.

Similar to phosphorylation and protein kinases, ubiquitylation and E3 ubiquitin ligases play important roles in cell division (39). For example, the cycling levels of cyclin B were partially explained by the ubiquitination (40, 41) and subsequent degradation of cyclin B by the APC/C (42, 43). Degradation of Emi1 (44) and Wee1 (45) via ubiquitylation of the Cul1-based SCF (Skp-Cullin-F box) complex is necessary for proper mitotic exit. Whereas phosphatases (such as Wee1 or PP2A (10)) have been well studied as antagonizers of cell division kinases, the role of deubiquitinating enzymes and the identification of their substrates remain to be fully explored (46).

Beyond these classical genetic and biochemical studies, modern approaches aimed at dissecting the mechanisms of cell division have greatly advanced our understanding of this dynamic process. Here, we present a broad overview of recent approaches that take a comprehensive and "-omics" view to identify novel components critical for cell division, to understand the function of the cell division machinery, and to analyze the pathways and other novel factors that contribute to cell division.

Genetic dissection of cell division

Although the aforementioned traditional yeast mutagenesis studies were seminal to the field of cell division, in the era of modern genomics, genetic analyses of cell division have become more targeted and efficient. The availability of RNAi and CRISPR-Cas9 gRNA (47) libraries has made studying gene expression knockdowns a viable option for discovering novel genes involved in cell division (Fig. 1, *upper left*). Approaches that screen these libraries are usually coupled with a high-throughput method of multiparametric data analysis, such as assessing mitotic progression via microscopy and DNA content or via the HeLa fluorescence ubiquitination cell cycle indicator (FUCCI) cell lines, which change color based on the cell cycle phase (48). As an example, our group performed an siRNA screen to assess the importance of ~600 mitotic microtubule-associated proteins for their function in cell division and used high content imagers to quantify the mitotic index and apoptotic index of each knockdown (49). Through this approach, we discovered StarD9, a novel protein involved in centrosome cohesion and whose depletion led to a dynamic unstable mitotic arrest (49). Combined with microscopy and computer-aided imaging, siRNA screens have now analyzed the importance of ~22,000 genes for cell division, uncovering novel proteins critical for this process (50).

Similarly, expression of fluorescently-tagged fusion proteins, by transfecting vectors encoding cDNAs (51) or bacterial artificial chromosomes containing a gene with its endogenous promoter (52), has enabled the identification of novel cell division proteins. The use of a fluorescently-tagged protein allows for an easy visual analysis for whether the protein has a relevant localization, such as at the kinetochores during mitosis, and is particularly useful when an antibody for the protein of interest is unavailable, either because the protein of interest is novel or because commercially available antibodies could not be validated. Combined with other analyses, such as proteomic data, these approaches have been used to identify novel protein complexes and pathways, such as a subunit of the APC/C (52), the MOZART family of tubulin-associated proteins (52), and the katanin family of microtubule-severing enzymes (53).

Together, these genetic approaches have defined a parts list of the critical factors that are required for proper cell division. Importantly, they have allowed for the dissection of key cell division processes like centrosome homeostasis, early mitotic spindle assembly, spindle assembly checkpoint function, and cytokinesis. These studies have also aided the understanding of human genetic diseases, like developmental disorders and cancers, that have cell division dysregulation at the core of their pathophysiology.

Proteomic dissection of cell division

Classical yeast two-hybrid screens have been used to identify novel protein–protein interactions (54, 55) and to define key domains or amino acids necessary for protein–protein interactions (Fig. 1, *upper left*) (56). However, modern proteomic approaches have greatly expanded the identification of novel protein–protein interactions and protein complexes involved in cell division. We outline two main approaches to the proteomic mapping of cell division: first, affinity-based purifications, based on the strength of protein–protein interactions; and second, proximity-based purifications, based on the spatiotemporal localization of the protein of interest. In affinity purifications, a tagged protein is expressed within cells, and the protein complexes are immunoprecipitated via antibodies that target the protein tag and are analyzed by MS (Fig. 1, *upper right*) (51, 57). We have used this approach to study various protein complexes of the cell division machinery, including enzymes that regulate the length of the mitotic spindle (58), ubiquitylation complexes that regulate cytokinesis (59), novel light chains of the dynein machinery (60), and a novel kinesin involved in centrosome cohesion (49, 61, 62). In proximity-

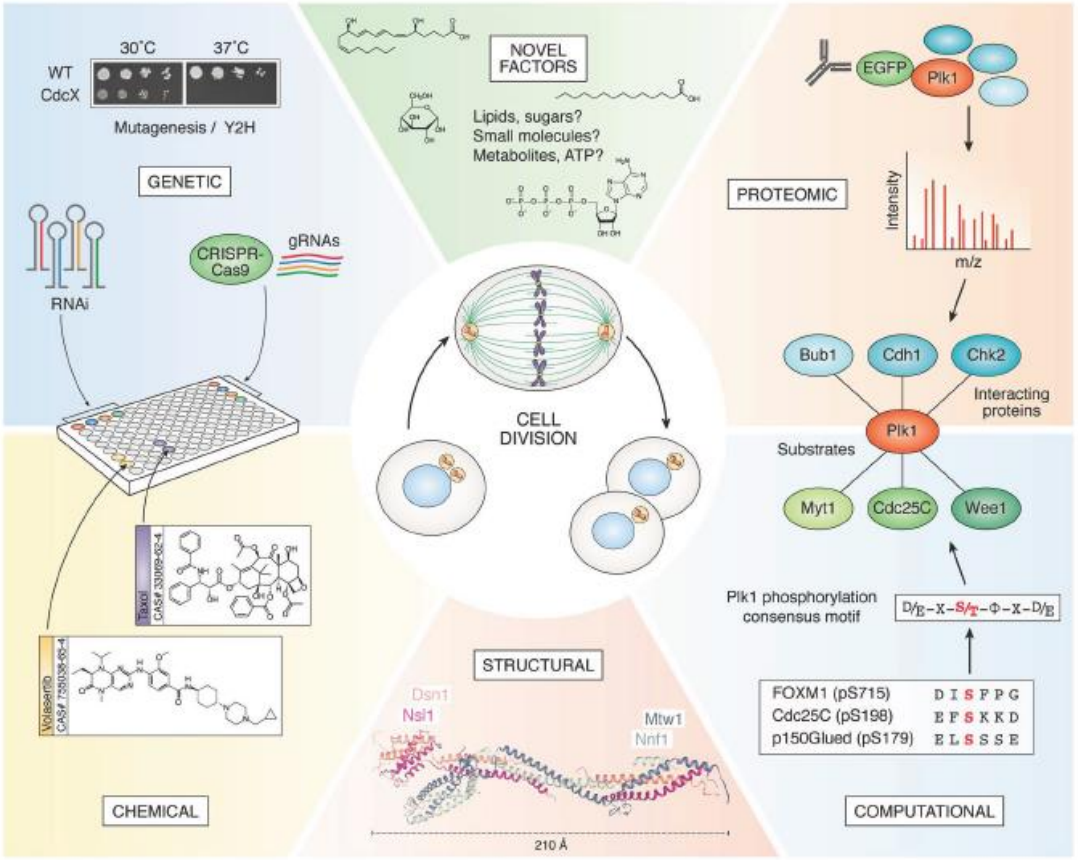

Figure 1. Overview of approaches used to dissect the mechanisms of cell division. Multiple approaches have been used to dissect the mechanisms of cell division, including genetic, proteomic, chemical, structural, and computational approaches. Figure contains the structure of the MIND complex from *Kluyveromyces lactis* (84) (Protein Data Bank code 5T58 (127), created using the NGL Viewer (128)). Examples of Plk1-interacting proteins are Bub1 (129), Cdh1 (130), and Chk2 (131). Examples of PLK1 substrates are FOXM1 (8), Cdc25C (132), p150Glued (133), Myt1 (134), and Wee1 (45).

based purifications, the protein of interest is tagged with a labeling enzyme such as a BirA biotin-ligase mutant called BioID (135) (or its derivatives BioID2 (136), TurboID, or miniTurboID (63)) or a peroxide-based enzyme APEX (64). Upon addition of the small ligand biotin to the cell culture media, these labeling enzymes modify proximal proteins with biotin via accessible lysine residues. Following the labeling step, the cells are lysed in denaturing conditions, biotinylated proteins are immunoprecipitated by binding to streptavidin beads, and protein complexes are analyzed by MS. Examples of proximity-based approaches include the identification of CDK1 protein interactors (65) and the spatial mapping of protein–protein associations within the centrosome (66).

Our group has been interested not only in defining novel components of the cell division machinery but also how these components interact with each other in a spatiotemporal manner. The mapping of cell division protein–protein interactions has been and will continue to be important for understanding how the cell division machinery coordinates to execute cell division with high fidelity. For example, protein interactors of a mitotic protein kinase could represent components of a protein complex, regulators of its activity or localization, and/or substrates for modification. Therefore, cell division protein–protein interaction networks are critical for defining protein function and more broadly how these proteins affect a specific pathway within the cell division program.

Chemical dissection of cell division

Natural and synthetic small molecules that target the cell division machinery are useful research tools that can be used in an acute and temporal manner to dissect the mechanisms of cell division. They can also serve as lead molecules for the development of therapeutics for treating proliferative diseases like cancer. However, these compounds have shown limited use in clinical trials, emphasizing the need to discover new or improved compounds and/or more viable biological targets. Moreover, many critical regulators of cell division have no specific inhibitors, hindering research to improve our understanding of their

1:1 stoichiometry of Aurora kinase B and Borealin, and visualized Aurora kinase B localization to the cytokinetic bridge (103).

Beyond microscopy, computational approaches have also been used to discover novel substrates of mitotic protein kinases. The basic structure of these algorithms is to use sequence information of known phosphorylation sites to identify a consensus phosphorylation motif and predict novel substrates, as outlined in Fig. 1 (*lower right*) for Plk1. Many computational tools that expand on this basic approach have been published (104, 105); we highlight a recent study that identified SPICE1 as an Aurora kinase A substrate via a computational algorithm and validated the interaction via biochemistry (106).

Given the wealth of information generated by chemical, proteomic, and genetic screens and cheminformatics and bioinformatics analyses, there is a pressing need to develop computational methods to integrate and analyze these data. In regard to this, our group recently used computational cell cycle profiling for prioritizing Food and Drug Administration–approved drugs with the potential for repurposing as anticancer therapies (68). Methods like this that combine and synthesize data sets from multiple sources into multiparametric analyses will become increasingly critical for developing a comprehensive view of cell division and how best to target it for therapeutic purposes.

Future perspectives

Although much has been discovered about the mechanisms that drive cell division, many novel factors that play a role in cell division are still being discovered. For example, endogenous RNA interference (RNAi) has been shown to regulate the expression of cell division proteins like Plk1 (107, 108), Mad1 (109), Bub1 (110), and Aurora kinase B (111). Many other RNAi have been shown to affect at least one aspect of cell division (112–116), and some have no identified targets (117). Given the clinical importance of these RNAi and the therapeutic potential of exogenous RNAi, a systematic understanding of how different forms of RNAi influence the proteins involved in cell division may help uncover novel levels of regulation for cell division.

In addition to RNAi, small molecules and reactive oxygen species (ROS) have been shown to play critical roles in mitotic progression. For example, folate deficiency leads to replicative stress during DNA replication and consequently to mis-segregation defects during mitosis (118). Similarly, the lipid family of phosphoinositides was shown to directly influence mitotic progression through proteins like NuMA (119) or phosphatases (120) and by regulating cytoskeletal elements (121, 122). Sterols have also been shown to play a role in cell division: cells deprived of cholesterol have difficulty undergoing cytokinesis (123), and the cholesterol derivative pregnenolone localizes to the spindle poles, binds Shugoshin 1, and promotes centriole cohesion (124). In *S. pombe*, intracellular concentrations of glucose affect Wee1 activity and thus cell size at mitotic entry (125). Whether glucose or other metabolites serve roles during mitosis in human cells is largely unexplored. Interestingly, in cancer cells, ROS levels are elevated during mitosis, leading to an increased oxidation of biomolecules, but the functional implications of this oxidation, if any, are unknown (126). Thus, comprehensive metabolomic, lipidomic, and nucleic acid studies of cell division are likely to yield interesting and previously underappreciated biological aspects of cell division (Fig. 1, *upper middle*).

Concluding remarks

Methods to dissect the mechanisms that govern cell division have progressed rapidly over the last few decades. The strategies discussed here allow for a genome- or proteome-wide assessment of proteins, drugs, and small molecules involved in cell division. In addition, advances in structural biology and computation have aided the study of cell division, particularly with regard to complex structures that are difficult to study with traditional biochemical techniques. Altogether, these approaches have allowed for the discovery and study of the ensemble of proteins and other factors necessary for proper cell division.

Acknowledgment—We thank the Journal of Biological Chemistry for artistic help in constructing Fig. 1.

References

1. Tomkins, D. J., and Sisken, J. E. (1984) Abnormalities in the cell-division cycle in Roberts syndrome fibroblasts: a cellular basis for the phenotypic characteristics? *Am. J. Hum. Genet.* **36**, 1332–1340 Medline
2. Hung, C. Y., Volkmar, B., Baker, J. D., Bauer, J. W., Gussoni, E., Hainzl, S., Klausegger, A., Lorenzo, J., Mihalek, I., Rittinger, O., Tekin, M., Dallman, J. E., and Bodamer, O. A. (2017) A defect in the inner kinetochore protein CENPT causes a new syndrome of severe growth failure. *PLoS ONE* **12**, e0189324 CrossRef Medline
3. Hanahan, D., and Weinberg, R. A. (2011) Hallmarks of Cancer: the next generation. *Cell* **144**, 646–674 CrossRef Medline
4. Macedo, J. C., Vaz, S., Bakker, B., Ribeiro, R., Bakker, P. L., Escandell, J. M., Ferreira, M. G., Medema, R., Foijer, F., and Logarinho, E. (2018) FoxM1 repression during human aging leads to mitotic decline and aneuploidy-driven full senescence. *Nat. Commun.* **9**, 2834 CrossRef Medline
5. Yang, Y., Varvel, N. H., Lamb, B. T., and Herrup, K. (2006) Ectopic cell cycle events link human Alzheimer's disease and amyloid precursor protein transgenic mouse models. *J. Neurosci.* **26**, 775–784 CrossRef Medline
6. Peter, M., Nakagawa, J., Dorée, M., Labbé, J. C., and Nigg, E. A. (1990) Identification of major nucleolar proteins as candidate mitotic substrates of cdc2 kinase. *Cell* **60**, 791–801 CrossRef Medline
7. Bischoff, J. R., Friedman, P. N., Marshak, D. R., Prives, C., and Beach, D. (1990) Human p53 is phosphorylated by p60-cdc2 and cyclin B-cdc2. *Proc. Natl. Acad. Sci. U.S.A.* **87**, 4766–4770 CrossRef Medline
8. Fu, Z., Malureanu, L., Huang, J., Wang, W., Li, H., van Deursen, J. M., Tindall, D. J., and Chen, J. (2008) Plk1-dependent phosphorylation of FoxM1 regulates a transcriptional programme required for mitotic progression. *Nat. Cell Biol.* **10**, 1076–1082 CrossRef Medline
9. Lammer, C., Wagerer, S., Saffrich, R., Mertens, D., Ansorge, W., and Hoffmann, I. (1998) The cdc25B phosphatase is essential for the G_2/M phase transition in human cells. *J. Cell Sci.* **111**, 2445–2453 Medline
10. Torres, J. Z., Ban, K. H., and Jackson, P. K. (2010) A specific form of phosphoprotein phosphatase 2 regulates anaphase-promoting complex/cyclosome association with spindle poles. *Mol. Biol. Cell.* **21**, 897–904 CrossRef Medline
11. Davey, N. E., and Morgan, D. O. (2016) Building a regulatory network with short linear sequence motifs: lessons from the Degrons of the anaphase-promoting complex. *Mol. Cell* **64**, 12–23 CrossRef Medline
12. Yu, Z. K., Gervais, J. L., and Zhang, H. (1998) Human CUL-1 associates with the SKP1/SKP2 complex and regulates p21(CIP1/WAF1) and cyclin

D proteins. *Proc. Natl. Acad. Sci. U.S.A.* **95**, 11324–11329 CrossRef Medline
13. Huang, X., Summers, M. K., Pham, V., Lill, J. R., Liu, J., Lee, G., Kirkpatrick, D. S., Jackson, P. K., Fang, G., and Dixit, V. M. (2011) Deubiquitinase USP37 is activated By CDK2 to antagonize APCCDH1 and promote S phase entry. *Mol. Cell* **42**, 511–523 CrossRef Medline
14. Bonacci, T., Suzuki, A., Grant, G. D., Stanley, N., Cook, J. G., Brown, N. G., and Emanuele, M. J. (2018) Cezanne/OTUD7B is a cell cycle-regulated deubiquitinase that antagonizes the degradation of APC/C substrates. *EMBO J.* **37**, e98701 CrossRef Medline
15. Hartwell, L. H., Mortimer, R. K., Culotti, J., and Culotti, M. (1973) Genetic control of the cell division cycle in yeast: V. genetic analysis of cdc mutants. *Genetics* **74**, 267–286 Medline
16. Nurse, P. (1975) Genetic control of cell size at cell division in yeast. *Nature* **256**, 547–551 CrossRef Medline
17. Lee, M. S., Ogg, S., Xu, M., Parker, L. L., Donoghue, D. J., Maller, J. L., and Piwnica-Worms, H. (1992) cdc25+ encodes a protein phosphatase that dephosphorylates p34cdc2. *Mol. Biol. Cell* **3**, 73–84 CrossRef Medline
18. Russell, P., and Nurse, P. (1986) cdc25+ functions as an inducer in the mitotic control of fission yeast. *Cell* **45**, 145–153 CrossRef Medline
19. Fantes, P. (1979) Epistatic gene interactions in the control of division in fission yeast. *Nature* **279**, 428–430 CrossRef Medline
20. Russell, P., and Nurse, P. (1987) Negative regulation of mitosis by wee1+, a gene encoding a protein kinase homolog. *Cell* **49**, 559–567 CrossRef Medline
21. Hindley, J., and Phear, G. A. (1984) Sequence of the cell division gene CDC2 from *Schizosaccharomyces pombe*; patterns of splicing and homology to protein kinases. *Gene* **31**, 129–134 CrossRef Medline
22. Conrad, M. N., and Newlon, C. S. (1983) *Saccharomyces cerevisiae* cdc2 mutants fail to replicate approximately one-third of their nuclear genome. *Mol. Cell. Biol.* **3**, 1000–1012 CrossRef Medline
23. Lundgren, K., Walworth, N., Booher, R., Dembski, M., Kirschner, M., and Beach, D. (1991) mik1 and wee1 cooperate in the inhibitory tyrosine phosphorylation of cdc2. *Cell* **64**, 1111–1122 CrossRef Medline
24. Gould, K. L., and Nurse, P. (1989) Tyrosine phosphorylation of the fission yeast cdc2+ protein kinase regulates entry into mitosis. *Nature* **342**, 39–45 CrossRef Medline
25. Hara, K., Tydeman, P., and Kirschner, M. (1980) A cytoplasmic clock with the same period as the division cycle in *Xenopus* eggs. *Proc. Natl. Acad. Sci. U.S.A.* **77**, 462–466 CrossRef Medline
26. Masui, Y., and Markert, C. L. (1971) Cytoplasmic control of nuclear behavior during meiotic maturation of frog oocytes. *J. Exp. Zool.* **177**, 129–145 CrossRef Medline
27. Gerhart, J., Wu, M., and Kirschner, M. (1984) Cell cycle dynamics of an M-phase-specific cytoplasmic factor in *Xenopus laevis* oocytes and eggs. *J. Cell Biol.* **98**, 1247–1255 CrossRef Medline
28. Lohka, M. J., Hayes, M. K., and Maller, J. L. (1988) Purification of maturation-promoting factor, an intracellular regulator of early mitotic events. *Proc. Natl. Acad. Sci. U.S.A.* **85**, 3009–3013 CrossRef Medline
29. Dunphy, W. G., Brizuela, L., Beach, D., and Newport, J. (1988) The *Xenopus* cdc2 protein is a component of MPF, a cytoplasmic regulator of mitosis. *Cell* **54**, 423–431 CrossRef Medline
30. Draetta, G., Luca, F., Westendorf, J., Brizuela, L., Ruderman, J., and Beach, D. (1989) cdc2 protein kinase is complexed with both cyclin A and B: evidence for proteolytic inactivation of MPF. *Cell* **56**, 829–838 CrossRef Medline
31. Evans, T., Rosenthal, E. T., Youngblom, J., Distel, D., and Hunt, T. (1983) Cyclin: a protein specified by maternal mRNA in sea urchin eggs that is destroyed at each cleavage division. *Cell* **33**, 389–396 CrossRef Medline
32. Pines, J., and Hunter, T. (1990) Human cyclin A is adenovirus E1A-associated protein p60 and behaves differently from cyclin B. *Nature* **346**, 760–763 CrossRef Medline
33. Tsai, L.-H., Harlow, E., and Meyerson, M. (1991) Isolation of the human cdk2 gene that encodes the cyclin A- and adenovirus E1A-associated p33 kinase. *Nature* **353**, 174–177 CrossRef Medline
34. Labbé, J. C., Capony, J. P., Caput, D., Cavadore, J. C., Derancourt, J., Kaghad, M., Lelias, J. M., Picard, A., and Dorée, M. (1989) MPF from starfish oocytes at first meiotic metaphase is a heterodimer containing one molecule of cdc2 and one molecule of cyclin B. *EMBO J.* **8**, 3053–3058 CrossRef Medline
35. Dessev, G., Iovcheva-Dessev, C., Bischoff, J. R., Beach, D., and Goldman, R. (1991) A complex containing p34cdc2 and cyclin B phosphorylates the nuclear lamin and disassembles nuclei of clam oocytes *in vitro*. *J. Cell Biol.* **112**, 523–533 CrossRef Medline
36. Peter, M., Nakagawa, J., Dorée, M., Labbé, J. C., and Nigg, E. A. (1990) *In vitro* disassembly of the nuclear lamina and M phase-specific phosphorylation of lamins by cdc2 kinase. *Cell* **61**, 591–602 CrossRef Medline
37. Chou, Y. H., Ngai, K. L., and Goldman, R. (1991) The regulation of intermediate filament reorganization in mitosis. p34cdc2 phosphorylates vimentin at a unique N-terminal site. *J. Biol. Chem.* **266**, 7325–7328 Medline
38. Yamashiro, S., Yamakita, Y., Hosoya, H., and Matsumura, F. (1991) Phosphorylation of non-muscle caldesmon by p34cdc2 kinase during mitosis. *Nature* **349**, 169–172 CrossRef Medline
39. Ong, J. Y., and Torres, J. Z. (2019) E3 ubiquitin ligases in cancer and their pharmacological targeting CrossRef
40. Hershko, A., Ganoth, D., Pehrson, J., Palazzo, R. E., and Cohen, L. H. (1991) Methylated ubiquitin inhibits cyclin degradation in clam embryo extracts. *J. Biol. Chem.* **266**, 16376–16379 Medline
41. Glotzer, M., Murray, A. W., and Kirschner, M. W. (1991) Cyclin is degraded by the ubiquitin pathway. *Nature* **349**, 132–138 CrossRef Medline
42. King, R. W., Peters, J. M., Tugendreich, S., Rolfe, M., Hieter, P., and Kirschner, M. W. (1995) A 20S complex containing CDC27 and CDC16 catalyzes the mitosis-specific conjugation of ubiquitin to cyclin B. *Cell* **81**, 279–288 CrossRef Medline
43. Sudakin, V., Ganoth, D., Dahan, A., Heller, H., Hershko, J., Luca, F. C., Ruderman, J. V., and Hershko, A. (1995) The cyclosome, a large complex containing cyclin-selective ubiquitin ligase activity, targets cyclins for destruction at the end of mitosis. *Mol. Biol. Cell* **6**, 185–197 CrossRef Medline
44. Margottin-Goguet, F., Hsu, J. Y., Loktev, A., Hsieh, H. M., Reimann, J. D., and Jackson, P. K. (2003) Prophase destruction of Emi1 by the SCF(βTrCP/Slimb) ubiquitin ligase activates the anaphase promoting complex to allow progression beyond prometaphase. *Dev. Cell.* **4**, 813–826 CrossRef Medline
45. Watanabe, N., Arai, H., Nishihara, Y., Taniguchi, M., Watanabe, N., Hunter, T., and Osada, H. (2004) M-phase kinases induce phospho-dependent ubiquitination of somatic Wee1 by SCFβ-TrCP. *Proc. Natl. Acad. Sci. U.S.A.* **101**, 4419–4424 CrossRef Medline
46. Mapa, C. E., Arsenault, H. E., Conti, M. M., Poti, K. E., and Benanti, J. A. (2018) A balance of deubiquitinating enzymes controls cell cycle entry. *Mol. Biol. Cell.* **29**, 2821–2834 CrossRef Medline
47. McKinley, K. L., and Cheeseman, I. M. (2017) Large-scale analysis of CRISPR/Cas9 cell-cycle knockouts reveals the diversity of p53-dependent responses to cell-cycle defects. *Dev. Cell* **40**, 405–420.e2 CrossRef Medline
48. Sakaue-Sawano, A., Kurokawa, H., Morimura, T., Hanyu, A., Hama, H., Osawa, H., Kashiwagi, S., Fukami, K., Miyata, T., Miyoshi, H., Imamura, T., Ogawa, M., Masai, H., and Miyawaki, A. (2008) Visualizing spatiotemporal dynamics of multicellular cell-cycle progression. *Cell* **132**, 487–498 CrossRef Medline
49. Torres, J. Z., Summers, M. K., Peterson, D., Brauer, M. J., Lee, J., Senese, S., Gholkar, A. A., Lo, Y.-C., Lei, X., Jung, K., Anderson, D. C., Davis, D. P., Belmont, L., and Jackson, P. K. (2011) The STARD9/Kif16a kinesin associates with mitotic microtubules and regulates spindle pole assembly. *Cell* **147**, 1309–1323 CrossRef Medline
50. Neumann, B., Walter, T., Hériché, J.-K., Bulkescher, J., Erfle, H., Conrad, C., Rogers, P., Poser, I., Held, M., Liebel, U., Cetin, C., Sieckmann, F., Pau, G., Kabbe, R., Wünsche, A., *et al.* (2010) Phenotypic profiling of the human genome by time-lapse microscopy reveals cell division genes. *Nature* **464**, 721–727 CrossRef Medline
51. Torres, J. Z., Miller, J. J., and Jackson, P. K. (2009) High-throughput generation of tagged stable cell lines for proteomic analysis. *Proteomics* **9**, 2888–2891 CrossRef Medline
52. Hutchins, J. R., Toyoda, Y., Hegemann, B., Poser, I., Hériché, J.-K., Sykora, M. M., Augsburg, M., Hudecz, O., Buschhorn, B. A., Bulkescher, J., Conrad,

C., Comartin, D., Schleiffer, A., Sarov, M., Pozniakovsky, A., *et al.* (2010) Systematic analysis of human protein complexes identifies chromosome segregation proteins. *Science* 328, 593–599 CrossRef Medline

53. Cheung, K., Senese, S., Kuang, J., Bui, N., Ongpipattanakul, C., Gholkar, A., Cohn, W., Capri, J., Whitelegge, J. P., and Torres, J. Z. (2016) Proteomic analysis of the mammalian Katanin family of microtubule-severing enzymes defines Katanin p80 subunit B-like 1 (KATNBL1) as a regulator of mammalian Katanin microtubule-severing. *Mol. Cell. Proteomics* 15, 1658–1669 CrossRef Medline
54. Jeong, A. L., Lee, S., Park, J. S., Han, S., Jang, C.-Y., Lim, J.-S., Lee, M. S., and Yang, Y. (2014) Cancerous inhibitor of protein phosphatase 2A (CIP2A) protein is involved in centrosome separation through the regulation of NIMA (never in mitosis gene A)-related kinase 2 (NEK2) protein activity. *J. Biol. Chem.* 289, 28–40 CrossRef Medline
55. Hwang, L. H., Lau, L. F., Smith, D. L., Mistrot, C. A., Hardwick, K. G., Hwang, E. S., Amon, A., and Murray, A. W. (1998) Budding yeast Cdc20: a target of the spindle checkpoint. *Science* 279, 1041–1044 CrossRef Medline
56. Vidal, M., Braun, P., Chen, E., Boeke, J. D., and Harlow, E. (1996) Genetic characterization of a mammalian protein–protein interaction domain by using a yeast reverse two-hybrid system. *Proc. Natl. Acad. Sci. U.S.A.* 93, 10321–10326 CrossRef Medline
57. Bradley, M., Ramirez, I., Cheung, K., Gholkar, A. A., and Torres, J. Z. (2016) Inducible LAP-tagged stable cell lines for investigating protein function, spatiotemporal localization and protein interaction networks. *J. Vis. Exp. 2016*, CrossRef
58. Xia, X., Gholkar, A., Senese, S., and Torres, J. Z. (2015) A LCMT1-PME-1 methylation equilibrium controls mitotic spindle size. *Cell Cycle* 14, 1938–1947 CrossRef Medline
59. Gholkar, A. A., Senese, S., Lo, Y.-C., Vides, E., Contreras, E., Hodara, E., Capri, J., Whitelegge, J. P., and Torres, J. Z. (2016) The X-linked-intellectual-disability-associated ubiquitin ligase Mid2 interacts with astrin and regulates astrin levels to promote cell division. *Cell Rep.* 14, 180–188 CrossRef Medline
60. Gholkar, A. A., Senese, S., Lo, Y.-C., Capri, J., Deardorff, W. J., Dharmarajan, H., Contreras, E., Hodara, E., Whitelegge, J. P., Jackson, P. K., and Torres, J. Z. (2015) Tctex1d2 associates with short-rib polydactyly syndrome proteins and is required for ciliogenesis. *Cell Cycle* 14, 1116–1125 CrossRef Medline
61. Senese, S., Cheung, K., Lo, Y.-C., Gholkar, A. A., Xia, X., Wohlschlegel, J. A., and Torres, J. Z. (2015) A unique insertion in STARD9's motor domain regulates its stability. *Mol. Biol. Cell* 26, 440–452 CrossRef Medline
62. Torres, J. Z. (2012) STARD9/Kif16a is a novel mitotic kinesin and antimitotic target. *Bioarchitecture* 2, 19–22 CrossRef Medline
63. Branon, T. C., Bosch, J. A., Sanchez, A. D., Udeshi, N. D., Svinkina, T., Carr, S. A., Feldman, J. L., Perrimon, N., and Ting, A. Y. (2018) Efficient proximity labeling in living cells and organisms with TurboID. *Nat. Biotechnol.* 36, 880–887 CrossRef Medline
64. Rhee, H.-W., Zou, P., Udeshi, N. D., Martell, J. D., Mootha, V. K., Carr, S. A., and Ting, A. Y. (2013) Proteomic mapping of mitochondria in living cells via spatially restricted enzymatic tagging. *Science* 339, 1328–1331 CrossRef Medline
65. Schopp, I. M., Amaya Ramirez, C. C., Debeljak, J., Kreibich, E., Skribbe, M., Wild, K., and Béthune, J. (2017) Split-BioID a conditional proteomics approach to monitor the composition of spatiotemporally defined protein complexes. *Nat. Commun.* 8, 15690 CrossRef Medline
66. Firat-Karalar, E. N., Rauniyar, N., Yates, J. R., 3rd., Stearns, T., and Stearns, T. (2014) Proximity interactions among centrosome components identify regulators of centriole duplication. *Curr. Biol.* 24, 664–670 CrossRef Medline
67. Senese, S., Lo, Y. C., Huang, D., Zangle, T. A., Gholkar, A. A., Robert, L., Homet, B., Ribas, A., Summers, M. K., Teitell, M. A., Damoiseaux, R., and Torres, J. Z. (2014) Chemical dissection of the cell cycle: probes for cell biology and anti-cancer drug development. *Cell Death Dis.* 5, e1462 CrossRef Medline
68. Lo, Y.-C., Senese, S., France, B., Gholkar, A. A., Damoiseaux, R., and Torres, J. Z. (2017) Computational cell cycle profiling of cancer cells for prioritizing FDA-approved drugs with repurposing potential. *Sci. Rep.* 7, 11261 CrossRef Medline
69. Lo, Y.-C., Senese, S., Li, C.-M., Hu, Q., Huang, Y., Damoiseaux, R., and Torres, J. Z. (2015) Large-scale chemical similarity networks for target profiling of compounds identified in cell-based chemical screens. *PLoS Comput. Biol.* 11, e1004153 CrossRef Medline
70. Lo, Y.-C., Senese, S., Damoiseaux, R., and Torres, J. Z. (2016) 3D chemical similarity networks for structure-based target prediction and scaffold hopping. *ACS Chem. Biol.* 11, 2244–2253 CrossRef Medline
71. McNamara, D. E., Senese, S., Yeates, T. O., and Torres, J. Z. (2015) Structures of potent anticancer compounds bound to tubulin. *Protein Sci.* 24, 1164–1172 CrossRef Medline
72. Xia, X., Lo, Y.-C., Gholkar, A. A., Senese, S., Ong, J. Y., Velasquez, E. F., Damoiseaux, R., and Torres, J. Z. (2019) Leukemia cell cycle chemical profiling identifies the G_2-phase leukemia specific inhibitor leusin-1. *ACS Chem. Biol.* 14, 994–1001 CrossRef Medline
73. Verma, R., Peters, N. R., D'Onofrio, M., Tochtrop, G. P., Sakamoto, K. M., Varadan, R., Zhang, M., Coffino, P., Fushman, D., Deshaies, R. J., and King, R. W. (2004) Ubistatins inhibit proteasome-dependent degradation by binding the ubiquitin chain. *Science* 306, 117–120 CrossRef Medline
74. Steegmaier, M., Hoffmann, M., Baum, A., Lénárt, P., Petronczki, M., Krssák, M., Gürtler, U., Garin-Chesa, P., Lieb, S., Quant, J., Grauert, M., Adolf, G. R., Kraut, N., Peters, J.-M., and Rettig, W. J. (2007) BI 2536, a potent and selective inhibitor of polo-like kinase 1, inhibits tumor growth *in vivo*. *Curr. Biol.* 17, 316–322 CrossRef Medline
75. Ditchfield, C., Johnson, V. L., Tighe, A., Ellston, R., Haworth, C., Johnson, T., Mortlock, A., Keen, N., and Taylor, S. S. (2003) Aurora B couples chromosome alignment with anaphase by targeting BubR1, Mad2, and Cenp-E to kinetochores. *J. Cell Biol.* 161, 267–280 CrossRef Medline
76. Gadea, B. B., and Ruderman, J. V (2005) Aurora kinase inhibitor ZM447439 blocks chromosome-induced spindle assembly, the completion of chromosome condensation, and the establishment of the spindle integrity checkpoint in *Xenopus* egg extracts. *Mol. Biol. Cell* 16, 1305–18 CrossRef Medline
77. Lénárt, P., Petronczki, M., Steegmaier, M., Di Fiore, B., Lipp, J. J., Hoffmann, M., Rettig, W. J., Kraut, N., and Peters, J.-M. (2007) The small-molecule inhibitor BI 2536 reveals novel insights into mitotic roles of polo-like kinase 1. *Curr. Biol.* 17, 304–315 CrossRef Medline
78. Zeng, X., Sigoillot, F., Gaur, S., Choi, S., Pfaff, K. L., Oh, D.-C., Hathaway, N., Dimova, N., Cuny, G. D., and King, R. W. (2010) Pharmacologic inhibition of the anaphase-promoting complex induces a spindle checkpoint-dependent mitotic arrest in the absence of spindle damage. *Cancer Cell* 18, 382–395 CrossRef Medline
79. Luo, X., Tang, Z., Rizo, J., and Yu, H. (2002) The Mad2 spindle checkpoint protein undergoes similar major conformational changes upon binding to either Mad1 or Cdc20. *Mol. Cell* 9, 59–71 CrossRef Medline
80. Luo, X., Tang, Z., Xia, G., Wassmann, K., Matsumoto, T., Rizo, J., and Yu, H. (2004) The Mad2 spindle checkpoint protein has two distinct natively folded states. *Nat. Struct. Mol. Biol.* 11, 338–345 CrossRef Medline
81. Hara, M., Özkan, E., Sun, H., Yu, H., and Luo, X. (2015) Structure of an intermediate conformer of the spindle checkpoint protein Mad2. *Proc. Natl. Acad. Sci. U.S.A.* 112, 11252–11257 CrossRef Medline
82. Yang, M., Li, B., Liu, C.-J., Tomchick, D. R., Machius, M., Rizo, J., Yu, H., and Luo, X. (2008) Insights into Mad2 regulation in the spindle checkpoint revealed by the crystal structure of the symmetric Mad2 dimer. *PLoS Biol.* 6, e50 CrossRef Medline
83. Hewitt, L., Tighe, A., Santaguida, S., White, A. M., Jones, C. D., Musacchio, A., Green, S., and Taylor, S. S. (2010) Sustained Mps1 activity is required in mitosis to recruit O-Mad2 to the Mad1–C-Mad2 core complex. *J. Cell Biol.* 190, 25–34 CrossRef Medline
84. Dimitrova, Y. N., Jenni, S., Valverde, R., Khin, Y., and Harrison, S. C. (2016) Structure of the MIND complex defines a regulatory focus for yeast kinetochore assembly. *Cell* 167, 1014–1027.e12 CrossRef Medline
85. Sironi, L., Mapelli, M., Knapp, S., De Antoni, A., Jeang, K.-T., and Musacchio, A. (2002) Crystal structure of the tetrameric Mad1-Mad2 core complex: implications of a "safety belt" binding mechanism for the spindle checkpoint. *EMBO J.* 21, 2496–2506 CrossRef Medline

86. Chao, W. C., Kulkarni, K., Zhang, Z., Kong, E. H., and Barford, D. (2012) Structure of the mitotic checkpoint complex. *Nature* **484**, 208–213 CrossRef Medline
87. Chang, L. F., Zhang, Z., Yang, J., McLaughlin, S. H., and Barford, D. (2014) Molecular architecture and mechanism of the anaphase-promoting complex. *Nature* **513**, 388–393 CrossRef Medline
88. Chang, L., Zhang, Z., Yang, J., McLaughlin, S. H., and Barford, D. (2015) Atomic structure of the APC/C and its mechanism of protein ubiquitination. *Nature* **522**, 450–454 CrossRef Medline
89. Brown, N. G., VanderLinden, R., Watson, E. R., Weissmann, F., Ordureau, A., Wu, K.-P., Zhang, W., Yu, S., Mercredi, P. Y., Harrison, J. S., Davidson, I. F., Qiao, R., Lu, Y., Dube, P., Brunner, M. R., *et al.* (2016) Dual RING E3 architectures regulate multiubiquitination and ubiquitin chain elongation by APC/C. *Cell* **165**, 1440–1453 CrossRef Medline
90. Yamaguchi, M., VanderLinden, R., Weissmann, F., Qiao, R., Dube, P., Brown, N. G., Haselbach, D., Zhang, W., Sidhu, S. S., Peters, J.-M., Stark, H., and Schulman, B. A. (2016) Cryo-EM of mitotic checkpoint complex-bound APC/C reveals reciprocal and conformational regulation of ubiquitin ligation. *Mol. Cell* **63**, 593–607 CrossRef Medline
91. Ng, C. T., Deng, L., Chen, C., Lim, H. H., Shi, J., Surana, U., and Gan, L. (2019) Electron cryotomography analysis of Dam1C/DASH at the kinetochore-spindle interface *in situ*. *J. Cell Biol.* **218**, 455–473 CrossRef Medline
92. Gonen, S., Akiyoshi, B., Iadanza, M. G., Shi, D., Duggan, N., Biggins, S., and Gonen, T. (2012) The structure of purified kinetochores reveals multiple microtubule-attachment sites. *Nat. Struct. Mol. Biol.* **19**, 925–929 CrossRef Medline
93. Hinshaw, S. M., and Harrison, S. C. (2019) The structure of the Ctf19c/CCAN from budding yeast. *Elife* **8**, e44239 CrossRef Medline
94. Novak, B., and Tyson, J. J. (1993) Numerical analysis of a comprehensive model of M-phase control in *Xenopus* oocyte extracts and intact embryos. *J. Cell Sci.* **106**, 1153–1168 Medline
95. Pomerening, J. R., Sontag, E. D., and Ferrell, J. E. (2003) Building a cell cycle oscillator: hysteresis and bistability in the activation of Cdc2. *Nat. Cell Biol.* **5**, 346–351 CrossRef Medline
96. Sha, W., Moore, J., Chen, K., Lassaletta, A. D., Yi, C.-S., Tyson, J. J., and Sible, J. C. (2003) Hysteresis drives cell-cycle transitions in *Xenopus laevis* egg extracts. *Proc. Natl. Acad. Sci. U.S.A.* **100**, 975–980 CrossRef Medline
97. Chen, K. C., Calzone, L., Csikasz-Nagy, A., Cross, F. R., Novak, B., and Tyson, J. J. (2004) Integrative analysis of cell cycle control in budding yeast. *Mol. Biol. Cell* **15**, 3841–3862 CrossRef Medline
98. Queralt, E., Lehane, C., Novak, B., and Uhlmann, F. (2006) Downregulation of PP2ACdc55 phosphatase by separase initiates mitotic exit in budding yeast. *Cell* **125**, 719–732 CrossRef Medline
99. Henze, R., Dittrich, P., and Ibrahim, B. (2017) A dynamical model for activating and silencing the mitotic checkpoint. *Sci. Rep.* **7**, 3865 CrossRef Medline
100. Mistry, H. B., MacCallum, D. E., Jackson, R. C., Chaplain, M. A., and Davidson, F. A. (2008) Modeling the temporal evolution of the spindle assembly checkpoint and role of Aurora B kinase. *Proc. Natl. Acad. Sci. U.S.A.* **105**, 20215–20220 CrossRef Medline
101. Civelekoglu-Scholey, G., Sharp, D. J., Mogilner, A., and Scholey, J. M. (2006) Model of chromosome motility in *Drosophila* embryos: adaptation of a general mechanism for rapid mitosis. *Biophys. J.* **90**, 3966–3982 CrossRef Medline
102. Lacroix, B., Letort, G., Pitayu, L., Sallé, J., Stefanutti, M., Maton, G., Ladouceur, A.-M., Canman, J. C., Maddox, P. S., Maddox, A. S., Minc, N., Nédélec, F., and Dumont, J. (2018) Microtubule dynamics scale with cell size to set spindle length and assembly timing. *Dev. Cell* **45**, 496–511.e6 CrossRef Medline
103. Cai, Y., Hossain, M. J., Hériché, J.-K., Politi, A. Z., Walther, N., Koch, B., Wachsmuth, M., Nijmeijer, B., Kueblbeck, M., Martinic-Kavur, M., Ladurner, R., Alexander, S., Peters, J.-M., and Ellenberg, J. (2018) Experimental and computational framework for a dynamic protein atlas of human cell division. *Nature* **561**, 411–415 CrossRef Medline
104. Ayati, M., Wiredja, D., Schlatzer, D., Maxwell, S., Li, M., Koyutürk, M., and Chance, M. R. (2019) CoPhosK: a method for comprehensive kinase substrate annotation using co-phosphorylation analysis. *PLOS Comput. Biol.* **15**, e1006678 CrossRef Medline
105. Song, J., Wang, H., Wang, J., Leier, A., Marquez-Lago, T., Yang, B., Zhang, Z., Akutsu, T., Webb, G. I., and Daly, R. J. (2017) PhosphoPredict: a bioinformatics tool for prediction of human kinase-specific phosphorylation substrates and sites by integrating heterogeneous feature selection. *Sci. Rep.* **7**, 6862 CrossRef Medline
106. Deretic, J., Kerr, A., and Welburn, J. P. I. (2019) A rapid computational approach identifies SPICE1 as an Aurora kinase substrate. *Mol. Biol. Cell.* **30**, 312–323 CrossRef Medline
107. Wang, Z.-D., Shen, L.-P., Chang, C., Zhang, X.-Q., Chen, Z.-M., Li, L., Chen, H., and Zhou, P.-K. (2016) Long noncoding RNA lnc-RI is a new regulator of mitosis via targeting miRNA-210–3p to release PLK1 mRNA activity. *Sci. Rep.* **6**, 25385 CrossRef Medline
108. Shi, W., Alajez, N. M., Bastianutto, C., Hui, A. B., Mocanu, J. D., Ito, E., Busson, P., Lo, K.-W., Ng, R., Waldron, J., O'Sullivan, B., and Liu, F.-F. (2010) Significance of Plk1 regulation by miR-100 in human nasopharyngeal cancer. *Int. J. Cancer* **126**, 2036–2048 CrossRef Medline
109. Bhattacharjya, S., Nath, S., Ghose, J., Maiti, G. P., Biswas, N., Bandyopadhyay, S., Panda, C. K., Bhattacharyya, N. P., and Roychoudhury, S. (2013) miR-125b promotes cell death by targeting spindle assembly checkpoint gene MAD1 and modulating mitotic progression. *Cell Death Differ.* **20**, 430–442 CrossRef Medline
110. Luo, M., Weng, Y., Tang, J., Hu, M., Liu, Q., Jiang, F., Yang, D., Liu, C., Zhan, X., Song, P., Bai, H., Li, B., and Shi, Q. (2012) MicroRNA-450a-3p represses cell proliferation and regulates embryo development by regulating Bub1 expression in mouse. *PLoS ONE* **7**, e47914 CrossRef Medline
111. Mäki-Jouppila, J. H., Pruikkonen, S., Tambe, M. B., Aure, M. R., Halonen, T., Salmela, A.-L., Laine, L., Børresen-Dale, A.-L., and Kallio, M. J. (2015) MicroRNA let-7b regulates genomic balance by targeting Aurora B kinase. *Mol. Oncol.* **9**, 1056–1070 CrossRef Medline
112. Hwang, W.-L., Jiang, J.-K., Yang, S.-H., Huang, T.-S., Lan, H.-Y., Teng, H.-W., Yang, C.-Y., Tsai, Y.-P., Lin, C.-H., Wang, H.-W., and Yang, M.-H. (2014) MicroRNA-146a directs the symmetric division of Snail-dominant colorectal cancer stem cells. *Nat. Cell Biol.* **16**, 268–280 CrossRef Medline
113. Roy, S., Hooiveld, G. J., Seehawer, M., Caruso, S., Heinzmann, F., Schneider, A. T., Frank, A. K., Cardenas, D. V., Sonntag, R., Luedde, M., Trautwein, C., Stein, I., Pikarsky, E., Loosen, S., Tacke, F., *et al.* (2018) microRNA 193a-5p regulates levels of nucleolar- and spindle-associated protein 1 to suppress hepatocarcinogenesis. *Gastroenterology* **155**, 1951–1966.e26 CrossRef Medline
114. Takacs, C. M., and Giraldez, A. J. (2016) miR-430 regulates oriented cell division during neural tube development in zebrafish. *Dev. Biol.* **409**, 442–450 CrossRef Medline
115. Pruikkonen, S., and Kallio, M. J. (2017) Excess of a Rassf1-targeting microRNA, miR-193a-3p, perturbs cell division fidelity. *Br. J. Cancer* **116**, 1451–1461 CrossRef Medline
116. Kriegel, A. J., Terhune, S. S., Greene, A. S., Noon, K. R., Pereckas, M. S., and Liang, M. (2018) Isomer-specific effect of microRNA miR-29b on nuclear morphology. *J. Biol. Chem.* **293**, 14080–14088 CrossRef Medline
117. Stein, P., Rozhkov, N. V., Li, F., Cárdenas, F. L., Davydenko, O., Vandivier, L. E., Gregory, B. D., Hannon, G. J., Schultz, R. M., and Schultz, R. M. (2015) Essential role for endogenous siRNAs during meiosis in mouse oocytes. *PLoS Genet.* **11**, e1005013 CrossRef Medline
118. Bjerregaard, V. A., Garribba, L., McMurray, C. T., Hickson, I. D., and Liu, Y. (2018) Folate deficiency drives mitotic missegregation of the human *FRAXA* locus. *Proc. Natl. Acad. Sci.* **115**, 13003–13008 CrossRef Medline
119. Kotak, S., Busso, C., and Gönczy, P. (2014) NuMA interacts with phosphoinositides and links the mitotic spindle with the plasma membrane. *EMBO J.* **33**, 1815–1830 CrossRef Medline
120. Sierra Potchanant, E. A., Cerabona, D., Sater, Z. A., He, Y., Sun, Z., Gehlhausen, J., and Nalepa, G. (2017) INPP5E preserves genomic stability through regulation of mitosis. *Mol. Cell. Biol.* **37**, e00500-16 CrossRef Medline
121. Zheng, P., Baibakov, B., Wang, X.-H., and Dean, J. (2013) PtdIns(3,4,5)P3 is constitutively synthesized and required for spindle translocation during meiosis in mouse oocytes. *J. Cell Sci.* **126**, 715–721 CrossRef Medline

122. Tuncay, H., Brinkmann, B. F., Steinbacher, T., Schürmann, A., Gerke, V., Iden, S., and Ebnet, K. (2015) JAM-A regulates cortical dynein localization through Cdc42 to control planar spindle orientation during mitosis. *Nat. Commun.* 6, 8128 CrossRef Medline
123. Fernández, C., Lobo, Md Mdel, V., Gómez-Coronado, D., and Lasunción, M. A. (2004) Cholesterol is essential for mitosis progression and its deficiency induces polyploid cell formation. *Exp. Cell Res.* 300, 109–120 CrossRef Medline
124. Hamasaki, M., Matsumura, S., Satou, A., Takahashi, C., Oda, Y., Higashiura, C., Ishihama, Y., and Toyoshima, F. (2014) Pregnenolone functions in centriole cohesion during mitosis. *Chem. Biol.* 21, 1707–1721 CrossRef Medline
125. Allard, C. A. H., Opalko, H. E., and Moseley, J. B. (2019) Stable Pom1 clusters form a glucose-modulated concentration gradient that regulates mitotic entry. *Elife* 8, e46003 CrossRef Medline
126. Patterson, J. C., Joughin, B. A., van de Kooij, B., Lim, D. C., Lauffenburger, D. A., and Yaffe, M. B. (2019) ROS and oxidative stress are elevated in mitosis during asynchronous cell cycle progression and are exacerbated by mitotic arrest. *Cell Syst.* 8, 163–167.e2 CrossRef Medline
127. Berman, H. M., Westbrook, J., Feng, Z., Gilliland, G., Bhat, T. N., Weissig, H., Shindyalov, I. N., and Bourne, P. E. (2000) The Protein Data Bank. *Nucleic Acids Res.* 28, 235–242 CrossRef Medline
128. Rose, A. S., Bradley, A. R., Valasatava, Y., Duarte, J. M., Prlic, A., and Rose, P. W. (2018) NGL viewer: web-based molecular graphics for large complexes. *Bioinformatics* 34, 3755–3758 CrossRef Medline
129. Jia, L., Li, B., and Yu, H. (2016) The Bub1–Plk1 kinase complex promotes spindle checkpoint signalling through Cdc20 phosphorylation. *Nat. Commun.* 7, 10818 CrossRef Medline
130. Bassermann, F., Frescas, D., Guardavaccaro, D., Busino, L., Peschiaroli, A., and Pagano, M. (2008) The Cdc14B-Cdh1-Plk1 axis controls the G_2 DNA-damage-response checkpoint. *Cell* 134, 256–267 CrossRef Medline
131. van Vugt, M. A., Gardino, A. K., Linding, R., Ostheimer, G. J., Reinhardt, H. C., Ong, S.-E., Tan, C. S., Miao, H., Keezer, S. M., Li, J., Pawson, T., Lewis, T. A., Carr, S. A., Smerdon, S. J., Brummelkamp, T. R., and Yaffe, M. B. (2010) A mitotic phosphorylation feedback network connects Cdk1, Plk1, 53BP1, and Chk2 to inactivate the G(2)/M DNA damage checkpoint. *PLoS Biol.* 8, e1000287 CrossRef Medline
132. Toyoshima-Morimoto, F., Taniguchi, E., and Nishida, E. (2002) Plk1 promotes nuclear translocation of human Cdc25C during prophase. *EMBO Rep.* 3, 341–348 CrossRef Medline
133. Li, H., Liu, X. S., Yang, X., Song, B., Wang, Y., and Liu, X. (2010) Polo-like kinase 1 phosphorylation of p150Glued facilitates nuclear envelope breakdown during prophase. *Proc. Natl. Acad. Sci. U.S.A.* 107, 14633–14638 CrossRef Medline
134. Nakajima, H., Toyoshima-Morimoto, F., Taniguchi, E., and Nishida, E. (2003) Identification of a consensus motif for Plk (Polo-like kinase) phosphorylation reveals Myt1 as a Plk1 substrate. *J. Biol. Chem.* 278, 25277–25280 CrossRef Medline
135. Roux, K. J., Kim, D. I., Raida, M., and Burke, B. (2012) A promiscuous biotin ligase fusion protein identifies proximal and interacting proteins in mammalian cells. *J. Cell Biol.* 196, 801–810 CrossRef Medline
136. Kim, D. I., Jensen, S. C., Noble, K. A., Kc, B., Roux, K. H., Motamedchaboki, K., and Roux, K. J. (2016) An improved smaller biotin ligase for BioID proximity labeling. *Mol. Biol. Cell.* 27, 1188–1196 CrossRef Medline

Appendix Chapter 2: Phase separation in cell division

This chapter is reproduced from

Joseph Y. Ong and Jorge Z. Torres. Phase separation in cell division. Review. Mol Cell. 2020 Aug 19;S1097-2765(20)30550-5. doi: 10.1016/j.molcel.2020.08.007 PMID: 32860741

Molecular Cell

CellPress

Review

Phase Separation in Cell Division

Joseph Y. Ong[1] and Jorge Z. Torres[1,2,3,*]
[1]Department of Chemistry and Biochemistry, University of California, Los Angeles, Los Angeles, CA 90095, USA
[2]Molecular Biology Institute, University of California, Los Angeles, Los Angeles, CA 90095, USA
[3]Jonsson Comprehensive Cancer Center, University of California, Los Angeles, Los Angeles, CA 90095, USA
*Correspondence: torres@chem.ucla.edu
https://doi.org/10.1016/j.molcel.2020.08.007

SUMMARY

Cell division requires the assembly and organization of a microtubule spindle for the proper separation of chromosomes in mitosis and meiosis. Phase separation is an emerging paradigm for understanding spatial and temporal regulation of a variety of cellular processes, including cell division. Phase-separated condensates have been recently discovered at many structures during cell division as a possible mechanism for properly localizing, organizing, and activating proteins involved in cell division. Here, we review how these condensates play roles in regulating microtubule density and organization and spindle assembly and function and in activating some of the key players in cell division. We conclude with perspectives on areas of future research for this exciting and rapidly advancing field.

INTRODUCTION

In biology, phase separation is the phenomenon whereby biomolecules form phase-separated condensates (also called membraneless compartments or coacervates) that have different physical and biological functions from the free, soluble macromolecule (Banani et al., 2017; Boeynaems et al., 2018). This process has recently emerged as being important for cellular processes such as RNA function (Bouchard et al., 2018), transcription (Han et al., 2020; Sabari et al., 2018), DNA repair (Duan et al., 2019), ubiquitylation (Bouchard et al., 2018; Dao et al., 2018; Sun et al., 2018; Yasuda et al., 2020), nuclear pore complex trafficking (Celetti et al., 2020; Milles et al., 2013), and cell division (Ding et al., 2019; Jiang et al., 2015; So et al., 2019; Trivedi et al., 2019). Underscoring the importance of phase-separated macromolecules to human physiology, their dysregulation has been linked to multiple disease states, including neurodegenerative diseases and cancer (Spannl et al., 2019), and possibly developmental disorders (Desai and Pethe, 2020; Hubstenberger et al., 2013; Plys et al., 2019; Schoenfelder et al., 2015).

In particular, the field of cell division has seen an emergence of advancements in understanding the molecular function of phase-separated macromolecules. Cell division is a highly dynamic process that relies on the proper formation of a bipolar microtubule-based spindle that functions as the primary mechanical structure for driving chromosome congression to the metaphase plate and for the equal segregation of DNA into two daughter cells (Lacroix et al., 2018). Three key features essential to microtubule spindle function are the spindle poles, the microtubule spindle itself, and kinetochores. The spindle poles anchor the minus ends of microtubules and serve as the nucleation sites for spindle microtubules. In most animal cells, the centrosome serves as the primary microtubule organizing center (MTOC) and spindle pole for the dividing cell (Azimzadeh, 2014). The spindle microtubules provide the structural framework for the spindle (Prosser and Pelletier, 2017) and include astral microtubules, which radiate toward the cell periphery; k-fibers (or kinetochore microtubules), which are captured at the kinetochore; and polar (or interpolar) microtubules, which extend toward the chromosomes but usually form an attachment to an opposing polar microtubule. The kinetochore, a large protein structure that bridges the interaction between a k-fiber and the centromeric DNA of chromosomes (Musacchio and Salmon, 2007), is important for the capture and movement of chromosomes.

Although the repertoire of proteins necessary for cell division has been well documented and characterized, what roles phase separation play in the fidelity of cell division is an exciting area of ongoing research. Phase separation serves as a novel and attractive mechanism for orchestrating the cell division machinery and for coordinating and organizing complex spatially and temporally sensitive processes. Phase separation has been documented at key cell division structures, namely, the spindle pole (centrosomal and acentrosomal), spindle body, kinetochore, inner centromere, chromosomes, and elsewhere (Figure 1; Table 1). In this review, we focus on the function, properties, and key components of phase separation at these cell division structures and provide perspectives on future avenues for understanding the role of phase separation within the context of mitosis and meiosis.

Properties of Phase Separation

Broadly, phase-separated components share a number of properties (Figure 2; Banani et al., 2017; Boeynaems et al., 2018). Free, soluble macromolecules, usually RNA, proteins, or RNA-protein complexes, can undergo phase separation to form membraneless condensates (Figure 2A). These condensates are usually spherical in appearance because of surface tension (Banani et al., 2017; Boeynaems et al., 2018). Moreover, their

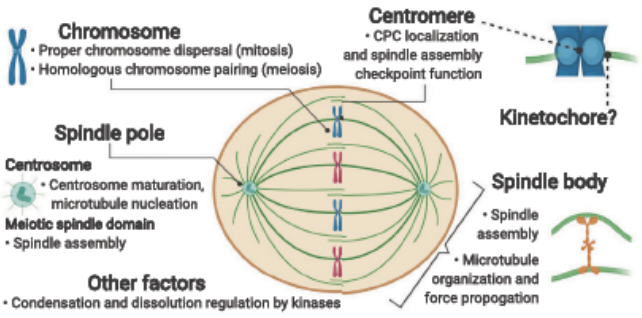

Figure 1. Potential Roles for Phase Separation in Cell Division
Many aspects of mitosis and meiosis are regulated by phase separation. Phase separation may play important roles in the organization of cellular structures and in spatial and temporal regulation of factors involved in cell division.

contents are selective (Banani et al., 2017; Boeynaems et al., 2018): some macromolecules are incorporated within the condensates (dark blue macromolecules), some are excluded from the condensates (red macromolecules), and some are neither included nor excluded and have equal concentrations within and outside the condensate. Macromolecules incorporated into the condensate tend to have higher concentrations than macromolecules in the bulk solution. In the case of enzymes and their substrates, this may lead to faster rates of reaction (Banani et al., 2017).

The formation of phase-separated condensates depends on a variety of factors. In general, macromolecules with intrinsically disordered, low complexity, or repetitive regions tend to form phase-separated condensates (Banani et al., 2017; Boeynaems et al., 2018). Condensation is usually mediated by post-translational modifications such as phosphorylation or poly(ADP-ribosylation) (PARylation) (Duan et al., 2019) and by multivalent interactions (Banani et al., 2017), particularly via hydrophobic or charged amino acid residue-mediated protein-protein interactions, RNA-RNA interactions, or protein-RNA interactions (Mittag and Parker, 2018). Condensation is generally promoted by molecular crowding (induced either by high concentrations of proteins or by the addition of a crowding agent such as PEG; Milles et al., 2013) and lower ionic strength solutions (Lin et al., 2015). Caution must be used when interpreting *in vitro* experiments using purified protein, however, as the concentrations of purified protein used to observe phase separation by microscopy are often much higher than physiological conditions. Moreover, experiments using crowding agents such as PEG must similarly be interpreted carefully, as the use of reagents such as PEG may result in artifacts that are not physiologically relevant. Although high concentrations of proteins and the use of crowding agents are used as aids to form and study phase-separated condensates *in vitro*, further experiments are necessary to confirm the existence and understand the role of phase-separated condensates within a cell. Phase-separated condensates may dissolve when diluted, in high salt solutions, or in the presence of small molecules that disrupt hydrophobic interactions, such as 1,6-hexanediol (Ding et al., 2019). In yeast, autophagy-related phase-separated condensates were promoted by an acidic pH of 6, the approximate pH of the yeast cytoplasm during starvation conditions (Fujioka et al., 2020).

Temperature may also play a role in phase separation, though how much of a role this plays within a mammalian system is unclear (Jiang et al., 2015).

Many phase-separated condensates have a liquid-like character, sometimes earning them the name liquid-liquid phase-separated (LLPS) condensates, as the liquid-like condensates are separated (another common term is "de-mixed") from the liquid of the cytoplasm (Hyman et al., 2014). These condensates are distinct from the bulk solution. When in close proximity, these condensates can fuse together, mixing their components and growing in size (Figure 2B; Banani et al., 2017). They may also undergo fission in the presence of an external force such as a shear force (Figure 2B; Banani et al., 2017). Within liquid-like condensates, macromolecules diffuse quickly, and the contents of the condensate undergo internal rearrangements at fast timescales, usually demonstrated by photobleaching experiments (Figure 2C; Banani et al., 2017). Macromolecules can also exchange in and out of the liquid-like condensate. For example, nuclear transport receptors enriched in nuclear pore complex-based gels recover quickly after photobleaching, suggesting that the nuclear transport receptors within the condensate exchange quickly and freely with their soluble counterpart (Schmidt and Görlich, 2015). In contrast, the nuclear pore complex-based gels, which are in a solid-like condensate because of aging over time (Celetti et al., 2020; Milles et al., 2013), do not recover after photobleaching, suggesting that the nuclear pore complex-based gels are more static and do not freely diffuse within the condensate or exchange with solution. In biological systems, this dynamic aspect of condensates may allow the equal distribution of protein complexes over a large cellular substructure.

Some condensates have been observed to "age" over time. Aged condensates can "harden" into solid-like or gel-like states (Celetti et al., 2020; Milles et al., 2013) wherein the dynamics of their internal rearrangements become slower, as demonstrated via photobleaching experiments (Figure 2D, top; Gouveia et al., 2019; Lin et al., 2015; Park et al., 2019), and their ability to fuse decreases (Figure 2D, bottom; Patel et al., 2015). Instead of fusing, aged condensates tend to clump, sometimes forming networks and amyloid-like aggregates (Lin et al., 2015). For proteins involved in amyloid diseases, the formation of these amyloids can be affected by patient-derived mutations and may play a role in disease progression (Conicella et al., 2016; Mackenzie et al., 2017; Molliex et al., 2015; Patel et al., 2015; Wegmann et al., 2018). In the nuclear pore complex, the formation of gel-like states may play a role in nuclear trafficking (Celetti et al., 2020; Milles et al., 2013; Schmidt and Görlich, 2015).

Table 1. Summary of Phase-Separated Condensates in Cell Division

Structure	Key Components	Properties	Biological Function	System
Spindle poles	centrosome: SPD-5 (*C. elegans*), Plk4 (*X. laevis* extracts and cultured human cells)	• SPD-5 condensates promoted by Plk1, incorporated centrosome factors, nucleated MTs, hardened over time	• concentrates tubulin and generates microtubule asters; promotes MTOC formation	*C. elegans* embryos (SPD-5) (Woodruff et al., 2017)
		• Plk4 condensates promoted by autophosphorylation, hardened over time, promoted centrosome maturation and stability	• centrosome maturation	recombinant Plk4 and *X. laevis* extracts (Gouveia et al., 2019), cultured human cells (Park et al., 2019)
	acentrosomal: centrosome and centrosome-associated proteins	• LISD promoted by Aurora A kinase activity, TACC3 binding to CHC17 and to microtubules	• promotes spindle assembly and formation of MTOC	recombinant proteins and mammalian oocytes (So et al., 2019)
Spindle body	tubulin, microtubule motors and crosslinkers	• tubulin polymers form tactoids that can fuse with other tactoids	• local range liquid-like state preserves microtubule spindle assembly and homeostasis	*X. laevis* extracts (Brugués and Needleman, 2014; Gatlin et al., 2009), purified tubulin and recombinant proteins (Edozie et al., 2019)
		• diffusion of microtubule-associated proteins • two bipolar spindles will fuse into one bipolar spindle in a dynein-dependent manner	• regulates microtubule orientation and density	
	Tau	• concentrates tubulin, promotes nucleation, elongation, and bundling of MTs	• unknown role in spindle assembly	recombinant proteins (Hernández-Vega et al., 2017)
	TPX2	• concentrates tubulin, promotes nucleation of MTs	• promotes mitotic spindle density and assembly	recombinant proteins, *X. laevis* extracts (King and Petry, 2020)
	BuGZ	• concentrates tubulin, promotes nucleation and bundling of MTs • incorporates and promotes activity of Aurora A kinase	• promotes mitotic spindle density and assembly	*X. laevis* extracts, recombinant proteins, and cultured human cells (Huang et al., 2018; Jiang et al., 2015)
Centromere	chromosomal passenger complex (INCENP, Borealin, Survivin)	• Borealin condensates promoted by Cdk1/Cyclin B kinase activity, microtubules, α-satellite DNA, and nucleosomes • nucleates microtubules; hardens *in vitro* and in cells	• promotes localization of CPC to inner centromere and midzone, spindle assembly checkpoint, and mitotic timing	Cultured human cells (Trivedi et al., 2019)

(*Continued on next page*)

Table 1. *Continued*

Structure	Key Components	Properties	Biological Function	System
Chromosomes	mitotic: Ki-67	• Ki-67 protein surfactant properties mediated via steric hindrance and/or electrostatic interactions	• Ki-67 promotes chromosome dispersal and promotes MT spindle formation	cultured human cells (Cuylen et al., 2016)
	meiotic: RNA binding proteins and lncRNA	• meiotic lncRNA droplets fuse with droplets of same RNA species	• lncRNA droplets promote pairing of homologous chromosomes	*S. pombe* (Ding et al., 2019)
Other	mostly stress granules, RNA splicing speckles, centrosome/ pericentriolar matrix	• DYRK3 promotes condensate dissolution at NEBD to release mitotic factors	• promotes spindle formation and mitotic timing	cultured human cells (Rai et al., 2018)

MT, microtubule; MTOC, microtubule organizing center; NEBD, nuclear envelope breakdown.

The physiological function, if any, of the aggregation of aged condensates in other biological systems is largely unknown.

Phase Separation at the Centrosome

The centrosome is the main MTOC of most eukaryotic cells and usually serves as the spindle pole in mitosis (Nigg and Holland, 2018; Prosser and Pelletier, 2017). Centrosomes are composed of two centrioles surrounded by pericentriolar matrix (PCM) that serves to scaffold proteins necessary for microtubule nucleation and anchoring (Azimzadeh, 2014). During interphase, the centrioles undergo a complex round of duplication and maturation into a centrosome before it can serve as a proper MTOC for cell division (Nigg and Holland, 2018). Many microtubule-associated proteins localize at the centrosome to provide structural support and cohesion and to promote microtubule nucleation, polymerization, and organization (Nigg and Holland, 2018). Of interest, recent examples have surfaced in which the phase separation of key centrosomal proteins is essential for centrosome maturation and homeostasis.

In the *C. elegans* embryo, SPD-5 is a protein with roles in centrosome maturation, and loss of SPD-5 leads to defects in spindle assembly (Laos et al., 2015). In a study to reconstitute centrosome morphology and microtubule organization *in vitro*, SPD-5 was found to form phase-separated condensates as a function of molecular crowding (Woodruff et al., 2017). Whereas newly formed, "young" SPD-5 condensates incorporated other SPD-5 into their condensates, older, "aged" SPD-5 condensates did not exhibit dynamic exchange with the solution or internal rearrangement after photobleaching *in vitro* (Woodruff et al., 2017). Within the embryo, the dynamics of SPD-5 at the centrosome also resembled that of the aged SPD-5 condensates (Woodruff et al., 2017). These data suggest that *in vivo*, SPD-5 undergoes a liquid-like to a solid-like rearrangement as a function of time or droplet size. Droplet formation was enhanced by Plk1 kinase activity and via incorporation of SPD-2 (mammalian homolog: Cep192), and in cells, key centrosomal proteins Plk1, SPD-2, TPXL-1 (mammalian homolog: TPX2), and Zyg-9 (mammalian homolog: CKAP5; also known as ch-TOG or the mammalian homolog of XMAP215) incorporated into these condensates at the centrosomes (Woodruff et al., 2017). The microtubule-associated protein EB1 was not incorporated into SPD-5 condensates *in vitro*, suggesting that these condensates are selective (Woodruff et al., 2017). In the presence of TPXL-1 and Zyg-9, SPD-5 condensates incorporated and concentrated tubulin both *in vitro* and *in vivo* (Woodruff et al., 2017). These SPD-5, Zyg-9, and TPXL-1 condensates also formed microtubule asters *in vitro* (Woodruff et al., 2017). These data indicate that phase separation at the centrosome is critical for its function as a MTOC.

In *Xenopus* egg extracts, the ability of Plk4 to form condensates was dependent on its kinase activity (Gouveia et al., 2019); in particular, in cultured human cells, Plk4 autophosphorylation on key residues in its cryptic polo box (CPB) domain promoted phase-separated condensates (Park et al., 2019). These Plk4 condensates concentrated tubulin and acted as the MTOC that recruited and ordered the centrosomal protein STIL and gamma-tubulin (Gouveia et al., 2019). During centrosome biogenesis and maturation, Plk4-Cep152 binding in a ring-like structure is first necessary for Plk4 localization to the centrioles (Park et al., 2014), then Plk4-STIL binding in a dot-like structure is necessary for the initiation of procentriole formation (Moyer and Holland, 2019). When Plk4 formed phase-separated condensates, the binding between Plk4 and Cep152 became weaker, whereas the binding between Plk4 and STIL became stronger (Park et al., 2019), suggesting a role for phase separation in procentriole formation. When in condensates, Plk4 also resisted ubiquitin-mediated degradation by excluding the ubiquitin ligase β-TrCP (Park et al., 2019), suggesting that phase separation may stabilize proteins by excluding the factors that degrade them. Unlike many other condensates, condensates made from recombinant Plk4 *in vitro* did not recover after photobleaching experiments, suggesting that Plk4 condensates resemble a more solid gel-like state (Gouveia et al., 2019; Park et al., 2019). These data suggest that, during centrosome maturation, Plk4 may transition from a liquid-like to a solid gel-like state (in a manner similar to SPD-5 in the *C. elegans* embryo), perhaps to prevent degradation factors or further maturation factors from accumulating at the centrosome. Alternatively, the hardening of the centrosome may serve to "cement" microtubules within the centrosome, to maintain an ordered array of microtubules, and to resist forces generated by microtubule motors. Phase separation then may serve as a means by which different protein interactions are controlled through time to spatially and temporally regulate centrosome maturation.

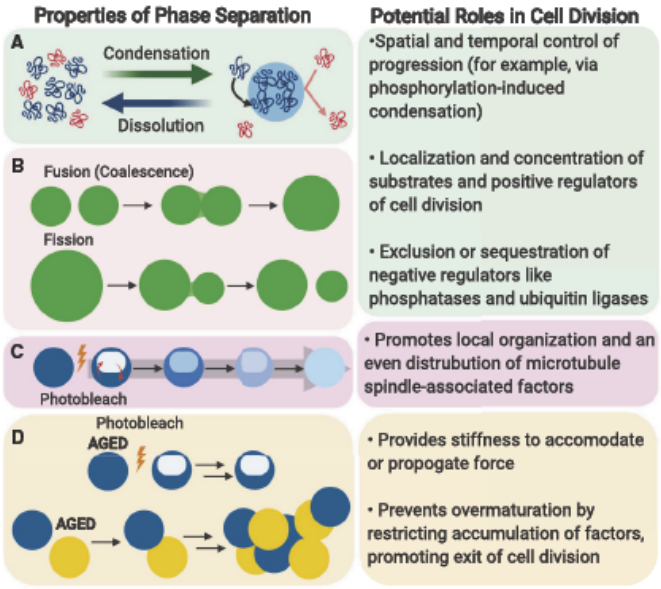

Figure 2. Phase-Separated Condensates Have Unique Chemical and Physical Properties

(A) Soluble macromolecules can condense to form phase-separated compartments. These compartments are selective in which macromolecules are incorporated and are distinct from the bulk solution. Condensates may dissolve back into free macromolecules. The factors that affect condensation or dissolution vary.

(B) Phase-separated condensates may exhibit liquid-like droplet behavior. Two or more condensates may fuse, increasing their size and mixing their contents. A condensate may also undergo fission to form two or more smaller condensates, usually in response to shear force.

(C) Within phase-separated condensates, macromolecules usually have faster rates of diffusion and internal rearrangement relative to macromolecules in solid or solid-like structures. Macromolecules in phase-separated condensates also tend to have fast rates of exchange with macromolecules in free solution.

(D) Phase-separated condensates can undergo "aging" wherein they harden over time. Macromolecules within aged condensates do not diffuse easily and aged condensates tend to aggregate instead of fusing.

Phase Separation at the Acentrosomal Meiotic Spindle Pole and Spindle Body

Whereas all eukaryotic cells form a microtubule spindle to divide, not all cells use centrosomes to nucleate microtubule spindles. For example, plants, fungi, and some algae all divide without centrosomes, instead using other organelles or protein complexes to organize their microtubules (Yi and Goshima, 2018). Among mammalian cells, the mammalian oocyte is unique in that although it expresses many centrosomal proteins, the oocyte lacks a centrosome and undergoes an acentrosomal cell division (Dumont and Desai, 2012). How these proteins are localized and organized to form a microtubule spindle within the oocyte, a large cell relative to other mammalian cells, is an active area of investigation.

Immunofluorescence microscopy of centrosome- and spindle-related proteins in mouse metaphase I oocytes identified a number of proteins that localized at the acentrosomal MTOC at the spindle poles (So et al., 2019). However, a number of other proteins localized in a structure that encompassed the MTOC as well as the spindle itself. This structure exhibited droplet-like behavior and high rates of diffusion, suggestive of phase separation (So et al., 2019). This structure, which the authors termed the liquid-like meiotic spindle domain (LISD), was disrupted by depletion of microtubule-associated protein TACC3, by depletion of CHC17 (a binding partner of TACC3), and by inhibition of Aurora A kinase activity (So et al., 2019).

In contrast to phase separation at the centrosome, the LISD did not appear to concentrate tubulin (So et al., 2019). However, disruption of the LISD resulted in reduced density of k-fibers and interpolar microtubules, spindle volume, and resulted in delays in meiotic progression (So et al., 2019). Consequently, the authors speculate that the LISD may serve at least two purposes: first, as the oocyte is a large cell, the formation of the LISD may sequester and concentrate important meiotic spindle proteins; second, the LISD may promote an even distribution of spindle proteins across the entire spindle, preventing the accumulation of a particular protein in a confined area (So et al., 2019).

Phase Separation at the Microtubule Spindle

The microtubule spindle is a large and dynamic cellular structure that needs to be assembled and disassembled every cell division. Moreover, it is a complicated machine: during cell division, microtubules undergo dynamic instability, wherein their lengths change rapidly because of fluctuating periods of growth and depolymerization, and the spindle itself is permeated with a number of microtubule motors and microtubule-associated proteins that also affect microtubule polymerization dynamics, force generation, and mechanical stress propagation (Prosser and Pelletier, 2017). How the spindle is organized across many length scales and how spindle architecture gives rise to the mechanical properties of the microtubule spindle are still under study (Lacroix et al., 2018). Phase separation has begun to describe how the microtubule spindle is organized at small and large length scales.

The foundation of the microtubule spindle is the tubulin dimer. Purified tubulin was observed not only to polymerize into filaments but also to form spindle-shaped, highly oriented domains (Edozie et al., 2019). These micron-scale almond shaped domains, which the authors termed tactoids, formed condense bundles in the presence of the *Arabidopsis thaliana* microtubule crosslinker MAP65 (human ortholog: PRC1) (Edozie et al., 2019). Tactoids that elongated and approached a neighboring tactoid

fused together into a longer tactoid, but only if the two tactoids were parallel along the long axis (end-to-end) (Edozie et al., 2019). Interestingly, via photobleaching experiments of the tactoids, MAP65 is able to quickly diffuse within the tactoid, but the polymerized tubulin of the microtubule itself cannot (Edozie et al., 2019). The ability of MAP65 to diffuse within the tactoid is reminiscent of the diffusion of proteins in the meiotic LISD and may suggest that phase separation-based diffusion may serve to distribute microtubule-associated proteins evenly within the meiotic and mitotic spindles. As these results come from an *in vitro* system using methylcellulose as a crowding agent and GMPCPP to stabilize the microtubule filaments, this system fails to account for many important aspects of microtubule dynamics, including the actions of molecular motors in shaping the microtubule spindle as well as the property of dynamic instability at microtubule ends. Nonetheless, these experiments suggest that, at least under some conditions, microtubules and microtubule crosslinkers such as MAP65 have the capacity to self-organize microtubules into local domains.

Mitotic spindles isolated from frog extracts display similar properties (Gatlin et al., 2009). Using microneedle manipulation, two metaphase mitotic spindles brought close together would fuse into one mitotic spindle (Gatlin et al., 2009). Unlike tubulin tactoids, mitotic spindles could fuse under a variety of orientations: both parallel and perpendicular mitotic spindles fused (Gatlin et al., 2009). The ability of these spindles to fuse was dependent on the activity of the motor protein dynein (Gatlin et al., 2009). Later experiments that used quantitative polarized light microscopy and computational modeling to study the *X. laevis* metaphase mitotic spindle demonstrated that the spindle is self-organized via local domains governed by microtubule polymerization dynamics, crosslinkers, and motors (Brugués and Needleman, 2014).

Given that recent experiments using microneedle manipulation to probe biomechanical properties of the spindle demonstrated that different regions of the spindle have different degrees of stiffness and viscosities (Suresh et al., 2020; Takagi et al., 2019), local phase-separated domains may serve to give rise to the morphology of the mitotic spindle and accounts for the generation and propagation of mechanical stress.

Phase separation may thus play a role in providing a physical means for microtubules to find and attach to kinetochores in the otherwise crowded microtubule spindle body. Which microtubule-associated proteins grant different biomechanical properties, how they are localized within the entire microtubule spindle, and how they are affected by phase separation within sub-regions or sub-condensates of the microtubule spindle, however, are not entirely clear. Moreover, tubulin itself is a highly modified protein (Janke and Magiera, 2020), and these modifications play important roles in cell division (Barisic and Maiato, 2016). Because post-translational modifications regulate the formation of phase-separated condensates, tubulin modifications that affect the phase separation properties of the microtubule spindle may also affect the organization, morphology, and mechanical properties of the microtubule spindle. For example, the velocity and the time bound to microtubules of molecular motor dynein, which is necessary for the fusion of *Xenopus* mitotic spindles (Gatlin et al., 2009), increases when dynein binds to acetylated tubulin (Alper et al., 2014). Although it is unknown whether tubulin post-translational modifications have any effect on the ability of dynein or other microtubule-associated proteins to induce phase separation of tubulin, these modifications nonetheless may regulate the phase separation properties of the microtubule spindle either directly through the ability of tubulin to assemble and associate with itself or indirectly, via the ability of microtubule-associated proteins to bind to microtubules.

Key proteins involved in assembling the microtubule spindle also exhibit phase separation properties. We highlight the roles of microtubule binding proteins tau, TPX2, and BuGZ. Tau is a microtubule-stabilizing protein that has been highly studied because aggregates of tau have been implicated in a number of neurodegenerative diseases (Wang and Mandelkow, 2016). Although a clear role for tau in mitosis or spindle assembly has not yet been identified, tau is differentially phosphorylated in mitosis (Pope et al., 1994; Tatebayashi et al., 2006) and decorates the microtubule spindle (Connolly et al., 1977; Preuss and Mandelkow, 1998). Tau regulates the activity of molecular motors such as kinesins and severing enzymes such as the katanins (Siahaan et al., 2019), two families of enzymes that play roles in shaping the mitotic spindle (Cheung et al., 2016; Mayr et al., 2007; Splinter et al., 2010; Stumpff et al., 2008), and overexpression of tau led to the formation of monopolar spindles and mitotic arrest in the *Drosophila melanogaster* wing disc (Bougé and Parmentier, 2016). In experiments with purified protein, tau formed liquid-like condensates (Hernández-Vega et al., 2017; Wegmann et al., 2018) that incorporated and concentrated tubulin dimers. These tau-tubulin drops served as sites for microtubule nucleation, and the tau droplets spread out along the emerging microtubule (Hernández-Vega et al., 2017). Tau-coated microtubules could fuse or bundle with each other, forming a network of parallel filaments (Hernández-Vega et al., 2017). Similar to MAP65 on tubulin tactoids, photobleaching experiments demonstrated that the fluorescence of tau on microtubule bundles, but not the tubulin itself, quickly recovered after photobleaching, suggesting that tau was able to diffuse along the microtubule length and with free tau in solution (Hernández-Vega et al., 2017). Moreover, tau condensates were observed to age and harden, promoting the formation of tau aggregates (Wegmann et al., 2018), though whether this aspect of tau condensates has any function in normal spindle assembly or is part of the progression of neurodegenerative diseases is unknown.

Similarly, purified TPX2, a microtubule nucleator that promotes branched microtubules from an existing microtubule filament (Petry et al., 2013), formed phase-separated condensates that incorporated and concentrated tubulin (King and Petry, 2020). In solution, these TPX2-tubulin condensates formed microtubule asters, and in *Xenopus* egg extracts, these TPX2-tubulin condensates served as microtubule nucleation points (King and Petry, 2020). Purified TPX2 preferentially formed droplets on existing microtubules and enhanced branched microtubule nucleation (King and Petry, 2020). Interestingly, importin-α/β, inhibitors of TPX2 nucleation (Schatz et al., 2003), dissolved TPX2-tubulin condensates (King and Petry, 2020). Given that the concentration of importin that can inhibit TPX2 is low near the chromosomes by nature of a Ran-GTP gradient (Kalab

et al., 2002), importin-mediated dissolution of TPX2 condensates may partly explain why TPX2 microtubule nucleation is high near the chromosomes and how TPX2 promotes correct spindle size and function (Bird and Hyman, 2008). Moreover, as TPX2 protects Aurora A from proteasome-mediated degradation (Giubettini et al., 2011), TPX2-based phase separation may play a role in stabilizing Aurora A by excluding ubiquitin ligases that target Aurora A for destruction.

BuGZ is a mitotic spindle (Jiang et al., 2014; Toledo et al., 2014) and kinetochore-associated (Jiang et al., 2014) protein that binds to and stabilizes Bub3, a protein that scaffolds and recruits proteins that monitor the proper attachment between microtubules and chromosomes through a mechanism known as the spindle assembly checkpoint to prevent improper cell division (Musacchio and Salmon, 2007). During mitosis, BuGZ facilitates the loading of Bub3 onto the kinetochore, and loss of BuGZ leads to a weakening of the spindle assembly checkpoint (Jiang et al., 2014; Toledo et al., 2014). Recombinant BuGZ was found to phase-separate in a temperature-dependent manner, as BuGZ condensates were disrupted at colder temperatures (Jiang et al., 2015). In *Xenopus* egg extracts, which allow the study of kinetochore-independent roles of BuGZ, disruption of BuGZ phase separation resulted in fewer microtubule-associated proteins associated with MTOCs generated from Aurora A kinase (Jiang et al., 2015). The microtubule aster-like MTOCs formed in the presence of phase separation-deficient BuGZ were also smaller and contained fewer microtubules than phase separation-capable BuGZ (Jiang et al., 2015). Moreover, *in vitro*, Aurora A could incorporate into BuGZ droplets, promoting Aurora A kinase activity (Huang et al., 2018).

The incorporation of Aurora A into BuGZ phase-separated condensates is particularly interesting given the kinetochore localization and function of BuGZ. Although Aurora A predominately functions in centrosome maturation and spindle assembly (Joukov and De Nicolo, 2018), Aurora A has also been demonstrated to phosphorylate a component of the kinetochore, Hec1 (DeLuca et al., 2018). BuGZ-based phase separation may thus function to enhance Aurora A phosphorylation both at the centrosome and at the kinetochores. However, the experiments demonstrating the phase separation properties of BuGZ were performed in *Xenopus* egg extracts. *Xenopus* egg extracts allow the study of phase separation of BuGZ with Aurora A (Huang et al., 2018) and microtubule-associated proteins (Jiang et al., 2015), but because these extracts lack chromosomes and kinetochores, the role of BuGZ phase separation at the kinetochores is unclear. For example, expression of mutant forms of BuGZ that lacked the ability to phase separate resulted in abnormal mitotic spindles in HeLa cells (Jiang et al., 2015). However, these mutant BuGZ constructs had a weaker association with tubulin (Jiang et al., 2015). As BuGZ promotes Bub3 loading on the kinetochores in a microtubule-dependent manner (Jiang et al., 2014; Toledo et al., 2014), it is possible that the observed spindle assembly defects may be attributed to errors in kinetochore-microtubule attachment from a lack of Bub3 and not necessarily to the phase separation properties of BuGZ. Further experiments are necessary to determine if BuGZ phase separation, the BuGZ-Bub3 interaction, or both are necessary for proper microtubule spindle formation. Interestingly, Aurora A binding partners TACC3 (So et al., 2019), TPX2 (King and Petry, 2020), and BuGZ (Huang et al., 2018) are all involved in phase-separated microtubule assembly processes, potentially suggesting an important role of Aurora A in mediating spindle assembly via phase separation.

Phase Separation at the Centromere

The centromere is a cellular substructure assembled around CENP-A nucleosomes located at centromeric DNA (McKinley and Cheeseman, 2016). One of the major regulators of cell division located within the centromere is the Aurora B kinase, whose kinase activity generally destabilizes incorrect kinetochore-microtubule attachments, delaying anaphase onset until proper kinetochore-microtubule attachments are formed (Hindriksen et al., 2017). Aurora B, together with Survivin, Borealin, and INCENP, form the chromosomal passenger complex (CPC) (Carmena et al., 2012).

Purified Survivin, Borealin, and INCENP formed phase-separated droplets *in vitro* and in cells at the inner centromere (Trivedi et al., 2019). *In vitro*, components of the inner centromere, including α-satellite RNA and DNA, histone H3 phosphorylated at Thr3, SGO1, phosphorylated HP1α, microtubules, and Aurora B, promoted the formation of these phase-separated droplets, were enriched in these phase-separated droplets, or both (Trivedi et al., 2019). In contrast, Mad2, an outer kinetochore protein, was excluded from CPC-based droplets (Trivedi et al., 2019). *In vitro*, the ability of Borealin to form phase-separated droplets was enhanced by Cdk1/Cyclin B phosphorylation. Disruption of phase separation of the CPC via expression of a mutant form of Borealin resulted in reduced localization of the CPC and Aurora B at the inner centromere and spindle midbody by about half (Trivedi et al., 2019). This result suggests that phase separation mediated by Borealin contributes to or enhances CPC localization and assembly but is not the only factor that contributes to CPC localization or assembly (Carmena et al., 2012; Hindriksen et al., 2017). Loss of CPC phase separation also resulted in a delay in mitotic progression, a weakening of the spindle assembly checkpoint, and an increase in the number of lagging chromosomes, though whether this is simply due to less Aurora B activity from reduced Aurora B localization or some other aspect of phase separation is unclear (Trivedi et al., 2019).

Given that Aurora B phosphorylates components of the kinetochore in early mitosis (Broad et al., 2020), phase separation of the centromere may serve to spatially separate Aurora B and the inner centromere from kinetochore proteins. This hypothesis is particularly intriguing given that Mad2 was excluded from the CPC-based droplets. In this way, the formation of phase-separated condensates at the centromere serves as a physical means of separating the kinetochore and centromere. Phase separation, then, along with other physical methods (Akiyoshi et al., 2010), may serve to decrease Aurora B activity at the kinetochore and promote the formation of stable kinetochore-microtubule attachments.

Aurora C is a homolog of Aurora B that is expressed predominantly in gametes and has important functions in meiosis (Quartuccio and Schindler, 2015). Similar to Aurora B, Aurora C binds INCENP and performs similar functions during meiotic divisions (Abdul Azeez et al., 2019). Whether Aurora C also undergoes

phase separation during meiosis is unknown. However, because the phase separation described here was reconstituted with Survivin, Borealin, and INCENP, all of which are also present and active in meiosis, phase separation may also play a role in the progression of meiosis and gamete formation. Perhaps Aurora C can change the localization and function of CPC-based condensates in meiosis to fine-tune the CPC for function in meiosis.

Phase Separation at the Chromosomes

Whereas chromatin and transcription factors form phase-separated compartments that aid in transcription (Han et al., 2020; Sabari et al., 2018), chromosomes themselves play roles in phase separation-mediated processes in cell division. In a small interfering RNA (siRNA) screen for proteins involved in chromosome separation, loss of Ki-67 in HeLa cells was observed to cause chromosomes to clump together (Cuylen et al., 2016). Microtubules were not able to access the kinetochores of clumped chromosomes, leading to mitotic failure (Cuylen et al., 2016). No one domain of Ki-67 was responsible for the proper separation of chromosomes; rather, Ki-67 acted as a molecular surfactant, coating the surface of the chromosome and using electrostatic and/or steric interactions to separate chromosomes from each other and to promote a functional mitosis (Cuylen et al., 2016).

In contrast, in meiosis, long noncoding RNA (lncRNA) may serve to join homologous chromosomes together. In *S. pombe* meiosis, *sme2* RNA is a lncRNA that accumulates at its gene locus and plays a role in facilitating the pairing of homologous recombination (Ding et al., 2019). Via microscopy of proteins that localized near the *sme2* lncRNA foci, two other genetic loci were identified (Ding et al., 2019). These two loci also coded for meiosis-specific lncRNA, and similar to *sme2* lncRNA, these two novel lncRNAs also accumulated and formed foci at their respective genomic locations (Ding et al., 2019). Each of the three chromosomes of *S. pombe* had one gene locus that exhibited fusion under physiological conditions (Ding et al., 2019). In particular, two *sme2* lncRNA foci (one on each homologous chromosome) would fuse, bringing the two chromosomes together for homologous recombination; the other two lncRNA behaved likewise (Ding et al., 2019). Interestingly, the different lncRNAs were phase separated from each other and would fuse only with the compartment that shared the same RNA species (Ding et al., 2019). In meiosis, then, phase separation of protein-lncRNA foci served to exclude non-homologous chromosomes and to physically join homologous chromosomes.

Other Factors in Phase Separation during Cell Division

Cell division is highly regulated by kinases such as the cyclin-dependent kinases, Polo kinases, and Aurora kinases (Malumbres and Barbacid, 2009; Mistry et al., 2008; van Vugt et al., 2010). Evidence for the role of kinases in promoting the formation of phase-separated condensates is growing. Many of the discussed condensates are promoted by phosphorylation (centrosomal SPD-5 by Plk1, centrosomal Plk4 by Plk4, the meiotic LISD by Aurora A, centromeric CPC by Cdk1), and in at least one case, kinase activity is enhanced by the formation of a phase-separated condensate (BuGZ enhancing Aurora A). A prime example of a kinase regulating condensate formation is DYRK3 (Wippich et al., 2013), which is a cell-cycled regulated kinase that increases in concentration from G1 to M phase and is degraded in late mitosis by the APC/C (Rai et al., 2018). DYRK3 localizes to and associates with proteins of multiple membraneless compartments such as the centrosome, stress granules, and splicing speckles (Rai et al., 2018). Overexpression of DYRK3 led to dissolution of these membraneless compartments, and chemical inhibition of DYRK3 stabilized them (Rai et al., 2018). These membraneless compartments dissolve during mitosis and reform at the end of mitosis dependent on DYRK3 kinase activity and the ratio of DYRK3 to substrate, which increases at nuclear envelope breakdown (NEBD) because of the mixing of the nucleoplasm and cytoplasm (Rai et al., 2018). Inhibition of DYRK3 kinase activity led to the persistence of membraneless compartments during mitosis and the sequestration of mitotic regulator BuGZ (Rai et al., 2018). The inhibition of DYRK3 consequently resulted in multipolar spindle formation and an increase in mitotic timing (Rai et al., 2018). Therefore, DYRK3 kinase activity may serve as a means of solubilizing or freeing mitotic factors from membraneless compartments in early mitosis for proper spindle assembly and cell division. However, these experiments were performed with only one chemical inhibitor of DYRK3, GSK-626616, and at the relatively high concentration of 1 μM. Given that GSK-626616 has known off-target effects at 1 μM, including other DYRK kinases and important signaling and cell cycle-related kinases such as ERK8, PIM1, JAK kinases, and NEK kinases (Wippich et al., 2013), further study of the role of DYRK3 and other kinases is necessary to understand how condensate formation and dissolution may serve as regulators of mitosis.

Conclusion and Perspectives

Phase separation is an increasingly studied phenomenon with emerging roles in regulating the fidelity of cell division. At the molecular level, phase-separated condensates concentrate and localize proteins of interest; thus, microtubules are more easily nucleated at the centromere, microtubule-associated proteins and motors are diffuse and spread throughout the microtubule spindle, and meiotic factors are sequestered and spread within a particular domain of the otherwise large oocyte. Phase-separated condensates also sequester other factors and provide a means of spatial regulation, as Plk4-condensates exclude ubiquitin ligases and the CPC-based centromeric condensate excluded the kinetochore protein Mad2. Finally, as the centrosome and centromere were both observed to harden over time and as lncRNA complexes in meiosis keep homologous chromosomes together, phase-separated condensates may serve a structural role, allowing the formation of an ordered microtubule array at the centrosome and for the accommodation of stresses and forces at the centromere and within the microtubule spindle.

To what extent does phase separation serve to organize cellular substructures? Understanding whether certain organelles or substructures exhibit properties of phase separation and how, if at all, those properties affect their function is an active area of research. For example, here, we highlighted the phase separation properties of centrosomal protein SPD-5 and Plk4 in centrosome maturation. However, other proteins involved in centrosome maturation do not undergo phase separation. Purified *D. melanogaster* centrosomal protein Centrosomin (human

ortholog: CDK5RAP2; probable *Drosophila* ortholog for *C. elegans*: SPD-5), for example, was found to form structures that resembled phase-separated aggregates by microscopy. In contrast to most phase-separated systems, however, Centrosomin did not dynamically rearrange after photobleaching, suggesting that these Centrosomin structures are not liquid-like phase-separated aggregates but a micron-scale ordered structure or a solid-like phase-separated condensate (Feng et al., 2017).

Do these data suggest that the centrosome is not regulated by phase separation? It is possible that the dynamic liquid-like state of Centrosomin could not be observed for technical reasons. Certain nuclear pore complex proteins have long been known to form aggregate-like gels (Milles et al., 2013), but it was only recently discovered, via innovative microfluidics and imaging systems, that nuclear pore complex proteins first transition through a liquid-like state before maturing into gel-like states (Celetti et al., 2020). There is a possibility that solid-like structures, such as Centrosomin-based structures, are simply "aged" liquid-like phase-separated structures and that technical details prevent the capture of the liquid-like states. Alternatively, cellular structures such as the centrosome may simply be composed of both ordered structures and phase-separated structures.

Much work has focused on how mitotic and meiotic structures are assembled by phase separation, but less work has focused on the relationship between phase separation and disassembly. As cells progress through cell division, the activity of kinases such as Plk1 or Aurora kinases generally decreases as they are degraded by the APC/C (Lindon and Pines, 2004; Stewart and Fang, 2005). Given the importance of kinase activity in forming phase-separated condensates (So et al., 2019; Woodruff et al., 2017), it is reasonable to hypothesize that condensates may dissolve as kinases and other mitotic and meiotic factors are degraded. Is it possible that force by the microtubule spindle has a role in physically breaking apart phase-separated condensates or in reducing the concentration of factors such that they no longer undergo phase separation? For example, CPC phase-separated condensates, which localize at the centromeres of two homologous chromosomes, likely experience both a physical force during the metaphase to anaphase transition and a change in the local concentration of CPC components, both factors which may cause its dissolution.

How a cell commits to enter and complete cell division has been an active area of study. In particular, the rapid events in cell division need to be executed in a non-reversible, temporally regulated, and sequential manner. Characteristics of kinases have been shown to assist in decisively executing events in cell division. For example, in mitosis, Cdk1 exhibits hysteresis and bistability, meaning that once Cdk1 is active, a small decrease in the concentration of its activator Cyclin B does not significantly inhibit Cdk1 activity (Pomerening et al., 2003; Sha et al., 2003). This mechanism prevents regression from mitosis because of a small change in Cyclin B levels. Moreover, Cdk1 is regulated by positive feedback loops at the entry to mitosis, allowing a rapid and irreversible entry into mitosis (Santos et al., 2012). Can phase separation play a similar role in promoting rapid and irreversible temporal regulation of cell division? As cell division-promoting factors accumulate, they may spontaneously phase separate as a function of concentration or other cellular events, such as NEBD (Rai et al., 2018). These phase-separated condensates may activate kinases by concentrating kinases and their substrates, excluding phosphatases or ubiquitin ligases, or other means (Fujioka et al., 2020; Huang et al., 2018). Thus, the formation of phase-separated condensates may also serve to enhance rapid and irreversible progression through the steps of cell division.

Post-translational modifications, particularly via kinases and ubiquitin ligases, play crucial roles at the heart of cell cycle progression and in the establishment of phase separation (Bouchard et al., 2018; Dao et al., 2018; Heinkel et al., 2019; Park et al., 2019; Su et al., 2016; Sun et al., 2018; Yasuda et al., 2020). Although phosphatases have been studied in regulating phase separation in other systems, they are largely unstudied in cell division. For example, phosphatases have been shown to abrogate phase separation in T cell receptors (Su et al., 2016) and in *M. tuberculosis* membrane proteins (Heinkel et al., 2019). Interestingly, although the *M. tuberculosis* phosphatase was incorporated into the phase-separated condensate, the phosphatase was also localized to distinct foci within the condensate, perhaps representing selective enrichment or phase-within-phase separation. Whether these findings apply to phosphatases in cell division remains to be uncovered. When kinase activity is essential, are phosphatases sequestered within their own condensates, and when phosphatase activity is required, do these condensates then fuse with condensates containing phosphorylated substrates? Such a mechanism would allow spatial regulation of phosphatases and their substrates.

Similarly, although phase separation may also be driven by ubiquitylation, the main ubiquitin ligase in cell division, the APC/C (Pines, 2011), has not yet been shown to undergo phase separation. However, the APC/C is active at and localizes to many structures during cell division (Acquaviva et al., 2004; Huang and Raff, 2002; Melloy and Holloway, 2004; Torres et al., 2010), many of which have been demonstrated to be sites of phase separation, so phase separation involving the APC/C or its substrates may be possible. Although the presence of poly-ubiquitin chains has been shown to induce phase separation (Sun et al., 2018), no deubiquitylases have yet been identified as agents of ubiquitin-mediated phase-separated condensate dissolution as phosphatases have for kinase-mediated condensates.

ACKNOWLEDGMENTS

We apologize to colleagues whose work could not be cited to keep this review to a reasonable length. This material is based upon work supported by the National Institutes of Health (NIH), National Institute of General Medical Sciences (NIGMS) (grant R01GM117475), and the National Science Foundation (grant MCB1912837) to J.Z.T. Any opinions, findings, and conclusions or recommendations expressed in this material are those of the authors and do not necessarily reflect the views of the NIH or the National Science Foundation. This work was also supported by an NIH-NIGMS Ruth L. Kirschstein National Research Service Award (GM007185) and a National Science Foundation Graduate Research Fellowship (DGE-1650604) to J.Y.O. Figures 1 and 2 were created using BioRender.com.

AUTHOR CONTRIBUTIONS

Conceptualization, J.Y.O; Writing – Original Draft, J.Y.O.; Writing – Review & Editing, J.Y.O and J.Z.T.; Supervision, J.Z.T.

REFERENCES

Abdul Azeez, K.R., Chatterjee, S., Yu, C., Golub, T.R., Sobott, F., and Elkins, J.M. (2019). Structural mechanism of synergistic activation of Aurora kinase B/C by phosphorylated INCENP. Nat. Commun. *10*, 3166.

Acquaviva, C., Herzog, F., Kraft, C., and Pines, J. (2004). The anaphase promoting complex/cyclosome is recruited to centromeres by the spindle assembly checkpoint. Nat. Cell Biol. *6*, 892–898.

Akiyoshi, B., Sarangapani, K.K., Powers, A.F., Nelson, C.R., Reichow, S.L., Arellano-Santoyo, H., Gonen, T., Ranish, J.A., Asbury, C.L., and Biggins, S. (2010). Tension directly stabilizes reconstituted kinetochore-microtubule attachments. Nature *468*, 576–579.

Alper, J.D., Decker, F., Agana, B., and Howard, J. (2014). The motility of axonemal dynein is regulated by the tubulin code. Biophys. J. *107*, 2872–2880.

Azimzadeh, J. (2014). Exploring the evolutionary history of centrosomes. Philos. Trans. R. Soc. B Biol. Sci. *369*, 20130453.

Banani, S.F., Lee, H.O., Hyman, A.A., and Rosen, M.K. (2017). Biomolecular condensates: organizers of cellular biochemistry. Nat. Rev. Mol. Cell Biol. *18*, 285–298.

Barisic, M., and Maiato, H. (2016). The tubulin code: a navigation system for chromosomes during mitosis. Trends Cell Biol. *26*, 766–775.

Bird, A.W., and Hyman, A.A. (2008). Building a spindle of the correct length in human cells requires the interaction between TPX2 and Aurora A. J. Cell Biol. *182*, 289–300.

Boeynaems, S., Alberti, S., Fawzi, N.L., Mittag, T., Polymenidou, M., Rousseau, F., Schymkowitz, J., Shorter, J., Wolozin, B., Van Den Bosch, L., et al. (2018). Protein phase separation: a new phase in cell biology. Trends Cell Biol. *28*, 420–435.

Bouchard, J.J., Otero, J.H., Scott, D.C., Szulc, E., Martin, E.W., Sabri, N., Granata, D., Marzahn, M.R., Lindorff-Larsen, K., Salvatella, X., et al. (2018). Cancer mutations of the tumor suppressor SPOP disrupt the formation of active, phase-separated compartments. Mol. Cell *72*, 19–36.e8.

Bougé, A.L., and Parmentier, M.L. (2016). Tau excess impairs mitosis and kinesin-5 function, leading to aneuploidy and cell death. Dis. Model. Mech. *9*, 307–319.

Broad, A.J., DeLuca, K.F., and DeLuca, J.G. (2020). Aurora B kinase is recruited to multiple discrete kinetochore and centromere regions in human cells. J. Cell Biol. *219*, 219.

Brugués, J., and Needleman, D. (2014). Physical basis of spindle self-organization. Proc. Natl. Acad. Sci. U S A *111*, 18496–18500.

Carmena, M., Wheelock, M., Funabiki, H., and Earnshaw, W.C. (2012). The chromosomal passenger complex (CPC): from easy rider to the godfather of mitosis. Nat. Rev. Mol. Cell Biol. *13*, 789–803.

Celetti, G., Paci, G., Caria, J., VanDelinder, V., Bachand, G., and Lemke, E.A. (2020). The liquid state of FG-nucleoporins mimics permeability barrier properties of nuclear pore complexes. J. Cell Biol. *219*, 219.

Cheung, K., Senese, S., Kuang, J., Bui, N., Ongpipattanakul, C., Gholkar, A., Cohn, W., Capri, J., Whitelegge, J.P., and Torres, J.Z. (2016). Proteomic analysis of the mammalian katanin family of microtubule-severing enzymes defines katanin p80 subunit B-like 1 (KATNBL1) as a regulator of mammalian katanin microtubule-severing. Mol. Cell. Proteomics *15*, 1658–1669.

Conicella, A.E., Zerze, G.H., Mittal, J., and Fawzi, N.L. (2016). ALS mutations disrupt phase separation mediated by α-helical structure in the TDP-43 low-complexity C-terminal domain. Structure *24*, 1537–1549.

Connolly, J.A., Kalnins, V.I., Cleveland, D.W., and Kirschner, M.W. (1977). Immunofluorescent staining of cytoplasmic and spindle microtubules in mouse fibroblasts with antibody to tau protein. Proc. Natl. Acad. Sci. U S A *74*, 2437–2440.

Cuylen, S., Blaukopf, C., Politi, A.Z., Müller-Reichert, T., Neumann, B., Poser, I., Ellenberg, J., Hyman, A.A., and Gerlich, D.W. (2016). Ki-67 acts as a biological surfactant to disperse mitotic chromosomes. Nature *535*, 308–312.

Dao, T.P., Kolaitis, R.M., Kim, H.J., O'Donovan, K., Martyniak, B., Colicino, E., Hehnly, H., Taylor, J.P., and Castañeda, C.A. (2018). Ubiquitin modulates liquid-liquid phase separation of UBQLN2 via disruption of multivalent interactions. Mol. Cell *69*, 965–978.e6.

DeLuca, K.F., Meppelink, A., Broad, A.J., Mick, J.E., Peersen, O.B., Pektas, S., Lens, S.M.A., and DeLuca, J.G. (2018). Aurora A kinase phosphorylates Hec1 to regulate metaphase kinetochore-microtubule dynamics. J. Cell Biol. *217*, 163–177.

Desai, D., and Pethe, P. (2020). Polycomb repressive complex 1: regulators of neurogenesis from embryonic to adult stage. J. Cell. Physiol. *235*, 4031–4045.

Ding, D.Q., Okamasa, K., Katou, Y., Oya, E., Nakayama, J.I., Chikashige, Y., Shirahige, K., Haraguchi, T., and Hiraoka, Y. (2019). Chromosome-associated RNA-protein complexes promote pairing of homologous chromosomes during meiosis in Schizosaccharomyces pombe. Nat. Commun. *10*, 5598.

Duan, Y., Du, A., Gu, J., Duan, G., Wang, C., Gui, X., Ma, Z., Qian, B., Deng, X., Zhang, K., et al. (2019). PARylation regulates stress granule dynamics, phase separation, and neurotoxicity of disease-related RNA-binding proteins. Cell Res. *29*, 233–247.

Dumont, J., and Desai, A. (2012). Acentrosomal spindle assembly and chromosome segregation during oocyte meiosis. Trends Cell Biol. *22*, 241–249.

Edozie, B., Sahu, S., Pitta, M., Englert, A., do Rosario, C.F., and Ross, J.L. (2019). Self-organization of spindle-like microtubule structures. Soft Matter *15*, 4797–4807.

Feng, Z., Caballe, A., Wainman, A., Johnson, S., Haensele, A.F.M., Cottee, M.A., Conduit, P.T., Lea, S.M., and Raff, J.W. (2017). Structural basis for mitotic centrosome assembly in flies. Cell *169*, 1078–1089.e13.

Fujioka, Y., Alam, J.M., Noshiro, D., Mouri, K., Ando, T., Okada, Y., May, A.I., Knorr, R.L., Suzuki, K., Ohsumi, Y., and Noda, N.N. (2020). Phase separation organizes the site of autophagosome formation. Nature *578*, 301–305.

Gatlin, J.C., Matov, A., Groen, A.C., Needleman, D.J., Maresca, T.J., Danuser, G., Mitchison, T.J., and Salmon, E.D. (2009). Spindle fusion requires dynein-mediated sliding of oppositely oriented microtubules. Curr. Biol. *19*, 287–296.

Giubettini, M., Asteriti, I.A., Scrofani, J., De Luca, M., Lindon, C., Lavia, P., and Guarguaglini, G. (2011). Control of Aurora-A stability through interaction with TPX2. J. Cell Sci. *124*, 113–122.

Gouveia, S.M., Zitouni, S., Kong, D., Duarte, P., Gomes, B.F., Sousa, A.L., Tranfield, E.M., Hyman, A., Loncarek, J., and Bettencourt-Dias, M. (2019). PLK4 is a microtubule-associated protein that self-assembles promoting de novo MTOC formation. J. Cell Sci. *132*, jcs219501.

Han, X., Yu, D., Gu, R., Jia, Y., Wang, Q., Jaganathan, A., Yang, X., Yu, M., Babault, N., Zhao, C., et al. (2020). Roles of the BRD4 short isoform in phase separation and active gene transcription. Nat. Struct. Mol. Biol. *27*, 333–341.

Heinkel, F., Abraham, L., Ko, M., Chao, J., Bach, H., Hui, L.T., Li, H., Zhu, M., Ling, Y.M., Rogalski, J.C., et al. (2019). Phase separation and clustering of an ABC transporter in *Mycobacterium tuberculosis*. Proc. Natl. Acad. Sci. U S A *116*, 16326–16331.

Hernández-Vega, A., Braun, M., Scharrel, L., Jahnel, M., Wegmann, S., Hyman, B.T., Alberti, S., Diez, S., and Hyman, A.A. (2017). Local nucleation of microtubule bundles through tubulin concentration into a condensed tau phase. Cell Rep. *20*, 2304–2312.

Hindriksen, S., Lens, S.M.A., and Hadders, M.A. (2017). The ins and outs of Aurora B inner centromere localization. Front. Cell Dev. Biol. *5*, 112.

Huang, J.Y., and Raff, J.W. (2002). The dynamic localisation of the Drosophila APC/C: evidence for the existence of multiple complexes that perform distinct functions and are differentially localised. J. Cell Sci. *115*, 2847–2856.

Huang, Y., Li, T., Ems-McClung, S.C., Walczak, C.E., Prigent, C., Zhu, X., Zhang, X., and Zheng, Y. (2018). Aurora A activation in mitosis promoted by BuGZ. J. Cell Biol. *217*, 107–116.

Hubstenberger, A., Noble, S.L., Cameron, C., and Evans, T.C. (2013). Translation repressors, an RNA helicase, and developmental cues control RNP phase transitions during early development. Dev. Cell *27*, 161–173.

Hyman, A.A., Weber, C.A., and Jülicher, F. (2014). Liquid-liquid phase separation in biology. Annu. Rev. Cell Dev. Biol. *30*, 39–58.

Janke, C., and Magiera, M.M. (2020). The tubulin code and its role in controlling microtubule properties and functions. Nat. Rev. Mol. Cell Biol. *21*, 307–326.

Jiang, H., He, X., Wang, S., Jia, J., Wan, Y., Wang, Y., Zeng, R., Yates, J., 3rd, Zhu, X., and Zheng, Y. (2014). A microtubule-associated zinc finger protein, BuGZ, regulates mitotic chromosome alignment by ensuring Bub3 stability and kinetochore targeting. Dev. Cell *28*, 268–281.

Jiang, H., Wang, S., Huang, Y., He, X., Cui, H., Zhu, X., and Zheng, Y. (2015). Phase transition of spindle-associated protein regulate spindle apparatus assembly. Cell *163*, 108–122.

Joukov, V., and De Nicolo, A. (2018). Aurora-PLK1 cascades as key signaling modules in the regulation of mitosis. Sci. Signal. *11*, eaar4195.

Kalab, P., Weis, K., and Heald, R. (2002). Visualization of a Ran-GTP gradient in interphase and mitotic Xenopus egg extracts. Science *295*, 2452–2456.

King, M.R., and Petry, S. (2020). Phase separation of TPX2 enhances and spatially coordinates microtubule nucleation. Nat. Commun. *11*, 270.

Lacroix, B., Letort, G., Pitayu, L., Sallé, J., Stefanutti, M., Maton, G., Ladouceur, A.-M., Canman, J.C., Maddox, P.S., Maddox, A.S., et al. (2018). Microtubule dynamics scale with cell size to set spindle length and assembly timing. Dev. Cell *45*, 496–511.e6.

Laos, T., Cabral, G., and Dammermann, A. (2015). Isotropic incorporation of SPD-5 underlies centrosome assembly in C. elegans. Curr. Biol. *25*, R648–R649.

Lin, Y., Protter, D.S.W., Rosen, M.K., and Parker, R. (2015). Formation and maturation of phase-separated liquid droplets by RNA-binding proteins. Mol. Cell *60*, 208–219.

Lindon, C., and Pines, J. (2004). Ordered proteolysis in anaphase inactivates Plk1 to contribute to proper mitotic exit in human cells. J. Cell Biol. *164*, 233–241.

Mackenzie, I.R., Nicholson, A.M., Sarkar, M., Messing, J., Purice, M.D., Pottier, C., Annu, K., Baker, M., Perkerson, R.B., Kurti, A., et al. (2017). TIA1 mutations in amyotrophic lateral sclerosis and frontotemporal dementia promote phase separation and alter stress granule dynamics. Neuron *95*, 808–816.e9.

Malumbres, M., and Barbacid, M. (2009). Cell cycle, CDKs and cancer: a changing paradigm. Nat. Rev. Cancer *9*, 153–166.

Mayr, M.I., Hümmer, S., Bormann, J., Grüner, T., Adio, S., Woehlke, G., and Mayer, T.U. (2007). The human kinesin Kif18A is a motile microtubule depolymerase essential for chromosome congression. Curr. Biol. *17*, 488–498.

McKinley, K.L., and Cheeseman, I.M. (2016). The molecular basis for centromere identity and function. Nat. Rev. Mol. Cell Biol. *17*, 16–29.

Melloy, P.G., and Holloway, S.L. (2004). Changes in the localization of the Saccharomyces cerevisiae anaphase-promoting complex upon microtubule depolymerization and spindle checkpoint activation. Genetics *167*, 1079–1094.

Milles, S., Huy Bui, K., Koehler, C., Eltsov, M., Beck, M., and Lemke, E.A. (2013). Facilitated aggregation of FG nucleoporins under molecular crowding conditions. EMBO Rep. *14*, 178–183.

Mistry, H.B., MacCallum, D.E., Jackson, R.C., Chaplain, M.A.J., and Davidson, F.A. (2008). Modeling the temporal evolution of the spindle assembly checkpoint and role of Aurora B kinase. Proc. Natl Acad. Sci. U S A *105*, 20215–20220.

Mittag, T., and Parker, R. (2018). Multiple modes of protein-protein interactions promote RNP granule assembly. J. Mol. Biol. *430*, 4636–4649.

Molliex, A., Temirov, J., Lee, J., Coughlin, M., Kanagaraj, A.P., Kim, H.J., Mittag, T., and Taylor, J.P. (2015). Phase separation by low complexity domains promotes stress granule assembly and drives pathological fibrillization. Cell *163*, 123–133.

Moyer, T.C., and Holland, A.J. (2019). PLK4 promotes centriole duplication by phosphorylating STIL to link the procentriole cartwheel to the microtubule wall. eLife *8*, 8.

Musacchio, A., and Salmon, E.D. (2007). The spindle-assembly checkpoint in space and time. Nat. Rev. Mol. Cell Biol. *8*, 379–393.

Nigg, E.A., and Holland, A.J. (2018). Once and only once: mechanisms of centriole duplication and their deregulation in disease. Nat. Rev. Mol. Cell Biol. *19*, 297–312.

Park, S.Y., Park, J.E., Kim, T.S., Kim, J.H., Kwak, M.J., Ku, B., Tian, L., Murugan, R.N., Ahn, M., Komiya, S., et al. (2014). Molecular basis for unidirectional scaffold switching of human Plk4 in centriole biogenesis. Nat. Struct. Mol. Biol. *21*, 696–703.

Park, J.-E., Zhang, L., Bang, J.K., Andresson, T., DiMaio, F., and Lee, K.S. (2019). Phase separation of Polo-like kinase 4 by autoactivation and clustering drives centriole biogenesis. Nat. Commun. *10*, 4959.

Patel, A., Lee, H.O., Jawerth, L., Maharana, S., Jahnel, M., Hein, M.Y., Stoynov, S., Mahamid, J., Saha, S., Franzmann, T.M., et al. (2015). A liquid-to-solid phase transition of the ALS protein FUS accelerated by disease mutation. Cell *162*, 1066–1077.

Petry, S., Groen, A.C., Ishihara, K., Mitchison, T.J., and Vale, R.D. (2013). Branching microtubule nucleation in Xenopus egg extracts mediated by augmin and TPX2. Cell *152*, 768–777.

Pines, J. (2011). Cubism and the cell cycle: the many faces of the APC/C. Nat. Rev. Mol. Cell Biol. *12*, 427–438.

Plys, A.J., Davis, C.P., Kim, J., Rizki, G., Keenen, M.M., Marr, S.K., and Kingston, R.E. (2019). Phase separation of Polycomb-repressive complex 1 is governed by a charged disordered region of CBX2. Genes Dev. *33*, 799–813.

Pomerening, J.R., Sontag, E.D., and Ferrell, J.E., Jr. (2003). Building a cell cycle oscillator: hysteresis and bistability in the activation of Cdc2. Nat. Cell Biol. *5*, 346–351.

Pope, W.B., Lambert, M.P., Leypold, B., Seupaul, R., Sletten, L., Krafft, G., and Klein, W.L. (1994). Microtubule-associated protein tau is hyperphosphorylated during mitosis in the human neuroblastoma cell line SH-SY5Y. Exp. Neurol. *126*, 185–194.

Preuss, U., and Mandelkow, E.M. (1998). Mitotic phosphorylation of tau protein in neuronal cell lines resembles phosphorylation in Alzheimer's disease. Eur. J. Cell Biol. *76*, 176–184.

Prosser, S.L., and Pelletier, L. (2017). Mitotic spindle assembly in animal cells: a fine balancing act. Nat. Rev. Mol. Cell Biol. *18*, 187–201.

Quartuccio, S.M., and Schindler, K. (2015). Functions of Aurora kinase C in meiosis and cancer. Front. Cell Dev. Biol. *3*, 50.

Rai, A.K., Chen, J.-X., Selbach, M., and Pelkmans, L. (2018). Kinase-controlled phase transition of membraneless organelles in mitosis. Nature *559*, 211–216.

Sabari, B.R., Dall'Agnese, A., Boija, A., Klein, I.A., Coffey, E.L., Shrinivas, K., Abraham, B.J., Hannett, N.M., Zamudio, A.V., Manteiga, J.C., et al. (2018). Coactivator condensation at super-enhancers links phase separation and gene control. Science *361*, eaar3958.

Santos, S.D.M., Wollman, R., Meyer, T., and Ferrell, J.E., Jr. (2012). Spatial positive feedback at the onset of mitosis. Cell *149*, 1500–1513.

Schatz, C.A., Santarella, R., Hoenger, A., Karsenti, E., Mattaj, I.W., Gruss, O.J., and Carazo-Salas, R.E. (2003). Importin alpha-regulated nucleation of microtubules by TPX2. EMBO J. *22*, 2060–2070.

Schmidt, H.B., and Görlich, D. (2015). Nup98 FG domains from diverse species spontaneously phase-separate into particles with nuclear pore-like permselectivity. eLife *4*, e04251.

Schoenfelder, S., Sugar, R., Dimond, A., Javierre, B.M., Armstrong, H., Mifsud, B., Dimitrova, E., Matheson, L., Tavares-Cadete, F., Furlan-Magaril, M., et al. (2015). Polycomb repressive complex PRC1 spatially constrains the mouse embryonic stem cell genome. Nat. Genet. *47*, 1179–1186.

Sha, W., Moore, J., Chen, K., Lassaletta, A.D., Yi, C.-S., Tyson, J.J., and Sible, J.C. (2003). Hysteresis drives cell-cycle transitions in Xenopus laevis egg extracts. Proc. Natl. Acad. Sci. U S A *100*, 975–980.

Siahaan, V., Krattenmacher, J., Hyman, A.A., Diez, S., Hernández-Vega, A., Lansky, Z., and Braun, M. (2019). Kinetically distinct phases of tau on

microtubules regulate kinesin motors and severing enzymes. Nat. Cell Biol. *21*, 1086–1092.

So, C., Seres, K.B., Steyer, A.M., Mönnich, E., Clift, D., Pejkovska, A., Möbius, W., and Schuh, M. (2019). A liquid-like spindle domain promotes acentrosomal spindle assembly in mammalian oocytes. Science *364*, eaat9557.

Spannl, S., Tereshchenko, M., Mastromarco, G.J., Ihn, S.J., and Lee, H.O. (2019). Biomolecular condensates in neurodegeneration and cancer. Traffic *20*, 890–911.

Splinter, D., Tanenbaum, M.E., Lindqvist, A., Jaarsma, D., Flotho, A., Yu, K.L., Grigoriev, I., Engelsma, D., Haasdijk, E.D., Keijzer, N., et al. (2010). Bicaudal D2, dynein, and kinesin-1 associate with nuclear pore complexes and regulate centrosome and nuclear positioning during mitotic entry. PLoS Biol. *8*, e1000350.

Stewart, S., and Fang, G. (2005). Destruction box-dependent degradation of aurora B is mediated by the anaphase-promoting complex/cyclosome and Cdh1. Cancer Res. *65*, 8730–8735.

Stumpff, J., von Dassow, G., Wagenbach, M., Asbury, C., and Wordeman, L. (2008). The kinesin-8 motor Kif18A suppresses kinetochore movements to control mitotic chromosome alignment. Dev. Cell *14*, 252–262.

Su, X., Ditlev, J.A., Hui, E., Xing, W., Banjade, S., Okrut, J., King, D.S., Taunton, J., Rosen, M.K., and Vale, R.D. (2016). Phase separation of signaling molecules promotes T cell receptor signal transduction. Science *352*, 595–599.

Sun, D., Wu, R., Zheng, J., Li, P., and Yu, L. (2018). Polyubiquitin chain-induced p62 phase separation drives autophagic cargo segregation. Cell Res. *28*, 405–415.

Suresh, P., Long, A.F., and Dumont, S. (2020). Microneedle manipulation of the mammalian spindle reveals specialized, short-lived reinforcement near chromosomes. eLife *9*, e53807.

Takagi, J., Sakamoto, R., Shiratsuchi, G., Maeda, Y.T., and Shimamoto, Y. (2019). Mechanically distinct microtubule arrays determine the length and force response of the meiotic spindle. Dev. Cell *49*, 267–278.e5.

Tatebayashi, Y., Planel, E., Chui, D.H., Sato, S., Miyasaka, T., Sahara, N., Murayama, M., Kikuchi, N., Yoshioka, K., Rivka, R., and Takashima, A. (2006). c-jun N-terminal kinase hyperphosphorylates R406W tau at the PHF-1 site during mitosis. FASEB J. *20*, 762–764.

Toledo, C.M., Herman, J.A., Olsen, J.B., Ding, Y., Corrin, P., Girard, E.J., Olson, J.M., Emili, A., DeLuca, J.G., and Paddison, P.J. (2014). BuGZ is required for Bub3 stability, Bub1 kinetochore function, and chromosome alignment. Dev. Cell *28*, 282–294.

Torres, J.Z., Ban, K.H., and Jackson, P.K. (2010). A specific form of phospho protein phosphatase 2 regulates anaphase-promoting complex/cyclosome association with spindle poles. Mol. Biol. Cell *21*, 897–904.

Trivedi, P., Palomba, F., Niedzialkowska, E., Digman, M.A., Gratton, E., and Stukenberg, P.T. (2019). The inner centromere is a biomolecular condensate scaffolded by the chromosomal passenger complex. Nat. Cell Biol. *21*, 1127–1137.

van Vugt, M.A.T.M., Gardino, A.K., Linding, R., Ostheimer, G.J., Reinhardt, H.C., Ong, S.-E., Tan, C.S., Miao, H., Keezer, S.M., Li, J., et al. (2010). A mitotic phosphorylation feedback network connects Cdk1, Plk1, 53BP1, and Chk2 to inactivate the G(2)/M DNA damage checkpoint. PLoS Biol. *8*, e1000287.

Wang, Y., and Mandelkow, E. (2016). Tau in physiology and pathology. Nat. Rev. Neurosci. *17*, 5–21.

Wegmann, S., Eftekharzadeh, B., Tepper, K., Zoltowska, K.M., Bennett, R.E., Dujardin, S., Laskowski, P.R., MacKenzie, D., Kamath, T., Commins, C., et al. (2018). Tau protein liquid-liquid phase separation can initiate tau aggregation. EMBO J. *37*, e98049.

Wippich, F., Bodenmiller, B., Trajkovska, M.G., Wanka, S., Aebersold, R., and Pelkmans, L. (2013). Dual specificity kinase DYRK3 couples stress granule condensation/dissolution to mTORC1 signaling. Cell *152*, 791–805.

Woodruff, J.B., Ferreira Gomes, B., Widlund, P.O., Mahamid, J., Honigmann, A., and Hyman, A.A. (2017). The centrosome is a selective condensate that nucleates microtubules by concentrating tubulin. Cell *169*, 1066–1077.e10.

Yasuda, S., Tsuchiya, H., Kaiho, A., Guo, Q., Ikeuchi, K., Endo, A., Arai, N., Ohtake, F., Murata, S., Inada, T., et al. (2020). Stress- and ubiquitylation-dependent phase separation of the proteasome. Nature *578*, 296–300.

Yi, P., and Goshima, G. (2018). Microtubule nucleation and organization without centrosomes. Curr. Opin. Plant Biol. *46*, 1–7.

Appendix Chapter 3: Human Protein-l-isoaspartate O-Methyltransferase Domain-Containing Protein 1 (PCMTD1) Associates with Cullin-RING Ligase Proteins

This chapter is reproduced from

> Rebeccah A. Warmack, Eric Z. Pang, Esther Peluso, Jonathan D. Lowenson, Joseph Y. Ong, Jorge Z. Torres, Steven G. Clarke. The human protein-L-isoaspartate O-methyltransferase domain-containing protein 1 (PCMTD1) associates with Cullin-RING ligase proteins. Biochemistry. 2022 Apr 29. doi: 10.1021/acs.biochem.2c00130. PMID: 35486881

This chapter describes a rather peculiar working model of protein degradation. Whereas most E3 ubiquitin ligases are specific for a particular subset of proteins, the working model for the E3 ubiquitin ligase PCMTD1 is that it can target any protein with an isoaspartyl residue, a form of protein damage generally caused by protein age. Whether or not this model holds true is still to be determined, as we were unable to determine any definitive substrates for PCMTD1, although affinity mass spectrometry has given us some interesting leads.

Biochemistry

pubs.acs.org/biochemistry Article

Human Protein-L-isoaspartate *O*-Methyltransferase Domain-Containing Protein 1 (PCMTD1) Associates with Cullin-RING Ligase Proteins

Rebeccah A. Warmack,† Eric Z. Pang,† Esther Peluso, Jonathan D. Lowenson, Joseph Y. Ong, Jorge Z. Torres, and Steven G. Clarke*

Cite This: *Biochemistry* 2022, 61, 879–894 Read Online

ACCESS | Metrics & More | Article Recommendations | Supporting Information

ABSTRACT: The spontaneous L-isoaspartate protein modification has been observed to negatively affect protein function. However, this modification can be reversed in many proteins in reactions initiated by the protein-L-isoaspartyl (D-aspartyl) *O*-methyltransferase (PCMT1). It has been hypothesized that an additional mechanism exists in which L-isoaspartate-damaged proteins are recognized and proteolytically degraded. Herein, we describe the protein-L-isoaspartate *O*-methyltransferase domain-containing protein 1 (PCMTD1) as a putative E3 ubiquitin ligase substrate adaptor protein. The N-terminal domain of PCMTD1 contains L-isoaspartate and *S*-adenosylmethionine (AdoMet) binding motifs similar to those in PCMT1. This protein also has a C-terminal domain containing suppressor of cytokine signaling (SOCS) box ubiquitin ligase recruitment motifs found in substrate receptor proteins of the Cullin-RING E3 ubiquitin ligases. We demonstrate specific PCMTD1 binding to the canonical methyltransferase cofactor *S*-adenosylmethionine (AdoMet). Strikingly, while PCMTD1 is able to bind AdoMet, it does not demonstrate any L-isoaspartyl methyltransferase activity under the conditions tested here. However, this protein is able to associate with the Cullin-RING proteins Elongins B and C and Cul5 *in vitro* and in human cells. The previously uncharacterized PCMTD1 protein may therefore provide an alternate maintenance pathway for modified proteins in mammalian cells by acting as an E3 ubiquitin ligase adaptor protein.

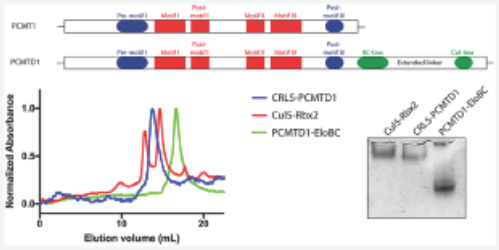

INTRODUCTION

Proteins can accumulate a number of nonenzymatic post-translational modifications over time that alter the normal enzymatic function and threaten protein stability. These modifications include oxidation, carbonylation, glycation, deamidation, and isomerization, which can occur by inter- or intramolecular reactions.[1] Despite this variety of damaging alterations, few protein repair mechanisms have been characterized. Examples of protein repair pathways include methionine sulfoxide reductases, protein deglycation, and L-isoaspartate methylation.[2−4] The latter is accomplished *via* the protein-L-isoaspartyl (D-aspartyl) *O*-methyltransferase (PCMT1) enzyme. By methylating L-isoaspartate and D-aspartate sites, PCMT1 allows for subsequent reformation of L-aspartate.[4]

In parallel, many modified proteins are funneled to the lysosome or the proteosome in mammalian cells for degradation.[5] While the lysosome is a powerful protein degradation system capable of breaking down whole aggregates, organelles, and aged cytosolic proteins, proteasomal degradation is highly regulated and is monitored by the ubiquitin−proteosome system. The latter system involves over 600 E3 ubiquitin ligases in eukaryotic cells where targeted substrates are recognized.[6,7] Among the E3 ubiquitin ligases, the Cullin-RING ligase (CRL) family is the largest subset.[8] These E3 ubiquitin ligases contain conserved RING domains that recruit Cullin scaffold proteins. Full complex formation positions an E2 enzyme opposite bound substrates for ubiquitin transfer.[9]

The Elongin−Cullin−suppressor of cytokine signaling (SOCS) box family is a subgroup of the RING ligase family.[10] This group is characterized by the presence of a SOCS box motif found in the C-terminus of the complex's substrate adaptor protein (the SOCS box-containing protein).[10] This motif consists of both a Cul-box and a BC-box, which facilitate interactions with Cullin 5 (Cul5), and the heterodimer adaptor

Received: March 7, 2022
Revised: April 15, 2022
Published: April 29, 2022

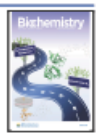

https://doi.org/10.1021/acs.biochem.2c00130
Biochemistry 2022, 61, 879−894

Table 1. Bacterial Expression Plasmids Used in This Study

plasmid	description	marker	source or reference
pET28a+-rhPCMT	pET28a(+) vector expressing N-terminally 6xHis-tagged human PCMT sequence	Kan^r	gift from Dr. Bruce Downie (Addgene catalog # 34852)
pMAPLe4−PCMTD1	pMAPLe4 vector expressing full-length N-terminally 6xHis-tagged human PCMTD1 sequence (residues 1−357)	Kan^r	this study
pMAPLe4−PCMTD1$^{1-231}$	pMAPLe4 vector expressing truncated N-terminally 6His-tagged human PCMTD1 sequence (residues 1−231)	Kan^r	this study
ELONGIN BC (XX01TCEB1A-c001)	Elongin B and Elongin C coexpression plasmids; full-length human Elongin B and amino acids 17−112 of human Elongin C	Clm^r	Addgene (catalog # 110274)
pET28a_Cul5	pET28a vector expressing Cul5 with an N-terminal 6xHis-tag, GB1 tag, and TEV cleavage site (6xHis−GB1−TEV−Cul5)	Kan^r	gift from Dr. Elizabeth Komives
pET11a_Rbx2	pET11a vector expressing untagged Rbx2	Amp^r	gift from Dr. Elizabeth Komives

proteins Elongins B and C, respectively. The SOCS box-containing E3 ligase adaptor protein and the Elongins interact with the N-terminus of the Cul5 scaffold protein, while the C-terminal domain of Cul5 binds Rbx1 or Rbx2 for recruitment of an activated E2 ligase. The open-ring structure of this complex allows coordination between a substrate (recruited to this complex by the SOCS box-containing E3 ligase) to an activated E2 ligase bound to the tail end of the complex. This allows for ubiquitin transfer to a lysine on the surface of the substrate protein.[11]

A degradation pathway for L-isoaspartate-damaged proteins was proposed when levels of L-isoaspartate residues in proteins unexpectedly plateaued with respect to age in tissues yet appeared in urinary peptides of transgenic mice lacking the L-isoaspartate repair enzyme, PCMT1, in all cell types except neurons.[12] In this work, we describe a potential pathway for such degradation with the initial characterization of protein-L-isoaspartate *O*-methyltransferase domain-containing protein 1 (PCMTD1).[13] At its N-terminus, PCMTD1 contains L-isoaspartate and *S*-adenosylmethionine (AdoMet) binding motifs comparable to the PCMT1 enzyme. The protein also contains an extended SOCS box motif within its C-terminus. Previous reports have linked mutations or deletions of the PCMTD1 and PCMTD2 genes to neurodevelopmental disorders,[14,15] viral activation,[16] and cancer.[17] Thus, the biochemical characterization of these poorly understood proteins may be of clinical importance.

Using recombinantly expressed constructs, we show that the human PCMTD1 protein interacts with Elongins B and C and Cul5. We observe that the interaction with Elongins B and C appears to stabilize recombinantly expressed PCMTD1 protein levels. Furthermore, using a truncated variant of PCMTD1, the C-terminal SOCS box motif has been found essential for Cul5 and Elongin B and C interactions. While the PCMTD1 enzyme binds the methyltransferase cofactor AdoMet, it has no detectable methyltransferase activity when tested against canonical PCMT1 L-isoaspartate-containing substrates *in vitro*. Lastly, we observe interactions between recombinantly purified preparations of PCMTD1−EloBC and Cul5−Rbx2 subcomplexes, which suggests that these proteins oligomerize into a larger protein complex reminiscent of other Cullin-RING E3 ligases. Although specific substrates have yet to be identified, the PCMTD1 protein may represent a novel protein damage-specific E3 ubiquitin ligase when complexed with components of the Cullin-RING E3 ligase.

EXPERIMENTAL PROCEDURES

Reagents and Plasmids. Full-length (1−357) and truncated (1−231) PCMTD1 were expressed as N-terminal 6xHis-tagged constructs in pMAPle4 vectors designed and generated in the UCLA DOE Protein Expression Technology Core. The vector includes a pBR322 origin and lacI gene. Transgenes in this vector are expressed as an N-terminal MBP−TVMV−6xHis fusion protein. This vector also coexpresses the TVMV protease, which allows for intracellular processing of the fusion protein transgene yielding a target protein with a TEV-cleavable N-terminal 6xHis-tag. Elongins were expressed on the ELONGIN BC plasmid (XX01TCEB1A-c001), which was a gift from Dr. Nicola Burgess-Brown (Addgene plasmid #110274). The plasmid encoding the recombinant human L-isoaspartyl protein methyltransferase (rhPIMT) with an N-terminal polyhistidine tag was a generous gift from Dr. Bruce Downie (available as plasmid #34852 from Addgene). Plasmids for the recombinant expression of 6xHis−GB1−TEV−Cul5 (pET28a_Cul5) and untagged Rbx2 (pET11a_Rbx2) were generous gifts from Dr. Elizabeth Komives. pGLAP2 plasmids (Addgene plasmid #19703) for PCMTD1 and enhanced green fluorescent protein (EGFP) were constructed from their respective pDONR221 plasmids using LR Clonase II (Invitrogen, catalog #11791020) with standard cloning techniques.

Protein BLAST, Sequence Identification and Alignment, and Phylogenetic Analyses. For PCMTD1 sequence alignment and subsequent phylogenetic analyses, an NCBI protein BLAST search was first performed.[18] The protein sequence for PCMTD1 isoform 1 was used as a query against the nonredundant protein sequence (nr) database with nonredundant RefSeq proteins (WP) excluded. The blastp (protein−protein BLAST) algorithm was used. The max number of target sequences selected was 5000 with an expected threshold cutoff of 1×10^{-6}. All other parameters were left as default. This search yielded 4118 sequences. PCMTD1 isoform 1 sequences from organisms were manually selected resulting in a total of 399 sequences selected. These sequences were imported into JALVIEW 2.11.1.0[19] and aligned using the T-Coffee algorithm with default settings unless otherwise noted,[20] and sequences were color-coded according to ClustalX rules. T-Coffee alignments were imported into the MEGAX program,[21] and trees were generated using the phylogeny tool with maximum likelihood methods. Default methods for maximum likelihood analysis were used and are as follows: test of phylogeny (none), substitution model (Jones−Taylor−Thornton (JTT) model), rates among sites (uniform rates), data subset to use (use all sites), ML heuristic method (nearest-neighbor-interchange (NNI)), and branch swap filter (none). Multiple sequence alignment of PCMT with the PCMTDs was done with Clustal Omega[22] and UniProt accession numbers P22061-1

https://doi.org/10.1021/acs.biochem.2c00130
Biochemistry 2022, 61, 879−894

(PCMT1), Q96MG8-1 (PCMTD1), and Q9NV79-1 (PCMTD2).

Recombinant Protein Expression and Purification. Plasmids used for recombinant protein purification are described in Table 1. The PCMTD1−EloBC coexpression strain was created by cotransforming competent BL21(DE3) cells with pMAPLe4−PCMTD1 and ELONGIN BC. The PCMTD1$^{1-231}$ expression strain was created by transforming competent BL21(DE3) cells with pMAPLe−PCMTD1$^{1-231}$. The PCMTD1$^{1-231}$−EloBC coexpression strain was created by cotransforming competent *Escherichia coli* BL21(DE3) strains with the pMAPLe−PCMTD1$^{1-231}$ and ELONGIN BC plasmids. The Cul5−Rbx2 coexpression strain was created by sequentially transforming competent BL21(DE3) cells with pET28a_Cul5, pET11a_Rbx2, and ELONGIN BC. All transformants were selected by plating on Luria−Bertani (LB) agar with appropriate antibiotics.

For growth and expression, the PCMTD1−EloBC coexpression strain was grown in LB media and induced with 0.5 mM isopropyl β-D-1-thiogalactopyranoside (IPTG) for 3 h at 37 °C when OD_{600} = 0.5−0.7. The PCMTD1$^{1-231}$ and PCMTD1$^{1-231}$−EloBC expression strains were also grown in LB media but were instead induced overnight for 16−18 h at 18 °C with 1 mM IPTG. These strains were also induced when OD_{600} = 0.5−0.7. The Cul5−Rbx2 coexpression strain was grown in M9 minimal media supplemented with casein enzymatic hydrolysate (M9-NZ). This strain was induced at an OD_{600} of 1.0 with 0.5 mM IPTG. Just prior to induction, M9-NZ was supplemented with $ZnCl_2$ to a final concentration of 200 μM to stabilize Rbx2-containing cultures. Cul5−Rbx2 was induced for 16−18 h at 18 °C.

Following expression, cells for all expression strains were spun down for 15 min at 5000*g* at 4 °C and frozen at −80 °C until lysis and purification. Thawed cells were resuspended in 5 mL/g pellet of lysis buffer (50 mM *N*-(2-hydroxyethyl)-piperazine-*N*′-ethanesulfonic acid (HEPES), pH 7.6, 300 mM NaCl, 5% glycerol, 1 mM β-mercaptoethanol (βME), 1 mM phenylmethylsulfonyl fluoride (PMSF), and 1 ethylenediaminetetraacetic acid (EDTA)-free Pierce protease inhibitor tablet per 50 mL). Lysis was performed by three passes through an Avestin Emulsiflex at 15,000 psi with incubations on ice to minimize the temperatures of lysates. Lysates were then spun at 13,000 rpm for 50 min at 4 °C. Filtered lysates were then loaded onto three 5 mL HisTrap HP columns equilibrated with wash buffer (50 mM HEPES, pH 7.6, 150 mM NaCl, 5% glycerol, 20 mM imidazole, 1 mM βME) on a Bio-Rad Biologic FPLC system. Proteins were eluted from the column over two steps, first a linear gradient of 0−100% elution buffer (50 mM HEPES, pH 7.6, 150 mM NaCl, 5% glycerol, 300 mM imidazole, 1 mM βME) over 60 min, followed by a 100% elution buffer wash for 30 min at 1 mL/min. Fractions containing the purified protein were pooled and loaded onto a HiPrep 16/60 Sephacryl S-200 HR gel filtration column equilibrated with gel filtration buffer (50 mM HEPES, pH 7.6, 150 mM NaCl, 1 mM βME). Gel filtration was performed by running 1.7 column volumes (CVs) of gel filtration buffer at 0.4 mL/min after protein samples were injected into the column. Fractions containing purified proteins were pooled and concentrated with 10 kDa molecular weight cut-off (MWCO) Amicon centrifugal filters prior to storage at −80 °C with 5% glycerol. Protein concentrations were determined by a TCA-Lowry assay.[23]

Antibodies Used in This Study. The primary antibodies used in this study were mouse anti-Elongin B (1:2000, Santa Cruz Biotechnology, catalog # sc-135895), mouse anti-Elongin C (1:2000, Santa Cruz Biotechnology, catalog # sc-166554), mouse anti-6xHis (1:2000, Proteintech, catalog # 66005-1-lg), mouse anti-GAPDH (1:3000, ProteinTech, catalog # 60004-1-Ig), mouse anti-FLAG antibody conjugated to Dylight 800 (1:10,000, Rockland, catalog # 200-345-383), rabbit anti-rhPCMT1 (1:1000, noncommercial; a kind gift from Dr. Mark Mamula), rabbit anti-Cul5 (1:2000, Bethyl Laboratories, catalog # A302-173A), goat anti-S-Tag (1:100, GeneTex, catalog # GTX19321), and rabbit anti-FLAG (1:200, Cell Signaling Technology, catalog # 14793).

Secondary antibodies used in this study were goat antimouse IgG (H + L) cross-adsorbed Alexa Fluor 488 (1:2000, Thermo Fisher, catalog # A-11001; Figures 8C and S4), goat antirabbit IgG (H + L) Alexa Fluor Plus 647 (1:2000, Thermo Fisher, catalog # A32733; Figure 7A), donkey antimouse IRDye 800CW (1:10,000, LI-COR, catalog #926-32212; Figure 7B), donkey antirabbit IRDye 680RD (1:10,000, LI-COR, catalog # 926-68073; Figure 7B), and antirabbit horseradish peroxidase (HRP) conjugated (1:100,000, Abcam, catalog # ab6721) visualized with Amersham ECL immunoblotting detection reagent (GE Healthcare, catalog # RPN2106; Figure 6).

Expression and Solubility Trials of PCMTD1 and PCMTD1−EloBC. Fifty milliliter cultures of either PCMTD1 alone or PCMTD1−EloBC strains were inoculated at a starting OD_{600} of 0.05. When cultures reached 0.5 OD_{600}, an uninduced aliquot corresponding to 0.4 OD of cells was removed, and the expression of constructs was induced by the addition of 0.5 mM IPTG. Expression continued for 4.5 h at 37 °C. Then, an induced aliquot corresponding to 0.4 OD of cells was removed and cells were pelleted at 5000*g* at 4 °C. Cell pellets were resuspended in 12.5 mL of lysis buffer (50 mM HEPES, pH 7.6, 300 mM NaCl, 5% glycerol, 1 mM βME, 1 mM PMSF, and 1 EDTA-free Pierce protease inhibitor tablet per 50 mL) and lysed using a 550 Sonic Dismembrator at a 50% duty cycle with 15 rounds of 30 s on, 30 s off. Debris was pelleted at 13,000 rpm at 4 °C. The resultant supernatant was removed as the soluble fraction, and the pellet was resuspended in 12.5 mL lysis buffer as the insoluble fraction. Ten microliters of the uninduced, induced, soluble, and insoluble samples were analyzed by SDS-PAGE and anti-His immunoblot detection.

PCMTD1 Degradation Trials within Tetracycline-Treated *E. coli*. Fifty milliliter expression cultures were inoculated from PCMTD1 or PCMTD1−EloBC overnight cultures at a starting OD_{600} = 0.05. When expression cultures reached OD_{600} = 0.4, uninduced aliquots of cells were removed and expression was induced with 0.5 mM IPTG at 37 °C. After 30 min, an aliquot of cells corresponding to 0.4 OD of cells was taken as an induced sample. Then, tetracycline (Sigma-Aldrich, catalog # T7660) was added at a final concentration of 25 μg/mL. Aliquots corresponding to 0.4 OD of cells were removed at 10 min, 30 min, 1 h, 2 h, and 3 h time intervals after tetracycline addition and analyzed by both Coomassie staining or Ponceau staining and anti-His immunoblot detection.

[^{3}H]AdoMet:Protein Ultraviolet Light Cross-Linking Experiments. In a final volume of 60 μL, 3.85 μM protein was mixed with 0.5 μM *S*-adenosyl-L-[methyl-^{3}H] methionine ([^{3}H]AdoMet; PerkinElmer Life Sciences; 75−85 Ci/mmol, 0.55 mCi/mL in 10 mM H_2SO_4/ethanol (9:1, v/v)) in 50 mM

https://doi.org/10.1021/acs.biochem.2c00130
Biochemistry 2022, 61, 879−894

tris−HCl, pH 7.6. Where indicated in the figure legend, 0.5 mM of either nonradioactive *S*-adenosylhomocysteine or adenosine triphosphate (ATP) was added. Reactions were placed into NUNC 96-well clear-bottom plates and exposed to 254 nm ultraviolet light at 4 °C for 1 h. The reaction was stopped by adding 15 μL 5× SDS-PAGE sample buffer (250 mM tris−HCl, pH 6.8, 10% SDS, 50% glycerol, 5% βME, and 0.05% bromophenol blue). Samples were heated at 95 °C for 3 min and separated on a 4−20%, 10-well ExpressPlus PAGE gel (Genscript, catalog # M42010) at 140 V for 1 h. Gels were stained with Coomassie (0.1% (w/v) Brilliant Blue R-250, 10% (v/v) glacial acetic acid, and 50% (v/v) methanol) for 1 h and destained with 10% (v/v) acetic acid and 15% (v/v) methanol. For fluorography, gels were subsequently incubated with EN^{3}HANCE (PerkinElmer Life Sciences, catalog number 6NE9701) for 1 h, incubated in water for 30 min, and dried before the gels were exposed to film (Denville Scientific, 8 × 10-in. Hyblot CI) for the length of time designated in the figure legends at −80 °C.

Determination of L-Isoaspartate-Methylation Levels by the Methanol Vapor Diffusion Assay. PCMT1 was used as an analytical reagent to quantify L-isoaspartate levels; it was purified as a His-tagged enzyme from the expression plasmid #34852 available from Addgene.com as described by Patananan et al.[24] with a specific activity at 37 °C of 5,300 pmol of methyl esters formed on KASA(isoD)LAKY/min/mg of enzyme. The isoaspartate-containing substrates used in this assay were the synthetic peptide KASA(isoD)LAKY and the protein ovalbumin (SIGMA A5503). In a final volume of 100 μL, 10 pmol of PCMT1 or 15 pmol PCMTD1−EloBC was incubated with 25 pmol KASA(isoD)LAKY or 500 pmol ovalbumin (typically ∼6% isomerized). Final concentrations in the reactions included 135 mM bis−tris−HCl, pH 6.4, and 10 μM *S*-adenosyl-L-[methyl^{3}H]methionine ([^{3}H]AdoMet) (prepared by a 1600-fold isotopic dilution of a stock of 72 Ci/mmol [^{3}H]AdoMet (PerkinElmer Life Sciences, NET155H00) with nonisotopically labeled AdoMet (*p*-toluenesulfonate salt; Sigma-Aldrich A2408)). The reaction was stopped by adding 10 μL of 2 M sodium hydroxide, and 100 μL of the 110 μL mixture was transferred to a 9 × 2.5 cm^2 piece of folded thick filter paper (Bio-Rad; catalog number 1650962) wedged in the neck of a 20 mL scintillation vial above 5 mL scintillation reagent (Safety Solve, Research Products International, catalog number 121000), tightly capped, and incubated at room temperature. After 2 h, the folded filter papers were removed, the caps were replaced, and the vials were counted thrice for 5 min each in a Beckman LS6500 scintillation counter. Background radioactivity in a reaction containing no substrate was determined by incubating the recombinant human PCMT1 or PCMTD1−EloBC, 135 mM bis−tris−HCl buffer, and 10 μM [^{3}H]AdoMet, as described above. Samples were analyzed in triplicate.

Animal Husbandry. *Pcmt1*−/− animals were generated through breeding of *Pcmt1*+/− animals and maintained as reported previously.[12,25] These animals have been interbred for 20 years to obtain a genetically homogeneous population. *Pcmt1*−/− and *Pcmt1*+/+ offspring were used in this study. Mice were kept on a 12 h light/dark cycle and allowed ad libitum access to water and NIH-31 7013 pellet chow (18% protein, 6% fat, 5% fiber, Harlan Teklad, Madison, WI).

Preparation of Wild-Type and *Pcmt1* Knockout Mouse Tissue Lysates. Fifty-two day old wild-type and *Pcmt1* knockout mice were euthanized in a CO_2 chamber. Brain tissue was removed and weighed, and 5 mL/g tissue of ice-cold lysis buffer (250 mM sucrose, 10 mM tris−HCl, pH 7.4, 1 mM ethylenediaminetetraacetic acid (EDTA), 1 mM phenylmethylsulfonyl fluoride (PMSF); one Roche protease inhibitor cocktail tablet) was added per 50 mL buffer. Tissues were homogenized with a Fisher LR400A Lab-Stirrer with a Potter-Elvejem Teflon and glass homogenizer at approximately 300 rpm and then spun at 20,000*g* for 20 min at 4 °C. The supernatant was removed as the soluble extract and stored at −20 °C until future use.

SDS-PAGE Fluorography for the Analysis of Methyltransferase Activity. Twenty-five micrograms of wild-type and *Pcmt1* knockout mouse brain cytosolic proteins were incubated in a 30 μL reaction volume with 6 μg recombinant human PCMT1 or PCMTD1−EloBC, and 0.3 μM *S*-adenosyl-L-[methyl-^{3}H] methionine (PerkinElmer Life Sciences; 75−85 Ci/mmol, 0.55 mCi/mL in 10 mM H_2SO_4/ethanol (9:1, v/v)) in 74 mM bis−tris−HCl, pH 6.4, for 2 h at 37 °C. The reaction was stopped by adding 5× SDS-PAGE sample buffer and boiling at 95 °C for 3 min. Samples were then separated on a gel, and Coomassie staining and fluorography were performed as described above.

Cell Culturing Conditions. HeLa Flp-In TRex and hTERT-RPE-1 cells were maintained in Dulbecco's modified Eagle's medium (DMEM)/F12 media (Hyclone, catalog # SH30023.01) supplemented with 10% fetal bovine serum (FBS) by volume (Atlanta Biological, catalog #S10350; note this FBS contains no detectable tetracycline to avoid expression of the doxycycline-inducible proteins until the addition of doxycycline) and penicillin/streptomycin (Gibco, catalog #15140148). Cells were passaged using trypsin (Gibco, catalog # 25300054) and in cell culture plates (Thermo, catalog #150350 and 140685).

To generate cell lines expressing doxycycline-inducible pGLAP2 PCMTD1 and EGFP, 4 μg of pOG44 (encoding Flippase recombinase) and 1 μg of pGLAP2 PCMTD1 or EGFP were transfected with 15 μL of Fugene 6 (Promega, catalog # E2691) into one well of a six-well plate of HeLa Flp-In TRex cells at 66% confluency. Forty-eight hours after transfection, the cells were expanded into a 10 cm plate and allowed to grow for another 48 h. The cells were selected with 400 μg/mL of hygromycin B (Gibco, catalog # 10687010) for 2 weeks, whereupon untransfected (control) HeLa Flp-In TRex cells died and hygromycin-resistant colonies were visible in both pGLAP2 PCMTD1 and pGLAP2 EGFP plates. The colonies were allowed to grow in media without hygromycin for 2 weeks before the colonies were pooled together and used for experiments.

Ni-NTA and S-Tag Pulldowns for the Analysis of PCMTD1−Cul5 Interactions *In Vitro* and in Cells. For Ni-NTA pulldowns, 1.12 nmol of N-terminal His-tagged PCMTD1−EloBC or PCMTD1$^{1-231}$ was immobilized by gentle rocking onto 100 μL HisPur Ni-NTA resin (Thermo Fisher, catalog # 88221) pre-equilibrated with wash buffer (50 mM HEPES, pH 7.6, 150 mM NaCl, 5% glycerol, 1 mM βME, 20 mM imidazole) for 1 h at RT. hTERT-RPE-1 (retinal pigment epithelial cells) cell lysate samples were then freshly prepared by incubating 110 μL cell lysis buffer (50 mM HEPES, pH 7.6, 150 mM NaCl, 1 mM PMSF, 1% NP40, 1 mM βME) with 3 × 10^6 hTERT-RPE-1 cells (lysate C_F ∼ 0.4 mg/mL) on ice for 12 min with gentle mixing. Lysates were then cleared by a 13,300*g* spin at 4 °C for 10 min. Following immobilization of purified proteins to the Ni-NTA resin, 110

https://doi.org/10.1021/acs.biochem.2c00130
Biochemistry 2022, 61, 879−894

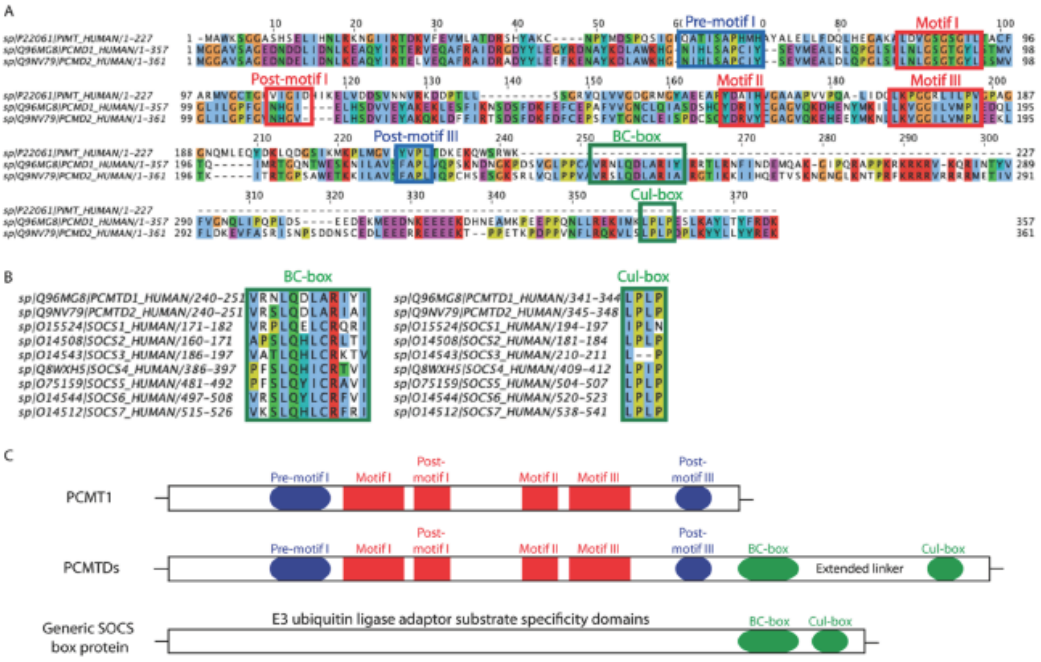

Figure 1. Sequence alignment of human PCMT1 (PIMT), the PCMTD proteins, and SOCS box proteins. (A) Sequence alignment of PCMT1 with PCMTD1 and PCMTD2. For conserved residues, the color scheme is as follows: hydrophobic (blue), positive charge (red), negative charge (magenta), polar (green), cysteine (pink), glycine (orange), proline (yellow), and aromatic (cyan). Sequences outlined in blue correspond to PCMT1 isoaspartyl-binding motifs, while sequences outlined in red represent PCMT1 AdoMet binding motifs. Residues boxed in green in the PCMTD proteins comprise the BC-box and Cul5 box binding motifs of the SOCS box domain. (B) Sequence alignment of the C-terminal region of PCMTD1 and PCMTD2 (residues 225–357) with the SOCS box proteins. Residues boxed in green comprise the BC-box and Cul5 box binding motifs of the SOCS box domain. (C) Domain comparison of PCMT1, the PCMTDs, and SOCS box proteins. Blue boxes correspond to PCMT1 isoaspartyl-binding motifs, red boxes correspond to PCMT1 AdoMet binding motifs, and green boxes represent the BC-box and Cul5 box binding motifs of the SOCS box domain.

μL of cell lysate was directly added to the Ni-NTA resin and rocked for 2 h at RT. The resin was then washed three times. After the final wash, immobilized proteins and potential binding partners were eluted with 160 μL elution buffer (50 mM HEPES, pH 7.6, 150 mM NaCl, 5% glycerol, 1 mM βME, 300 mM imidazole). Samples were then analyzed by Coomassie staining and immunoblot detection.

For S-Tag pulldowns, two wells of a six-well plate each of HeLa pGLAP2 PCMTD1 and pGLAP2 EGFP were plated at a 66% confluency. For each cell line, one well was left without doxycycline as a control, and to the other well, 0.1 μg/mL of doxycycline was added for 18 h. The cells were lysed in 120 μL LAP200 buffer supplemented with dithiothreitol (DTT), protease inhibitors, and 1% NP40. Five microliters of lysate was added to 2 μL of 6× Laemmli buffer and boiled for 5 min at 95 °C. From the remaining doxycycline-induced lysates, 110 μL was added to 50 μL of S-protein agarose beads (Millipore, catalog # 69704) in 250 μL of LAP200 without NP40 (for a final concentration of about 0.3% NP40) and allowed to bind, rotating end over end, for 2 h at 4 °C. The beads were pelleted by centrifugation at 500*g* for 2 min at 4 °C and washed with 250 μL of LAP200 with 0.33% NP40 four times. After the final wash, the beads were pelleted, the supernatant was aspirated, and 20 μL of 6× Laemmli buffer was added. The beads were boiled for 5 min at 95 °C. The resulting proteins were subjected to SDS-PAGE and immunoblot detection.

CRL5–PCMTD1 Complex Constitution and Analytical Gel Filtration Chromatography. CRL5–PCMTD1 was made by incubating Cul5–Rbx2 and PCMTD1–EloBC at a molar ratio of 1.1:1 for 2 h at room temperature with gentle rocking. CRL5–PCMTD1, Cul5–Rbx2, and PCMTD1–EloBC were then concentrated to 0.2 mg/mL prior to analytical gel filtration chromatography. Four hundred microliters of concentrated samples were then injected and ran on a Superdex 200 Increase 10/300 GL column with an AKTAprime plus FPLC system for 2 CVs with gel filtration buffer (50 mM HEPES, pH 7.6, 150 mM NaCl, 5% glycerol, 1 mM βME at 0.3 mL/min).

Native-PAGE. Protein samples for native-PAGE were prepared by mixing four parts of protein sample with one part of 5× native sample buffer (124 mM tris base, pH 6.8, 3.8 mM bromophenol blue, 50% glycerol, 1.43 M βME) without heating. Five micrograms of total protein was loaded onto a 10-well 4–20% gel (Genscript, catalog # M42010). Gels were electrophoresed with a native running buffer (50 mM tris, pH 7.4, 50 mM 3-(*N*-morpholino)propanesulfonic acid (MOPS), 1 mM EDTA) at 30 V until the dye front migrated to the

https://doi.org/10.1021/acs.biochem.2c00130
Biochemistry 2022, 61, 879–894

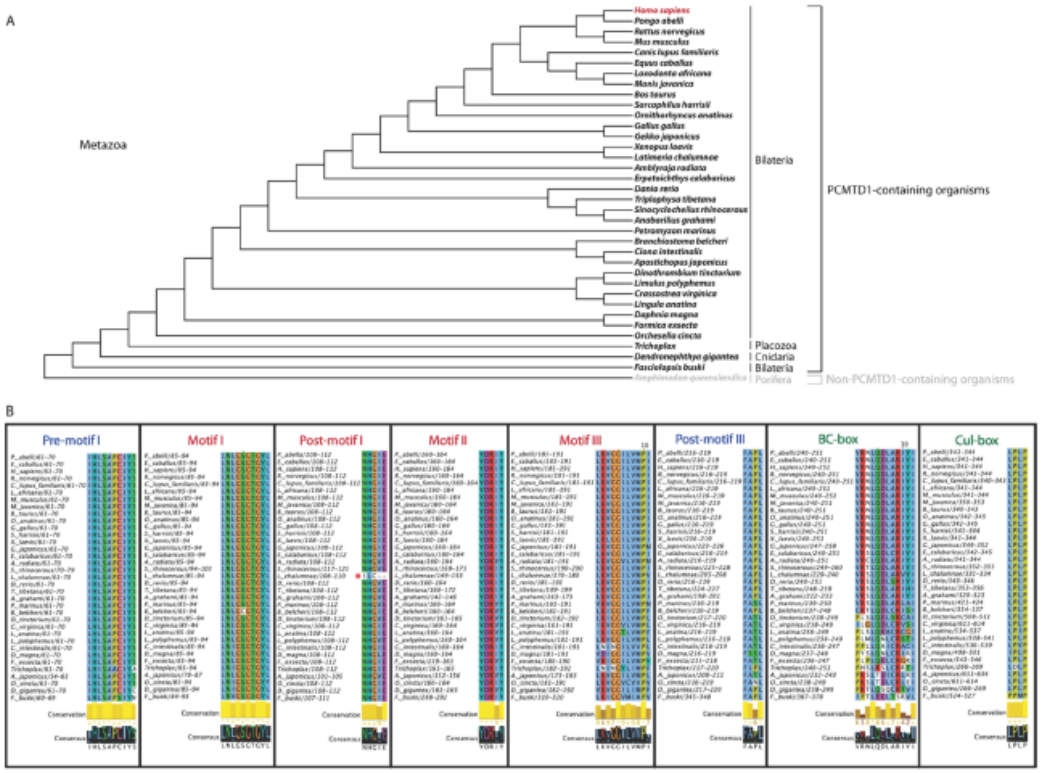

Figure 2. PCMTD1 is present within select metazoan phyla and is well conserved in most chordate organisms. (A) A protein BLAST search was performed against PCMTD1 isoform 1. At least one species from each phylum that was identified were selected, and a multiple sequence alignment was performed. Organisms are designated as belonging to the superphyla bilateria, cnidaria, or placozoa. A PCMT1-like protein lacking any similar PCMTD1 C-terminal domain was identified in porifera and used to root the tree; no significant matches were identified in ctenophora. The phylogenetic tree of the full-length PCMTD1 sequences was generated utilizing the maximum likelihood method in MEGAX, as described in the Experimental Procedures and rooted in the outgroup species *Amphimedon queenslandica* PCMT1-like protein. (B) T-Coffee multiple sequence alignment of PCMTD1 motifs from the selected organisms in panel (A). AdoMet binding motifs are labeled in red, L-isoaspartyl recognition motifs are labeled in blue, and SOCS box motifs are labeled in green. For conserved residues, the color scheme is as follows: hydrophobic (blue), positive charge (red), negative charge (magenta), polar (green), cysteine (pink), glycine (orange), proline (yellow), and aromatic (cyan).

bottom of the gel. Gels were then stained and destained with Coomassie as described above.

RESULTS

PCMTD Proteins Contain Both L-Isoaspartyl Methyltransferase and Cullin-RING Ligase Motifs. Figure 1A displays an alignment of the primary sequences of human PCMT1 (227 residues), PCMTD1 (357 residues), and PCMTD2 (361 residues). PCMTD1 and PCMTD2 share approximately 26% similarity with PCMT1. Similar regions include both motifs common for seven β-strand methyltransferases and motifs specific for L-isoaspartyl binding.[26] Notably, PCMTD1 and PCMTD2 contain several conserved residues which directly interact with isoaspartyl substrates and AdoMet through hydrogen-bonding and hydrophobic interactions (Figure 1A).[27] However, PCMTD1 and PCMTD2 have ~130 additional residues comprising a novel C-terminal domain. Encompassed within the additional ~130 amino acids of the PCMTD proteins are two motifs that comprise the SOCS box recruitment domain: the BC-box and the Cul-box that are found in E3 ubiquitin ligases. Both of these motifs align well with other human SOCS box proteins, with the PCMTD1 BC-box and Cul-box motifs having an average of 54 and 73% sequence identities, respectively, compared across the seven human SOCS proteins (Figures 1B and S1). The BC-box is a 12-residue motif that recruits proteins Elongin B and Elongin C, which are Cullin-RING E3 ubiquitin ligase adaptor proteins. Elongins B and C form a heterodimer, which mediates interactions between SOCS box-containing proteins with Cul5 to form a partial Cullin-RING E3 ubiquitin ligase complex.[28] A leucine at the +4 position within the BC-box has been shown to be critical for this interaction[29,30] and is conserved within the sequences of both PCMTD1 and PCMTD2 (Figures 1B and S1). In contrast to other SOCS box-containing proteins, which contain an 11-residue spacer separating the Cul- and BC-boxes, the Cul-box in PCMTD1 and PCMTD2 is separated from the BC-box by ~90 residues,

https://doi.org/10.1021/acs.biochem.2c00130
Biochemistry 2022, 61, 879−894

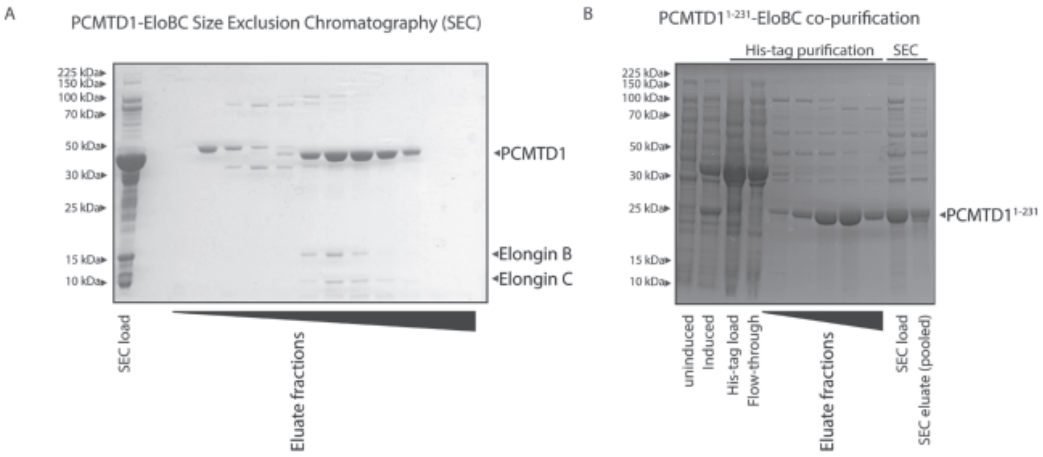

Figure 3. C-terminus of PCMTD1 facilitates interactions between PCMTD1 and Elongins B and C. (A) SDS-PAGE results of sequential fractions collected during size exclusion chromatography of His-tag purified preparations of PCMTD1−EloBC reveal that PCMTD1 and Elongins B and C coeluted as a complex. (B) His-tag purification and size exclusion chromatography result in the purification of $PCMTD1^{1-231}$ alone when $PCMTD1^{1-231}$ is coexpressed with Elongins B and C. This suggests that $PCMTD1^{1-231}$ does not interact with Elongins B and C.

which generates a novel extended SOCS box motif (Figure 1C).

PCMTD1 Is Present within Certain Metazoan Phyla and Is Highly Conserved in Chordates. Using BLAST and phylogenetic analyses, a tree was generated displaying PCMTD1 protein sequence similarities from select organisms representative of all phyla in which PCMTD1 was identified (Figure 2A).[31] Unlike the PCMT1 methyltransferase, which is present within bacteria, archaea, and eukaryota, PCMTD1 was only found within select phyla of the metazoan kingdom.[24] Specifically, this previously uncharacterized protein was found within the superphyla bilateria, cnidaria, and placozoa but not within ctenophora, porifera, nor choanoflagellatea. Interestingly, SOCS box-containing proteins have been identified in bilateria, cnidaria, placozoa, ctenophora, and porifera, in addition to a putative SOCS box-containing protein found in the choanoflagellate *Salpingoeca rosetta*.[32,33] These observations may suggest that the PCMTD proteins originated from a gene duplication event within the last common ancestor of the bilateria, cnidaria, and placozoa superphyla. Phylogenetic analysis indicates that the human PCMTD1 sequence is on average 76% identical to sequences across the chordate phylum (Figure 2A). PCMTD1 sequence alignment across representative organisms is shown in Figure 2B. Across all phyla shown, the AdoMet binding motifs and the L-isoaspartyl recognition motifs are on average 88 and 89% identical, respectively (Figure 2B). While the Cul-box of the SOC box motif is 92% identical, there is more variation within the BC-box at 62% identity averaged across the species shown here. At this point, it is unclear what the roles of the variant BC-box are in lower organisms. However, the +4 leucine is perfectly conserved within the BC-box, suggesting strong positive selective pressure. This residue is also conserved across all human SOCS box-containing proteins (Figure S1).

As mentioned above, the human PCMTD1 and PCMTD2 sequences represent a unique extension of the canonical SOCS box motifs due to the insertion of +90 residues between the BC-box and the Cul-box, compared to the canonical +11 residues within previously characterized SOCS box-containing proteins (Figures 1B and S1B). Interestingly, the tunicate *Ciona intestinalis*, the arthropods *Daphnia magna*, *Formica exsecta*, *Limulus polyphemus*, *Dinothrombium tinctorium*, and *Orchesella cincta*, the mollusk *Crassostrea virginica*, and the echinoderm *Apostichopus japonicus* each has over 200 residues between the BC-box and the Cul-box of their PCMTD1 sequences, with the longest distance being 386 residues within *A. japonicus*. In stark contrast, the cnidarian *Dendronephthya gigantea* and the placozoan *Trichoplax*, which are approximately as distantly related to humans as the previously listed organisms, have 15 and 12 residues extending between their BC- and Cul-boxes. Within these elongated interim sequences, there are several stretches with conserved residues including a positive patch corresponding to residues 275-KRKRKR-280 in the human PCMTD1 sequence (Figure S2C), as well as a highly negative patch corresponding to residues 303-EEDEKMEEDNKEEEKD-319 in the human PCMTD1 sequence (Figure S2G−L). The positive and negative patches within the human PCMTD1 sequence are on average 96 and 61% similar to the other chordate sequences, respectively.

A protein BLAST query of the linker region of the nonredundant protein database using human PCMTD1 residues Arg252−Lys340 did not reveal significant sequence similarities with any non-PCMTD proteins. The C-terminal domains of both human PCMTD1 and PCMTD2 are predicted to exist as independent isoforms lacking the methyltransferase domain (PCMTD1 isoform 2 and PCMTD2 isoform 3, respectively), resulting from alternative splicing (Figure S3).[34−37] Given the presence of the BC-box, the Cul-box, and the large region of residues with unknown purposes, it is possible that these are active isoforms with distinct functions from the full-length PCMTD proteins.

Recombinant Human PCMTD1 Expression Is Stabilized by Coexpression with Elongins B and C. The BC-box found within the SOCS box motif is conserved for Elongins B and C binding. To investigate the function of the BC-box identified within the PCMTD1 sequence, His-tagged

https://doi.org/10.1021/acs.biochem.2c00130
Biochemistry 2022, 61, 879−894

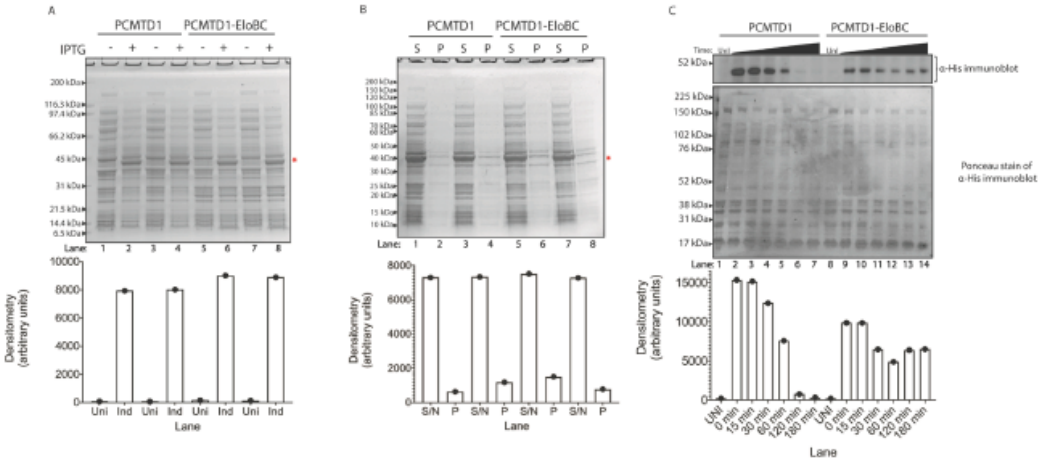

Figure 4. Elongins B and C help stabilize recombinant PCMTD1. (A) Coomassie-stained SDS-PAGE gel of PCMTD1 IPTG-induced expression with (lanes 6 and 8, replicates) and without Elongins B and C from whole cell lysates (lanes 2 and 4, replicates). The lower panel represents densitometric quantification of the PCMTD1 band (indicated by a red asterisk). (B) Coomassie-stained SDS-PAGE gel of the supernatant (S) and pellet (P) of lysed *E. coli* expressing either PCMTD1 alone (lanes 1–4) or PCMTD1–EloBC (lanes 5–8). The lower panel represents densitometric quantification of the PCMTD1 band indicated by a red asterisk. (C) *E. coli* cells expressing PCMTD1 alone (lanes 1–7) or PCMTD1 with Elongins B and C (lanes 8–14) were treated with 25 μg/mL tetracycline, as described in the Experimental Procedures section. Lanes 1 and 8 represent whole cell lysates from uninduced cultures. Succeeding lanes represent whole cell lysates from induced cultures treated with tetracycline at increasing time points. The lower panel represents densitometric quantification of the PCMTD1 band detected by an anti-His immunoblot.

PCMTD1 was recombinantly coexpressed with untagged Elongins B and C proteins in *E. coli* (Figure 3A). PCMTD1 and Elongins B and C were purified within the same fractions in immobilized metal affinity chromatography and size exclusion chromatography (Figures 3A and S4A). Thus, the association and complex formation between PCMTD1 and Elongins B and C, now termed PCMTD1–EloBC, were demonstrated (Figure 3A). Cotransformation and subsequent coexpression of a C-terminally truncated construct of His-tagged PCMTD1, PCMTD1$^{1-231}$, and Elongins B and C in *E. coli* resulted in the purification of PCMTD1$^{1-231}$ alone after size exclusion chromatography (Figures 3B and S4B). These results suggest that the BC-box found within the C-terminus of PCMTD1 facilitates the interactions between PCMTD1 and Elongins B and C.

For SOCS box-containing proteins, several regions responsible for the E3 ubiquitin ligase complex association have been suggested to be intrinsically disordered in the absence of Elongins B and C.[38−40] To investigate the nature of the effects Elongins B and C may have on PCMTD1 expression, recombinant expression trials for constructs of PCMTD1 alone and PCMTD1 coexpressed with Elongins B and C were compared in duplicate *E. coli* cultures. Uninduced and induced whole cell lysates were analyzed by SDS-PAGE (Figure 4A). Densitometry of the band corresponding to induced PCMTD1 suggested that there were modest increases of ∼11% in the expression or stability of PCMTD1 with the coexpression of the Elongins (Figure 4A, lower panel). The lysates from induced cultures were then separated into soluble supernatant (S) and insoluble pellet (P) fractions. These samples were analyzed by SDS-PAGE, and densitometry performed on the band corresponding to PCMTD1 revealed no detectable increases in the solubility of PCMTD1 with the Elongins. To explore the stability of the PCMTD1 protein, *E. coli* cultures were grown to mid-log phase and the PCMTD1 constructs were induced with IPTG. After 30 min of expression, the protein synthesis inhibitor tetracycline was added to cells and aliquots of the culture were taken at increasing time points. Lysates were separated by SDS-PAGE, and levels of PCMTD1 were evaluated by both Coomassie stain and immunoblot against the N-terminal His-tag (Figure 4C). While the PCMTD1-alone culture has higher initial signal at 30 min of expression, the protein levels decrease steeply after 1 h of treatment with tetracycline and are completely depleted after 2 h (Figure 4C, lanes 2–7). Strikingly, while the PCMTD1–Elongins samples display lower levels of initial signal, His-PCMTD1 could be detected by immunoblot throughout the course of the tetracycline treatment (Figure 4C, lanes 9–14). This result was replicated, indicating that the Elongins help stabilize recombinant PCMTD1 protein levels (Figure S5). Thus, all subsequent *in vitro* experiments were performed with the recombinantly coexpressed complex of PCMTD1 and Elongins B and C (PCMTD1–EloBC; Figure 4).

PCMTD1–EloBC Specifically Binds to the Methyltransferase Cofactor AdoMet. To assess possible binding between AdoMet and PCMTD1, PCMTD1–EloBC or PCMTD1$^{1-231}$ purified proteins were incubated with *S*-adenosyl-[methyl-^{3}H]-L-methionine ([^{3}H]AdoMet) and exposed to a UV light source with or without the addition of *S*-adenosylhomocysteine (AdoHcy) or adenosine 5′triphosphate (ATP). Cross-linking results were then monitored with SDS-PAGE and fluorography. Signals observed on the film correspond to the PCMTD1 band within the gel, indicating that PCMTD1–EloBC is able to cross-link to [^{3}H]AdoMet (Figure 5). Addition of the methyltransferase site-specific inhibitor, AdoHcy, inhibited cross-linking between [^{3}H]-

https://doi.org/10.1021/acs.biochem.2c00130
Biochemistry 2022, 61, 879−894

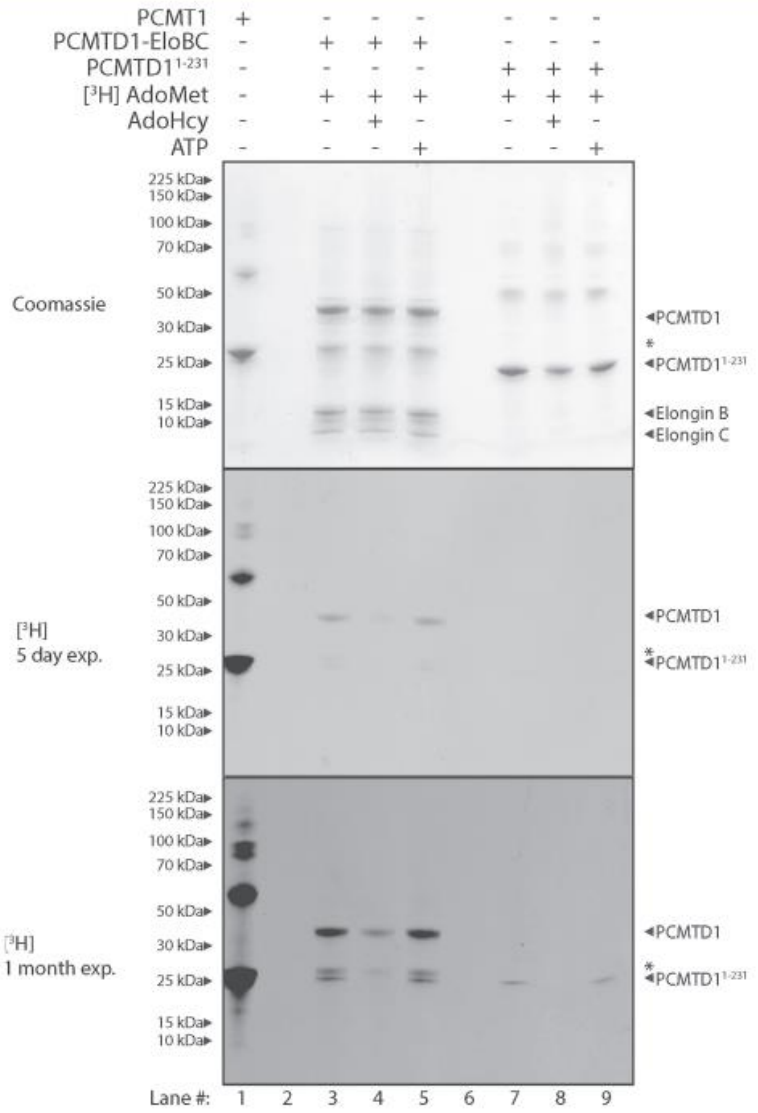

Figure 5. PCMTD1 site-specifically binds [^{3}H]AdoMet. The Coomassie-stained SDS-PAGE gel (upper panel) and fluorography (lower two panels) show [^{3}H]AdoMet cross-linked to the PCMT1 positive control (lane 1), PCMTD1−EloBC (lanes 3 and 5), and PCMTD1$^{1-231}$ (lanes 7 and 9) at pH 7.6. A known inhibitor of site-specific [^{3}H]AdoMet binding to PCMT1 (AdoHcy) was able to abrogate [^{3}H]AdoMet binding for both PCMTD1−EloBC (lane 4) and PCMTD1$^{1-231}$ (lane 8). ATP was not able to inhibit binding between PCMTD1−EloBC or PCMTD1$^{1-231}$ to [^{3}H]AdoMet (lanes 5 and 9). The film was exposed for 5 days (middle panel) and 30 days (lower panel) for the same experiments. Asterisks indicate potential PCMTD1 degradation products.

AdoMet and PCMTD1−EloBC. However, ATP did not inhibit binding. Together, these results suggest that PCMTD1−EloBC is able to site-specifically cross-link to [^{3}H]AdoMet. PCMT1 exhibits similar binding behavior, whereas bovine serum albumin, a negative control, exhibits no binding activity to [^{3}H]AdoMet in cross-linking reactions (data not shown).

Performing these experiments with the truncated PCMTD1$^{1-231}$ variant shows that AdoMet binding is localized in the PCMT1-homologous N-terminus of PCMTD1. PCMTD1$^{1-231}$ similarly cross-links [^{3}H]AdoMet in a site-specific manner (Figure 5). The signal for binding was lower in comparison to PCMTD1−EloBC. This may be caused by allosteric effects induced by the interactions between

https://doi.org/10.1021/acs.biochem.2c00130
Biochemistry 2022, 61, 879−894

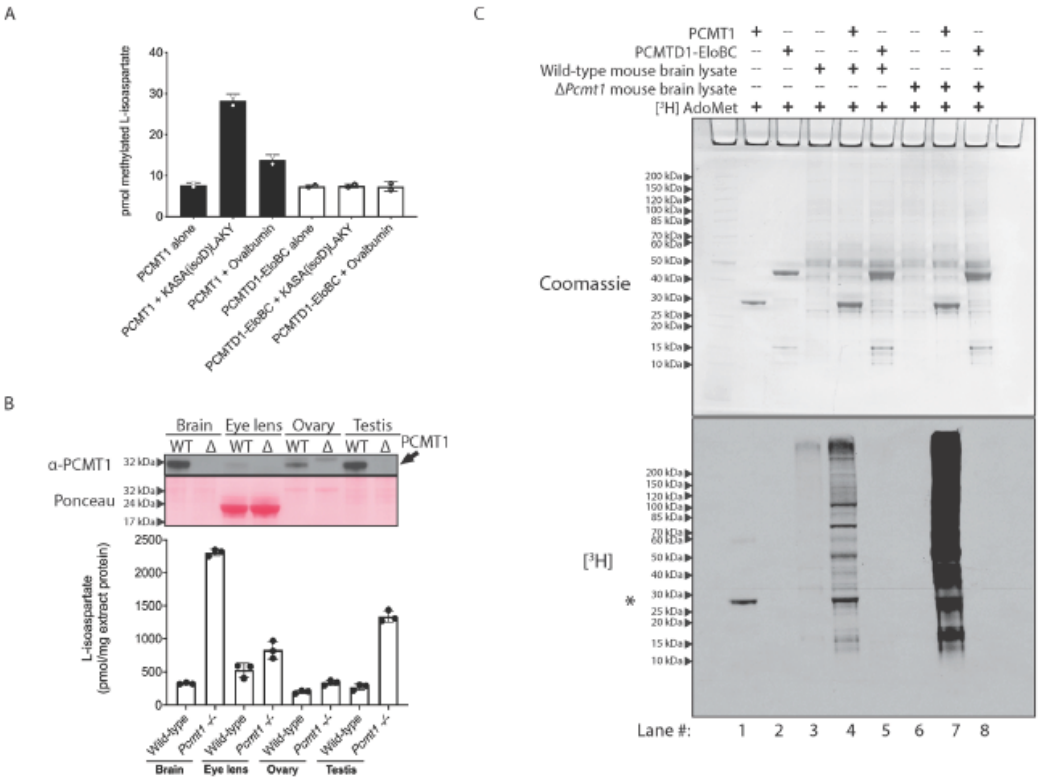

Figure 6. PCMTD1–EloBC does not display methyltransferase activity. (A) L-Isoaspartate-specific methylation of 30 pmol of the KASA(isoD)LAKY peptide and 500 pmol of ovalbumin were detected by a methanol vapor diffusion assay, as described in the Experimental Procedures. The assay was performed in duplicate; error bars represent range. (B) Mouse tissue extracts from wild-type (WT) or Δ*Pcmt1* mice were tested for the presence of PCMT1 with an anti-*rh*PCMT1 antibody (upper panel). The extracts were then tested for L-isoaspartate content using the vapor diffusion assay, as described in the Experimental Procedures. Assays were performed in triplicate: error bars represent standard deviation. (C) Total methylation was investigated by incubation of proteins with *S*-adenosyl-L-[methyl-^{3}H] methionine ([^{3}H]AdoMet) and either wild-type mouse brain lysate or *Pcmt1* knockout mouse brain lysate, as described in the Experimental Procedures. All [^{3}H]-labeled proteins were separated by sodium dodecyl sulfate-polyacrylamide gel electrophoresis (SDS-PAGE). Proteins were visualized by Coomassie staining (upper panel), and [^{3}H]-methylated proteins were detected by fluorography (lower panel) by exposure to film for 6 days. Asterisk represents PCMT1 automethylation.

PCMTD1 and the adaptor proteins, Elongins B and C. These effects may enhance binding between AdoMet and PCMTD1–EloBC when compared to AdoMet binding of the truncated variant of PCMTD1.

PCMTD1–EloBC Complex Does Not Display Methyltransferase Activity. The sequence conservation of the AdoMet- and L-isoaspartyl-binding sites between PCMT1 and PCMTD1 suggests that this protein may retain similar L-isoaspartyl-methylation activity. Using L-isoaspartate-containing peptide and protein substrates of the canonical repair enzyme PCMT1, we tested for L-isoaspartyl methylation by PCMTD1–EloBC *via* a methanol vapor diffusion assay, which takes advantage of the greater base lability of isoaspartyl methyl esters compared to other sites of methylation (Figure 6A). The canonical L-isoaspartyl repair methyltransferase PCMT1 is able to methylate the synthetic L-isoaspartyl-containing peptide KASA(isoD)LAKY at a near 1:1 stoichiometric ratio. In addition, PCMT1 was able to methylate ovalbumin, a known PCMT1 substrate, at an ~3% stoichiometric ratio, which is consistent with previous studies (Figure 6A).[41] Incubation of substrates with the PCMTD1–EloBC, however, did not show any methylation of L-isoaspartate above the enzyme-alone background (Figure 6A). Furthermore, methylation activity is not observed with the truncated variant of PCMTD1 in similar assays (data not shown).

It is possible that the KASA(isoD)LAKY peptide and the ovalbumin protein are not preferred L-isoaspartate substrates for PCMTD1 or that it is a protein methyltransferase that does not methylate L-isoaspartate residues. To test these hypotheses, we incubated PCMT1 and PCMTD1–EloBC with mouse tissue lysates and [^{3}H]AdoMet. Using [^{3}H]AdoMet at an undiluted specific activity of ~80 Ci/mmol, it would be possible to detect as little as 1 fmol of methylated product (176 dpm). Tissue extracts from both *Pcmt1*−/− mice and WT mice were prepared from brain, eye lens, ovaries, and testes. PCMT1 was then used to quantify L-isoaspartate levels within

https://doi.org/10.1021/acs.biochem.2c00130
Biochemistry 2022, 61, 879−894

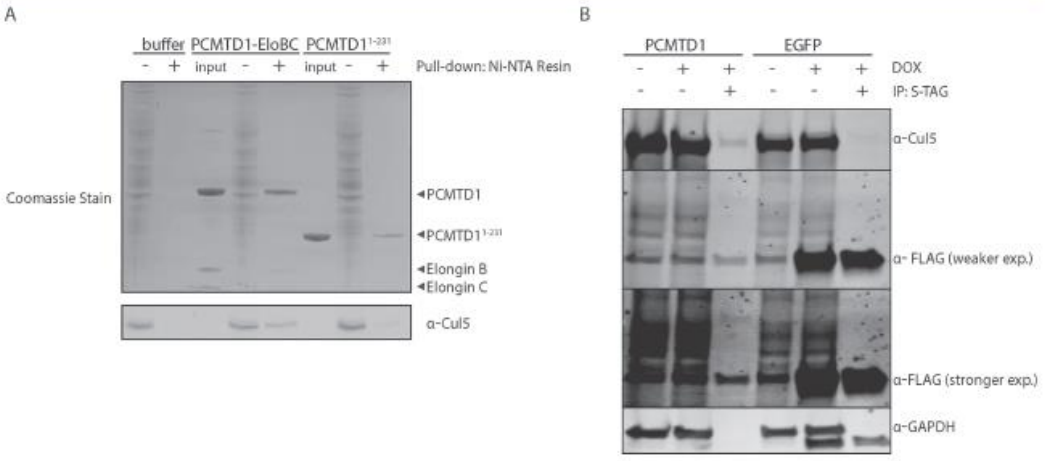

Figure 7. PCMTD1 associates with Cul5 *in vitro* and in cells. (A) PCMTD1's interaction with Cul5 was verified *in vitro* using pulldown assays where recombinant purified proteins were immobilized to Ni-NTA resin as bait. Input lanes represent purified protein stocks used as bait protein that was immobilized onto Ni-NTA resin for pulldown assays. Fresh RPE-1 lysates used as prey are indicated by adjacent − lanes. Proteins eluted from Ni-NTA resin are indicated by the + lanes. The bait proteins were able to coimmunoprecipitate Cul5 as shown by immunoblotting. (B) PCMTD1 was also able to associate with Cul5 in cells. FLAG-S-Tag-PCMTD1 or EGFP expression was induced with 0.1 μg/mL doxycycline in HeLa cells, and the resulting lysates were subjected to immunoprecipitation against the S-Tag and blotted for the indicated proteins. FLAG-S-Tag-PCMTD1, but not FLAG-S-Tag-EGFP, was able to coimmunoprecipitate Cul5. The blot was not stripped between the different antibodies, so the EGFP band is still present in the GAPDH image.

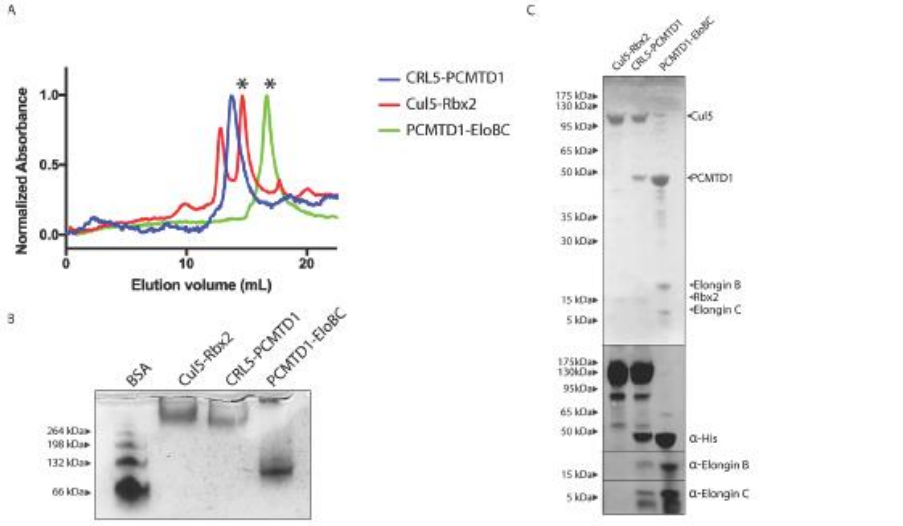

Figure 8. PCMTD1−EloBC interacts with Cul5−Rbx2 to form a PCMTD1−EloBC−Cul5−Rbx2 (CRL5−PCMTD1) complex. (A) Analytical gel filtration suggests that the Cul5−Rbx2 and PCMTD1−EloBC subcomplexes interact to form a larger complex. The CRL5−PCMTD1 complex was formed by incubating purified preparations of Cul5−Rbx2 to PCMTD1−EloBC at a 1.1:1 molar ratio for 2 h at room temperature (RT). Asterisks (*) indicate fractions used for creating this complex. The elution profile CRL5−PCMTD1 (green), PCMTD1−EloBC (blue), and Cul5−Rbx2 (red) were then determined with analytical gel filtration in separate runs. The shift to an earlier elution volume for CRL5−PCMTD1 compared to that for Cul5−Rbx2 and PCMTD1−EloBC suggests that some interaction between these subcomplexes occurs. (B) Shifts in gel mobility and banding pattern in native-PAGE further suggest that a complex is formed between PCMTD1−EloBC and Cul5−Rbx2. (C) SDS-PAGE followed by Coomassie staining and immunoblotting of the singular blue peak or peaks indicated by an asterisk (*) after gel filtration reveal that the blue peak collected during gel filtration contains all protein components for CRL5−PCMTD1.

https://doi.org/10.1021/acs.biochem.2c00130
Biochemistry 2022, 61, 879−894

proteins in each extract sample (Figure 6B). Because *Pcmt1*−/− mice brain extracts contained the highest level of L-isoaspartate protein damage overall, this tissue extract was used for subsequent assays (Figure 6B). In the lanes containing *Pcmt1*−/− mouse brain extract and repair enzyme PCMT1, a significant signal as a result of methylation was observed. As expected, methylation signal was more intense in reactions with PCMT1 and brain extract from *Pcmt1*−/− mice (lanes 4 and 7, Figure 6C). Due to endogenous PCMT1 homologues present in WT mice, the background methylation signal was seen in WT mouse brain lysate but was absent in *Pcmt1*−/− mice. In lanes 5 and 8 in which PCMTD1−EloBC was incubated with WT and *Pcmt*−/− lysates, no significant signal is observed above the lysate-alone lanes 3 and 6. Thus, while the PCMTD1−EloBC complex is able to bind AdoMet, it does not exhibit any detectable protein methyltransferase activity in these *in vitro* assays.

PCMTD1 Associates with Known Components of the Cullin-RING E3 Ubiquitin Ligase. The PCMTD1 C-terminus contains the SOCS box domain, which facilitates the formation of a Cullin-RING E3 ubiquitin ligase complex within SOCS box-containing proteins (Figure 1). Within this domain, the BC-box is responsible for recruiting the heterodimeric adaptor proteins Elongin B and C.[28] As shown above, *E. coli* cotransformed with plasmids expressing full-length PCMTD1 and Elongins B and C allowed for the purification of complexed PCMTD1−EloBC. Within the SOCS box, the Cul-box motif further mediates the complex formation between SOCS box-containing proteins and Cul5. To investigate interactions with Cullin-RING ligase component proteins, His-tagged PCMTD1−EloBC was immobilized onto the Ni-NTA resin. We found that recombinant Ni-NTA-immobilized PCMTD1−EloBC was able to pulldown and coelute endogenous Cul5 from RPE-1 cell lysates, as demonstrated with an anti-Cul5 immunoblot (Figure 7A). Using the truncated PCMTD1$^{1-231}$ construct, only a small amount of Cul5 coimmunoprecipitation was seen. These results suggest that the recombinant PCMTD1−EloBC interacts with Cul5 and these interactions may be facilitated by the C-terminus of PCMTD1. To investigate whether Cul5 could interact with PCMTD1 in human cells, HeLa cell lines expressing doxycycline-inducible FLAG- and S-tagged PCMTD1 or EGFP were generated. Tagged PCMTD1 and EGFP were precipitated with S-protein agarose beads, and the subsequent immunoblots were probed for endogenous Cul5. Cul5 coprecipitated with PCMTD1 but not with EGFP (Figure 7B). This suggests that complex formation may occur between PCMTD1 and Cul5 within human cell lysates.

To test whether PCMTD1 is truly capable of forming a complete Cullin-RING E3 ligase complex with Cul5 and Rbx2 *in vitro*, recombinantly purified preparations of Cul5−Rbx2 and PCMTD1−EloBC were incubated together to promote oligomerization into PCMTD1−EloBC−Cul5−Rbx2 (CRL5−PCMTD1). This sample was then chromatographed on an analytical gel filtration column. The CRL5−PCMTD1 complex elutes earlier than Cul5−Rbx2 and PCMTD1−EloBC when chromatographed under identical conditions (Figure 8A). These results suggest that Cul5−Rbx2 and PCMTD1−EloBC do indeed oligomerize to form a larger complex *in vitro*. Native-PAGE analysis of these samples suggests that protein migration behavior of CRL5−PCMTD1 resembles Cul5−Rbx2 more than PCMTD1−EloBC (Figure 8B). This may be caused by particle shape differences in comparison with CRL5−PCMTD1 to PCMTD1−EloBC—oligomerization into the larger complex may cause CRL5−PCMTD1 to adopt a nonglobular shape that may be important for its proposed enzymatic functions. SDS-PAGE followed by Coomassie staining and immunoblotting verifies that the CRL5−PCMTD1 peak collected during analytical gel filtration does indeed contain the proposed protein components needed for constituting the CRL5−PCMTD1 complex (Figure 8C). Together, these results suggest that PCMTD1 is indeed capable of forming an E3 ubiquitin ligase complex through direct interactions with these CRL proteins, which is reminiscent of other substrate adaptor proteins implicated in the Cullin-Ring E3 ligase family.

DISCUSSION

Disruption of protein homeostasis by protein misfolding or aggregation can be the result of numerous factors including cellular stress, inherited mutations, or protein aging. Aging can contribute to errors within protein homeostasis through the damage and aggregation of long-lived proteins and through the disruption of the protein homeostasis network.[42] A thorough understanding of the proteins involved in this network and their substrates helps inform the therapeutic design for related diseases.[43] The function of the PCMTD1 and PCMTD2 proteins was previously proposed to be a link between the methylation and ubiquitylation of the protein age-related modification, L-isoaspartate, based on their interactions with Elongins and Cullins.[44] However, we have not detected any methyltransferase activity for these proteins. PCMTD1 and PCMTD2 have also been linked to various disease states including neurodevelopmental disorders and cancer.[14−17] These proteins therefore potentially represent an important part of the protein homeostasis network but they remain largely uncharacterized.

In this study, we have developed both recombinant bacterial and mammalian cell systems for the expression and characterization of PCMTD1 in complex with Cullin-RING ligase (CRL) proteins. PCMTD1 and PCMTD2 are 79% identical, and it is likely that they have similar mechanisms. Our PCMTD1 constructs demonstrated consistent interactions between PCMTD1, Elongins B and C, and Cul5 across *in vitro* and in cell experiments (Figures 3 and7). Importantly, C-terminally truncated PCMTD1 constructs did not associate with Elongins B and C, supporting the role of the C-terminally localized PCMTD1 SOCS box motif in Elongin recruitment (Figure 3). SOCS box-containing proteins perform a variety of regulatory functions within the cell, including SOCS1 ubiquitination of Jak2, Asb2 targeting of actin-binding filaments in leukemia cells, and VHL ubiquitination of HIF-1α.[45−47] It is clear from these few examples that the 80+ SOCS box proteins in the human genome play a significant role in maintaining cellular and human health, and thus an understanding of the putative PCMTD SOCS box protein mechanisms and targets is of utmost importance.

While substrates for the PCMTD proteins have yet to be identified, the discovery of the PCMTD1 association with CRL proteins in both recombinant and cellular contexts is an important step forward in our understanding of the SOCS box motif. Outside of the PCMTD proteins, the degenerate sequence between the BC-box and the Cul-box is typically 10 amino acids (Figure 1).[10] In both PCMTD1 and PCMTD2, this linker region is comprised of ∼90 residues (Figure 1). This study demonstrates that the extended linker does not disrupt

https://doi.org/10.1021/acs.biochem.2c00130
Biochemistry 2022, 61, 879−894

the association between PCMTD1, Elongins B and C, and Cul5 (Figures 3 and 7). Phylogenetic analysis of the PCMTD1 extended linker sequence across select metazoan phyla indicates a wide variety in sequence lengths ranging from 12 to 386 residues, with the average length being 145 residues, and the mode of these sequence lengths being 89 residues (Figure S2). When compared to previous PCMT1 crystal structures, the predicted structural models from AlphaFold demonstrate that the length of this linker could allow for a loop to wrap around the PCMTD1 globular core (PCMT1-homologous region) to extend over the presumed substrate binding site, where canonical L-isoaspartate binding motifs are localized, without disrupting the BC- or Cul-boxes (Figure S6).[48] If accurate, these models would indicate that the extended linker may play a role in substrate recruitment, binding, or release. Mutational studies, including the removal of this extended linker, could shed light on its role in future studies.

Purification of the full-length PCMTD1 alone proved difficult, while either coexpression with Elongins B and C or truncation of the PCMTD1 C-terminal domain allowed for robust purification of the PCMTD1−EloBC complex or PCMTD1$^{1-231}$, respectively (Figure 3). Expression and solubility tests revealed only modest increases in the expression of PCMTD1 in the presence of Elongins B and C (Figure 4A,B). Intriguingly, when PCMTD1 protein levels were monitored in induced cultures by immunoblot at various time points after the addition of a protein synthesis inhibitor, the results showed nearly complete loss of signal from the N-terminal His-tag of PCMTD1 after 120 min without Elongins (Figure 4C). In contrast, when PCMTD1 was coexpressed with Elongins, a strong signal from the N-terminal His-tag persisted throughout all time points. Loss of signal in the PCMTD1-alone samples may be explained by occlusion of the tag through misfolding, aggregation, or interacting partners or degradation of the PCMTD1 protein. While a faint band is seen near the molecular weight of PCMTD1 (42 kDa) in the Ponceau-stained blot, protein degradation cannot be ruled out, as the PCMTD1 construct also produces cleaved maltose binding protein after protein expression, which is approximately the same polypeptide molecular weight as PCMTD1 (42.5 kDa). The association between PCMTD1 and Elongins B and C within the *E. coli* expression system may prevent interaction with other partners that may occlude the His-tag from immunoblot detection or it may stabilize inherently disordered portions of the protein that may otherwise trigger unfolding or aggregation. The predicted AlphaFold model of PCMTD1 shows the lowest confidence metrics in the extended C-terminal linker region between the BC-box and the Cul-box, which may be an indicator of disorder within the protein structure (Figure S6). It is possible that Elongins B and C binding at the BC-box help order this region and prevent aggregation or degradation. Future biochemical and structural studies of PCMTD1 alone and in the presence of Elongins B and C may shed light on their stabilization of PCMTD1 protein levels.

PCMTD1 appears to associate better with Cul5 in our *in vitro* reconstitution experiments compared to either of our pulldown strategies (Figures 7 and 8). These results may be due to the sources from which PCMTD1 and Cul5 were derived in these experiments. For instance, recombinant PCMTD1 and Cul5 expressed in *E. coli* may not have their respective posttranslational modifications or other supplemental binding partners when found within their endogenous mammalian environments. However, these experiments still collectively suggest that a direct interaction occurs between PCMTD1 and Cul5.

In addition to demonstrating the interaction between PCMTD1 and CRL proteins, we have shown that PCMTD1 and PCMTD1$^{1-231}$ associate with the methyltransferase cofactor AdoMet (Figure 5). Sequence comparisons, as well as structural comparisons between the PCMT1 structure and the AlphaFold predicted the PCMTD1 structure, reveal a few disruptive substitutions in the AdoMet binding domains, which corresponds with the observation that PCMTD1−EloBC is able to bind AdoMet (Figures 1 and5). Interestingly, the C-terminally truncated PCMTD1 construct PCMTD1$^{1-231}$ appears to exhibit decreased binding to AdoMet with respect to PCMTD1−EloBC (Figure 5). The PCMT1 crystal structure reveals that the C-terminus is approximately 8 Å away from the AdoMet binding site, while the predicted AlphaFold model of PCMTD1 shows the C-terminus extending from this point to form the SOCS box domain and further wrap around the PCMT1-homologous region (Figure S6).[49] It is possible that the removal of this extended C-terminus disrupts the PCMT1-homologous region of PCMTD1 adjacent to the AdoMet binding pocket, thereby lowering the affinity of the truncated PCMTD1 for the methyltransferase cofactor. There may also be an additional role for Elongins B and C in which the adaptor protein binding may allosterically enhance the association between PCMTD1 and AdoMet. Elongins B and C binding have been shown to induce conformational rearrangements of the substrate binding interface for ASB9, another Cullin-RING E3 ubiquitin ligase.[46]

Surprisingly, despite evidence for AdoMet binding and conservation of the L-isoaspartyl-binding and AdoMet binding motifs within PCMTD1, no methyltransferase activity against L-isoaspartate-containing substrates or L-isoaspartate-rich tissue extracts was observed (Figure 6). The PCMTD1 construct is N-terminally 6xHis-tagged, and it is possible that the tag interferes with substrate binding; however, the recombinant PCMT1 construct used in this study is similarly N-terminally 6xHis-tagged and exhibits robust methyltransferase activity (Figure 6). Additionally, the isoaspartyl-binding site within the PCMT1 structure lies adjacent to the AdoMet binding pocket, and PCMTD1−EloBC is still able to bind AdoMet (Figures S6B and 5). While the radiolabeling methods used in this study are sufficient to detect as little as 1 fmol of methylation, further testing of different conditions and substrates may be necessary to detect PCMTD1 methyltransferase activity or demonstrate that the methyltransferase activity of this protein has been lost.

The cellular localization of the PCMTD proteins may affect their proposed physiological roles and enzymatic functions. We do note that these proteins contain a candidate nuclear localization signal—specifically 275-KRKRKR-280 in PCMTD1. Fluorescence microscopy of overexpressed PCMTD1 shows localization within the nucleus as well as the cytosol (Figure S7), consistent with Elongins B and C and Cul5 localization.[50,51] This localization may be driven by its proposed basic nuclear localization signal (^{275}KRKRKR^{280}), but given the small size of the pGLAP2 PCMTD1 construct used here (~50 kDa), the observed nuclear localization may also be due to diffusion into the nucleus.[52] Consistent with the idea of small proteins diffusing through the nuclear pore complex into the nucleus, our pGLAP2 EGFP (~30 kDa)

https://doi.org/10.1021/acs.biochem.2c00130
Biochemistry 2022, 61, 879−894

construct was also observed within the nucleus in our experiments (Figure S7).

This study adds to the limited knowledge available for the biochemical mechanisms of PCMTD1 and PCMTD2, and to the best of the authors' knowledge, only one previous study has included biochemical experiments with these proteins.[44] We have built on the previous study by investigating the interactions between PCMTD1 and CRL components, as well as its AdoMet binding and putative methyltransferase function. These results showed specific interactions with CRL components with the C-terminus of PCMTD1 and AdoMet binding within the N-terminus. These results suggest that the PCMTD proteins may be Cullin-RING E3 ubiquitin ligases that may recognize substrates that contain L-isoaspartate residues. Future work exploring the substrate specificity, ubiquitination activity, and structure of these proteins will reveal much about the mechanism and function of these proteins. This would represent a significant step forward in our understanding of RING ligase targeting, as recognition of L-isoaspartate in proteins would be the first example of an age-specific molecular switch. In this way, PCMTD1 and PCMTD2 may help maintain a functional proteome within the cell through the regular turnover of age-damaged proteins.

■ ASSOCIATED CONTENT

Supporting Information

The Supporting Information is available free of charge at https://pubs.acs.org/doi/10.1021/acs.biochem.2c00130.

Sequence variation across different human SOCS box-containing proteins (Figure S1); conserved regions between the PCMTD1 BC-box and Cul-box across metazoan phyla (Figure S2); multiple human isoforms of PCMTD result from alternative splicing (Figure S3); Elongins B and C copurifies with full-length PCMTD1 but not with truncated PCMTD1$^{1-231}$ (Figure S4); Elongins B and C help stabilize the recombinant PCMTD1 replicate experiment (Figure S5); AlphaFold predicted structural model of human PCMTD1 (Figure S6); and microscopy of pGLAP2 EGFP and PCMTD1 constructs (Figure S7) (PDF)

Accession Codes

PCMT1: P22061-1, PCMTD1: Q96MG8-1, PCMTD2: Q9NV79-1, EloB: Q15370-1, EloC: Q15369-2, Cul5: Q93034, Rbx2: Q9WTZ1.

■ AUTHOR INFORMATION

Corresponding Author

Steven G. Clarke − *Department of Chemistry and Biochemistry and Molecular Biology Institute, University of California, Los Angeles, Los Angeles, California 90095, United States;* orcid.org/0000-0002-7303-6632; Email: clarke@mbi.ucla.edu

Authors

Rebeccah A. Warmack − *Department of Chemistry and Biochemistry and Molecular Biology Institute, University of California, Los Angeles, Los Angeles, California 90095, United States;* Present Address: Division of Chemistry and Chemical Engineering, California Institute of Technology, 1200 E. California Blvd., Pasadena, California 91125, United States

Eric Z. Pang − *Department of Chemistry and Biochemistry and Molecular Biology Institute, University of California, Los Angeles, Los Angeles, California 90095, United States*

Esther Peluso − *Department of Chemistry and Biochemistry and Molecular Biology Institute, University of California, Los Angeles, Los Angeles, California 90095, United States*

Jonathan D. Lowenson − *Department of Chemistry and Biochemistry and Molecular Biology Institute, University of California, Los Angeles, Los Angeles, California 90095, United States*

Joseph Y. Ong − *Department of Chemistry and Biochemistry and Molecular Biology Institute, University of California, Los Angeles, Los Angeles, California 90095, United States*

Jorge Z. Torres − *Department of Chemistry and Biochemistry and Molecular Biology Institute, University of California, Los Angeles, Los Angeles, California 90095, United States;* orcid.org/0000-0002-2158-889X

Complete contact information is available at: https://pubs.acs.org/10.1021/acs.biochem.2c00130

Author Contributions

†R.A.W. and E.Z.P. contributed equally to this work.

Funding

This work was supported by the National Science Foundation grant MCB-1714569 (to S.G.C.), the National Institutes of Health grant R35GM139539 (to J.Z.T), and by funds from the UCLA Academic Senate Faculty Research Program, the Life Extension Foundation, Inc., and the Elizabeth and Thomas Plott Chair in Gerontology of the UCLA Longevity Center (to S.G.C.). R.A.W. and J.Y.O. were supported by the National Institutes of Health Ruth L. Kirschstein National Research Service Award GM007185. E.Z.P. was supported by the NIH NIGMS-funded predoctoral fellowship (T32GM136614). J.Y.O. was supported by a National Science Foundation Graduate Research Fellowship DGE-1650604 and by a UCLA Whitcome Predoctoral Fellowship in Molecular Biology. The content is solely the responsibility of the authors and does not necessarily represent the official views of the National Institutes of Health.

Notes

The authors declare no competing financial interest.

This study was performed in accordance with animal use protocols approved by the UCLA Animal Research Committee (Protocol 1993-109-64). Mice were scheduled to be euthanized if they met any early removal criteria (kyphosis, lack of grooming behavior). However, this did not occur with any of the animals in our study.

Figures and tables were arranged in Adobe Illustrator. Signals from fluorographs were quantified by densitometry using ImageJ.[53]

All data described in the manuscript are contained within the manuscript. Additional data are available upon request.

■ ACKNOWLEDGMENTS

The authors would like to acknowledge Dr. Mark Arbing and the UCLA DOE Protein Expression Core for aid in the design and synthesis of the plasmids used within this study. The authors would also like to thank Austin Gable, Georgiana Salant, Andrea Hadjikyriacou, Kennen MacKay, Calvin Lin, and Dylan Valencia for their contributions at the initial stages of this project.

construct was also observed within the nucleus in our experiments (Figure S7).

This study adds to the limited knowledge available for the biochemical mechanisms of PCMTD1 and PCMTD2, and to the best of the authors' knowledge, only one previous study has included biochemical experiments with these proteins.[44] We have built on the previous study by investigating the interactions between PCMTD1 and CRL components, as well as its AdoMet binding and putative methyltransferase function. These results showed specific interactions with CRL components with the C-terminus of PCMTD1 and AdoMet binding within the N-terminus. These results suggest that the PCMTD proteins may be Cullin-RING E3 ubiquitin ligases that may recognize substrates that contain L-isoaspartate residues. Future work exploring the substrate specificity, ubiquitination activity, and structure of these proteins will reveal much about the mechanism and function of these proteins. This would represent a significant step forward in our understanding of RING ligase targeting, as recognition of L-isoaspartate in proteins would be the first example of an age-specific molecular switch. In this way, PCMTD1 and PCMTD2 may help maintain a functional proteome within the cell through the regular turnover of age-damaged proteins.

■ ASSOCIATED CONTENT

Supporting Information

The Supporting Information is available free of charge at https://pubs.acs.org/doi/10.1021/acs.biochem.2c00130.

Sequence variation across different human SOCS box-containing proteins (Figure S1); conserved regions between the PCMTD1 BC-box and Cul-box across metazoan phyla (Figure S2); multiple human isoforms of PCMTD result from alternative splicing (Figure S3); Elongins B and C copurifies with full-length PCMTD1 but not with truncated PCMTD1$^{1-231}$ (Figure S4); Elongins B and C help stabilize the recombinant PCMTD1 replicate experiment (Figure S5); AlphaFold predicted structural model of human PCMTD1 (Figure S6); and microscopy of pGLAP2 EGFP and PCMTD1 constructs (Figure S7) (PDF)

Accession Codes

PCMT1: P22061-1, PCMTD1: Q96MG8-1, PCMTD2: Q9NV79-1, EloB: Q15370-1, EloC: Q15369-2, Cul5: Q93034, Rbx2: Q9WTZ1.

■ AUTHOR INFORMATION

Corresponding Author

Steven G. Clarke − *Department of Chemistry and Biochemistry and Molecular Biology Institute, University of California, Los Angeles, Los Angeles, California 90095, United States;* orcid.org/0000-0002-7303-6632; Email: clarke@mbi.ucla.edu

Authors

Rebeccah A. Warmack − *Department of Chemistry and Biochemistry and Molecular Biology Institute, University of California, Los Angeles, Los Angeles, California 90095, United States;* Present Address: Division of Chemistry and Chemical Engineering, California Institute of Technology, 1200 E. California Blvd., Pasadena, California 91125, United States

Eric Z. Pang − *Department of Chemistry and Biochemistry and Molecular Biology Institute, University of California, Los Angeles, Los Angeles, California 90095, United States*

Esther Peluso − *Department of Chemistry and Biochemistry and Molecular Biology Institute, University of California, Los Angeles, Los Angeles, California 90095, United States*

Jonathan D. Lowenson − *Department of Chemistry and Biochemistry and Molecular Biology Institute, University of California, Los Angeles, Los Angeles, California 90095, United States*

Joseph Y. Ong − *Department of Chemistry and Biochemistry and Molecular Biology Institute, University of California, Los Angeles, Los Angeles, California 90095, United States*

Jorge Z. Torres − *Department of Chemistry and Biochemistry and Molecular Biology Institute, University of California, Los Angeles, Los Angeles, California 90095, United States;* orcid.org/0000-0002-2158-889X

Complete contact information is available at: https://pubs.acs.org/10.1021/acs.biochem.2c00130

Author Contributions

†R.A.W. and E.Z.P. contributed equally to this work.

Funding

This work was supported by the National Science Foundation grant MCB-1714569 (to S.G.C.), the National Institutes of Health grant R35GM139539 (to J.Z.T), and by funds from the UCLA Academic Senate Faculty Research Program, the Life Extension Foundation, Inc., and the Elizabeth and Thomas Plott Chair in Gerontology of the UCLA Longevity Center (to S.G.C.). R.A.W. and J.Y.O. were supported by the National Institutes of Health Ruth L. Kirschstein National Research Service Award GM007185. E.Z.P. was supported by the NIH NIGMS-funded predoctoral fellowship (T32GM136614). J.Y.O. was supported by a National Science Foundation Graduate Research Fellowship DGE-1650604 and by a UCLA Whitcome Predoctoral Fellowship in Molecular Biology. The content is solely the responsibility of the authors and does not necessarily represent the official views of the National Institutes of Health.

Notes

The authors declare no competing financial interest.

This study was performed in accordance with animal use protocols approved by the UCLA Animal Research Committee (Protocol 1993-109-64). Mice were scheduled to be euthanized if they met any early removal criteria (kyphosis, lack of grooming behavior). However, this did not occur with any of the animals in our study.

Figures and tables were arranged in Adobe Illustrator. Signals from fluorographs were quantified by densitometry using ImageJ.[53]

All data described in the manuscript are contained within the manuscript. Additional data are available upon request.

■ ACKNOWLEDGMENTS

The authors would like to acknowledge Dr. Mark Arbing and the UCLA DOE Protein Expression Core for aid in the design and synthesis of the plasmids used within this study. The authors would also like to thank Austin Gable, Georgiana Salant, Andrea Hadjikyriacou, Kennen MacKay, Calvin Lin, and Dylan Valencia for their contributions at the initial stages of this project.

Takiguchi, S.; Watanabe, S.; Yosida, M.; Hotuta, T.; Kusano, J.; Kanehori, K.; Takahashi-Fujii, A.; Hara, H.; Tanase, T.; Nomura, Y.; Togiya, S.; Komai, F.; Hara, R.; Takeuchi, K.; Arita, M.; Imose, N.; Musashino, K.; Yuuki, H.; Oshima, A.; Sasaki, N.; Aotsuka, S.; Yoshikawa, Y.; Matsunawa, H.; Ichihara, T.; Shiohata, N.; Sano, S.; Moriya, S.; Momiyama, H.; Satoh, N.; Takami, S.; Terashima, Y.; Suzuki, O.; Nakagawa, S.; Senoh, A.; Mizoguchi, H.; Goto, Y.; Shimizu, F.; Wakebe, H.; Hishigaki, H.; Watanabe, T.; Sugiyama, A.; Takemoto, M.; Kawakami, B.; Yamazaki, M.; Watanabe, K.; Kumagai, A.; Itakura, S.; Fukuzumi, Y.; Fujimori, Y.; Komiyama, M.; Tashiro, H.; Tanigami, A.; Fujiwara, T.; Ono, T.; Yamada, K.; Fujii, Y.; Ozaki, K.; Hirao, M.; Ohmori, Y.; Kawabata, A.; Hikiji, T.; Kobatake, N.; Inagaki, H.; Ikema, Y.; Okamoto, S.; Okitani, R.; Kawakami, T.; Noguchi, S.; Itoh, T.; Shigeta, K.; Senba, T.; Matsumura, K.; Nakajima, Y.; Mizuno, T.; Morinaga, M.; Sasaki, M.; Togashi, T.; Oyama, M.; Hata, H.; Watanabe, M.; Komatsu, T.; Mizushima-Sugano, J.; Satoh, T.; Shirai, Y.; Takahashi, Y.; Nakagawa, K.; Okumura, K.; Nagase, T.; Nomura, N.; Kikuchi, H.; Masuho, Y.; Yamashita, R.; Nakai, K.; Yada, T.; Nakamura, Y.; Ohara, O.; Isogai, T.; Sugano, S. Complete sequencing and characterization of 21,243 full-length human cDNAs. *Nat. Genet.* **2004**, *36*, 40−45.

(36) Bechtel, S.; Rosenfelder, H.; Duda, A.; Schmidt, C.; Ernst, U.; Wellenreuther, R.; Mehrle, A.; Schuster, C.; Bahr, A.; Blöcker, H.; Heubner, D.; Hoerlein, A.; Michel, G.; Wedler, H.; Köhrer, K.; Ottenwälder, B.; Poustka, A.; Wiemann, S.; Schupp, I. The full-ORF clone resource of the German cDNA Consortium. *BMC Genomics* **2007**, *8*, No. 399.

(37) The MGC Project Team. The status, quality, and expansion of the NIH full-length cDNA project: the Mammalian Gene Collection (MGC). *Genome Res.* **2004**, *14*, 2121−2127.

(38) Zheng, N.; Schulman, B. A.; Song, L.; Miller, J. J.; Jeffrey, P. D.; Wang, P.; Chu, C.; Koepp, D. M.; Elledge, S. J.; Pagano, M.; Conaway, R. C.; Conaway, J. W.; Harper, J. W.; Pavletich, N. P. Structure of the Cul1-Rbx1-Skp1-F boxSkp2 SCF ubiquitin ligase complex. *Nature* **2002**, *416*, 703−709.

(39) Babon, J. J.; Sabo, J. K.; Soetopo, A.; Yao, S.; Bailey, M. F.; Zhang, J. G.; Nicola, N. A.; Norton, R. S. The SOCS box domain of SOCS3: structure and interaction with the elonginBC-cullin5 ubiquitin ligase. *J. Mol. Biol.* **2008**, *381*, 928−940.

(40) Lumpkin, R. J.; Baker, R. W.; Leschziner, A. E.; Komives, E. A. Structure and dynamics of the ASB9 CUL-RING E3 Ligase. *Nat Commun.* **2020**, *11*, No. 2866.

(41) Lowenson, J. D.; Clarke, S. Structural elements affecting the recognition of L-isoaspartyl residues by the L-isoaspartyl/D-aspartyl protein methyltransferase: implications for the repair hypothesis. *J. Biol. Chem.* **1991**, *266*, 19396−19406.

(42) Pey, A. L. *Protein Homeostasis and Disease*, Academic Press, 2020; Chapter 2.

(43) Calamini, B.; Morimoto, R. I. Protein Homeostasis as a Therapeutic Target for Diseases of Protein Conformation. *Curr. Top. Med. Chem.* **2013**, *12*, 2623−2640.

(44) Mahrour, N.; Redwine, W. B.; Florens, L.; Swanson, S. K.; Martin-Brown, S.; Bradford, W. D.; Staehling-Hampton, K.; Washburn, M. P.; Conaway, R. C.; Conaway, J. W. Characterization of Cullin-box sequences that direct recruitment of Cul2-Rbx1 and Cul5-Rbx2 modules to Elongin BC-based ubiquitin ligases. *J. Biol. Chem.* **2008**, *283*, 8005−8013.

(45) Razinia, Z.; Baldassarre, M.; Bouaouina, M.; Lamsoul, I.; Lutz, P. G.; Calderwood, D. A. The E3 ubiquitin ligase specificity subunit ASB2α targets filamins for proteasomal degradation by interacting with the filamin actin-binding domain. *J. Cell Sci.* **2011**, *124*, 2631−2641.

(46) Ungureanu, D.; Saharinen, P.; Junttila, I.; Hilton, D. J.; Silvennoinen, O. Regulation of Jak2 through the ubiquitin-proteasome pathway involves phosphorylation of Jak2 on Y1007 and interaction with SOCS-1. *Mol. Cell. Biol.* **2002**, *22*, 3316−3326.

(47) Iwai, K.; Yamanaka, K.; Kamura, T.; Minato, N.; Conaway, R. C.; Conaway, J. W.; Klausner, R. D.; Pause, A. Identification of the von Hippel−Lindau tumor-suppressor protein as part of an active E3 ubiquitin ligase complex. *Proc. Natl. Acad. Sci. U.S.A.* **1999**, *96*, 12436−12441.

(48) Jumper, J.; Evans, R.; Pritzel, A.; Green, T.; Figurnov, M.; Ronneberger, O.; Tunyasuvunakool, K.; Bates, R.; Žídek, A.; Potapenko, A.; Bridgland, A.; Meyer, C.; Kohl, S. A. A.; Ballard, A. J.; Cowie, A.; Romera-Paredes, B.; Nikolov, S.; Jain, R.; Adler, J.; Back, T.; Petersen, S.; Reiman, D.; Clancy, E.; Zielinski, M.; Steinegger, M.; Pacholska, M.; Berghammer, T.; Bodenstein, S.; Silver, D.; Vinyals, O.; Senior, A. W.; Kavukcuoglu, K.; Kohli, P.; Hassabis, D. Highly accurate protein structure prediction with AlphaFold. *Nature* **2021**, *596*, 583−589.

(49) Ryttersgaard, C.; Griffith, S. C.; Sawaya, M. R.; MacLaren, D. C.; Clarke, S.; Yeates, T. O. Crystal structure of human L-isoaspartyl methyltransferase. *J. Biol. Chem.* **2002**, *277*, 10642−10646.

(50) Zhang, Z.; Huang, Q.; Wang, Z.; Zou, J.; Yu, Z.; Strauss, J. F., III; Zhang, Z. Elongin B is a binding partner of the male germ cell nuclear speckle protein sperm-associated antigen 16S (SPAG16S) and is regulated post-transcriptionally in the testis. *Reprod., Fertil. Dev.* **2019**, *31*, 962.

(51) Weems, J. C.; Slaughter, B. D.; Unruh, J. R.; Hall, S. M.; McLaird, M. B.; Gilmore, J. M.; Washburn, M. P.; Florens, L.; Yasukawa, T.; Aso, T.; Conaway, J. W.; Conaway, R. C. Assembly of the Elongin A Ubiquitin Ligase Is Regulated by Genotoxic and Other Stresses. *J. Biol. Chem.* **2015**, *290*, 15030−15041.

(52) Timney, B. L.; Raveh, B.; Mironska, R.; Trivedi, J. M.; Kim, S. J.; Russel, D.; Wente, S. R.; Sali, A.; Rout, M. P. Simple rules for passive diffusion through the nuclear pore complex. *J. Cell Biol.* **2016**, *215*, 57−76.

(53) Schneider, C. A.; Rasband, W. S.; Eliceiri, K. W. NIH Image to ImageJ: 25 years of image analysis. *Nat. Methods* **2012**, *9*, 671−675.

https://doi.org/10.1021/acs.biochem.2c00130
Biochemistry 2022, 61, 879−894

Appendix Chapter 4: Synonymous Mutation Generator: a web tool for designing RNAi-resistant sequences

This chapter is reproduced from

Joseph Y. Ong. Synonymous Mutation Generator: a web tool for designing RNAi-resistant sequences. bioRxiv. 2021.01.02.425100. doi: https://doi.org/10.1101/2021.01.02.425100

Synonymous Mutation Generator: a web tool for designing RNAi-resistant sequences

Joseph Y. Ong

Department of Chemistry and Biochemistry, University of California, Los Angeles, Los Angeles, California, United States of America

Corresponding author:
E-mail: jong2@ucla.edu

Abstract

RNA interference (RNAi) is a useful technique for knocking down a protein of interest, allowing for the study of the function of a gene product. However, RNAi techniques are prone to off-target effects, such as non-specific knockdown of genes besides the protein of interest. An important control and companion to RNAi knockdown experiments is the rescue experiment, wherein gene function is restored by expression of an RNAi-resistant construct of the protein of interest. Generating an RNAi-resistant construct of the protein of interest involves generating silent mutations within the coding sequence of the protein so that the resulting amino acid product is the same, but the protein mRNA is no longer a target for the RNAi. Here, Synonymous Mutation Generator, a Python-based web tool that takes an input DNA coding sequence and outputs a synonymous DNA coding sequence that is RNAi-resistant, is described. This web tool should be a useful resource for researchers cloning RNAi-resistant constructs. Synonymous Mutation Generator is easy to use and can be found at jong2.pythonanywhere.com, and the source code is available on GitHub.

Introduction

RNA interference (RNAi) is an established genetic technique for understanding protein function. RNAi, including short interfering RNA (siRNA) and small hairpin RNA (shRNA), enables specific and selective repression of a gene of interest, allowing for functional studies with high-throughput. Commercial genome-wide libraries of short interfering RNA (siRNA)[1,2] and small hairpin RNA (shRNA)[3,4] have both been used in a variety of screens to identify genes of interest in an unbiased manner. Thus, having tools to properly design RNAi experiments is an important component toward thorough and careful science.

The mechanisms of RNAi function have been well-documented[5] and will only be briefly summarized here. For most molecular biology experiments involving RNAi, an exogenous siRNA or shRNA is expressed or transfected within a cell or tissue of interest. The RNAi is then processed into single-stranded RNA of about 21 nucleotides complimentary to the mRNA of the protein target. This complementarity between the mature RNAi and the target mRNA grants RNAi its specificity. Together with the RISC complex, the RNAi binds to the target mRNA, leading to the degradation, inhibition of translation, or deadenylation (removal of the 3' poly(A) tail and subsequent mRNA decay) of the target mRNA. Altogether, the resulting protein product is produced at lower rates, allowing for phenotypic assessment when the protein is knocked down.

Importantly, RNAi techniques have been well-documented as having off-target effects[6]. For example, the kinetochore protein Mad2 (gene *MAD2L1*) is frequently knocked down by RNAi not complimentary to and not designed to target Mad2 mRNA transcripts[7]. As a result, care must be taken when designing and interpreting RNAi experiments. One important control is the rescue experiment, where the RNAi is co-expressed with an RNAi-resistant construct coding for the protein of interest. The RNAi-resistant construct allows for the expression of the protein of interest should restore the loss of function phenotype observed with the RNAi alone, assuming the RNAi has no off-target effects.

In addition to performing the rescue experiment with the wild-type protein of interest, rescue experiments can also be performed with alleles of the protein to gain greater genetic control over which protein construct is expressed. For example, siRNA

can be co-transfected with RNAi-resistant protein constructs containing mutations such as point mutations or domain deletions. RNAi and RNAi-resistant protein complementation approaches like these suppress the endogenous, RNAi-sensitive protein and allow a more controlled analysis of the mutant allele. These experiments have been used to determine the consequence of post-translational modifications like phosphorylation[8] or to determine which domain or isoform[9,10] of a protein is responsible for a phenotype.

The most straight-forward approach towards these RNAi and protein complementation experiments is to use RNAi that targets the 5' or 3' untranslated regions (UTR) of the mRNA of the target gene. In this way, the protein of interested is knocked down by the RNAi and the desired rescue construct can be expressed from an exogenous source (with UTRs that are not recognized by the RNAi). However, in many cases, RNAi must be designed against the coding sequence of the protein. To perform these experiments, an RNAi-resistant construct must first be cloned.

Ideally, to make the most RNAi-resistant construct, the number of nucleotide differences between the RNAi and the RNAi-resistant sequence would be maximized (that is, the degree of complementarity between the RNAi and RNAi-resistant sequence would be minimized). Generating these nucleotide differences involves making silent mutations that cause the protein coding sequence to differ from the RNAi target but do not change the protein encoded by the DNA. While there are web tools for generating silent mutations in DNA sequences[11] (such as WatCut, http://watcut.uwaterloo.ca/template.php?act=silent_new), these tools are mainly for creating or removing restriction enzyme sites for cloning, and the output sequence contains only one silent mutation, probably not enough to render the modified sequence RNAi-resistant. One web tool for generating RNAi-resistant mutations is *C. elegans* Codon Adaptor[12] (https://worm.mpi-cbg.de/codons/cgi-bin/optimize.py). *C. elegans* Codon Adaptor receives an input DNA protein coding sequence with a start and stop codon and modifies some codons of the sequence such that within every 7 consecutive codons, at least 2 have been mutated into a synonymous codon. However, this approach still means that within an RNAi target sequence, 5 of 7 codons might still be the same and thus might still be targets of the RNAi. Moreover, *C. elegans* Codon Adaptor uses *C. elegans* codon frequency tables to determine the alternative codon, and human codon frequency and *C. elegans* codon frequency are different enough such that use of *C. elegans* Codon Adaptor may not be ideal for use in mammalian systems, such as experiments using cultured human cells (see Discussion).

Here, a web tool for generating silent mutations within a protein coding sequence is described. Synonymous Mutation Generator takes an input human DNA sequence and outputs a synonymous DNA sequence that codes for the same amino acids but should be resistant to RNAi targeting the original sequence. Synonymous Mutation Generator is easy to use and freely available online at jong2.pythonanywhere.com.

Results

To devise a program that would generate a synonymous DNA sequence from a given user input sequence, a Python-based script that operates similar to DNA translation scripts was used. Similar to how DNA translation scripts match a codon with a corresponding amino acid, a script that would match a codon to a synonymous codon was employed. The first step was to generate a dictionary of alternative codons that could be used to "translate" a given codon to a synonymous codon.

To generate a dictionary of alternative codons, each of the 59 codons that can code for one amino acid were examined. No alternative codons were generated for the Met (ATG) or Trp (TGG) codons, as these amino acids only have one codon, or for the three stop codons. For the amino acids encoded by only two codons (Asn, Asp, Cys, Glu, His, Lys, Phe, Tyr), identifying the best alternative codon was straightforward: the alternative codon was the other codon that preserved the identity of the amino acid. For the remaining amino acids encoded by more than two codons (Ala, Arg, Gly, Ile, Leu, Pro, Ser, Thr, Val), rules for designing which codon would be the best synonymous codon were adapted from the prior work[13]. In particular, the synonymous codon that caused the greatest number of nucleotide mismatches were chosen (favoring mismatches in the first or second position), avoiding making mutations that would result in wobble base pairing (namely, avoiding A to G and C to T mutations in the third position, as these mutations would allow the RNAi to still target these synonymous codons[14]) and favored codons with the highest usage frequency[15] to promote translation efficiency[16]. The Kazusa database described by Nakamura et al. was the main database used for human codon frequency[15], but the frequencies here were checked against the GenScript human codon frequency table (https://www.genscript.com/tools/codon-frequency-table). There were no major disagreements between these two sources. The complete alternative codon table is found in **Table 1** and an example of how an alternative codon was determined is given in **Box 1**.

Box 1. Example of alternative codon determination

For example, to determine the alternative codons for the six codons that code for Leu:

Leu		
Codon	**Frequency (Kazusa)**	**Alternative Codon**
CTG	0.40	CTC
CTC	0.20	CTG
CTT	0.13	TTG
TTG	0.13	CTC
TTA	0.08	CTC
CTA	0.07	TTA

For CTG, the alternative codon that would cause the greatest number of nucleotide matches is TTA (two mismatches). However, TTA is a codon of much lower frequency and was avoided. The remaining codons all have one mismatch with CTG. Of these, CTC was chosen because it avoids wobble base pairing and has the highest frequency.

For CTC, the alternative codon that would cause the greatest number of mismatches is TTG or TTA (two mismatches). However, both of these codons are of much lower frequency and were avoided. The remaining codons all have one mismatch with CTC. Of these, CTG was chosen because it avoids wobble base pairing and has the highest frequency.

For CTT, the alternative codon that would cause the greatest number of nucleotide mismatches is TTG or TTA (two mismatches). TTG was chosen because it has a higher frequency than TTA.

To generate a dictionary of alternative codons, each of the 59 codons that can code for one amino acid were examined. No alternative codons were generated for the Met (ATG) or Trp (TGG) codons, as these amino acids only have one codon, or for the three stop codons. For the amino acids encoded by only two codons (Asn, Asp, Cys, Glu, His, Lys, Phe, Tyr), identifying the best alternative codon was straightforward: the alternative codon was the other codon that preserved the identity of the amino acid. For the remaining amino acids encoded by more than two codons (Ala, Arg, Gly, Ile, Leu, Pro, Ser, Thr, Val), rules for designing which codon would be the best synonymous codon were adapted from the prior work[13]. In particular, the synonymous codon that caused the greatest number of nucleotide mismatches were chosen (favoring mismatches in the first or second position), avoiding making mutations that would result in wobble base pairing (namely, avoiding A to G and C to T mutations in the third position, as these mutations would allow the RNAi to still target these synonymous codons[14]) and favored codons with the highest usage frequency[15] to promote translation efficiency[16]. The Kazusa database described by Nakamura et al. was the main database used for human codon frequency[15], but the frequencies here were checked against the GenScript human codon frequency table (https://www.genscript.com/tools/codon-frequency-table). There were no major disagreements between these two sources. The complete alternative codon table is found in **Table 1** and an example of how an alternative codon was determined is given in **Box 1**.

Box 1. Example of alternative codon determination

For example, to determine the alternative codons for the six codons that code for Leu:

Leu		
Codon	**Frequency (Kazusa)**	**Alternative Codon**
CTG	0.40	CTC
CTC	0.20	CTG
CTT	0.13	TTG
TTG	0.13	CTC
TTA	0.08	CTC
CTA	0.07	TTA

For CTG, the alternative codon that would cause the greatest number of nucleotide matches is TTA (two mismatches). However, TTA is a codon of much lower frequency and was avoided. The remaining codons all have one mismatch with CTG. Of these, CTC was chosen because it avoids wobble base pairing and has the highest frequency.

For CTC, the alternative codon that would cause the greatest number of mismatches is TTG or TTA (two mismatches). However, both of these codons are of much lower frequency and were avoided. The remaining codons all have one mismatch with CTC. Of these, CTG was chosen because it avoids wobble base pairing and has the highest frequency.

For CTT, the alternative codon that would cause the greatest number of nucleotide mismatches is TTG or TTA (two mismatches). TTG was chosen because it has a higher frequency than TTA.

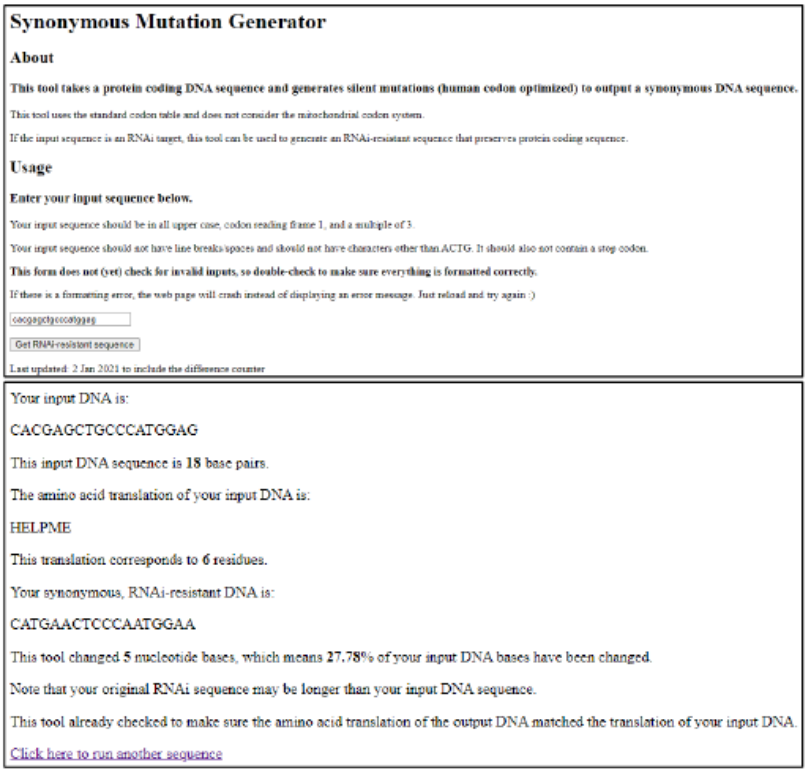

Figure 1. Using Synonymous Mutation Generator.
Top: The user inputs the DNA sequence in the text box at the bottom of the page and clicks "Get RNAi-resistant sequence". The input sequence is "cacgagctgcccatggag". *Bottom:* Synonymous Mutation Generator reiterates the input DNA sequence, translates the DNA sequence into amino acids, returns the synonymous, RNAi-resistant DNA sequence, and details the number of mutations made.

Examples

As a guide, four worked examples using human genes to demonstrate the use of Synonymous Mutation Generator have been included in **Table 2**. The examples generate RNAi-resistant sequences for 4 examples: (1) three shRNAs from Sigma Mission shRNA collection against Lamin A (*LMNA*), (2) five shRNAs from the Dharmacon GIPZ shRNA collection against microtubule severing enzyme katanin subunit A1 (*KATNA1*), (3) three siRNAs against E3 ubiquitin ligase Cullin 3 (*CUL3*), and (4) four siRNAs against cholesterol trafficking membrane protein NPC1 (*NPC1*). These proteins were chosen semi-randomly*. One example, using Sigma Mission

* Author's note: I simply picked proteins of varying function I have encountered throughout my career. I specifically chose *KATNA1* because there is a possibility that I may obtain an shRNA sequence against *KATNA1* and may be able to demonstrate the cloning of an shRNA-resistant construct of *KATNA1*. If this plan comes to fruition, I will update this manuscript.

shRNA TRCN0000061835 against Lamin A, is worked out visually in **Figure 2** and will be discussed here, but all examples described in **Table 2** have parallel comments demonstrating the use of Synonymous Mutation Generator.

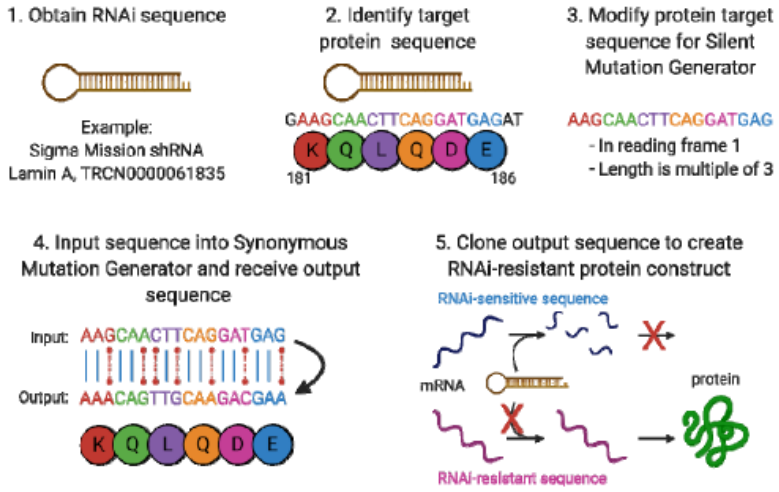

Figure 2. Example for using Synonymous Mutation Generator.
Step 1: The RNAi sequence is obtained from the manufacturer or designer. Here, Sigma Mission shRNA TRCN0000061835 against Lamin A is used as an example.
Step 2: The protein sequence targeted by the RNAi is determined. Here, the Lamin A shRNA sequence GAAGCAACTTCAGGATGAGAT targets amino acid residues 181-186, KQLQDE.
Step 3: The target protein sequence is modified to remove nucleotides such that the sequence is in the first codon reading frame and is a multiple of three. Here, the initial nucleotide G and final nucleotides AT were removed to give input sequence AAGCAACTTCAGGATGAG.
Step 4: The modified sequence is used as an input to Synonymous Mutation Generator and a corresponding, synonymous DNA sequence is obtained. Here, the output sequence from Synonymous Mutation Generator is AAACAGTTGCAAGACGAA. Note the output DNA sequence also codes for the same amino acids.
Step 5: The output sequence is cloned into a vector of choice. As the output sequence contains mutations that distinguish it from the RNAi target, the vectors containing the output sequence should be resistant to the RNAi.

Worked example for Sigma Mission shRNA TRCN0000061835 against Lamin A

Step 1: The RNAi sequence is obtained from the manufacturer or designer.

The sequence for shRNA TRCN0000061835 against Lamin A was obtained from the manufacturer's website and is given as follows:

CCGGGAAGCAACTTCAGGATGAGATCTCGAGATCTCATCCT
GAAGTTGCTTCTTTTTG

Note that this is not the mature RNA sequence that targets Lamin A. Rather, Sigma provides the entire DNA sequence of the translated hairpin RNA. Some manufacturers simply provide the portion of the RNAi sequence that targets the protein of interest.

Step 2: The protein sequence targeted by the RNAi is determined.

To identify the portion of shRNA TRCN0000061835 that targets Lamin A, an alignment of three shRNAs against Lamin A was performed to identify shared (corresponding to vector backbone sequences) and unique (the Lamin A-specific RNAi sequences) regions of DNA (**Figure 3A**). This RNAi sequence lies on the stem of the shRNA (**Figure 3B**). This analysis allowed the identification of a 21-nucleotide protein targeting sequence:

GAAGCAACTTCAGGATGAGAT

Translation of this sequence using web tool Expasy Translate[19] and subsequent manual alignment of the translation identified this sequence as corresponding to Lamin A amino acid residues 181-186, KQLQDE (see **Figure 2 Step 2**).

For manufacturers who provide only the RNAi sequence (and no backbone or other information), only translation and alignment to identify the targeted amino acid residues is necessary. Some manufacturers provide the anti-sense sequence (that is, the reverse complement of the protein coding DNA sequence) and/or provide the sequence as RNA sequences. The sequence must be converted into a DNA sequence (by changing U to T) and the protein coding sense orientation.

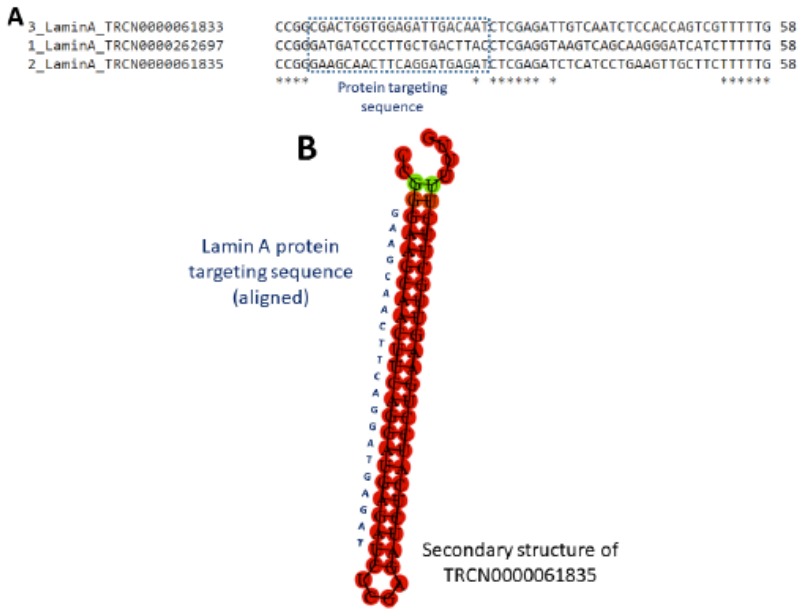

Figure 3. Identification of protein targeting sequence of TRCN0000061835. (A) Clustal Omega[20] alignment of three shRNAs against Lamin A from the Sigma Mission shRNA collection. The DNA sequence that did not align was determined to be the RNAi sequence that targeted Lamin A. (B) Predicted structure of the RNA product of TRCN0000061835 by Vienna RNA Websuite[21]. The identified Lamin A protein targeting sequence for TRCN0000061835 is located along the shRNA stem.

Step 3: The target protein sequence is modified to remove nucleotides such that the sequence is in the first codon reading frame and is a multiple of three.

Synonymous Mutation Generator reads the input DNA sequence as a series of codons. The tool does not read in multiple reading frames, nor does it accept incomplete codons as an input. As such, the sequence must be given in the first codon reading frame and as a multiple of three. As the identified protein target sequence was in the second codon reading frame, the initial nucleotide G was removed to shift the target sequence into the first reading frame. The last two nucleotides AT were removed to delete the terminal incomplete codon, making the sequence a multiple of three.

The resulting modified sequence is (compare **Figure 2 Step 3** to Figure 2 Step 2):

AAGCAACTTCAGGATGAG

In some cases, when the protein targeting sequence is already in the first codon reading frame and a multiple of three, no modification is necessary.

Step 4: The modified sequence is used as an input to Synonymous Mutation Generator and a corresponding, synonymous DNA sequence is obtained.

The modified sequence was input (**as in Figure 1**) into Synonymous Mutation Generator at jong2.pythonanywhere.com. The output sequence from Synonymous Mutation Generator was:

AAACAGTTGCAAGACGAA

Step 5: The output sequence is cloned into a vector of choice.

(Note: This cloning step was not performed for shRNA TRCN0000061835 against Lamin A and is presented as a description of the next step.)

Using the nucleotide sequence for Lamin A (NCBI NM_170707.4), the TRCN0000061835 Lamin A RNAi-sensitive (not mutated) sequence is:

ATGGAGACC…GAGGCCAA**GAAGCAACTTCAGGATGAGAT**
GCTGCGG…AGCATCATGTAA (the RNAi target is bolded)

The RNAi-resistant sequence would then be cloned into a vector of choice, replacing the RNAi target. Any cloning method could be used. The resulting RNAi-resistant sequence would read:

ATGGAGACC…GAGGCCAA**G**<u>AAACAGTTGCAAGACGAA</u>**AT**G
CTGCGG…AGCATCATGTAA (the TRCN0000061835 Lamin A RNAi-resistant sequence is underlined)

Note that there are still three nucleotides (the initial G and the terminal AT, bolded) that are still present in the RNAi-resistant sequence. Both RNAi-sensitive sequence and RNAi-resistant Lamin A constructs translate to:

MET… EAK**KQLQDE**MLR…SIM[Term] (the RNAi-targeted amino acids are bolded)

As the output sequence contains nucleotide mutations that distinguish it from the RNAi target, the mRNA product of the vector containing the output sequence should be resistant to the RNAi.

Discussion

RNA interference experiments are complemented by expression of a construct that restore the function of the target gene. These experiments may include expressing the wild-type protein to demonstrate that the observed RNAi-related phenotype can be rescued by re-expression of the RNAi target or may include molecular biology experiments, wherein an alternative construct (such as a point mutant or a truncation mutant of the target protein) is expressed. Introducing an RNAi-resistant construct of the target protein is necessary for these complementation experiments. Here, Synonymous Mutation Generator was designed as a tool for cloning such an RNAi-resistant construct. Synonymous Mutation Generator is a web tool that takes a user

human DNA input sequence (such as the target of RNAi) and generates a synonymous DNA output sequence. The resulting DNA output sequence codes for the same amino acids but, as it contains mutations that differentiate it from the RNAi target sequence, should be resistant to RNAi.

While the resulting output DNA sequences from Synonymous Mutation Generator codes for the same amino acids as the input sequence, such mutations in DNA sequence are not necessarily silent. Synonymous Mutation Generator does not account for factors like maintaining GC content or predict structural elements. As a result, sequences generated by Synonymous Mutation Generator may be more or less thermodynamically stable than the original transcript and may contain secondary structural elements that inhibit translation[22]. Synonymous Mutation Generator does not consider whether or not splice sites have been introduced within the coding sequence[23]. These are all factors that may influence how "silent" these synonymous mutations are.

Even though multiple codons can code for a given amino acid, not all codons are used equally. This phenomenon is known as codon usage bias, and a derivative of this bias is the codon adaptation index (CAI)[24]. Briefly, a protein coding DNA sequence with a higher CAI (maximum value: 1) uses the highest frequency codons, and the protein will be maximally expressed. In contrast, a protein encoded by DNA with a lower CAI will have lower expression. Modulating the CAI of a protein coding sequence allows for control over protein expression[12]. When generating an RNAi-resistant sequence, *C. elegans* Codon Adaptor allows for adjusting the CAI of a protein and control over protein expression levels. Synonymous Mutation Generator does not take into account the CAI of the input or output DNA sequences. In fact, since Synonymous Mutation Generator was designed to pick a codon of higher usage, the CAI of a given input protein is expected to increase. Whether or not this increase in CAI of the ~6 codons needed to generate an RNAi protein will significantly change the expression of the protein is unknown and must be tested in a case-by-case basis.

However, as *C. elegans* Codon Adaptor was designed for use with *C. elegans*, the codon frequency (and thus the output DNA sequence) was optimized using *C. elegans*, not human codon frequency. One advantage of Synonymous Mutation Generator is that the codon frequency (and thus the alternative codon in the output DNA sequence) is optimized for human expression. The codon biases between *C. elegans* and humans are different enough such that one may reconsider using *C. elegans* Codon Adaptor for use with human proteins (see example in **Box 2**).

Box 2. The human and *C. elegans* codon bias differ enough such that a strong codon in *C. elegans*, like GGA, may not be the ideal synonymous codon in human systems. For example, comparing the human and *C. elegans* codon frequency for Gly (from the Kizusa database):

Gly		
Codon	**Human frequency**	***C. elegans* frequency**
GGC	0.34	0.12
GGA	0.25	0.59
GGG	0.25	0.08
GGT	0.16	0.20

Finally, while Synonymous Mutation Generator mutates all input codons (for most typical 21-nucleotide RNAi sequences, at least 5 input codons and up to 7), whether or not all these codons need to be mutated to obtain an RNAi-resistant sequence is unclear. For example, in a *Drosophila melanogaster* embryo lysate system, a mismatch between siRNA and target mRNA sequence of only a single nucleotide out of a 21-nucleotide siRNA effectively abrogated the ability of an siRNA to degrade the mRNA target[25]. Whether ~6 codons of an RNAi target (as Synonymous Mutation Generator mutates) or only a couple nucleotides need to be mutated to generate an RNAi-resistant construct is unclear. However, given advancements in cloning techniques, cloning the output sequence should be straightforward, whether ~6 codons of a siRNA target or just a couple nucleotides need to be mutated[26,27].

Conclusions

Synonymous Mutation Generator, a web tool for easy generation of synonymous human DNA protein coding sequences, is described. Synonymous Mutation Generator receives a user input sequence of human DNA and outputs a DNA sequence that codes for the same amino acids but has a different coding sequence. The resulting output DNA can be cloned to generate a protein-coding DNA construct whose mRNA product will be resistant to RNAi that target the original DNA sequence. Synonymous Mutation Generator should be useful for researchers who use RNAi and want to implement RNAi knockdown and rescue experiments.

Abbreviations used

CAI: codon adaptation index
shRNA: small hairpin RNA
siRNA: short interfering RNA
RNAi: RNA interference
UTR: untranslated region of mRNA

Acknowledgements

Any opinions, findings, and conclusions or recommendations expressed in this material are those of the authors and do not necessarily reflect the views of the funders, including the National Institutes of Health and the National Science Foundation. This work was supported by a NIH-NIGMS Ruth L. Kirschstein National Research Service Award GM007185, a National Science Foundation Graduate Research Fellowship DGE-1650604, and a Whitcome Pre-doctoral Fellowship in Molecular Biology from the UCLA MBI to J.Y.O. Figure 2 was created with BioRender.com. The author also acknowledges support from National Science Foundation grant MCB1912837.

The author has no competing interests.

References

1. Torres, J. Z. *et al.* The STARD9/Kif16a Kinesin Associates with Mitotic Microtubules and Regulates Spindle Pole Assembly. *Cell* **147**, 1309–1323 (2011).
2. Neumann, B. *et al.* Phenotypic profiling of the human genome by time-lapse microscopy reveals cell division genes. *Nature* **464**, 721–727 (2010).

3. Huang, C. *et al.* Identification of XBP1-u as a novel regulator of the MDM2/p53 axis using an shRNA library. *Sci. Adv.* **3**, e1701383 (2017) PMID: 29057323.
4. Tschöp, K. *et al.* A kinase shRNA screen links LATS2 and the pRB tumor suppressor. *Genes Dev.* **25**, 814–830 (2011) PMID: 21498571.
5. Wilson, R. C. & Doudna, J. A. Molecular mechanisms of RNA interference. *Annu. Rev. Biophys.* **42**, 217–239 (2013) PMID: 23654304.
6. Davidson, B. L. & McCray, P. B. Current prospects for RNA interference-based therapies. *Nature Reviews Genetics* vol. 12 329–340 (2011) PMID: 21499294.
7. Diaz□Martinez, L. A. *et al.* Genome□wide si RNA screen reveals coupling between mitotic apoptosis and adaptation . *EMBO J.* **33**, 1960–1976 (2014) PMID: 25024437.
8. Agarwal, S. *et al.* Cdt1 stabilizes kinetochore–microtubule attachments via an Aurora B kinase–dependent mechanism. *J. Cell Biol.* **217**, 3446–3463 (2018) PMID: 30154187.
9. Chatterjee, P. *et al.* Otoferlin Deficiency in Zebrafish Results in Defects in Balance and Hearing: Rescue of the Balance and Hearing Phenotype with Full-Length and Truncated Forms of Mouse Otoferlin. *Mol. Cell. Biol.* **35**, 1043–1054 (2015) PMID: 25582200.
10. Guo, J. *et al.* The transmembrane nucleoporin Pom121 ensures efficient HIV-1 pre-integration complex nuclear import. *Virology* **521**, 169–174 (2018) PMID: 29957337.
11. Karnik, A., Karnik, R. & Grefen, C. SDM-Assist software to design site-directed mutagenesis primers introducing ' silent' restriction sites. *BMC Bioinformatics* **14**, (2013) PMID: 23522286.
12. Redemann, S. *et al.* Codon adaptation-based control of protein expression in C. elegans. *Nat. Methods* **8**, 250–252 (2011) PMID: 21278743.
13. Massengill, M. T., Young, B. M., Lewin, A. S. & Ildefonso, C. J. Co-delivery of a Short-Hairpin RNA and a shRNA-resistant replacement gene with adeno-associated virus: An allele-independent strategy for autosomal-dominant retinal disorders. in *Methods in Molecular Biology* vol. 1937 235–258 (Humana Press Inc., 2019). PMID: 30706401.
14. Saxena, S., Jónsson, Z. O. & Dutta, A. Small RNAs with Imperfect Match to Endogenous mRNA Repress Translation. *J. Biol. Chem.* **278**, 44312–44319 (2003) PMID: 12952966.
15. Nakamura, Y., Gojobori, T. & Ikemura, T. Codon usage tabulated from international DNA sequence databases: Status for the year 2000. *Nucleic Acids Research* vol. 28 292 (2000) PMID: 10592250.
16. Fu, J., Dang, Y., Counter, C. & Liu, Y. Codon usage regulates human KRAS expression at both transcriptional and translational levels. *J. Biol. Chem.* **293**, 17929–17940 (2018) PMID: 30275015.
17. Langer, S. *et al.* The E3 Ubiquitin-Protein Ligase Cullin 3 Regulates HIV-1 Transcription. *Cells* **9**, (2020) PMID: 32882949.
18. Sahay, G. *et al.* Efficiency of siRNA delivery by lipid nanoparticles is limited by endocytic recycling. *Nat. Biotechnol.* **31**, 653–658 (2013) PMID: 23792629.
19. Gasteiger, E. *et al.* ExPASy: The proteomics server for in-depth protein knowledge and analysis. *Nucleic Acids Res.* **31**, 3784–3788 (2003) PMID: 12824418.
20. Sievers, F. & Higgins, D. G. Clustal Omega for making accurate alignments of

many protein sequences. *Protein Sci.* **27**, 135–145 (2018) PMID: 28884485.
21. Gruber, A. R., Lorenz, R., Bernhart, S. H., Neuböck, R. & Hofacker, I. L. The Vienna RNA websuite. *Nucleic Acids Res.* **36**, W70–W74 (2008) PMID: 18424795.
22. Soemedi, R. *et al.* The effects of structure on pre-mRNA processing and stability. *Methods* vol. 125 36–44 (2017) PMID: 28595983.
23. Brunak, S., Engelbrecht, J. & Knudsen, S. Prediction of human mRNA donor and acceptor sites from the DNA sequence. *J. Mol. Biol.* **220**, 49–65 (1991) PMID: 2067018.
24. Sharp, P. M. & Li, W. H. The codon adaptation index-a measure of directional synonymous codon usage bias, and its potential applications. *Nucleic Acids Res.* **15**, 1281–1295 (1987) PMID: 3547335.
25. Elbashir, S. M., Martinez, J., Patkaniowska, A., Lendeckel, W. & Tuschl, T. Functional anatomy of siRNAs for mediating efficient RNAi in Drosophila melanogaster embryo lysate. *EMBO J.* **20**, 6877–6888 (2001) PMID: 11726523.
26. Li, C. *et al.* FastCloning: A highly simplified, purification-free, sequence- and ligation-independent PCR cloning method. *BMC Biotechnol.* **11**, 92 (2011) PMID: 21992524.
27. Jacobus, A. P. & Gross, J. Optimal Cloning of PCR Fragments by Homologous Recombination in Escherichia coli. *PLoS One* **10**, e0119221 (2015).

Supporting information

Table 1. Alternative Codon Dictionary. Gives the codon, corresponding amino acid, and the determined alternative codon used by Synonymous Mutation Generator.

Table 2. Worked examples for Synonymous Mutation Generator. Includes a total of 4 examples: (1) three shRNAs from Sigma Mission shRNA collection against Lamin A (*LMNA*), (2) five shRNAs from the Dharmacon GIPZ shRNA collection against microtubule severing enzyme katanin subunit A1 (*KATNA1*), (3) three siRNAs against E3 ubiquitin ligase Cullin 3 (*CUL3*), and (4) four siRNAs against cholesterol trafficking membrane protein NPC1 (*NPC1*).

Appendix Chapter 5: Leukemia cell cycle chemical profiling identifies the G2-phase leukemia specific inhibitor leusin-1

This chapter is reproduced from

> Xiaoyu Xia, Yu-Chen Lo, Ankur A. Gholkar, Silvia Senese, Joseph Y. Ong, Erick F. Velasquez, Robert Damoiseaux, Jorge Z. Torres. Leukemia Cell Cycle Chemical Profiling Identifies the G2-phase Leukemia Specific Inhibitor Leusin-1. ACS Chem Biol. 2019 May 17;14(5):994-1001. doi: 10.1021/acschembio.9b00173 PMID:31046221

This chapter describes my work in characterizing a small molecule inhibitor of cell growth, Leusin-1. Determining the target of small molecules has been an interesting question in my PhD research experience. In collaboration with the Backus lab at UCLA, we are also working to determine the target and mechanism of some cysteine-reactive compounds. In particular, the compounds of interest can react with Cys of some proteins, and these reacted proteins are then targeted for degradation, presumably through proteasomal degradation. The working model behind the Backus lab project is quite interesting: a protein of interest (whether the SARS-CoV-2 protein nsp14 or the human proteins Nup153, Aurora Kinase A, or PCMT1) reacts with the compound, the compound acts as a molecular glue to recruit an E3 ubiquitin ligase (perhaps HUWE1), and the protein is ubiquitylated and degraded. We can observe a number of cell division related defects when we add these drugs in cells: namely, depending on the drug, we observe monopolar spindles, poor spindle separation and poor establishment of spindle bipolarity, and multipolar spindle formation and PCM fragmentation. Altogether, working with and studying these small molecules has been a fascinating aspect of my PhD experience.

ACS chemical biology

Articles

Cite This: ACS Chem. Biol. 2019, 14, 994−1001

pubs.acs.org/acschemicalbiology

Leukemia Cell Cycle Chemical Profiling Identifies the G2-Phase Leukemia Specific Inhibitor Leusin-1

Xiaoyu Xia,[†] Yu-Chen Lo,[†,‡] Ankur A. Gholkar,[†] Silvia Senese,[†] Joseph Y. Ong,[†] Erick F. Velasquez,[†] Robert Damoiseaux,[§,∥] and Jorge Z. Torres[*,†,⊥,#]

[†]Department of Chemistry and Biochemistry, [‡]Program in Bioengineering, [§]Department of Molecular and Medical Pharmacology, [∥]California NanoSystems Institute, [⊥]Jonsson Comprehensive Cancer Center, and [#]Molecular Biology Institute, University of California, Los Angeles, California 90095, United States

Supporting Information

ABSTRACT: Targeting the leukemia proliferation cycle has been a successful approach to developing antileukemic therapies. However, drug screening efforts to identify novel antileukemic agents have been hampered by the lack of a suitable high-throughput screening platform for suspension cells that does not rely on flow-cytometry analyses. We report the development of a novel leukemia cell-based high-throughput chemical screening platform for the discovery of cell cycle phase specific inhibitors that utilizes chemical cell cycle profiling. We have used this approach to analyze the cell cycle response of acute lymphoblastic leukemia CCRF-CEM cells to each of 181420 druglike compounds. This approach yielded cell cycle phase specific inhibitors of leukemia cell proliferation. Further analyses of the top G2-phase and M-phase inhibitors identified the leukemia specific inhibitor 1 (Leusin-1). Leusin-1 arrests cells in G2 phase and triggers an apoptotic cell death. Most importantly, Leusin-1 was more active in acute lymphoblastic leukemia cells than other types of leukemias, non-blood cancers, or normal cells and represents a lead molecule for developing antileukemic drugs.

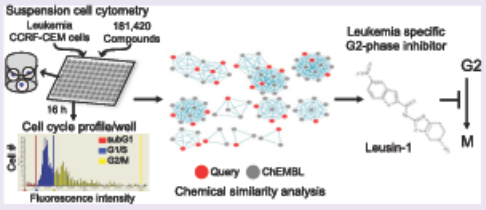

Acute lymphoblastic leukemia (ALL) originates from single B- or T-lymphocyte progenitors that proliferate and accumulate, resulting in the suppression of normal hematopoesis.[1] The disease is most common in children but can occur in any age group.[1] A successful strategy in the treatment of leukemias has been to inhibit leukemia cell proliferation by targeting DNA synthesis, protein synthesis, cell cycle progression, and proliferation-promoting signaling cascades.[1] Although some antileukemic drugs have been successful at treating specific types of leukemias, most have limited efficacies, mainly due to leukemia cell drug resistance mechanisms, a lack of specificity, and toxic side effects.[2−5] Therefore, there is a critical need to identify novel antileukemic drugs with improved chemical properties and efficacy.

Leukemia drug discovery studies have mainly relied on predefined targets identified by genetic abnormalities, differential gene expression, or protein abundance between normal and disease states.[4,7] Traditional target-based drug discovery is then used to identify inhibitors of these targets.[8] However, this process often relies on *in vitro* activity assays, and candidate inhibitors identified using this approach are frequently not cell-permeable, lose their activity, or have unintended consequences within the context of the cell, primarily due to off-target effects.[9] As an alternative approach, chemical genetic drug discovery approaches have utilized cell-based assays to identify anticancer agents, which has been highly successful with adherent cancer cells.[9] However, the difficulty in utilizing suspension cells for high-throughput chemical screens has hampered the progress in identifying novel inhibitors of bloodborne cancers. Therefore, only a limited number of compounds have been tested for their anticancer activities on human acute myeloid leukemia or lymphoma cells.[10,11] For example, flow-cytometry-based approaches have been used to develop leukemia cell cycle profile responses to compounds.[11] However, these approaches were time-consuming, expensive, and not amenable to high-throughput screening (only capable of processing ∼1000 compounds/day).[11] As an alternative, end point cell viability assays like Alamar Blue staining have been used to identify compounds that inhibit leukemia cell proliferation.[10] However, these approaches lack critical information with regard to the phase of the cell cycle in which these compounds are active that could inform their mechanism of action.[10]

Here, we report the development and application of a novel leukemia suspension cell-based high-throughput chemical screening approach for leukemia cell cycle profiling and antileukemic drug discovery. This approach has practical advantages over previous leukemia drug screening approaches, which include the saving of time and money and compatibility with current screening platforms that are used for adherent cell

Received: March 4, 2019
Accepted: May 2, 2019
Published: May 2, 2019

DOI: 10.1021/acschembio.9b00173
ACS Chem. Biol. 2019, 14, 994−1001

chemical screening. This approach is capable of generating a cell cycle profile response for each test compound and allows for easy comparison and ranking of compounds based on leukemia cell responses. Using this approach, we identified novel G1/S-, G2-, and M-phase specific leukemia inhibitors with diverse chemotypes. Importantly, we discovered and characterized the leukemia specific inhibitor 1 (Leusin-1), which specifically arrests leukemia cells during G2 phase and triggers an apoptotic cell death. Leusin-1 showed specificity toward acute lymphoblastic leukemia cells compared to other types of leukemias, nonbloodborne cancers, or normal cells and represents a lead molecule for antileukemic drug development.

RESULTS AND DISCUSSION

Discovery of Leukemia Cell Cycle Modulators. The limited efficacy, lack of specificity, and toxic side effects of current antileukemic drugs[2−5] inspired us to establish an integrated high-throughput suspension cell-based strategy for identifying small molecule cell cycle modulators for use in dissecting the mechanisms of leukemia cell proliferation and for the development of novel leukemia therapies (Figure 1A). Briefly, human CCRF-CEM acute lymphoblastic leukemia (ALL) cells were plated into 384-well plates. A diverse compound library (181420 small druglike molecules) encompassing a broad chemical space was used to place one compound per well at a final concentration of 10 μM. The cells were fixed 16 h later and stained with the DNA-selective stain Vybrant DyeCycle Green, which emits a fluorescent signal when exited at 488 nm that is proportional to the DNA mass of a cell. Plates were then scanned with an Acumen eX3 fluorescence microplate cytometer using its 488 nm laser, and a cell cycle histogram profile was generated for each compound (Figure 1A). Cell cycle profiles were ranked according to percent G1/S-phase arrest and percent G2/M-phase arrest (Figure 1B,C and Table S1). An example of a compound from each class and its associated cell cycle profile are shown in panels D and E of Figure 1. Compounds that arrested cells in G1/S phase with >2 standard deviations (SDs) from the dimethyl sulfoxide (DMSO) control or in G2/M phase with >80% of the Taxol control were retested in triplicate to confirm their bioactivity. In total, 30 G1/S-phase and 471 G2/M-phase inhibitors were reconfirmed and accounted for an overall hit rate of 0.28% (Figure 1F and Table S1).

Antileukemic Compound Chemical Analysis. The chemical structures and potential targets of the G1/S-phase and G2/M-phase hit antileukemic compounds were analyzed using CSNAP (Chemical Similarity Network Analysis Pull-down), a recently developed computational compound target inference approach based on chemical similarity networks.[12−15] Specifically, CSNAP compared hit compounds to compounds with annotated targets from the ChEMBL database that shared a high degree of chemical similarity (see Methods for similarity search parameters). The annotated and hit compounds were then ordered into chemical similarity networks where nodes represented compounds and edges represented compound similarities. Using a similarity threshold of 0.6, previously determined to be the optimal threshold for clustering six known drug classes into separate subnetworks from a training compound set,[12] the networks were further partitioned into multiple subnetworks that shared similar chemotypes. The chemical similarity networks were used to predict the targets of query compounds based on a nearest-

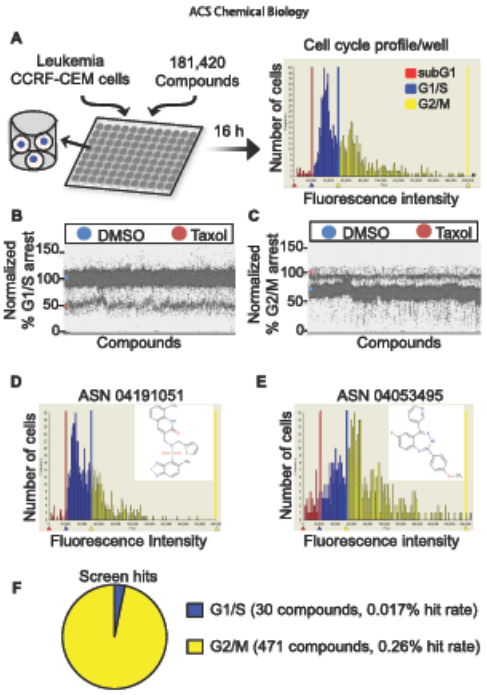

Figure 1. Overview of the leukemia suspension cell-based high-throughput cell cycle profiling chemical screening approach and summary of screening results. (A) Summary of the screening approach in which leukemia CCRF-CEM cells were treated with each of 181420 compounds (at 10 μM) for 16 h. Cells were then fixed and stained with Vybrant DyeCycle Green, and a cytometer was used to generate a cell cycle profile for each compound on the basis of the fluorescence intensity that is proportional to a cell's DNA mass. The fluorescence intensity is in arbitrary units (x-axis), and the total number of cells is on the y-axis. (B and C) Graphs show the percent G1/S-phase and G2/M-phase arrest (y-axis) for each of the 181420 compounds (x-axis). The cutoffs for G1/S-phase inhibitors was set at >2 SDs from the average of the DMSO controls. The cutoff for G2/M-phase inhibitors was set at >80% of the Taxol positive control average. (D and E) Examples of compounds arresting the cell cycle in G1/S phase and G2/M phase and their cell cycle profiles. (F) Summary of screen hits. In total, 30 G1/S-phase inhibitors and 471 G2/M-phase inhibitors were identified with an overall 0.28% hit rate. For panels B−F, see also Table S1.

neighbor scoring function, S-score, that ranks the frequency of targets from annotated compounds in the neighborhood of each query.[16] For our analysis, we generated two chemical similarity networks that corresponded to G1/S- and G2/M-phase networks (Figure 2A,B and Table S2). We visualized the number of predicted targets observed in each cell cycle phase using a heat map in which the color intensity was scaled and normalized according to the S-score of each target (Figure 2C,D and Table S2). Furthermore, we identified the most abundant targets by determining the accumulated S-score ($\sum S$-Score) across both G1/S- and G2/M-phase compounds (Figure 2C,D and Table S2). This analysis grouped the 30 G1/

DOI: 10.1021/acschembio.5b00173
ACS Chem. Biol. 2019, 14, 994−1001

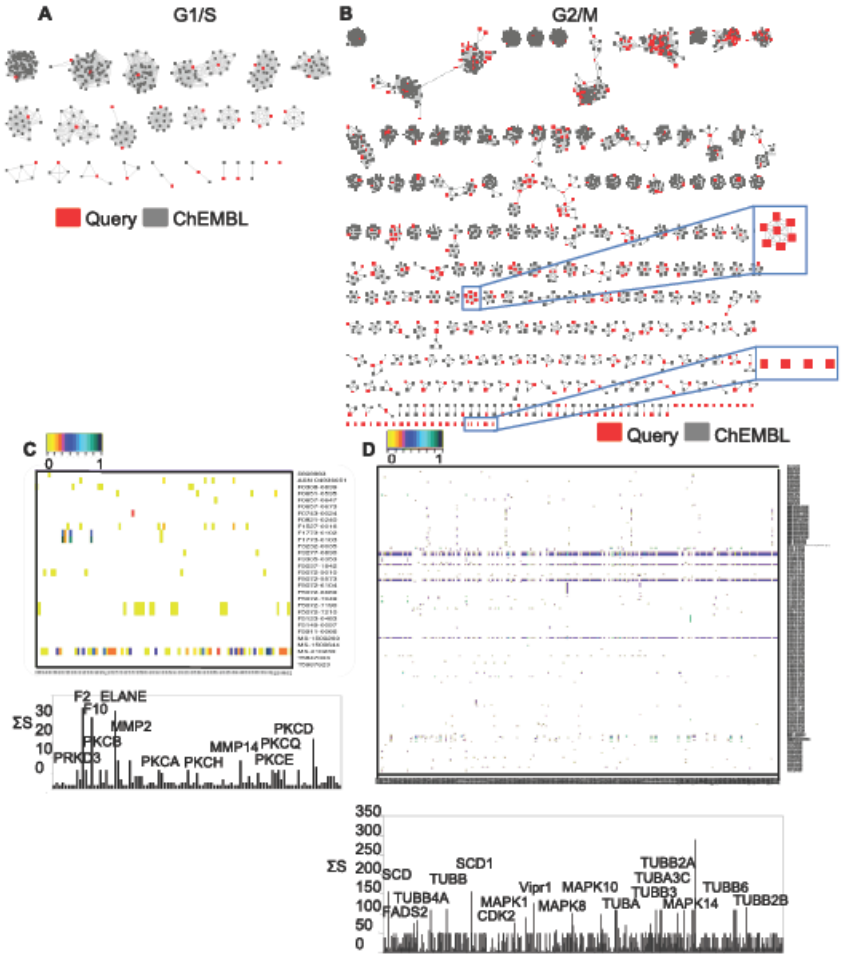

Figure 2. Chemical analysis of leukemia G1/S-phase and G2/M-phase specific inhibitors. (A) CSNAP chemical similarity network of G1/S-phase inhibitors. Note that these compounds are organized into 25 chemotypic clusters and two compounds remained orphaned. Query compounds are colored red, and ChEMBL compounds gray. (B) CSNAP chemical similarity network of G2/M-phase inhibitors. These compounds are organized into 96 chemotypic clusters, and 45 compounds remained orphaned. Query compounds are colored red, and ChEMBL compounds gray. (C and D) Heat map summaries of CSNAP *S*-scores, scaled from 0 to 1. The cumulative *S*-score ($\sum S$-score) of each assigned target in the target spectrum and the major predicted targets and off-targets are indicated. For panels A–D, see also Table S2.

S-phase compounds into 25 chemotype clusters and the 471 G2/M-phase compounds into 96 chemotype clusters (Figure 2A,B and Table S2). The top predicted targets for G1/S-phase inhibitors were proteins involved in signaling pathways that promote cell growth and proliferation (Figure 2C and Table S2). The top predicted targets for G2/M-phase inhibitors were tubulin isoforms (Figure 2D and Table S2). Because of our interest in cell division, we sought to analyze the G2/M-phase network further. However, due to the overabundance of screening campaigns aimed at discovering microtubule-targeting agents, we eliminated all chemotype clusters that were predicted to be targeting microtubules (α/β-tubulin) from further consideration. This resulted in four remaining chemotype clusters and 45 orphan compounds that did not share significant chemical similarity with other compounds in the ChEMBL database (for example, see the boxed compounds in Figure 2B). Two compounds from each novel chemotype cluster and the 45 orphan compounds (total of 53 compounds) were selected, resynthesized, and subjected to further evaluation in secondary assays (Table S3).

G2/M-Phase Antileukemic Compound Potency. To assess the potential of the 53 selected compounds as antileukemic agents, we tested them for their ability to inhibit CCRF-CEM ALL cell viability. For viability assays, cells were

DOI: 10.1021/acschembio.5b00173
ACS Chem. Biol. 2019, 14, 994–1001

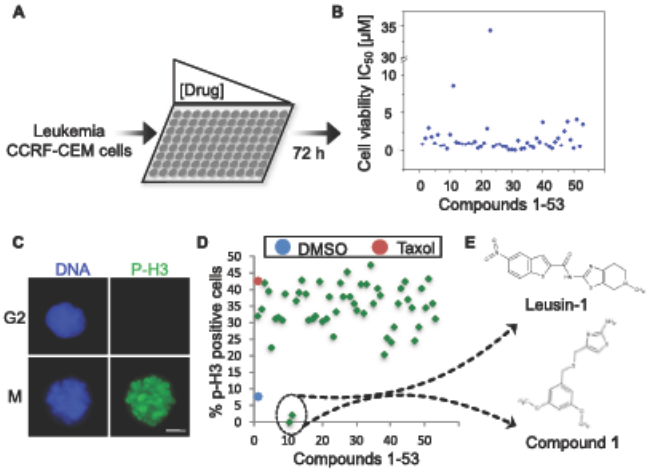

Figure 3. Leukemia G2/M-phase inhibitor potency. (A) CCRF-CEM cells were treated with increasing concentrations (from 95.37 pM to 50 μM) of each compound for 72 h, and the cell viability was assessed using the CellTiter-Glo assay. (B) Summary graph showing the cell viability IC_{50} of each compound (x-axis) on a micromolar scale (y-axis). Note that 53 compounds have an IC_{50} of <5 μM. See also Table S3. (C) Assay for measuring the percentage of mitotic cells. Cells were stained with Hoechst 33342 DNA dye (to measure total cells) and Alexa Fluor 488-pH3 antibodies (to measure the number of mitotic cells). The scale bar indicates 5 μm. (D) Summary of the percentage of cells in mitosis (y-axis) for each of the 53 compounds (x-axis). (E) Chemical structures of Leusin- I and compound 1 G2-phase inhibitors.

treated with each compound for 72 h, and their viability was measured using the CellTiter-Glo luminescent cell viability assay (Promega), which measures total ATP levels (indicative of metabolically active cells) using a luminometer at a wavelength of 560 nm (Figure 3A,B). These assays were carried out in triplicate with a 20-step series of 2-fold dilutions (from 50 μM to 95.37 pM) for each compound, and their cell viabilities, IC_{50} (half-maximal inhibitory concentration), were derived (Figure 3B and Table S3). This analysis revealed that most compounds (51) had an IC_{50} of <5 μM (Figure 3B and Table S3).

Multiparametric Phenotypic Analysis of Leukemia G2/M-Phase Inhibitors. To further explore the mechanism of action of G2/M-phase inhibitors, we analyzed the cellular response of cells to these inhibitors by immunofluorescence (IF) microscopy. Due to the difficulty in performing IF microscopy on CCRF-CEM cells, HeLa cells were treated with each of the 53 compounds at a concentration corresponding to their CCRF-CEM cell viability (IC_{90}) for 16 h. Cells were then fixed, permeabilized, co-stained for DNA and α-tubulin, and imaged at 63× magnification. Surprisingly, 51 compounds arrested cells with depolymerized microtubules, indicating that they represented novel chemotypes that were targeting microtubules (Table S3). Consistently, staining of the cells with a FITC fluorescently labeled antibody that recognizes the mitotic marker phosphorylated histone H3 (p-H3[17,18]) indicated that 51 compounds had an increased percentage of cells arrested in mitosis [% mitotic cells = (number of p-H3 positive cells)/(total number of cells that stained positive with the Hoechst 33342 DNA dye)] compared to controls (Figure 3C,D). However, *N*-(5-methyl-4,5,6,7-tetrahydrothiazolo[5,4-*c*]pyridin-2-yl)-5-nitrobenzo[*b*]thiophene-2-carboxamide hydrochloride [leukemia specific inhibitor 1 (Leusin-1)] and 4-{[(3,5-dimethoxybenzyl)thio]methyl}thiazol-2-amine (compound 1) induced a decrease in the percentage of mitotic cells (Figure 3D,E and Table S3). In HeLa cells, Leusin-1 and compound 1 had no effect on the interphase microtubule cytoskeletal network or the mitotic microtubule spindle, even at the high concentration of 137 μM for Leusin-1 or 180 μM for compound 1 (Figure 4A and Figure S1). Further testing of Leusin-1 and compound 1, using an *in vitro* microtubule polymerization assay, showed that they had no effect on microtubule polymerization, similar to the DMSO control (Figure 4B). In contrast, Taxol increased the rate of microtubule polymerization, whereas colchicine and nocodazole abolished microtubule polymerization (Figure 4B). However, compound 1 proved to be an unstable compound and lost activity over time in suspension. Therefore, we selected Leusin-1 for further analysis on the basis of its novel chemotype, its stable biochemical properties, and its inhibition of leukemia cell division through a G2-phase arresting and non-microtubule targeting mechanism. To further verify that Leusin-1 was a G2-phase inhibitor, we treated CCRF-CEM cells with thymidine (G1/S-phase arrest), Taxol (M-phase arrest), RO-3306 (G2-phase arrest[19]), or Leusin-1 and analyzed the status of cell cycle biochemical markers by immunoblot analysis. Consistently, Taxol, RO-3306, and Leusin-1 arrested cells with lower levels of Cyclin E (levels peak at G1/S phase) and increased levels of Cyclin B (levels peak at G2/M phase) (Figure 4C). However, unlike Taxol, RO-3306 and Leusin-1 also arrested cells with lower levels of p-H3 (present in only M phase) and increased levels of Cyclin A (levels peak in G2 phase) (Figure 4C). Additionally, flow-cytometry analyses of CCRF-CEM cells treated with either DMSO, nocodazole, or Leusin-1 showed that Leusin-1 was arresting cells in G2/M phase (Figure S2). Together, these

DOI: 10.1021/acschembio.5b00173
ACS Chem. Biol. 2019, 14, 994−1001

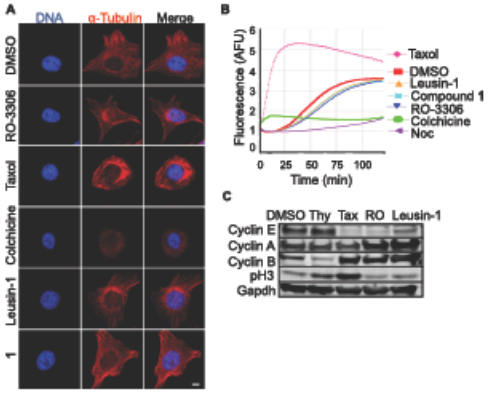

Figure 4. Leusin-1 and compound 1 do not target tubulin. (A) Immunofluorescence microscopy of HeLa cells treated with DMSO, Leusin-1 (137 μM), compound 1 (180 μM), Taxol (100 nM), colchicine (366 nM), or RO-3306 (10 μM) for 3 h and co-stained for α-tubulin (anti-α-tubulin antibodies, red) and DNA (Hoechst 33342, blue). The scale bar indicates 10 μm. For a summary of phenotypic classification for all 53 G2/M-phase inhibitors, see Table S3. (B) Summary of *in vitro* microtubule polymerization reactions in the presence of DMSO or 3 μM Leusin-1, compound 1, colchicine, nocodazole, RO-3306, or Taxol. Note that Leusin-1 and compound 1 have no effect on microtubule polymerization. The time is in minutes (x-axis), and AFU denotes arbitrary fluorescence units (y-axis). (C) CCRF-CEM cells were treated with DMSO, thymidine (2 mM), Taxol (100 nM), RO-3306 (10 μM), or Leusin-1 (5 μM) for 24 h. Extracts were prepared and immunoblotted for Cyclin A, B, and E and for the phospho-histone H3 (p-H3 ser10) marker of mitotic cells. Note that Leusin-1-treated cells have low p-H3 and stabilized Cyclin A and B levels, indicative of a failure to enter mitosis, similar to RO-3306. In contrast, Taxol-treated cells arrest in mitosis with high levels of p-H3 and Cyclin A levels are lower.

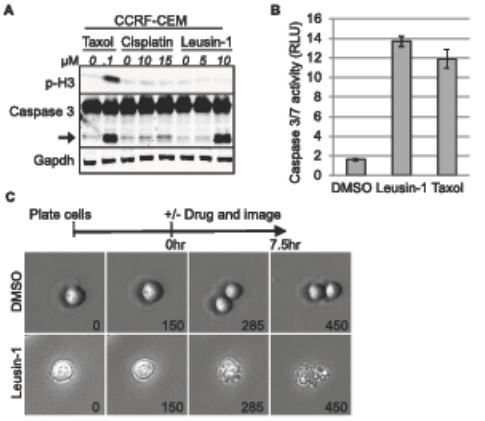

Figure 5. Leusin-1 arrests cells in G2 phase and triggers an apoptotic cell death. (A) CCRF-CEM cells were treated with DMSO or the indicated concentrations of Leusin-1, Taxol, or cisplatin for 48 h. Extracts were prepared and immunoblotted for p-H3, caspase-3, and Gapdh. Note that Leusin-1- and cisplatin-treated cells have low p-H3 levels, indicative of a failure to enter mitosis. In contrast, Taxol-treated cells arrest in mitosis with high levels of p-H3. Also note that Leusin-1 and Taxol treatment led to caspase-3 cleavage (the cleaved product is labeled with an arrow). (B) CCRF-CEM cells were treated with DMSO, Leusin-1 (5 μM), or Taxol (100 nM) for 48 h, and the caspase-3/7 activity was quantified using the Caspase-Glo luminescent caspase activity assay. RLU indicates relative light units. Data are presented as the average ± SDs. Note that Leusin-1 induced caspase-3/7 activation, similar to Taxol, indicative of apoptosis. (C) Live-cell time-lapse microscopy of CCRF-CEM cells treated with DMSO or Leusin-1 (5 μM). Note that Leusin-1-treated cells fail to divide and undergo apoptosis.

data indicated that Leusin-1 was arresting CCRF-CEM cells specifically in G2 phase through a nonmicrotubule targeting mechanism.

Leusin-1 Arrests Cells in G2 Phase and Triggers an Apoptotic Cell Death. To determine the consequences of arresting cells in G2 phase with Leusin-1, we analyzed the biochemical response of cells treated with Leusin-1. CCRF-CEM cells were treated with Leusin-1, cisplatin (G2-phase inhibitor), or Taxol (M-phase inhibitor), and protein extracts were prepared after 48 h. Consistent with our previous data, immunoblot analyses of protein samples using antibodies directed against p-H3 (phosphorylated in mitosis) indicated that Leusin-1 and cisplatin arrested cells with limited p-H3 staining, indicative of a G2-phase arrest, whereas Taxol arrested cells with increased p-H3 levels, indicative of a M-phase arrest (Figure 5A). Interestingly, Leusin-1 induced the cleavage of caspase-3, indicative of apoptotic pathway activation (Figure 5A). These data indicated that Leusin-1 arrested cells prior to mitosis and triggered an apoptotic cell death. To further test this, CCRF-CEM cells were treated with DMSO, Leusin-1, or Taxol for 48 h and the extent of caspase-3/7 activation was measured using the Caspase-Glo luminescent caspase activity assay.[20] This assay revealed that Leusin-1 was indeed inducing an apoptotic cell death similar to that seen with Taxol treatment (Figure 5B). Next, we performed live-cell time-lapse microscopy on CCRF-CEM cells treated with DMSO or Leusin-1. DMSO-treated cells were able to divide normally, whereas Leusin-1-treated cells never divided and eventually underwent apoptosis (Figure 5C and Movies S1 and S2). Together, these data indicated that Leusin-1 was arresting cells in G2 phase and triggering an apoptotic cell death.

Leusin-1 Is an ALL Specific Inhibitor. To determine whether Leusin-1 was active against a broad array of cancers or was specific for leukemias, we treated a diverse panel of cancer cell lines and normal cell lines with Leusin-1 for 72 h. These included cervical adenocarcinoma (HeLa), breast adenocarcinoma (MCF-7), melanoma (M233), osteosarcoma (U-2 OS), lung adenocarcinoma (NCI-H560), acute lymphoblastic leukemia (CCRF-CEM), retinal pigment epithelial (hTERT-RPE), lymphoma (Jeko-1), and colorectal carcinoma (HCT 116) cells. Cell viability IC_{50} was then quantified and compared to that of the DMSO control (Figure 6A). Interestingly, Leusin-1 showed specificity for CCRF-CEM cells compared to all other adherent types of cancers (CCRF-CEM cell viability IC_{50} for Leusin-1 = 2.64 μM compared to values 4–50-fold higher for all other cell lines) (Figure 6A). To determine if Leusin-1 was active against all leukemias (non-adherent cells) or only a subset of leukemias, we analyzed the efficacy of Leusin-1 on a panel of leukemia cell lines. These included acute lymphoblastic leukemia (ALL; CCRF-CEM

DOI: 10.1021/acschembio.5b00173
ACS Chem. Biol. 2019, 14, 994–1001

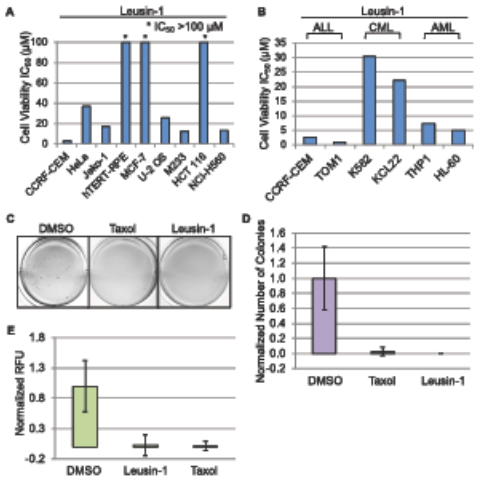

Figure 6. Leusin-1 inhibits ALL proliferation. (A) A broad panel of cancer cell lines was treated with increasing concentrations of Leusin-1 for 72 h, and their cell viability IC_{50} was assessed using the CellTiter-Glo assay. The graph shows the summary of results for cell viability IC_{50} (*y*-axis) for each cell line (*x*-axis). (B) A panel of leukemia cells were treated with increasing concentrations of Leusin-1, and cell viability IC_{50} (*y*-axis) was determined for each cell line (*x*-axis): ALL (CCRF-CEM and TOM1), AML (HL-60 and THP1), and CML (K562 and KCL22). (C and D) ALL clonogenic assay. ALL CCRF-CEM cells were treated with DMSO, Leusin-1 (2 μM), or Taxol (50 nM) for 3 weeks, and the percent colony formation, normalized to DMSO, was quantified. Data are represented as the average percent ± SDs. (E) ALL transformation assay. ALL CCRF-CEM cells were treated with DMSO, Leusin-1 (2 μM), or Taxol (50 nM) for 7 days, and the total fluorescence was quantified. Data are represented as the average percent ± SDs.

and TOM1), acute myeloid leukemia (AML; HL-60 and THP1), and chronic myeloid leukemia (CML; K562 and KCL22) cell lines. Surprisingly, ALL cell lines were the most sensitive to Leusin-1 (CCRF-CEM IC_{50} = 2.66 μM and TOM1 IC_{50} = 0.877 μM, compared to values of 5−30 μM for all other leukemia cell lines) (Figure 6B). These results indicated that Leusin-1 was most potent against acute lymphoblastic leukemias.

Leusin-1 Inhibits ALL Colony Formation. Next, we assessed the ability of Leusin-1 to inhibit CCRF-CEM colony formation using two separate clonogenic assays (Figure 6C−E). First, an agar-based colony formation assay was performed in the presence of DMSO, Taxol, or Leusin-1; colony formation was visualized with crystal violet stain, and the total number of colonies was quantified. Interestingly, Leusin-1 was able to inhibit colony formation like Taxol (Figure 6C,D). Next, we analyzed the effect of Leusin-1 on colony formation using the CytoSelect Cell Transformation Assay kit (Cell Biolabs, Inc.), which measures the total number of viable cells in agar solutions. Consistently, Leusin-1 inhibited colony formation like Taxol (Figure 6E). Together, these data indicated that Leusin-1 was inhibiting CCRF-CEM colony formation.

Conclusions. Cell cycle checkpoints ensure that the progression of the cell cycle from one phase to another is regulated with precision and occurs with high fidelity.[21] Dysregulation of the G1/S-, S-, G2-, and M-phase cell cycle checkpoints can lead to abnormal cell proliferation and carcinogenesis.[21] A strategy for developing leukemia therapeutics has been to develop inhibitors that perturbed the cell cycle and lead to a cell cycle arrest and subsequent apoptotic cell death.[22,23] However, the difficulty of analyzing the cell cycle response of suspension cells to chemical treatments has hampered leukemia cell-based high-throughput drug discovery efforts. Although a limited number of compounds have been screened in acute myeloid leukemia and lymphoma cells, these studies have relied on flow cytometry that is not easily amenable to high-throughput screening or on end point assays that lack critical information about the cell cycle phase where these compounds are active.[10,11] To address this, we engineered our high-throughput cell cycle profiling chemical screening platform to be compatible with suspension leukemia cells and screened 181420 druglike compounds in leukemia CCRF-CEM cells.[14] Importantly, this approach bypasses the need for flow cytometry and makes use of a laser scanning cytometer that is a staple of modern screening platforms. The use of laser scanning cytometery has the added benefits of reducing screening costs and screening run time while increasing throughput and the impact of data analyses. In comparison to end point chemical screens that use cell viability to select hit compounds, this approach provides a cell cycle profile for each drug that not only provides information about cell viability (cell death is represented by the subG1 population of cells) but also provides critical information about the cell cycle phase in which the drug is active. This additional cell cycle chemical profiling information can be used to better focus downstream experimentation to define the drug mechanism of action. Additionally, when coupled with chemical similarity analyses, like CSNAP, the cell cycle profile can be used to validate drug target predictions. For example, a hit drug predicted to be an analogue of Taxol (a known M-phase inhibitor) would be expected to have a cell cycle profile with an increased percentage of cells in M phase. Thus, this approach has several advantages that should help expedite leukemia drug discovery and characterization.

Our leukemia cell cycle chemical profiling approach yielded novel G1/S-, G2-, and M-phase specific inhibitors of acute lymphoblastic leukemia cell proliferation, which included novel chemotypes that were targeting each cell cycle phase. Although we did not pursue the M-phase microtubule-targeting agents, it is important to note that microtubule-targeting agents continue to be used broadly for the treatment of cancer and the new chemotypes discovered in this study could be used to develop more effective microtubule-targeting therapeutics.[24] Our data indicate that Leusin-1 is an exciting molecule to pursue for developing new acute lymphoblastic leukemia therapies. First, Leusin-1 potently arrests the leukemia cell cycle in G2 phase and triggers an apoptotic cell death, thereby inhibiting leukemia cell proliferation. Second, Leusin-1 is not a microtubule-targeting agent, which is often associated with numerous side effects like neurotoxicities and neutropenia.[24] Third, in comparison to other leukemia therapeutics, either in the clinic or approved for the treatment of leukemias like vinblastine by the Food and Drug Administration, Leusin-1 appears to have a greater specificity for leukemia cells (ALL in particular) compared to other cancer cell types and normal cells. This Leusin-1 specificity for acute lymphoblastic leukemias represents a vantage point for the development of

DOI: 10.1021/acschembio.5b00173
ACS Chem. Biol. 2019, 14, 994−1001

therapeutics with a more favorable therapeutic window. Future studies related to defining the Leusin-1 mechanism of action should help to elucidate the underlying sensitivity of acute lymphoblastic leukemias to Leusin-1.

METHODS

Compounds. Leusin-1 and compound 1 were purchased from Life Chemicals Inc. at >95% purity. For ^{1}H NMR of Leusin-1 and compound 1, see Figure S3.

Cell Culture. All human cell lines, with the exception of M233, were purchased from ATCC. Their identities were verified by short-tandem repeat profiling. Cells were passaged for <6 months following receipt and were maintained in 5% CO_2 at 37 °C in RPMI 1640 medium (CCRF-CEM, Jeko-1, NCI-H560, TOM1, KCL22, and THP1), DMEM/F12 (HeLa and hTERT-RPE), McCoy's 5A (U-2 OS and HCT 166), IMDM (K562 and HL-60), or EMEM (MCF-7) with 10% fetal bovine serum (FBS), 2 mM L-glutamine, and antibiotics. M233 was established from a patient biopsy under UCLA IRB Approval 02-08-067, as described previously.[25] M233 was genotyped using the Oncomap3 platform for 33 genes, Affymetrix Gene Chip for SNP, and Ion Torrent for next-generation sequencing, passaged for <6 months following verification, and maintained in RPMI 1640 medium with 10% FBS and antibiotics in 5% CO_2 at 37 °C. All media were purchased from ThermoFisher.

High-Throughput Screening. Screening conditions were as described previously,[14] with the following modifications. CCRF-CEM cells were plated in 384-well plates (1000 cells/well) and treated with 10 μM drugs for 16 h. Cells were fixed with 4% paraformaldehyde and stained with 2.5 μM Vybrant DyeCycle Green (Invitrogen) for 3 h at room temperature. Plates were scanned with an Acumen eX3 (TTP Labtech) fluorescence cytometer using its 488 nm laser, and a cell cycle histogram profile was generated for each well. For the G2/M-phase secondary screen, 16 h after the addition of the drug HeLa cells were fixed with 4% paraformaldehyde, permeabilized with 0.1% Triton X-100/phosphate-buffered saline (PBS), and stained with Alexa Fluor 488 phospho-histone-H3 (Ser10, Cell Signaling) and 0.25 μg/mL Hoechst 33342 for 1 h. Plates were washed twice with PBS using a microplate washer (BioTek) and then imaged with an ImageXpress Micro (Molecular Devices) high-content fluorescence microscope. Data analysis was performed using the CDD (Collaborative Drug Discovery) software, and outputs were exported to Excel.

Compound Potency. For cell viability IC_{50}, CCRF-CEM cells were treated with a 20-step series of 2-fold dilutions (from 50 μM to 95.37 pM). Cell viability IC_{50} was determined using the CellTiter-Glo Assay (Promega), which measures total ATP levels. Plates were read with a Tecan M1000 microplate reader at 540 nm, and CDD software was used for generating IC_{50} and IC_{90} values.

Immunofluorescence and Time-Lapse Microscopy. Immunofluorescence microscopy was carried out as described previously[26] using HeLa cells, except that images were captured with a Leica DMI6000 microscope (Leica Microsystems) and deconvolved with Leica deconvolution software. Time-lapse microscopy was performed as described previously.[17] Briefly, CCRF-CEM cells were treated with DMSO or Leusin-1 (5 μM), and 10 Z-stack images (0.9 μm steps) were captured at 15 min intervals. Images were deconvolved and converted to AVI movie files.

Apoptosis Assays. CCRF-CEM cells were treated with the indicated drugs for 48 h, and the Caspase-Glo luminescent caspase activity assay (Promega) was used to measure the activity of effector caspases, as a readout of apoptosis. Plates were scanned with a luminometer at a wavelength of 520 nm, and the apoptotic index [(total caspase activity)/(total number of cells)] per well was measured. Quantitation is in relative light units (RLU) compared to the DMSO control.

Leukemia Clonogenic Assays. Five thousand CCRF-CEM cells per well were grown in six-well plates with semisolid RPMI 1640 medium containing 10% FBS, 0.45% agarose, and drug (1% DMSO, 2 μM Leusin-1, or 50 nM Taxol). A layer of 500 μL of medium containing the corresponding drug was added on top, and plates were incubated in 5% CO_2 at 37 °C for 3 weeks. Fresh medium was replenished twice a week. Colonies (>30 cells) were scored and visualized after the addition of 0.005% crystal violet overnight.

Leukemia Cell Transformation Assay. The CytoSelect 96 Well Cell Transformation Assay kit (Cell Biolabs, Inc.) was used for assessing soft agar colony formation following the manufacturer's instructions for 7 days. Fluorescent signals from cells treated with DMSO, Leusin-1 (2 μM), or Taxol (50 nM) were normalized after subtracting the value from the no cell blank, and the mean values of the samples were plotted as relative light units (RLU).

CSNAP Chemical Analysis. CSNAP was used to predict the targets of G1/S-phase and G2/M-phase inhibitors as described previously.[12] Briefly, compounds were queried in annotated ChEMBL database version 18 using the following search parameters: Tanimoto cutoff of 0.75 and z-score cutoff of 2.5. The ChEMBL target annotations were retrieved from the database on the basis of the following criteria: confidence score of 4 and binding assay type. Finally, chemical similarity networks and ligand−target interaction fingerprints (LTIFs) were analyzed using Cytoscape and the R statistical package, respectively.

***In Vitro* Tubulin Polymerization Assays.** Tubulin polymerization reactions were carried out according to the manufacturer's instructions (Cytoskeleton, BK011P) in the presence of DMSO and 3 μM Leusin-1, compound 1, Taxol, or colchicine. Polymerization was monitored with a Tecan M1000 microplate reader at 420 nm for 120 min at 37 °C.

Antibodies. The following antibodies were used in this study: phospho-histone-H3 Alexa Fluor 488 (Ser10) (Cell Signaling, catalog no. 3465); α-tubulin (Serotec, catalog no. MCAP77G); caspase-3 (Cell Signaling Technology, catalog no. 9665); p-H3 (Cell Signaling, catalog no. 9701); Cyclin A, Cyclin B, and Cyclin E (Santa Cruz Biotechnology, catalog nos. sc-751, sc-245, and sc-481, respectively); and Gapdh (GeneTex, catalog no. GTX627408). FITC- and Cy3-conjugated secondary antibodies were from Jackson Immuno Research.

Software. The CSNAP program is available as a web server http://services.mbi.ucla.edu/CSNAP/.

Statistical Analysis. The quality of the screen was assessed by calculating the Z′ factor [Z' factor $= 1 - 3(\sigma_p + \sigma_n)/(|\mu_p - \mu_n|)$], which takes into account the dynamic range of the assay and the variance of the data.[27] The screen was performed with an average plate Z′ factor of 0.48 ± 0.06, close to the optimal performance range of 0.5−1.[27]

ASSOCIATED CONTENT

Supporting Information

The Supporting Information is available free of charge on the ACS Publications website at DOI: 10.1021/acschembio.9b00173.

Figures S1−S3, including ^{1}H NMR spectra for Leusin-1 and compound 1, and descriptions of Tables S1−S3 and Movies S1 and S2 (PDF)

Table S1 (XLSX)

Table S2 (XLS)

Table S3 (XLS)

Movie S1 (MOV)

Movie S2 (MOV)

AUTHOR INFORMATION

Corresponding Author

*Department of Chemistry and Biochemistry, UCLA, Los Angeles, CA 90095. Phone: 310-206-2092. E-mail: torres@chem.ucla.edu.

ORCID

Jorge Z. Torres: 0000-0002-2158-889X

DOI: 10.1021/acschembio.9b00173
ACS Chem. Biol. 2019, 14, 994−1001

Author Contributions

X.X. and J.Z.T. initiated the project, designed experiments, and analyzed results with input from all authors. A.A.G., S.S., J.Y.O., and E.F.V. performed biochemical and cellular assays. Y.-C.L. performed CSNAP chemical analyses. R.D. provided compound procurement and compound structure preparation.

Notes

The authors declare no competing financial interest.

■ ACKNOWLEDGMENTS

Work performed in the Molecular Screening Shared Resource was supported by the National Cancer Institute of the National Institutes of Health under Grant P30CA016042. J.Z.T. was supported by a Jonsson Cancer Center Foundation seed grant, the V Foundation for Cancer Research V Scholar Award, the Research Corporation for Science Advancement Cottrell Scholar Award, and University of California Cancer Research Coordinating Committee Funds. J.Y.O. was supported by Ruth L. Kirschstein National Research Service Award GM007185. E.F.V. was supported by a UCLA Molecular Biology Institute Whitcome Fellowship.

■ REFERENCES

(1) Pui, C. H., and Jeha, S. (2007) New therapeutic strategies for the treatment of acute lymphoblastic leukaemia. *Nat. Rev. Drug Discovery 6*, 149−165.

(2) Vagace, J. M., De la Maya, M. D., Caceres-Marzal, C., Gonzalez de Murillo, S., and Gervasini, G. (2012) Central nervous system chemotoxicity during treatment of pediatric acute lymphoblastic leukemia/lymphoma. *Critical Reviews in Oncology/Hematology 84*, 274.

(3) Shaffer, B. C., Gillet, J. P., Patel, C., Baer, M. R., Bates, S. E., and Gottesman, M. M. (2012) Drug resistance: Still a daunting challenge to the successful treatment of AML. *Drug Resist. Updates 15*, 62−69.

(4) Woessner, D. W., Lim, C. S., and Deininger, M. W. (2011) Development of an effective therapy for chronic myelogenous leukemia. *Cancer J. 17*, 477−486.

(5) Wierda, W. G., Chiorazzi, N., Dearden, C., Brown, J. R., Montserrat, E., Shpall, E., Stilgenbauer, S., Muneer, S., and Grever, M. (2010) Chronic lymphocytic leukemia: new concepts for future therapy. *Clin Lymphoma Myeloma Leuk 10*, 369−378.

(6) Iacobucci, I., Papayannidis, C., Lonetti, A., Ferrari, A., Baccarani, M., and Martinelli, G. (2012) Cytogenetic and molecular predictors of outcome in acute lymphocytic leukemia: recent developments. *Curr. Hematol Malig Rep 7*, 133−143.

(7) Kristensen, V. N., Lingjaerde, O. C., Russnes, H. G., Vollan, H. K., Frigessi, A., and Borresen-Dale, A. L. (2014) Principles and methods of integrative genomic analyses in cancer. *Nat. Rev. Cancer 14*, 299−313.

(8) Martell, R. E., Brooks, D. G., Wang, Y., and Wilcoxen, K. (2013) Discovery of novel drugs for promising targets. *Clin. Ther. 35*, 1271−1281.

(9) Cong, F., Cheung, A. K., and Huang, S. M. (2012) Chemical genetics-based target identification in drug discovery. *Annu. Rev. Pharmacol. Toxicol. 52*, 57−78.

(10) McDermott, S. P., Eppert, K., Notta, F., Isaac, M., Datti, A., Al-Awar, R., Wrana, J., Minden, M. D., and Dick, J. E. (2012) A small molecule screening strategy with validation on human leukemia stem cells uncovers the therapeutic efficacy of kinetin riboside. *Blood 119*, 1200−1207.

(11) Gasparetto, M., Gentry, T., Sebti, S., O'Bryan, E., Nimmanapalli, R., Blaskovich, M. A., Bhalla, K., Rizzieri, D., Haaland, P., Dunne, J., and Smith, C. (2004) Identification of compounds that enhance the anti-lymphoma activity of rituximab using flow cytometric high-content screening. *J. Immunol. Methods 292*, 59−71.

(12) Lo, Y. C., Senese, S., Li, C. M., Hu, Q., Huang, Y., Damoiseaux, R., and Torres, J. Z. (2015) Large-scale chemical similarity networks for target profiling of compounds identified in cell-based chemical screens. *PLoS Comput. Biol. 11*, e1004153.

(13) Lo, Y. C., Senese, S., Damoiseaux, R., and Torres, J. Z. (2016) 3D Chemical Similarity Networks for Structure-Based Target Prediction and Scaffold Hopping. *ACS Chem. Biol. 11*, 2244−2253.

(14) Senese, S., Lo, Y. C., Huang, D., Zangle, T. A., Gholkar, A. A., Robert, L., Homet, B., Ribas, A., Summers, M. K., Teitell, M. A., Damoiseaux, R., and Torres, J. Z. (2014) Chemical dissection of the cell cycle: probes for cell biology and anti-cancer drug development. *Cell Death Dis. 5*, e1462.

(15) Lo, Y. C., Senese, S., France, B., Gholkar, A. A., Damoiseaux, R., and Torres, J. Z. (2017) Computational Cell Cycle Profiling of Cancer Cells for Prioritizing FDA-Approved Drugs with Repurposing Potential. *Sci. Rep. 7*, 11261.

(16) Lo, Y. C., Rensi, S. E., Torng, W., and Altman, R. B. (2018) Machine learning in chemoinformatics and drug discovery. *Drug Discovery Today 23*, 1538−1546.

(17) Torres, J. Z., Summers, M. K., Peterson, D., Brauer, M. J., Lee, J., Senese, S., Gholkar, A. A., Lo, Y. C., Lei, X., Jung, K., Anderson, D. C., Davis, D. P., Belmont, L., and Jackson, P. K. (2011) The STARD9/Kif16a Kinesin Associates with Mitotic Microtubules and Regulates Spindle Pole Assembly. *Cell 147*, 1309−1323.

(18) Hendzel, M. J., Wei, Y., Mancini, M. A., Van Hooser, A., Ranalli, T., Brinkley, B. R., Bazett-Jones, D. P., and Allis, C. D. (1997) Mitosis-specific phosphorylation of histone H3 initiates primarily within pericentromeric heterochromatin during G2 and spreads in an ordered fashion coincident with mitotic chromosome condensation. *Chromosoma 106*, 348−360.

(19) Vassilev, L. T., Tovar, C., Chen, S., Knezevic, D., Zhao, X., Sun, H., Heimbrook, D. C., and Chen, L. (2006) Selective small-molecule inhibitor reveals critical mitotic functions of human CDK1. *Proc. Natl. Acad. Sci. U. S. A. 103*, 10660−10665.

(20) Chowdhury, I., Tharakan, B., and Bhat, G. K. (2008) Caspases - an update. *Comp. Biochem. Physiol., Part B: Biochem. Mol. Biol. 151*, 10−27.

(21) Williams, G. H., and Stoeber, K. (2012) The cell cycle and cancer. *J. Pathol 226*, 352−364.

(22) Halicka, H. D., Seiter, K., Feldman, E. J., Traganos, F., Mittelman, A., Ahmed, T., and Darzynkiewicz, Z. (1997) Cell cycle specificity of apoptosis during treatment of leukaemias. *Apoptosis 2*, 25−39.

(23) Ghelli Luserna di Rora', A., Iacobucci, I., and Martinelli, G. (2017) The cell cycle checkpoint inhibitors in the treatment of leukemias. *J. Hematol. Oncol. 10*, 77.

(24) Arnst, K. E., Banerjee, S., Chen, H., Deng, S., Hwang, D. J., Li, W., and Miller, D. D. (2019) Current advances of tubulin inhibitors as dual acting small molecules for cancer therapy. *Med. Res. Rev.*, DOI: 10.1002/med.21568.

(25) Sondergaard, J. N., Nazarian, R., Wang, Q., Guo, D., Hsueh, T., Mok, S., Sazegar, H., MacConaill, L. E., Barretina, J. G., Kehoe, S. M., Attar, N., Von Euw, E., Zuckerman, J. E., Chmielowski, B., Comin-Anduix, B., Koya, R. C., Mischel, P. S., Lo, R. S., and Ribas, A. (2010) Differential sensitivity of melanoma cell lines with BRAFV600E mutation to the specific Raf inhibitor PLX4032. *J. Transl. Med. 8*, 39.

(26) Torres, J. Z., Ban, K. H., and Jackson, P. K. (2010) A Specific Form of Phospho Protein Phosphatase 2 Regulates Anaphase-promoting Complex/Cyclosome Association with Spindle Poles. *Mol. Biol. Cell 21*, 897−904.

(27) Zhang, J. H., Chung, T. D., and Oldenburg, K. R. (1999) A Simple Statistical Parameter for Use in Evaluation and Validation of High Throughput Screening Assays. *J. Biomol. Screening 4*, 67−73.

DOI: 10.1021/acschembio.5b00173
ACS Chem. Biol. 2019, 14, 994−1001

Appendix Chapter 6: Supplemental File 1 for Chapter 2 (SPOP)

Table 1: List of plasmids

Item #	Plasmid name	Plasmid Source	Plasmid Identifier/Catalog Number
1	pDONR221 (empty vector)	Invitrogen	12536017
2	pgLAP1 (empty vector)	Addgene	Addgene Plasmid #19702
3	pCS2-3xHA (empty vector)	Torres lab (UCLA)	PMID: 26929214
4	pCS2-Myc (empty vector)	Torres lab (UCLA)	PMID: 26929214
5	pCS2-FLAG-S Tag (empty vector)	Torres lab (UCLA)	PMID: 26929214
6	pEGFPx3-Nup153	Jan Ellenberg (EMBL Heidelberg)	PMID: 11448991
7	pDONR221 Nup50 (no stop codon)	DNASU plasmid repository	HsCD00296748
8	pDONR221 KPNA6 (no stop codon)	DNASU plasmid repository	HsCD00040555
9	pCS2-3xHA Cdc20	Peter Jackson lab (Stanford University)	PMID: 15469984

10	pCS2-3xHA Plk1	Peter Jackson lab (Stanford University)	PMID: 15469984
11	pDONR223 SPOP WT	Addgene	Addgene Plasmid #81856
12	pDONR223 SPOP F102C	Addgene	Addgene Plasmid #81642
13	pDONR223 SPOP E50K	Addgene	Addgene Plasmid #81631
14	pDONR221 Nup153	This paper	
15	pDONR221 Nup50	This paper	
16	pDONR221 KPNA6	This paper	
17	pDONR221 Cdc20	This paper	
18	pDONR221 Plk1	This paper	
19	pCS2-FLAG-S Tag Cdc20	This paper	
20	pCS2-FLAG-S Tag Plk1	This paper	
21	pCS2-FLAG-S Tag Nup50	This paper	
22	pCS2-FLAG-S Tag KPNA6	This paper	
23	pCS2-FLAG-S Tag LCMT1	Torres lab (UCLA)	PMID: 25839665
24	pgLAP1 SPOP WT	This paper	
25	pgLAP1 SPOP F102C	This paper	
26	pGLAP1 SPOP E50K	This paper	
27	pCS2-FLAG-S Tag Nup153	This paper	
28	pCS2-Myc Nup153	This paper	

29	pgLAP1 Nup153 NPC (aa 1-619)	This paper
30	pgLAP1 Nup153 NPCZnF (aa 1-872)	This paper
31	pgLAP1 Nup153 ZnF (aa 620-873)	This paper
32	pgLAP1 Nup153 ZnFFG (aa 620-1475)	This paper
33	pgLAP1 Nup153 FG (aa 873-1475)	This paper
34	pCS2-FLAG-S Nup153 NPC (aa 1-619)	This paper
35	pCS2-FLAG-S Tag Nup153 NPCZnF (aa 1-872)	This paper
36	pCS2-FLAG-S Tag Nup153 ZnF (aa 620-873)	This paper
37	pCS2-FLAG-S Tag Nup153 ZnFFG (aa 620-1475)	This paper
38	pCS2-FLAG-S Tag Tag Nup153 FG (aa 873-1475)	This paper
39	pCS2-FLAG-S Tag Nup153 NPC 304AAA	This paper
40	pCS2-FLAG-S Tag Nup153 NPC 480AAA	This paper
41	pCS2-FLAG-S Tag Nup153 NPC 562AAA	This paper
42	pCS2-FLAG-S Tag Nup153 NPC 3xAAA (304AAA, 480AAA, 562AAA)	This paper

43	pCS2-3xHA SPOP WT	This paper	
44	pCS2-3xHA SPOP F102C	This paper	
45	pOG44	Invitrogen	V600520
46	pgLAP2-SPOP WT	This paper	
47	pgLAP2 (empty vector)	Addgene	Addgene Plasmid #19703

Table 2: List and sequence of oligonucleotides

#	Name	Sequence (given 5' to 3')	Comments
1	SPOP siRNA #100		Millipore Sigma siRNA ID: SASI_Hs01_00034100
	Sense	GUCAACAUUUCUGGCCAGA[dT][dT]	
	Antisense	UCUGGCCAGAAAUGUUGAC[dT][dT]	
2	SPOP siRNA #101		Millipore Sigma siRNA ID: SASI_Hs01_00034101
	Sense	GAAAUGGUGUUUGCGAGUA[dT][dT]	
	Antisense	UACUCGCAAACACCAUUUC[dT][dT]	
3	SPOP siRNA #102		Millipore Sigma siRNA ID: SASI_Hs01_00034102

	Sense	GAGCAAAUGAUAAACUGAA[dT][dT]	
	Antisense	UUCAGUUUAUCAUUUGCUC[dT][dT]	
4	Nup153 N-term Fwd (Start aa 1)	GGGGACAAGTTTGTACAAAAAAGCAGGCTTCGAAGGAGATAGAACCATG GCCTCGGGAGCCGGAGG	Used to attach Gateway cloning sites to Nup153
5	Nup153 NPC Rev (End aa 619)	GGGGACCACTTTGTACAAGAAAGCTGGGTCCTA CGATGCGAAACCAGGGCTTTTCAG	Used to attach Gateway cloning sites to Nup153
6	Nup153 ZnF Fwd (Start aa 620)	GGGGACAAGTTTGTACAAAAAAGCAGGCTTCGAAGGAGATAGAACCATG GGGCCGAAGATAGATTCTGTTGC	Used to attach Gateway cloning sites to Nup153
7	Nup153 ZnF Rev (End aa 872)	GGGGACCACTTTGTACAAGAAAGCTGGGTCCTA CAAACATTTGGTAGAGTCTGCC	Used to attach Gateway cloning sites to Nup153

8	Nup153 FG Fwd (Start aa 873)	GGGGACAAGTTTGTACAAAAAAGCAGGCTTCGAAGGAGATAGAACCATG GCATGTGAAAGTGCAAAGCCAGG	Used to attach Gateway cloning sites to Nup153
9	Nup153 C-term Rev (End aa 1475)	GGGGACCACTTTGTACAAGAAAGCTGGGTCCTATTTCCTGCGTCTAACAG CAGTCTTTATCTTGC	Used to attach Gateway cloning sites to Nup153
10	Nup153 1-330 Rev (End aa 330)	GGGGACCACTTTGTACAAGAAAGCTGGGTCCTAGGATGGAATTCTTTTTG CATCC	Used to attach Gateway cloning sites to Nup153
11	Nup153 331-619 Fwd (Start aa 331)	GGGGACAAGTTTGTACAAAAAAGCAGGCTTCGAAGGAGATAGAACCATG GGGATTGTTTCTTCTCCTCTGAATTC	Used to attach Gateway cloning sites to Nup153
12	Nup153 1-167	GGGGACCACTTTGTACAAGAAAGCTGGGTCCTACTTTACAAGGGAAAATC CCG	Used to attach

	Rev (End aa 167)		Gateway cloning sites to Nup153 Used to attach Gateway cloning sites to Nup153 Used with QuickChange Lightning to mutate Nup153 residues Used with QuickChange Lightning to mutate Nup153 residues Used with QuickChange Lightning to mutate
13	Nup153 168-330 (Start aa 168)	GGGGACAAGTTTGTACAAAAAAGCAGGCTTCGAAGGAGATAGAACCATGGAAATTAAAGATTCTACC	
14	Nup153 303VTST > VAAAT #1	CAATATTCGCCGAGCTGTTGCAGCGGCCACACCGTAAGATTGTGCAC	
15	Nup153 303VTST > VAAAT #2	GTGCACAATCTTACGGTGTGGCCGCTGCAACAGCTCGGCGAATATTG	
16	Nup153 479ITSS >	CTAAAATTAAAGGTAGGCAGTGAAGCAGCGGCGATCGGTAGAGAGATTTTCGGTAAT	

	IAAAS #1		Nup153 residues
17	Nup153 479ITSS > IAAAS #2	ATTACCGAAAATCTCTCTACCGATCGCCGCTGCTTCACTGCCTACCTTTAATTTTAG	Used with QuickChange Lightning to mutate Nup153 residues
18	Nup153 561GSST > GAAAT #1	GCTGAACTACTTATAATTGGTTCTAAAGTAGCAGCAGCACCAGAAAGTTCTGCTGTTTTTGCAACAGG	Used with QuickChange Lightning to mutate Nup153 residues
19	Nup153 561GSST > GAAAT #2	CCTGTTGCAAAAACAGCAGAACTTTCTGGTGCTGCTGCTACTTTAGAACCAATTATAAGTAGTTCAGC	Used with QuickChange Lightning to mutate Nup153 residues
20	Nup153	TATTCGCCGAGCACCGTAAGATTGTGCACTGAGT	Used with QuickChange Lightning to

	del303-7 #1		mutate Nup153 residues Used with QuickChange Lightning to
21	Nup153 del303-7 #2	ACTCAGTGCACAATCTTACGGTGCTCGGCGAATA	mutate Nup153 residues Used with QuickChange Lightning to
22	Nup153 del312-316 #1	AAAGGGCTTGACATCTTTATTCGCCGAGCTGTTGAAC	mutate Nup153 residues Used with QuickChange Lightning to
23	Nup153 del312-316 #2	GTTCAACAGCTCGGCGAATAAAGATGTCAAGCCCTTT	mutate Nup153 residues Used with QuickChange Lightning to
24	Nup153 1-330	ATTGCAGTCTTTAGAGAAGATGGCAAAAAGAATTCCATCCTAGG	mutate Nup153 residues Used with QuickChange Lightning to

	del319-324 #1		mutate Nup153 residues Used with QuickChange Lightning to mutate Nup153 residues Used with QuickChange Lightning to mutate Nup153 residues Used with QuickChange Lightning to mutate Nup153 residues Used with QuickChange Lightning to
25	Nup153 1-330 del319-324 #2	CCTAGGATGGAATTCTTTTTGCCATCTTCTCTAAAGACTGCAAT	
26	Nup153 219Term #1	AGCTGAACGTTCTCACTCACTCTAACAGCACACTGC	
27	Nup153 219Term #2	GCAGTGTGCTGTTAGAGTGAGTGAGAACGTTCAGCT	
28	Nup153	GGATTGAAGAATTCCCAAGTGACTAGGAAAGTGTTCCAAAGGCAGAC	

	241Term #1		mutate Nup153 residues Used with QuickChange Lightning to
29	Nup153 241Term #2	GTCTGCCTTTGGAACACTTTCCTAGTCACTTGGGAATTCTTCAATCC	mutate Nup153 residues Used with QuickChange Lightning to
30	Nup153 276Term #1	GCAGCAGCTGCTGTAAGACAGTAGAAACTACGAAATACACCTTATC	mutate Nup153 residues Used with QuickChange Lightning to
31	Nup153 276Term #2	GATAAGGTGTATTTCGTAGTTTCTACTGTCTTACAGCAGCTGCTGC	mutate Nup153 residues Used with QuickChange Lightning to
32	Nup153	CTGGTCACACCCTAAGATTGTGCACTGAGTTGC	mutate Nup153 residues Used with QuickChange Lightning to

	301Term #1		mutate Nup153 residues Used with QuickChange Lightning to mutate Nup153 residues Used with QuickChange Lightning to mutate Nup153 residues Used with QuickChange Lightning to mutate Nup153 residues
	Nup153		
33	301Term #2	GCAACTCAGTGCACAATCTTAGGGTGTGACCAG	
	Nup153		
34	del300-330 #1	ATTCAGAGGAGAAGAAACAATTTGTGCACTGAGTTGCTTAGC	
	Nup153		
35	del300-330 #2	GCTAAGCAACTCAGTGCACAAATTGTTTCTTCTCCTCTGAAT	

36	Nup153 Double Del del312-316 #1	ATTCAGAGGAGAAGAAACAATTTGTGCACTGAGTTGCTTAGC	This primer was used with QuickChange Lightning to delete residues 312-316 using the Nup153 1-330 del303-307 and del319-324 as a template. The previous set of primers could not be used as deleting nucleotides coding for amino acids 303-307 and 319-324 removed some of the

			annealing regions for the previous primer set.
37	Nup153 Double Del del312-316 #2	GCTAAGCAACTCAGTGCACAAATTGTTTCTTCTCCTCTGAAT	This primer was used with QuickChange Lightning to delete residues 312-316 using the Nup153 1-330 del303-307 and del319-324 as a template. The

			previous set of primers could not be used as deleting nucleotides coding for amino acids 303-307 and 319-324 removed some of the annealing regions for the previous primer set.
38	Gapdh qPCR, fwd	TGCACCACCAACTGCTTAGC	Adapted from PMID: 19036168
39	Gapdh qPCR, rev	GGCATGGACTGTGGTCATGAG	Adapted from PMID: 19036168

40	SPOP qPCR, fwd	TGCTGACAAGTATGCCCTGG	These primers were also verified to detect overexpressed SPOP; designed using NCBI Primer-BLAST tool to span an exon and produce a product of 193 bp
41	SPOP qPCR, rev	TTCCACCCAGAGGTCTCCAA	These primers were also verified to detect overexpressed SPOP; designed using NCBI Primer-BLAST tool to span

			an exon and produce a product of 193 bp
42	Plk1 N-term, fwd	GGGGACAAGTTTGTACAAAAAAGCAGGCTTCGAAGGAGATAGAACCATG GGGAGTGCTGCAGTGACTGC	Used to attach Gateway cloning sites to Plk1
43	Plk1 C-term, rev	GGGGACCACTTTGTACAAGAAAGCTGGGTCCTAGGAGGCCTTGAGACGG TTGCTGG	Used to attach Gateway cloning sites to Plk1
44	Cdc20 N-term, fwd	GGGGACAAGTTTGTACAAAAAAGCAGGCTTCGAAGGAGATAGAACCATG GCACAGTTCGCGTTCGAGA	Used to attach Gateway cloning sites to Cdc20
45	Cdc20 C-term, rev	GGGGACCACTTTGTACAAGAAAGCTGGGTCCTATCAGCGGATGCCTTGGT GGATG	Used to attach Gateway

			cloning sites to Cdc20 Used to attach Gateway cloning sites to KPNA6
46	KPNA6 N-term, fwd	GGGGACAAGTTTGTACAAAAAAGCAGGCTTCGAAGGAGATAGAACCATG GAGACCATGGCGAGCCCAG	
47	KPNA6 C-term, rev	GGGGACCACTTTGTACAAGAAAGCTGGGTCCTATAGCTGGAAGCCCTCCA TGGG	Used to attach Gateway cloning sites to KPNA6 Used to attach Gateway cloning sites to Nup50 Used to attach Gateway cloning sites to Nup50
48	Nup50 N-term, fwd	GGGGACAAGTTTGTACAAAAAAGCAGGCTTCGAAGGAGATAGAACCATG ATGGCCAAAAGAAATGCCGAG	
49	Nup50 C-term, rev	GGGGACCACTTTGTACAAGAAAGCTGGGTCCTAGGCATCCTTTTTCTCCA GTAAAATTTTG	

Table 3: List of primary antibodies

Primary antibodies for IB were diluted in blocking buffer (0.5% (w/v) BSA + 0.1% Tween 20 (v/v) in PBS) + 0.1% (w/v) sodium azide. Secondary antibodies for IB were diluted into blocking buffer.

Item #	Name	Company	Catalog Number	Notes
1	HA	CST	3724S	Used for IB at 1:1000; used for IF at 1:250
2	HA	Abcam	ab18181	Used for IB at 1:1000; used for IF at 1:250
3	FLAG800	Rockland	200-345-383	Used for IB at 1:10,000; note this antibody is already conjugated to a fluorophore and does not require a secondary antibody
4	Nup153	Abcam	ab84872	Used for IB at 1:1000; used for IF at 1:100
5	Nup50	Abcam	ab151567	Used for IB at 1:1000
6	KPNA6	ProteinTech	12366-2-AP	Used for IB at 1:1000
7	Daxx	Sigma	D7810-.2ML	Used for IB at 1:10,000
8	DEK	ProteinTech	16448-1-AP	Used for IB at 1:1000
9	SPOP	ProteinTech	16750-1-AP	Used for IB at 1:500
10	CREST	Antibodies Incorporated	15-234	Used for IF at 1:200
11	Mad1	GeneTex	GTX109519	Used for IF at 1:100; must be used with MeOH fixation
12	Myd88	ProteinTech	23230-1-AP	Used for IB at 1:1000
13	Caprin1	ProteinTech	15112-1-AP	Used for IB at 1:1000

	Poly		BML-	
14	ubiquitin	Enzo	PW8805	Used for IB at 1:1000
15	GFP	Abcam	ab13970	Used for IB at 1:1000; used for IF at 1:100
16	Myc	ProteinTech	60003-2-1G	Used for IF at 1:250
17	Nup98	Abcam	ab50610	Used for IB at 1:1000
	Lamin	Santa Cruz		
18	A/C	BioTech	sc-376248	Used for IB at 1:500; used for IF at 1:100
		Millipore		
19	pHH3	Sigma	06-570	Used for IB at 1:1000
	Alpha			
20	tubulin	BioRad	MCA77G	Used for IB at 1:1000; used for IF at 1:250
21	Gapdh	ProteinTech	60004-1-Ig	Used for IB at 1:3000
22	S-Tag	GeneTex	GTX19321	Used for IB at 1:1000

Table 4: List of secondary antibodies

Secondary antibodies for IB

All IB secondaries were purchased from LI-COR Biotechnology, resuspended in 800 microliters of 50% glycerol (stock concentration = 0.625 mg/mL), stored at 4C in the dark, and used at 1:10,000

Item

#	Name	Catalog #
1	IRDye® 800CW Donkey anti-Goat IgG (H + L), 0.5 mg	926-32214
2	IRDye® 800CW Donkey anti-Rabbit IgG (H + L), 0.5 mg	926-32213
3	IRDye® 800CW Goat anti-Rat IgG (H + L), 0.5 mg	926-32219
4	IRDye® 800CW Donkey anti-Mouse IgG (H + L), 0.5 mg	926-32212
5	IRDye® 800CW Donkey anti-Chicken IgG (H + L), 0.5 mg	926-32218
6	IRDye® 680RD Donkey anti-Goat IgG (H + L), 0.5 mg	926-68074
7	IRDye® 680RD Goat anti-Rat IgG (H + L), 0.5 mg	926-68076
8	IRDye® 680RD Donkey anti-Rabbit IgG (H + L), 0.5 mg	926-68073
9	IRDye® 680RD Donkey anti-Mouse IgG (H + L), 0.5 mg	926-68072
10	IRDye® 680RD Donkey anti-Chicken IgG (H + L), 0.5 mg	926-68075

Secondary antibodies for IF

All IF secondaries were purchased from Jackson ImmunoResearch Laboratories, resuspended in 400 microliters of 50% glycerol (stock concentration = 1.25 mg/mL), stored at -20C in the dark, and used at 1:500

#	Name	Catalog #
1	Fluorescein (FITC) AffiniPure Donkey Anti-Rat IgG (H+L)	712-095-150
2	Fluorescein (FITC) AffiniPure Donkey Anti-Rabbit IgG (H+L)	711-095-152
3	Fluorescein (FITC) AffiniPure Donkey Anti-Mouse IgG (H+L)	715-095-151
4	Fluorescein (FITC) AffiniPure Donkey Anti-Chicken IgY (IgG) (H+L)	703-095-155
5	Cy™5 AffiniPure Donkey Anti-Rat IgG (H+L)	712-175-150
6	Cy™5 AffiniPure Donkey Anti-Rabbit IgG (H+L)	711-175-152
7	Cy™5 AffiniPure Donkey Anti-Mouse IgG (H+L)	715-175-151
8	Cy™5 AffiniPure Donkey Anti-Human IgG (H+L)	709-175-149
9	Cy™3 AffiniPure Donkey Anti-Rat IgG (H+L)	712-165-153
10	Cy™3 AffiniPure Donkey Anti-Rabbit IgG (H+L)	711-165-152
11	Cy™3 AffiniPure Donkey Anti-Mouse IgG (H+L)	715-165-151

Appendix Chapter 7: Supplemental File 1 for Chapter 3

Table 1: List of plasmids

#	Plasmid name	Source (Catalog Number)	Notes
1	pGLAP1 (empty vector)	Addgene, #19702	For mammalian expression; backbone (empty) vector codes for EGFP-S Tag-(protein)
2	pCS2 FLAG DEST	PMID: 26748699	For IVT and mammalian expression; Gateway-compatible vector; backbone (empty) vector codes for FLAG-S Tag-(protein)
3	pCS2 HA DEST	PMID: 26748699	For IVT and mammalian expression; Gateway-compatible vector; backbone (empty) vector codes for 3xHA-(protein)
4	pENTR221 Cul3	Thermo Fisher Scientific, Ultimate ORF Clone IOH26262	Gateway vector containing human Cul3 coding sequence with stop codon, matching NM_003590.4
5	pCS2 HA Cul3	(This study)	For IVT and mammalian expression; generated via

			Gateway cloning; codes for 3xHA-Cul3
6	pENTR223 KCTD1	DNASU, HsCD00288028	Gateway vector containing human KCTD1 without stop codon; matches BC063652.1 except for the addition of nucleotides TAC (coding for Tyr) at the 3' end of the sequence
7	pDONR223 KCTD3	DNASU, HsCD00353755	Gateway vector containing human KCTD3 without stop codon, matching HQ258497
8	pDONR221 KCTD4	DNASU, HsCD00076174	Gateway vector containing human KCTD4 with stop codon, matching BC018063
9	pDONR221 KCTD5	DNASU, HsCD00829069	Gateway vector containing human KCTD5 without stop codon; sequence matches NM_018992.4 except for the addition of nucleotides TTG (coding for Leu) at the 3’ end of the sequence
10	pDONR223 KCTD8	DNASU, HsCD00353710	Gateway vector containing human KCTD8 without stop codon, matching HQ258617

11	pDONR223 KCTD9	DNASU, HsCD00352800	Gateway vector containing human KCTD9 without stop codon, matching HQ447786
12	pENTR223 KCTD12	DNASU, HsCD00515338	Gateway vector containing human KCTD12 without stop codon, matching BC013764.1
13	pDONR221 KCTD14	DNASU, HsCD00044794	Gateway vector containing human KCTD14 with stop codon, matching BC001062; note that this sequence codes for Isoform 3b (Uniprot Q9BQ13-2) and is distinct from the protein isoform NDUFC2-KCTD14 (Uniprot E9PQ53)
14	pENTR223 KCTD16	DNASU, HsCD00511508	Gateway vector containing human KCTD16 without stop codon, matching BC113435.1
15	pDONR221 KCTD18	DNASU, HsCD00718393	Gateway vector containing human KCTD18 without stop codon, matching NM_001321547.2
16	pDONR223 KCTD19	DNASU, HsCD00398604	Gateway vector containing human KCTD19 without stop codon, matching HQ258662

17	pENTR221 KCTD1 stop	(This study)	Generated via PCR amplification of coding sequence (appending a stop codon) and BP reaction into empty pDONR221 plasmid
18	pENTR221 KCTD9 stop	(This study)	Generated via PCR amplification of coding sequence (appending a stop codon) and BP reaction into empty pDONR221 plasmid
19	pENTR221 KCTD16 stop	(This study)	Generated via PCR amplification of coding sequence (appending a stop codon) and BP reaction into empty pDONR221 plasmid
20	pENTR221 KCTD18 stop	(This study)	Generated via PCR amplification of coding sequence (appending a stop codon) and BP reaction into empty pDONR221 plasmid
21	pDONR223 KCTD3 stop	(This study)	Generated via inserting a stop codon with QuikChange Lightning at end of coding sequence

22	pDONR221 KCTD5 stop	(This study)	Generated via inserting a stop codon with QuikChange Lightning at end of coding sequence
23	pDONR223 KCTD8 stop	(This study)	Generated via inserting a stop codon with QuikChange Lightning at end of coding sequence
24	pDONR223 KCTD12 stop	(This study)	Generated via inserting a stop codon with QuikChange Lightning at end of coding sequence
25	pDONR223 KCTD19 stop	(This study)	Generated via inserting a stop codon with QuikChange Lightning at end of coding sequence
26	pGLAP1 KCTD1	(This study)	For mammalian expression; generated via Gateway cloning; codes for EGFP-S Tag-KCTD
27	pGLAP1 KCTD3	(This study)	For mammalian expression; generated via Gateway cloning; codes for EGFP-S Tag-KCTD
28	pGLAP1 KCTD4	(This study)	For mammalian expression; generated via Gateway cloning; codes for EGFP-S Tag-KCTD

29	pGLAP1 KCTD5	(This study)	For mammalian expression; generated via Gateway cloning; codes for EGFP-S Tag-KCTD
30	pGLAP1 KCTD8	(This study)	For mammalian expression; generated via Gateway cloning; codes for EGFP-S Tag-KCTD
31	pGLAP1 KCTD9	(This study)	For mammalian expression; generated via Gateway cloning; codes for EGFP-S Tag-KCTD
32	pGLAP1 KCTD12	(This study)	For mammalian expression; generated via Gateway cloning; codes for EGFP-S Tag-KCTD
33	pGLAP1 KCTD14	(This study)	For mammalian expression; generated via Gateway cloning; codes for EGFP-S Tag-KCTD
34	pGLAP1 KCTD16	(This study)	For mammalian expression; generated via Gateway cloning; codes for EGFP-S Tag-KCTD
35	pGLAP1 KCTD18	(This study)	For mammalian expression; generated via Gateway cloning; codes for EGFP-S Tag-KCTD

36	pGLAP1 KCTD19	(This study)	For mammalian expression; generated via Gateway cloning; codes for EGFP-S Tag-KCTD
37	pCS2 FLAG KCTD1	(This study)	For IVT and mammalian expression; generated via Gateway cloning; codes for FLAG-S Tag-KCTD
38	pCS2 FLAG KCTD3	(This study)	For IVT and mammalian expression; generated via Gateway cloning; codes for FLAG-S Tag-KCTD
39	pCS2 FLAG KCTD4	(This study)	For IVT and mammalian expression; generated via Gateway cloning; codes for FLAG-S Tag-KCTD
40	pCS2 FLAG KCTD5	(This study)	For IVT and mammalian expression; generated via Gateway cloning; codes for FLAG-S Tag-KCTD
41	pCS2 FLAG KCTD8	(This study)	For IVT and mammalian expression; generated via Gateway cloning; codes for FLAG-S Tag-KCTD
42	pCS2 FLAG KCTD9	(This study)	For IVT and mammalian expression; generated via Gateway cloning; codes for FLAG-S Tag-KCTD

43	pCS2 FLAG KCTD12	(This study)	For IVT and mammalian expression; generated via Gateway cloning; codes for FLAG-S Tag-KCTD
44	pCS2 FLAG KCTD14	(This study)	For IVT and mammalian expression; generated via Gateway cloning; codes for FLAG-S Tag-KCTD
45	pCS2 FLAG KCTD16	(This study)	For IVT and mammalian expression; generated via Gateway cloning; codes for FLAG-S Tag-KCTD
46	pCS2 FLAG KCTD18	(This study)	For IVT and mammalian expression; generated via Gateway cloning; codes for FLAG-S Tag-KCTD
47	pCS2 FLAG KCTD19	(This study)	For IVT and mammalian expression; generated via Gateway cloning; codes for FLAG-S Tag-KCTD
48	pDONR221	Thermo Fisher Scientific, 12536017	Backbone (empty) vector for Gateway cloning
49	pGLAP2 (empty vector)	Addgene, #19703	For mammalian expression; backbone (empty) vector codes for FLAG-S Tag-(protein)
50	pGLAP2 Cul3	(This study)	For mass spectrometry

pCS2 FLAG DEST protein sequence (where the last M is the initiator Met of the tagged protein):

MDYKDDDDKAGGGGENLYFQGGGGGKETAAAKFERQHMDSGGGGINYNGHQTSLYKKVGTM...

pCS2 HA DEST protein sequence (where the last M is the initiator Met of the tagged protein):

MYPYDVPDYAYPYDVPDYAYPYDVPDYAGRPEFKDQTSLYKKAGTM...

Table 2: List and sequence of oligonucleotides

#	Primer name	Primer sequence (5' to 3')	Notes
1	KCTD1_fwd	GGGGACAAGTTTGTACAAAAAAGCAGGCTTCGAAGGAGATAGAACCATGGGGTCAAGACCTCTGATCACTAG	Used to amplify out coding sequence with stop codon added; PCR product used for BP reaction with empty pDONR221
2	KCTD1_revStop	GGGGACCACTTTGTACAAGAAAGCTGGGTCCTAGTCCAGAGGCTCTTGCTTTATCCGG	Used to amplify out coding sequence with stop codon added; PCR product used for BP reaction with empty pDONR221
3	KCTD9_fwd	GGGGACAAGTTTGTACAAAAAAGCAGGCTTCGAAGGAGATAGAACCATGGGGAGGCGGGTGACCCTGTTCC	Used to amplify out coding sequence with stop codon added; PCR product used for BP reaction with empty pDONR221
4	KCTD9_revStop	GGGGACCACTTTGTACAAGAAAGCTGGGTCCTATCTGACACTTTGTGACATGTG	Used to amplify out coding sequence with stop codon added; PCR product used for BP reaction with empty pDONR221
5	KCTD16_fwd	GGGGACAAGTTTGTACAAAAAAGCAGGCTTCGAAGGAGATAGAACCATGGCTCTGAGTGGAAACTGTAGTCG	Used to amplify out coding sequence with stop codon added; PCR product used

			for BP reaction with empty pDONR221
6	KCTD16_revStop	GGGGACCACTTTGTACAAGAAAGCTGGGTCCTATAGATGATACTTCCTTAAAAGTTC	Used to amplify out coding sequence with stop codon added; PCR product used for BP reaction with empty pDONR221
7	KCTD18_fwd	GGGGACAAGTTTGTACAAAAAAGCAGGCTTCGAAGGAGATAGAACCATGGAAGGCCACAAGGCAGAAGAAG	Used to amplify out coding sequence with stop codon added; PCR product used for BP reaction with empty pDONR221
8	KCTD18_revStop	GGGGACCACTTTGTACAAGAAAGCTGGGTCCTAATTTCCCTTGTTCTTCCCGTTC	Used to amplify out coding sequence with stop codon added; PCR product used for BP reaction with empty pDONR221
9	KCTD3_QCL_stop1	CAGGAGTACAGCTTGTAATTGCCAACTTTCTTGTAC	Used to insert a stop codon at the end of the protein coding sequence with QuikChange Lightning
10	KCTD3_QCL_stop2	GTACAAGAAAGTTGGCAATTACAAGCTGTACTCCTG	Used to insert a stop codon at the end of the protein coding sequence with QuikChange Lightning

11	KCTD5_QCL_stop1	CTCAAGGATGTTGTGAGACCCAGCTTTC	Used to insert a stop codon at the end of the protein coding sequence with QuikChange Lightning
12	KCTD5_QCL_stop2	GAAAGCTGGGTCTCACAACATCCTTGAG	Used to insert a stop codon at the end of the protein coding sequence with QuikChange Lightning
13	KCTD8_QCL_stop1	GTTGCAGAAGTATGGGTTATAATTGCCAAC TTTCTTGTAC	Used to insert a stop codon at the end of the protein coding sequence with QuikChange Lightning
14	KCTD8_QCL_stop2	GTACAAGAAAGTTGGCAATTATAACCCATA CTTCTGCAAC	Used to insert a stop codon at the end of the protein coding sequence with QuikChange Lightning
15	KCTD12_QCL_stop1	GTCTTCTGCAGGGAGTAATTGCCAACTTTC TTGTAC	Used to insert a stop codon at the end of the protein coding sequence with QuikChange Lightning
16	KCTD12_QCL_stop2	GTACAAGAAAGTTGGCAATTACTCCCTGCA GAAGAC	Used to insert a stop codon at the end of the protein coding sequence with QuikChange Lightning
17	KCTD19_QCL_stop1	GTACCTACAAGAGGACTAATTGCCAACTTT CTTGTAC	Used to insert a stop codon at the end of the protein coding sequence with QuikChange Lightning

1	KCTD19_	GTACAAGAAAGTTGGCAATTAGTCCTCTTG	Used to insert a stop codon
8	QCL_stop	TAGGTAC	at the end of the protein
	2		coding sequence with
			QuikChange Lightning